Ministry of Higher Education and Scientific Research

Hassiba Benbouali University of Chlef

Faculty of Technology

Department of Electrotechnical

THESE

Submitted in fulfillment of the requirements for the degree of

DOCTORATE (LMD)

Option: Electrical Control

By

Benali ALOUACHE

Title:

Modeling and intelligent load frequency control of an islanded microgrid.

(Fr : Modélisation et contrôle intelligent de la fréquence de charge d'un microgrid ilôté)

Defended on 11/04/2026 in front of the jury composed of:

Bachir BELMADANI	Professor	UHB-Chlef	President
M'hamed HELAIMI	Professor	UHB-Chlef	Supervisor
Elhadj BOUNADJA	Professor	UHB-Chlef	Examiner
Asma TOUALBIA	MCA	UHB-Chlef	Examiner
Abdelkadir YOUSFI	Professor	Université of Khemis Miliana	Examiner
Abdelkader BELHADJ DJILLALI	MCA	UHB-Chlef	Invited
Ismail BOUYAKOUB	MCA	UHB-Chlef	Invited


بسم الله الرحمن الرحيم

List of Publications

1- Alouache B., Helaimi M., Djilali A.B., Gabbar H.A., Allouache H., Yahdou A. Optimal tuning of multi-stage PID controller for dynamic frequency control of microgrid system under climate change scenarios. Electrical Engineering & Electromechanics, 2025, no. 1, pp. 8-15. doi: https://doi.org/10.20998/2074-272X.2025.1.02

2- Hidayet Meroua Sefiani, et al. "Thermal Performance Enhancement of Elliptical Absorbers in Cylindrical-Parabolic Solar Collectors: A CFD-Based Comparative Study." Scientific African - Elsevier, 1 Mar. 2025, pp. e02664–e02664, https://doi.org/10.1016/j.sciaf.2025.e02664. Accessed 18 Sept. 2025.

List of conferences

International Communications

1. Aloouache B, Helaimi M, Belhadj djilali ABD, Bordji N and Yamani H; Frequency fluctuations control of Microgrid System based on PID Controller; The 6th International Conference on Electrotechnics Oran, November 14-15, 2023
2. ALOUACHE B, HELAIMI M, BELHADJ DJILALI ABD and YAHDOU A ; Frequency control of an isolated microgrid based on PID controller tuned by pole placement and Genetic Algorithm; 3rd International Conference on Energy, Materials and Environment ICEME2024 6th-07th May 2024, Khemis Miliana, Algeria
3. Alouache, Benali, et al. "Load Frequency PID Controller Design Based on Pole Placement Method of an Islanded Microgrid." Journal of Renewable Energies, 24 Oct. 2024, https://doi.org/10.54966/jreen.v1i3.1303.
4. Alouache Benali et al. "Frequency Control in Microgrid Isolated System Using PID Controller Using Ziegler Nichols Method and Genetic Algorithm." Advances in Science, Technology & Innovation/Advances in Science, Technology & Innovation, 1 Jan. 2025, pp. 205–209, https://doi.org/10.1007/978-3-031-71926-4_36.
5. Benali AlOUACHE, Mhamed HELAIMI, Abdelkadir BELHADJ DJILALI, Hadj ALLOUACHE and Adil YAHDOU; Frequency control in Microgrid isolated system using PID controller using Ziegler Nichols method and Genetic Algorithm; First International Conference on Green Hydrogen Artificial Intelligence Renewable Energy and Electrical Engineering Systems GHARES'24
6. Benali Alouache, M'hamed Helaimi, Hadj allouache , Hossam A. Gabbarb, Bachir BELMADANI and Youcef benettayeb; Intelligent frequency control using PSO- PID and fuzzy logic controller for Microgrid system based on renewable energies; International Conference on Green Engineering (ICGE-25)
7. youcef benettayeb , abderrahmane benbouali, toufik tahri, benali alouache; numerical simulation of sloped absorber surface effects on solar chimney plant performance; First International Conference on Power and Modern Electrical Systems (ICPMES 2024), October 29-31, 2024 Skikda, Algeria

8. youcef benettayeb , abderrahmane benbouali, toufik tahri, benali alouache; numerical simulation of sloped absoeber surface effects on solar chimney power plant performance; 1st International Seminar on Mechatronics Innovation Materials, Renewable Energy, and Artificial Intelligence (ISMIMREAI'24), November 13-14, 2024, Tipaza, Algeria

National Communications

1. ALOUACHE B, HELAIMI M, BELHADJ DJILALI ABD and YAHDOU A ; Modeling and intelligent load frequency control of an islanded microgrid; The Third Doctoral Symposium on Technology: Process, Mechanical and Electrical Engineering DST'03-2023 02Decembre 2023
2. ALOUACHE B, HELAIMI M, BELHADJ DJILALI ABD,ALLOUACHE H and YAHDOU A; Frequency stabilization in a renewable energy-driven Bella CoolaMicrogrid System using a PID controller; The Fourth Doctoral Symposium on Technology: Process, Mechanical, Electrical and Electronic Engineering – DST'04-2024 – September 29-30, 2024
3. Youcef benettayeb , Abderrahmane benbouali, Toufik tahri, Benali alouache ; design and experimrntal validation of a solar chimney power plant prototype; Third national Conference on Materials Sciences And Engineering, (MSE'25)
4. Benali AlOUACHE, Mhamed HELAIMI, Hadj ALLOUACHE, a Gabber hossam bachir BELMADANI, youcef BENETTAYEB; Optimization framework for energy and battery management systems bassed Genetic algorithms; Third national Conference on Materials Sciences and Engineering, (MSE'25)
5. Ahmed BERROUDJI, Ahmed LARBAOUI, Khatir TABTI, Benali ALOUACHE; Advanced fuzzy logic based power management for hybrid electric vehicles integrating fuel cells and supercapacitors under dynamic driving conditions; Third national Conference on Materials Sciences and Engineering, (MSE'25).
6. ALOUACHE BENALI, M'hamed Helaimi, Hadj allouache, Hossam A. Gabbarb , Bachir BELMADANI and Youcef benettayeb; Energy Balance Optimization in Microgrids with Intermittent Solar and Wind Resources via PSO; École Nationale Polytechnique National Conference on Process Engineering & Environment May, 21st & 22nd, 2025
7. BENETTAYEB Youcef, Abderrahmane BENBOUALI, Toufik TAHRI, Alouache Benali; Hybrid Bioenergy-Solar Chimney System for Enhanced Renewable Electricity Generation; École Nationale Polytechnique National Conference on Process Engineering & Environment May, 21st & 22nd, 2025

Acknowledgements

الحمد لله رب العالمين، حمدًا يليق بجلاله وعظيم سلطانه، عدد ما كان وعدد ما يكون، الحمد لله الذي بنعمته تتم الصالحات، وبتوفيقه تتحقق الغايات، وبهدايته يُستنار في دروب الظلمات. تم بفضل الله وتوفيقه تم إنجاز هذا العمل وإتمامه؛ فهو الذي يسر أسبابه، وسخر لي من المعينات والعون ما لا يُعد ولا يُحصى، فله الحمد أولًا وآخرًا، ظاهرًا وباطنًا.

I would like to express my deepest gratitude and sincere appreciation to my esteemed supervisor, **Professor Mohamed Halaimi**, for his valuable supervision, constructive guidance, and continuous follow-up throughout the preparation of this thesis. His support and encouragement were of great importance to me in this academic journey.

My heartfelt thanks also go to **Dr. Belhadj Abdelkader**, for his valuable contributions and assistance in co-supervising this work, and for his efforts towards its successful completion.

I am also greatly indebted to all my professors in the Department of Electrotechnics, whose knowledge, guidance, and encouragement have been a fundamental part of my academic and scientific formation.

I warmly extend my gratitude to my colleagues and friends, who accompanied me during this journey, offering support, encouragement, and motivation, which helped me persevere until the end.

Special thanks and heartfelt gratitude are due to my beloved parents, **Alouache Abdelrahman** and **Charati Fatima**, who, after الله, have been my greatest support throughout my life. Surrounded by their sincere prayers, patience, and continuous sacrifices, they are the true foundation of all that I have achieved. To them, I dedicate the fruit of this work as a small token of appreciation and gratitude for the love, care, and support they have selflessly given me.

Finally, I pray to الله to make what is written in these pages beneficial knowledge and sincere work for His sake, a source of reward for me and my parents, and a blessing for everyone who has contributed, whether by a helping hand, kind advice, or moral support, near or far, seen or unseen. May He make it a continuous good and a guiding light for those who come after me.

والله ولي التوفيق

DEDICATION

I dedicate this humble work:

To ﷲ, my Creator and Owner, to Whom I belong.

To my great teacher and messenger, Prophet Muhammad ﷺ.

To my beloved father, the pillar of my strength and support.

To my great mother, the symbol of courage and endless sacrifice.

To my dear brothers and sisters, and to all my honorable family.

To my esteemed professors, who never hesitated to guide and support us until this work was completed.

To my beloved friends, who were a source of strength and encouragement along this journey.

Alouache Benali

Abstract

This thesis presents a comprehensive study on the modeling, analysis, and control of hybrid microgrid systems with a primary focus on frequency stability. The work begins with a review of microgrid concepts, classifications, and applications, highlighting their role in reducing emissions, improving efficiency, and providing reliable power in isolated regions. Accurate mathematical models of renewable and conventional energy sources, as well as Plug-in Hybrid Electric Vehicles (PHEVs) as flexible storage units, were developed to capture system dynamics and support effective control design.

A Multi-Stage PID (MPID) controller was proposed and tuned using both conventional methods (ZN and CDM) and advanced optimization algorithms (CSA and ACO). Results showed significant improvements in frequency regulation compared to classical PID controllers. The study was further extended with Type-1 and Type-2 Fuzzy Logic, which enhanced robustness and adaptability against uncertainties and stochastic variations.

The findings confirm that frequency stability is a cornerstone for reliable microgrid operation, especially in islanded mode where renewable energy variability is most pronounced. By integrating advanced control strategies and flexible storage such as PHEVs, hybrid microgrids can achieve higher resilience, flexibility, and sustainability. The proposed framework offers valuable insights for researchers, engineers, and policymakers in developing efficient, clean, and decentralized energy systems that meet growing global electricity demands while supporting long-term energy security and environmental goals.

Keywords

Microgrid - Frequency Stability- Multi-Stage PID (MPID) Controller -Fuzzy Logic (Type-1 & Type-2) - Optimization Algorithms (CSA, ACO) -Ziegler–Nichols (ZN) Method - Coefficient Diagram Method (CDM) - Plug-in Hybrid Electric Vehicles (PHEVs)- Renewable Energy source - Robust Control

ملخص

تقدم هذه المذكرة دراسة شاملة حول النمذجة والتحليل والتحكم في أنظمة الميكروغريد الهجينة، مع التركيز على استقرار التردد. يبدأ العمل بمراجعة لمفهوم الميكروغريد وأنواعه وتطبيقاته، مبرزًا دوره في تقليل الانبعاثات وتحسين الكفاءة وضمان موثوقية الإمداد الكهربائي، خاصة في المناطق المعزولة. كما تم تطوير نماذج رياضية دقيقة لمصادر الطاقة المتجددة والتقليدية، إضافةً إلى دمج المركبات الكهربائية الهجينة القابلة للشحن (PHEVs) كوحدات تخزين مرنة لدعم استقرار النظام.

تم اقتراح متحكم متعدد المراحل (MPID) وضبطه باستخدام طرق تقليدية ZN) و CDM) إلى جانب خوارزميات تحسين متقدمة CSA) و .(ACOوأظهرت النتائج تحسنًا ملحوظًا في تنظيم التردد مقارنةً بالمتحكم PID التقليدي. كما تم تعزيز الدراسة باستخدام منطق ضبابي من النوع الأول والثاني، مما زاد من مرونة المتحكم وقدرته على مواجهة الاضطرابات العشوائية والتغيرات المفاجئة.

تؤكد النتائج أن استقرار التردد يمثل الركيزة الأساسية لتشغيل الميكروغريد بشكل موثوق، خاصة في الوضع المعزول حيث تزداد تقلبات مصادر الطاقة المتجددة. وبدمج استراتيجيات التحكم المتقدمة مع التخزين المرن مثل المركبات الكهربائية الهجينة، يمكن تحقيق أنظمة أكثر مرونة واستدامة. يوفر هذا العمل إطارًا علميًا وعمليًا يساهم في تطوير شبكات طاقة نظيفة ولامركزية وفعالة، قادرة على تلبية الطلب العالمي المتزايد على الكهرباء، مع دعم أهداف الاستدامة وتعزيز أمن الطاقة في مختلف الدول.

الكلمات المفتاحية

الميكروغريد الهجين - استقرار التردد - المتحكم متعدد المراحلPID - المنطق الضبابي (النوع الأول والثاني)- خوارزميات التحسين CSA-ACO) ، - طريقة زيغلر–نيكولز (ZN)- طريقة المخطط البياني للمعاملات(CDM) - المركبات الكهربائية الهجينة القابلة للشحن(PHEVs) - مصادر الطاقة المتجددة - التحكم المتين

Notation & Abbreviation

List of abbreviations

1PD-3DOF-PID	Three-Degree-Of-Freedom PID Controller
ACO	Ant Colony Optimization
CERTS	Consortium For Electric Reliability Technology Solutions
CSA	Cuckoo Search Algorithm
DEG	Diesel Engine Generator
DSM	Demand Side Management
ESS	Energy Storage Systems
EV	Electric Vehicles
FOPID	Fractional-Order Proportional Integral Derivative
GA	Genetic Algorithm
GWA	Grey Wolf Optimization
HEV	Hybrid Electric Vehicles
IBFOA	Improved Bacterial Optimization Algorithm
ITAE	Integral Time Absolute Error
KHA	Krill Herd Algorithm
LFC	Load Frequency Control
MESS	Mobile Energy Storage Systems
MF	Membership Functions
MG	Microgrid
MPC	Model Predictive Controller
MPID	Multistage Proportional-Integral-Derivative (MPID)
MPPT	Maximum Power Point Tracking
PD	Proportional Derivative
PFC	Primary Frequency Control
PHEV	Plug-In Hybrid Electric Vehicles
PI	Proportional Integral
PID	Proportional Integral Derivative
PSO	Particle Swarm Optimization
PV	Photovoltaic
RES	Renewable Energy Source
SFC	Secondary Frequency Control
SOC	State Of Charge
T1-FL	Type 1 Fuzzy Logic
T2-FL	Type 2 Fuzzy Logic
V2G	Vehicle-To-Grid
WTG	Wind Turbine Generator
AC	Alternating Current
DC	Direct Current
DG	Distributed Generation
DER	Distributed Energy Resources
PCC	Point of Common Coupling
CSP	Concentrated Solar Power
HAWT	Horizontal Axis Wind Turbines

FES	Flywheel Energy Storage
BEV	Battery Electric Vehicles
HEV	Hybrid Electric Vehicles
BMS	Battery Management Systems
EMS	Energie Management Systems
EVB	Electric Vehicle Batteries
VSI	Voltage Source Inverter
AVR	Automatic Voltage Regulator
ZN	Ziegler Nichols Method
CDM	Coefficient Diagram Method
ACO	Ant Colony Optimization

Liset of symbols

Δf	Frequency variations
ΔPL	Load changes
ΔP_{PV}	Solar power variation
ΔP_{WTR}	Wind power variation
ΔP_{DEG}	Diesel power variation
ΔP_{PHEV}	Change in output power provided to support the grid
D	Damping coefficient
I_{Ph}	Current generated by solar irradiation,
I_D	diode current
I_{sh}	leakage current through the shunt resistance.
β	temperature coefficient
NOCT	Nominal operating cell temperature
A_{PV}	Total area of the PV panels
η	Considered approximately constant,
I_{r0}	Solar irradiance at the steady operating point.
ΔI_r	Small increase or decrease in irradiance around that point
P_{PV0}	Power produced at the steady operating point
ρ	Air density
Cp	Coefficient of power defined by the Betz limit
ω	The angular velocity of the shaft
β	The pitch angle of the blade
$\eta_{generator}$	The efficiency of the generator
$\eta_{converter}$	The efficiency of the power converters
ΔV_w	The instantaneous change in wind speed
$K_{EV\max}$	The maximum value that the participation factor can reach
N_{EV}	The number of vehicles participating
ΔU_C	The centralized control signal generated by the controller
Y	The droop coefficient that smooths the system's response
M	Equivalent inertia constant of the hybrid power system.
Ps	Total average power generation.
Pt	Net average power of WTGs or PV to the system.
K	Gain.
T	Time constant.

Table of contents

General Introduction

.1 Context and Motivation of the Study 2

2. Key Research Gaps 3

3. Research Contributions 3

.4 Thesis Layout 4

Chapter I: Overview of Microgrids: Principles, Architecture and Applications

I.1. Introduction 7

I.2. The Need for Microgrid Systems 7

I.3. Overview of microgrid 7

I.4. History 8

I.5. The current state of microgrids worldwide 9

I.5.1. USA 10

I.5.2. India 10

I.5.3. Australia 10

I.5.4. Japan 10

I.5.5. European Union 10

I.5.6. Africa 11

I.6. Applications of Microgrids in Various Sectors 12

I.7. Energy Mix Analysis in Isolated Microgrid Systems 13

I.8. Topology and Structural Configuration of Microgrid Systems 14

I.8.1. Classification of MG Based on Operating Mode and System Structure 14

I.8.1.1. Classification According to Operating Mode 14

I.8.1.2. Classification of Microgrid Architectures Based on Bus Configuration 15

I.8.2. Voltage Levels in Microgrids 18

I.9. The microgrid system used in this thesis 18

I.10. Energy Sources and Constituent Elements of the Microgrid 20

I.10.1. Solar Energy 20

I.10.1.1. Solar Energy Utilization Technologies 20

I.10.1.2. Photovoltaic Systems (PV) 21

I.10.2. Wind energy 23

I.10.2.1. Classification of Wind Turbines 24

I.10.2.2. General Advantages of VAWT: 26
I.10.2.3. General Disadvantages of VAWT: 27
I.11. Storage Systems in Microgrids 27
I.11.1. Mechanical Storage Systems 27
I.11.1.1. Flywheel Energy Storage (FES) 27
I..11.1.2. Compressed Air Energy Storage (CAES) 28
I.11.2. Electrochemical Storage Systems 28
I.11.2.1. Lithium-Ion Battery 29
I.11.2.2. Lead-Acid Batteries 29
I.11.2.3. Fuel cell 30
I.11.2.4. Supercapacitors 31
I.12. Adopting Electric Vehicle Batteries as a Main Solution for Energy Storage 31
I.12.1. Types of Electric Vehicles 32
I.12.1.1. Battery Electric Vehicles (BEVs) 32
I.12.1.2. Plug-in Hybrid Electric Vehicles (PHEVs) 33
I.12.1.3. Hybrid Electric Vehicles (HEVs) 33
I.12.2. Reasons for Selecting Electric Vehicle Batteries in This Study 34
I.12.3. Components and Working Principle of Electric Vehicle Batteries 35
I.12.3.1. Advantages of Electric Vehicle Batteries: 35
I.12.3.2. Comparison Between Electric Vehicle Batteries and Other Energy Storage Systems 36
I.13. Major Technical Issues in Microgrid Operation 36
I.13.1. Application of Inverters 37
I.13.2. Microgrid Protection 37
I.13.3. Load Frequency Control 37
I.14. Previous Works on Frequency Deviation Control in Microgrid Systems 37
I.15. Conclusion 38

Chapter II: Modeling of Microgrid with Electric Vehicles

II.1. Introduction 40
II.2. Microgrid Component Modeling 41
II.2.1. Photovoltaic systems (PV) 44
II.2.2.1. Modelling of PV system 45
II.2.2. Wind Turbine Generator (WTG) 49
II.2.2.1. Modelling of WTG system 50
II.2.3. Plug-in Hybrid Electric Vehicles (PHEV) 54

II.2.3.1. Modelling of PHEV System 54
II.2.4. Diesel Energy Generator (DEG) 57
II.2.4.1. Modelling of DEG System 58
II.3. Design and Modeling of the Microgrid in MATLAB Environment 58
II.4. Modeling the Temporal Variations of Renewable Energy Sources and Load 50
II.4.1. Modeling Variations in Solar Energy 60
II.4.2. Modeling Variations in Wind Energy 60
II.4.3. Modeling Variations in Electrical Load 60
II.5. conclusion 60

Chapter III : Frequency Stabilization of Microgrid Using Multi-Stage PID Controller and Optimization Techniques

III.1. Introduction 62
III.2. Problem Statement and Motivation 63
III.3. Study of Two Controllers for Frequency Deviation Control in a MG System 65
III.3.1. PID controller structure 66
III.3.2. Multi-Stage PID (MPID) Controller Design 67
III.4. The Various Approaches to Optimization 67
III.4.1. Optimization methods 68
III.4.1.1. Coefficient diagram method (CDM) 68
III.4.1.2. Ziegler Nichols method (ZN) 73
III.4.2. Optimization algorithms. 76
III.4.2.1. Cuckoo Search Algorithm (CSA) 76
III.4.2.2. Ant Colony Optimization (ACO) 80
III.5. Simulation Results and Discussion 84
III.6. Analysis of results in general 99
III.7. Conclusion 101

Chapter IV: Enhancing MG Performance Using MPID Controller Tuned with Type-2 Fuzzy Logic

IV.1. Introduction 103
IV.2. Proposed MG structure 105
IV.3. Design of a proposed multistage PID controller optimized with T2-FL 108
IV.4. Generality on Fuzzy logic controller 110
IV.5. Structure and formulation of Type-2 Fuzzy Logic Control System 110
IV.5.1. Fuzzification 110
IV.5.2. Footprint of Uncertainty 112

IV.5.3. Fuzzy Rule Base 112
IV.5.4. Inference System 114
IV.5.5. Type-Reduction 115
IV.5.6. Defuzzification 115
IV.6. Results and Discussion 116
IV.7. Analysis of results in general 126
IV.8. Conclusion 127
General Conclusion 129

List of Figures

Chapter I

Figure I.1: The simplified schematic model of the Microgrid. 8
Figure II.2: Early Power Stations the Historical Roots of Microgrid 8
Figure I.3: Global MG Capacity Growth and Projected Total Spending by region (2020–2029) 11
Figure I.4: The Top 10 Microgrid Trends 2023 12
Figure I.5: Microgrid Applications (a) Military Base, (b) Hospital, (c) Remote Island, (d) Ship 13
Figure I.6: Rates of Energy Utilization in Microgrid Projects Worldwide 14
Figure I.7: Typology of Hybrid Energy Systems for Microgrids 14
Figure I.8: Operational Structure of a Switchable Microgrid Grid-Tied and Islanded Modes 15
Figure I.9: Simple diagram of a typical DC-MG 16
Figure I.10: Simple diagram of a typical AC-MG 17
Figure I.11: Simple diagram of a typical HMG.AC/DC 18
Figure I.12: Geographical Location of the Microgrid System in Bella Coola – British Columbia, Canada 19
Figure I.13: Composition and structure of bella coola microgrid. 19
Figure I.14: Diagram of a Central Tower CSP Power Generation System 20
Figure I.15: Photovoltaic Energy Conversion Process 22
Figure I.16: Photovoltaïque operation 22
Figure I.17: Principle of the wind energy 24
Figure I.18: Horizontal Axis Wind Turbine 25
Figure I.19: Darrieus turbine with blades curved in an elliptical arc shape. 25
Figure I.20. Helical Darrieus Turbine Design for Enhanced Efficiency and Vibration Reduction 26
Figure I.21: Straight-Bladed Darrieus Rotor with H-Shaped Configuration 26
Figure I.22: Operating Principle of a FES System 28
Figure I.23: Schematic Diagram of a CAES System 28
Figure I.24: Operating Mechanism of a Lithium-Ion Battery During Charge and Discharge Cycles 29
Figure I.25: Electrochemical Operation of a Lead-Acid Battery 30
Figure I.26: Basic Operating Principle of a Hydrogen Fuel Cell 31
Figure I.27: Operating Principle of Supercapacitors and Formation of the Electric Double Layer 31

Figure I.28 : Integration of Electric Vehicle Batteries into the Microgrid as Distributed Storage Systems 32
Figure I.29: Structure and Components of a Battery Electric Vehicle (BEV) 33
Figure I.30: Structure and Components of a Plug-in Hybrid Electric Vehicle (PHEV) 33
Figure I.31: Structure and Components of a Hybrid Electric Vehicle (HEV) 34
Figure I.32: Global Growth in Electric Car Sales (2013–2023) 34

Chapter II

Figure II.1: Overview structure of the MG system. 42
Figure II.2: PV Cell, PV Module, and Array of Modules. 45
Figure II.3: Model of the PV cell considering voltage and leakage current 46
Figure II.4: PV cell model in Orcad 47
Figures II.5: I-V and P-V Characteristics of the Cell under 1000 W/m² and Variable Temperature 48
Figure II.6: Components of a Wind Turbine System 50
Figure II.7: A Typical Wind Energy Conversion System 50
Figure II.8: Structure of Plug-in Hybrid Electric Vehicles (PHEVs) in modern MG 54
Figure II.9: Representing the charging and discharging EV 56
Figure II.10: Functional Block Representation of the Diesel Generator 57
Figure II.11: Proposed Overall Structure of the Integrated Microgrid System in MATLAB Environment 59
Figure II.12: Dynamic Model of Renewable Energy and Load Variations Incorporating Randomness and Sudden Changes 61
Figure II.13: Graphic of load, wind and PV power variation 62

Chapter III

Figure III.1: Simulation Results Prior to Enhancement 64
Figure III.2: Simplified Block Diagram of the Microgrid System with Controller 65
Figure III.3: PID controller models. 66
Figure III.4: Block diagram representation of a multistage PID controller (MPID). 67
Figure III.5: Mathematical model of the CDM method 68
Figure III.6: Flowchart of the CDM method for tuning the MPID controller parameters 73
Figure III.7: Flowchart of the ZN method for tuning the MPID controller parameters 76
Figure III.8: Flowchart of the CSA-MPID Controller Parameter Optimization 79
Figure III.9: The shortest path ants to find the pheromone 80

Figure III.10: Construction Graph of ACO-Based Optimization for MPID Controller Parameters 81
Figure III.11: Construction graph for MPID optimization n values per parameter 82
Figure III.12: Flowchart of ACO algorithm. 84
Figure III.13: Flowchart showing the interaction between MATLAB Simulink and the workspace for setting the frequency deviation parameter in the objective function 85
Figure III.14: Frequency response of MG against PV power variations 87
Figure III.15: Impact of Kpp optimization on the Δf response of the microgrid system. 88
Figure III.16: Multistep load disturbances in MG 89
Figure III.17: Δf dynamic response of PID and MPID controller based on CDM 89
Figure III.18: Frequency perturbation dynamic response of PID and MPID controller based on ZN 90
Figure III.19: Δf dynamic response of MPID controller based on CDM and ZN methods. 91
Figure III.20: Graphic of load and solar power variation 92
Figure III.21: Frequency response of MG against PV power variations 92
Figure III.22: Graphic of load and wind power variation 93
Figure III.23: Frequency response of MG against Wind power variations 93
Figure III.24: Graphic of load, wind and PV power variation 94
Figure III.25: Frequency response of MG against PV power variations, Wind power variations and multi-step load disturbance 94
Figure III.26: Δf of the MG under different ACO parameter tuning strategies using the MPID controller. 96
Figure III.27: Convergence over iterations for different ACO parameter tuning strategies 96
Figure III.28: Δf of the MG under different CSA parameter tuning strategies using the MPID controller. 96
Figure III.29: Convergence over iterations for different CSA parameter tuning strategies 98
Figure III.30: Δf dynamic response of PID and MPID controller based on ACO 99
Figure III.31: Convergence behavior across iterations under various ACO parameter tuning strategies 99
Figure III.32: Δf dynamic response of PID and MPID controller based on CSA 100
Figure III.33: Convergence behavior across iterations under various ACO parameter tuning strategies 100
Figure III.34: Frequency response of the MG under load variations 102
Figure III.35: Frequency response of MG against PV power variations 102
Figure III.36: Frequency response of MG against wind power variations 103
Figure III.37: Frequency response of MG against PV power variations, wind power variations, and multi-step load disturbance 103

Figure III.38: ITAE analysis over iterations for different control strategies..... 104

Chapter IV

Figure IV.1. Schematic of an integrated hybrid energy system combining renewable sources and EV charging with Type 2 fuzzy logic..... 108

Figure IV.2. Hybrid architecture of integrating Type-2 Fuzzy Logic with an MPID controller in a Microgrid system..... 109

Figure IV.*3*. Adaptive tuning mechanism of MPID controller parameters using T2-FL..... 110

Figure IV.4. Structure of Type-2 Fuzzy Logic in Microgrid using MATLAB..... 111

Figure IV.5. Flowchart of T2-FL logic controller..... 112

Figure IV.6. Membership functions (MF) for inputs and outputs in the T2-FL Logic..... 113

Figure IV.7. Membership Function Editor in MATLAB..... 114

Figure IV.8. Impact of membership function type on frequency deviation in the MG..... 117

Figure IV.9. Impact of membership function type on ITAE criterion in the MG..... 117

Figure IV.10. Performance comparison of PID and MPID controllers tuned with T1-FL 119

Figure IV.11. ITAE performance index results of PID and MPID controllers tuned with T1-FL 119

Figure IV.12. Performance comparison of PID and MPID controllers tuned with T*2*-FL 120

Figure IV.13. ITAE performance index results of PID and MPID controllers tuned with T*2*-FL 120

Figure IV.1*4*. Frequency deviation response of the MG under load variations using MPID controller with T1-FL and T2-FL..... 122

Figure IV.1*5*. Frequency deviation response of the MG under wind power fluctuations using MPID controller with T1-FL and T2-FL..... 123

Figure IV.1*6*. Frequency deviation response of the MG under solar power variations using MPID controller with T1-FL and T2-FL..... 124

Figure IV.17. Frequency deviation response of the MG under the combined influence of wind power and load variations using T1-FL and T2-FL 125

Figure IV.18. Variation of ITAE index over time comparing T1-FL-MPID and T2-FL-MPID controllers in the MG 126

Figure IV.19. Variation of RES (wind and solar) with load over time in the MG..... 127

Figure IV.20. Frequency deviation response of the MG during charging and discharging of the PHEV battery 127

Figure IV.21: Frequency deviation response of the microgrid under different states of charge (SOC) of electric vehicle batteries (a- 10%, b- 40%, c- 60%, and d- 80%) using the T1-FUZZY-MPID and T2-FUZZY-MPID controllers 130

List of Tables

Chapter I

Table I.1: Comparative Analysis of Electric Vehicle Batteries and Other Energy Storage Technologies..... 36

Chapter II

Table II.1: Parameters and Constants Used in Modeling the Microgrid Components 59

Chapter III

Table III.1: Calculation of PID Controller Parameters Based on $K0$and $T0$ 74

Table III.2: Performance measurement coefficients MPID-CDM against variation 86

Table III.3: Optimal parameters of the MPID and PID controller-based CDM and ZN 88

Table III.4: Comparison of the performance indicators of PID, MPID controllers using ZN and CDM..... 90

Table III.5: Performance evaluation of CDM-MPID and ZN-MPID controllers. 95

Table III.6: Optimal parameters of the MPID and PID controller-based CDM and ZN 98

Table III.7: Comparison of the performance indicators of PID, MPID controllers using ACO and CSA 101

Chapter IV

Table IV.1. T2-FL Logic Approach Rule Base for ΔKP and ΔKPP..... 113

Table IV.2. T2-FL Approach Rule Base for ΔKi. 113

Table IV.3. T2-FL Approach Rule Base for ΔKd. 114

Table IV.4. The optimal parameters of PID, and MPID controllers using T2-FL and T1-FL. 118

Table IV.5. Ratio variation in PHEVs..... 128

GENERAL INTRODUCTION

General Introduction

1. Context and Motivation of the Study

The world is currently witnessing a steady increase in electricity demand due to population growth and rapid technological development. This has exerted significant pressure on fossil resources, which are gradually depleting, in addition to their negative environmental impacts such as greenhouse gas emissions, global warming, and climate change. These challenges have driven the search for sustainable and efficient alternatives to conventional energy systems, with microgrids (MGs) emerging as one of the most prominent solutions. MGs are based on the principle of decentralized electricity generation through the integration of renewable energy sources (RESs) such as solar, wind, and hydropower with storage units and supporting conventional sources such as diesel generators and Plug-in Hybrid Electric Vehicles (PHEV) [1-2].

Microgrids have proven to be a practical solution for supplying energy to remote and islanded areas where extending conventional grids is either difficult or costly. They can operate in both grid-connected and islanded modes, offering strategic advantages in reducing transmission and distribution losses, enhancing reliability and flexibility, and contributing to emission reduction and sustainability targets [3]. Since the introduction of the microgrid concept in 1998 by CERTS, this field has become a central focus of modern power system research, particularly with continuous improvements in storage technologies and the decreasing cost of renewable energies, which have accelerated their worldwide deployment [4].

According to the International Renewable Energy Agency (IRENA), renewable energy production capacity is expected to increase globally by more than 85% by 2024, with China and the United States leading the transition, while developing countries such as India are projected to become the third-largest market, installing over 100 GW of solar and wind power. India alone has deployed more than 10,000 solar microgrids to provide electricity to rural communities that are not connected to the national grid. In Sub-Saharan Africa, MGs have contributed to reducing grid fluctuations and supporting positive energy growth, while in Puerto Rico, they were deployed after Hurricane Maria to ensure reliable, decentralized energy systems in the absence of a stable main grid [5].

Despite these advantages, microgrids face major technical challenges, most notably frequency stability. Their heavy reliance on intermittent renewable sources such as solar and wind power highly dependent on stochastic meteorological conditions often leads to fluctuations in generation that may not match load variations. This mismatch produces frequency deviations that can negatively affect power quality and system stability, and in extreme cases, may lead to total system collapse if not effectively mitigated. The challenge is further compounded by the fact that MGs have significantly lower inertia compared to conventional power systems, making frequency regulation more difficult. Consequently, researchers have extensively focused on developing both conventional and advanced control strategies, often enhanced with optimization algorithms, to reduce frequency deviations and ensure stable MG operation, particularly in islanded mode [6].

To address this challenge, various control strategies have been developed. While the conventional PID controller is characterized by its simplicity and ease of implementation, its performance becomes limited when dealing with nonlinear and uncertain operating conditions.

Therefore, more advanced approaches have been proposed, such as the Multi-Stage PID (MPID) controller, in addition to fuzzy logic techniques (Type-1 and Type-2), which provide greater flexibility in handling uncertainties. Furthermore, artificial intelligence and metaheuristic optimization algorithms including Coefficient Diagram Method (CDM), Ziegler–Nichols (ZN) tuning method, Clonal Selection Algorithm (CSA), and Ant Colony Optimization (ACO) have been employed to enhance parameter tuning and improve the efficiency of control system performance.

2. Key Research Gaps

Despite the large body of research published in the field of microgrids, several research gaps still remain, the most prominent of which are:

- ✓ Frequency stability under the intermittent nature of renewable energy sources: The problem of severe fluctuations caused by solar and wind power still persists and has not been effectively addressed through conventional controllers.
- ✓ Limitations of the classical PID controller: Its performance remains restricted when dealing with nonlinearity, uncertainties, and sudden large disturbances associated with renewable energy sources.
- ✓ Lack of advanced comparative studies: While some research has investigated advanced controllers such as MPID and fuzzy logic techniques of type-1 and type-2, comprehensive comparisons under realistic microgrid scenarios are still scarce, especially in terms of their integration.
- ✓ Integration of Plug-in Hybrid Electric Vehicles (PHEVs): Their role has not been sufficiently explored as mobile storage units within hybrid systems incorporating batteries and other storage units, despite their potential to provide additional flexibility in energy balancing.

3. Research Contributions

This thesis provides several key contributions in the field of microgrid frequency control, which can be summarized as follows:

1. Hybrid microgrid modeling: Development of accurate models for a hybrid microgrid that integrates renewable energy sources (solar PV and wind), conventional backup sources (diesel generator), and multiple storage units (batteries and plug-in hybrid electric vehicles – PHEVs), enabling realistic performance evaluation and frequency stability analysis.
2. Controller parameter tuning strategies: Application and comparative evaluation of both classical methods (Ziegler–Nichols (ZN), Coefficient Diagram Method (CDM)) and metaheuristic optimization algorithms (Cuckoo Search Algorithm (CSA), Ant Colony Optimization (ACO)) for controller parameter tuning.
3. Advanced controller evaluation: Comprehensive performance assessment of conventional PID, multistage PID (MPID), and fuzzy logic controllers (type-1 and type-2), highlighting their effectiveness in mitigating frequency fluctuations under different microgrid operating conditions.

4. Integration of PHEVs: Novel investigation of plug-in hybrid electric vehicles (PHEVs) as mobile storage units, analyzing their impact on enhancing flexibility and improving frequency stability in hybrid microgrids.

4. Thesis Layout

This thesis is organized into four main chapters, each addressing a key aspect of microgrid modeling, control, and performance enhancement:

Chapter I: Overview of Microgrids: Principles, Architecture, and Applications:

This chapter introduces the concept of microgrids, highlighting their historical development, fundamental principles, and structural architecture. It discusses the main components, classifications, and available energy sources, with emphasis on their role in providing reliable power in remote and desert areas. The chapter also explores the benefits, challenges, and real-world applications of microgrids, along with their future potential in sustainable energy systems.

Chapter II: Modeling of Microgrid with Electric Vehicles:

This chapter presents detailed modeling of the main components of the proposed microgrid, including renewable energy sources such as photovoltaic (PV) panels and wind turbine generators (WTG), in addition to auxiliary units like diesel generators and fuel cells. Special attention is given to the modeling of electric vehicle batteries as energy storage units, given their crucial role in balancing energy supply and demand. The chapter establishes the foundation for performance analysis under various operating conditions, while addressing the intermittent nature of renewable energy sources.

Chapter III: Frequency Stabilization of Microgrid Using Multi-Stage PID Controller and Optimization Techniques:

This chapter focuses on the challenge of frequency fluctuations caused by sudden changes in load demand or renewable generation. The Multi-Stage PID (MPID) controller is first introduced and tuned using classical approaches such as Ziegler–Nichols (ZN) and the Coefficient Diagram Method (CDM). To further improve dynamic performance, intelligent optimization techniques including the Cuckoo Search Algorithm (CSA) and Ant Colony Optimization (ACO) are applied. A comparative study between the conventional PID and MPID controllers is conducted under various disturbances, with frequency deviation responses analyzed and discussed.

Chapter IV: Enhancing MG Performance Using MPID Controller Tuned with Type-2 Fuzzy Logic:

This chapter investigates the use of advanced fuzzy logic techniques to improve frequency stability in islanded microgrids. The Multistage PID (MPID) controller is enhanced through tuning with Type-1 Fuzzy Logic (T1-FL) and Type-2 Fuzzy Logic (T2-FL), and its performance is compared with the conventional PID controller. While T1-FL provides an efficient tuning mechanism, T2-FL demonstrates superior capability in handling uncertainties and stochastic behavior of renewable energy sources. The simulation results highlight the strengths and limitations of each approach, with in-depth discussion of their practical implications for improving the reliability and efficiency of future microgrid systems.

Figure 1 presents a schematic overview and structural framework of the paper.

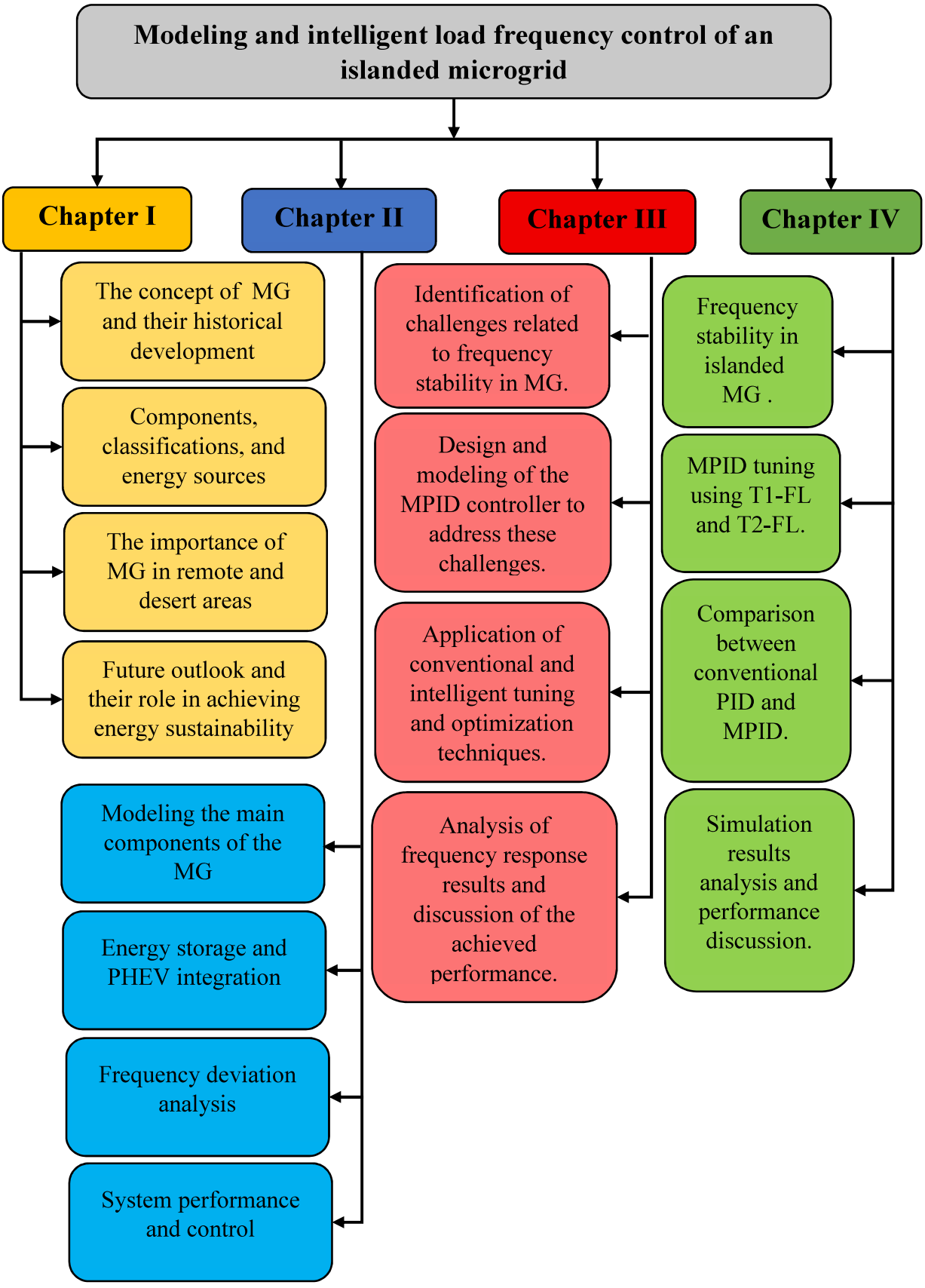

Figure 1: Schematic overview and structural framework of the paper.

CHAPTER I :

OVERVIEW OF MICROGRIDS PRINCIPLES, ARCHITECTURE AND APPLICATIONS

I.1. Introduction

With the growing global demand for electrical energy and the continuous depletion of fossil fuel resources alongside their harmful environmental impacts it has become essential to develop alternative energy systems that ensure sustainability and efficiency. Among the most promising innovations in this field is the microgrid system, which offers a decentralized approach to electricity generation by integrating renewable energy sources with advanced control and management technologies. Microgrids have gained particular importance in supplying remote and desert areas, where traditional grid extension is either costly or impractical. By enabling local energy production and ensuring supply continuity, microgrids represent a flexible and reliable solution.

This chapter provides a comprehensive introduction to microgrids, starting with their historical development, followed by an in-depth look at their main components, classifications, and available energy sources. It will also explore the benefits of microgrids, the technical and regulatory challenges they face, and their real-world applications. Finally, the chapter will offer a glimpse into the future potential of microgrids as a cornerstone of sustainable energy systems.

I.2. The Need for Microgrid Systems

With the growing global demand for reliable, sustainable, and flexible energy sources, microgrid systems have emerged as a vital solution to modern energy challenges. Traditional centralized power systems face limitations such as transmission losses, vulnerability to natural disasters, and difficulties in integrating renewable energy sources [7]. In contrast, microgrid systems offer decentralized power generation, enabling communities and facilities to operate either independently or in coordination with the main grid. These systems enhance energy security, reduce reliance on fossil fuels, and facilitate the integration of renewable sources such as solar and wind power. Additionally, they present a practical and cost-effective solution for remote or underserved areas lacking access to national electricity grids [8]. As a result, the demand for microgrid systems is rapidly increasing to meet the evolving needs for clean, reliable, and efficient energy. Energy. This growing interest is driving innovation in microgrid technology, leading to advancements in energy storage, management systems, and smart grid capabilities that further improve efficiency and adaptability. As communities and industries seek to achieve sustainability goals, microgrids are poised to have a major influence on the future of energy distribution [9].

I.3. Overview of microgrid

A microgrid is a smart, local, and self-sufficient energy system that integrates renewable energy sources such as solar panels and wind turbines, along with small-scale generators and energy storage systems like batteries. One of its key features is its dual-mode operation, allowing it to function either in connection with the main utility grid or independently in island mode during faults or emergencies [10]. This flexibility enables efficient energy distribution and demand management at the local level, reduces transmission losses, and enhances overall system reliability. The entire system is coordinated by a central controller, which manages the balance between generation and consumption and ensures optimal power distribution in real-time. Figure I.1 illustrates the basic structure of a microgrid, showing the interaction between its key components such as solar PV, wind turbines, batteries, critical loads, backup generators, and the main grid operating under the supervision of a centralized microgrid controller that

governs both grid connected and islanded modes. Microgrids represent a promising solution for achieving energy security, sustainability, and a smooth transition toward decentralized smart power networks [11].

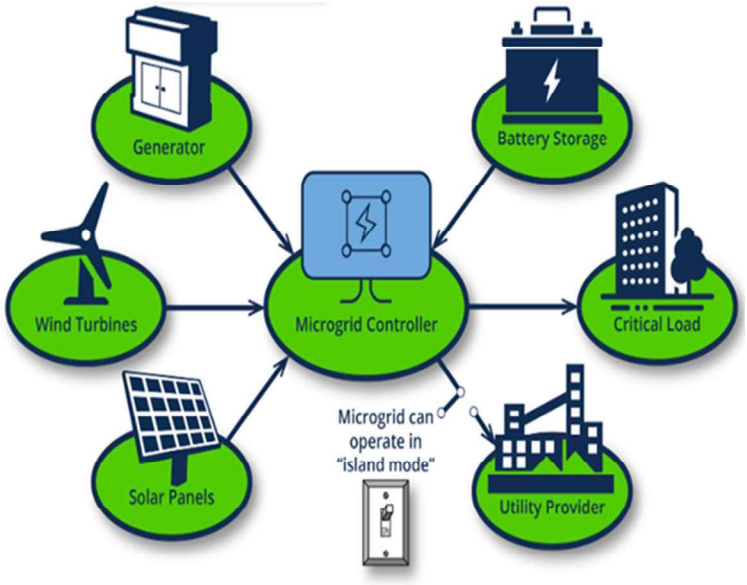

Figure I.1: The simplified schematic model of the Microgrid.

I.4. History

The concept of microgrids originated in 1882 with the establishment of the Pearl Street Station by Thomas Edison in New York City like the figure II.2. At the time, buildings were supplied with direct current (DC) electricity from a nearby power plant. However, with the advent of alternating current (AC), these localized systems were gradually replaced by centralized power grids. Despite this shift, microgrids continued to be used throughout the 20th century in remote areas, islands, and military bases in countries such as Canada, Russia, and Australia [12].

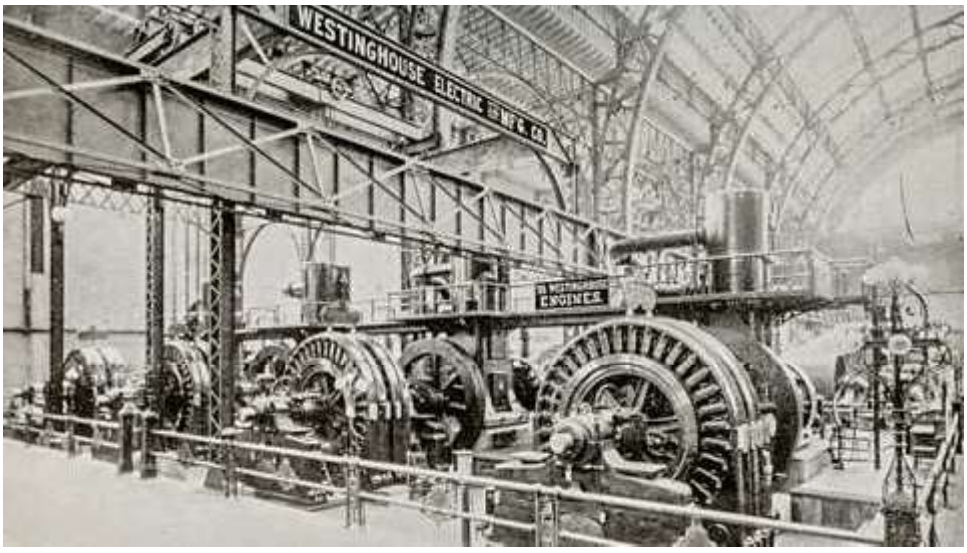

Figure II.2: Early Power Stations the Historical Roots of Microgrid

In the 1990s, renewed interest in microgrids emerged due to growing concerns about climate change and energy security. Countries like Germany and Japan began developing

microgrid systems based on renewable energy sources. In 2001, Professor R.H. Lasseter of the University of Wisconsin Madison reintroduced the modern concept of the microgrid, which was soon adopted and further developed by the Consortium for Electric Reliability Technology Solutions (CERTS) and the European Commission [13].

In 2002, the National Technical University of Athens (NTUA) launched a small laboratory microgrid for testing distributed resource (DR) control using multi-agent systems. In 2003, the University of Wisconsin built an 80 kVA laboratory microgrid, and another 480 V system was installed in Columbus, Ohio, to test the dynamic performance of microgrid components.

Between 2004 and 2006, several pilot projects were established globally, including the Sendai, Shimizu, and Tokyo Gas microgrids in Japan; the Labein microgrid in Spain; systems at Sandia National Laboratories and Palmdale in the U.S.; and the Mannheim project in Germany. During the same period, Italy's CESI RICERCA facility in Milan and the Control and Power Research Center at Imperial College London were also launched [13].

In 2006, China began integrating microgrids into its national R&D programs, including the 863 and 973 initiatives. Tsinghua University established a research microgrid incorporating distributed generation (DG), energy storage (ES), and loads. In 2008, Tianjin University focused on optimizing the dispatch of energy resources, while Hefei University of Technology concentrated on control strategies and energy management.

In 2010, China's State Grid Corporation China (SGCC) launched demonstration projects in Zhengzhou and Xi'an, integrating photovoltaic (PV) generation with energy storage. Additionally, the China Southern Power Grid Company built a combined cooling and power (CCP) microgrid demonstration in Foshan under the 863 Program. In 2011, the resilience of the Sendai microgrid was proven during the Great East Japan Earthquake, highlighting the importance of microgrids in disaster response and recovery [14].

Throughout the 2010s, rapid technological advancements enabled the integration of microgrids with smart grids, artificial intelligence, and advanced control systems. These developments facilitated rural electrification, grid flexibility, and energy autonomy. By 2020, decarbonization goals and renewable energy adoption made microgrids an essential component of national energy strategies in countries such as India, Australia, and Kenya. The COVID-19 pandemic further emphasized the role of autonomous microgrids in powering critical infrastructure like hospitals and emergency response centers. By 2022, microgrids began to incorporate electric vehicle (EV) smart charging and green hydrogen as emerging energy vectors. As of 2024, microgrids have become central to global energy transition strategies, enhanced by AI-driven predictive control, Internet of Things (IoT) technologies, and real-time optimization. These innovations have enabled microgrids to dynamically respond to fluctuations in demand and generation, supporting sustainability, reliability, and local energy independence [15-16].

I.5. The current state of microgrids worldwide

The global energy sector has witnessed significant transformations in recent years amid environmental challenges and increasing demand for electricity, prompting many countries to adopt microgrid technologies as an innovative and effective solution. According to a report issued by Navigant Research in 2023, more than 4,500 microgrid projects have been

implemented worldwide [17]. The Asia-Pacific region leads in terms of installed capacity, followed by North America, and then the Middle East and Africa.

I.5.1. USA

The United States is considered the birthplace of the microgrid concept, which first emerged through the Consortium for Electric Reliability Technology Solutions (CERTS). According to the Center for Climate and Energy Solutions, there are approximately 160 microgrid projects across the country, spread across states such as Alaska, Texas, New York, and California. One of the most notable examples is the Santa Rita Jail facility in California, which established an integrated microgrid relying on solar power, wind energy, and fuel cells following the energy crisis the state experienced in 2001 [17].

I.5.2. India

India is also one of the countries that have adopted microgrids as a means to provide electricity to rural and remote areas. According to reports from the Swiss company Hive Power, India hosts around 160 microgrid systems distributed across four states, with more than 80% of them relying on solar energy as the primary source. These projects reflect the government's efforts to promote sustainability and achieve energy equity in areas not served by traditional power grids [18].

I.5.3. Australia

The town of Heyfield in the state of Victoria serves as a promising model for implementing microgrids in small towns located on the outskirts of the grid. The My Town Microgrid Heyfield project is developing a flexible and sustainable energy system, funded by both the federal and state governments, with the goal of replicating the experience in similar towns across the country. Australia places particular emphasis on integrating renewable energy sources such as solar power and batteries into these systems [19].

I.5.4. Japan

Facing scarce natural resources and heavy reliance on energy imports, Japan gave early attention to microgrid technologies to reduce dependence on fossil fuels and achieve energy security. The Japanese model is distinguished by expanding the definition of microgrids to include traditional autonomous power systems, representing an extension of the American CERTS concept. One of Japan’s notable contributions is the FRIENDS concept (Flexible and Intelligent Energy Delivery Network System), which relies on FACTS technologies in distribution networks to enhance flexibility and response speed. Additionally, the New Energy and Industrial Technology Development Organization (NEDO) has played a pivotal role in coordinating research and projects among universities, companies, and national laboratories [20].

I.5.5. European Union

The European Union has adopted a clear policy to promote microgrids within a broader framework for the transition to smart grids. The European Commission launched the Smart Power Networks program in 2005, with its strategies being implemented starting in 2006, focusing on integrating Distributed Energy Resources (DER), smart technologies, and power

electronics for control. The European model is characterized by a mix of centralized and decentralized control, providing high-efficiency communication mechanisms such as CAN bus between digital protection units. Key contributors to the development of the European model include ABB, Fraunhofer IWES, the University of Manchester, and NTUA (Greece). This approach is considered a fundamental step toward the widespread integration of renewable energy sources into the European grid [21].

I.5.6. Africa

In several African countries such as Kenya, Nigeria, and Tanzania, microgrids have become a key tool in efforts to expand electricity access, especially in rural areas lacking national grid coverage. Startups like Power Gen and Mini Grid Africa play a prominent role in implementing projects that rely on low-cost solar energy. These models are characterized by operational simplicity and dependence on batteries to provide power throughout the day. Additionally, these projects receive support from international organizations such as UNDP and USAID, reflecting the developmental aspect of microgrid technologies in the developing world [22].

These two figures I.3 and I.4 show the overall distribution and development of microgrid systems worldwide. The map indicates that North America and parts of Europe currently serve as major hubs for these systems, reflecting North America's dominance in the largest share of microgrid capacity in terms of electrical power and investment over the past decade [23]. In contrast, the charts demonstrate significant and expected growth in both installed capacity and expenditure on this technology, reflecting a global trend towards increasing adoption of microgrids. The increase in investments is especially notable in the Asia-Pacific region, the Middle East, and Africa, underscoring the growing importance of decentralized and flexible energy solutions to address future challenges.

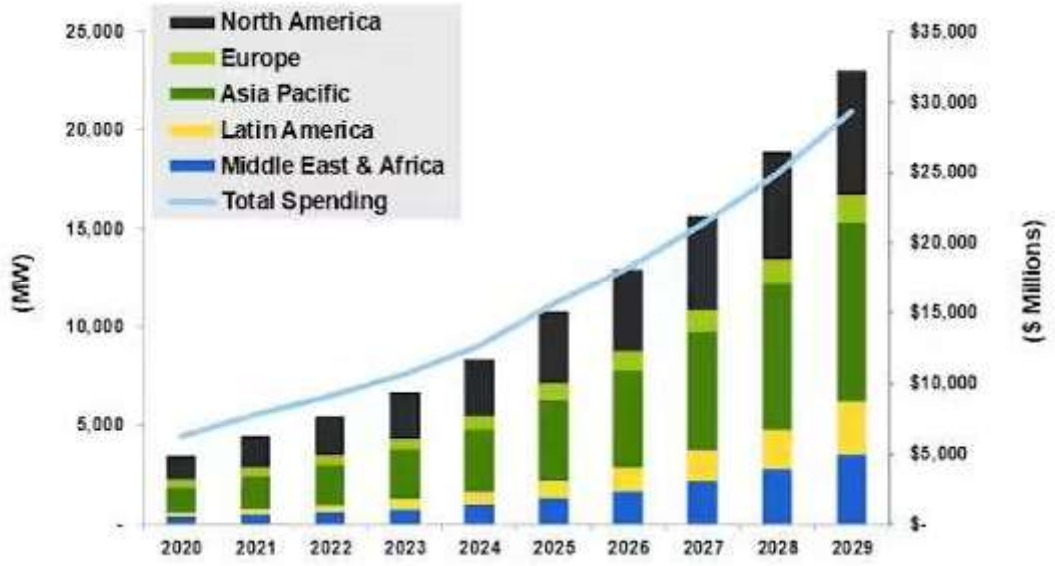

Figure I.3: Global Microgrid Capacity Growth and Projected Total Spending by region (2020–2029)

Figure I.4: The Top 10 Microgrid Trends 2023

I.6. Applications of Microgrids in Various Sectors

Microgrid systems are widely adopted across various sectors due to their ability to provide stable and reliable energy from local and renewable sources. In commercial and industrial settings, microgrids help reduce energy costs and enhance operational efficiency. They are commonly used in retail stores, call centers, carpentry workshops, small factories, and agricultural water pumping systems. In educational institutions such as universities and schools, microgrids facilitate the use of renewable energy to power entire campuses, thereby improving the sustainability of these facilities and reducing their carbon emissions. In remote areas that are not connected to the national power grid, microgrids offer an ideal solution for supplying independent electricity and reducing dependence on costly and polluting diesel generators. In critical infrastructure such as hospitals, military camps, and emergency centers as shown in Figure I.5, microgrids provide secure and sustainable energy, ensuring the continuity of essential services even during widespread power outages, thanks to their ability to operate in islanded mode. Thus, microgrids serve as flexible and integrated solutions to meet energy demands in a wide range of environments and applications.

a) b)

c) d)

Figure I.5: Microgrid Applications (a) Military Base, (b) Hospital, (c) Remote Island, (d) Ship

I.7. Energy Mix Analysis in Isolated Microgrid Systems

Figure I.6 illustrates the energy mix used in 5,554 operational isolated microgrid projects as of March 2024 (Bloomberg NEF, 2024). Approximately 63% of the identified projects rely on solar energy. In the figure, "solar microgrids" refer to systems powered exclusively by solar energy, while "solar hybrid microgrids" combine solar with at least one other source such as diesel, hydroelectric, or wind. Photovoltaic (PV) systems, which directly convert solar radiation into electricity, are the primary technology for solar-based electricity generation (IRENA, 2024). By 2024, the total installed PV capacity in Africa exceeded 13 GW, showing a significant increase from previous years (IRENA, 2024) [24].

Wind energy offers great potential in Africa, especially in the eastern, northern, and southern regions. However, its contribution to isolated microgrid systems remains limited. According to IRENA data (2024), onshore wind capacity in Africa surpassed 7 GW, although most of it is grid-connected, with few projects serving remote, off-grid communities. Small scale hydropower plants are well-suited for electrifying isolated areas. As of 2024, the cumulative installed capacity of such plants (under 10 MW) in Africa reached over 600 MW (IRENA, 2024). These installations typically divert river flows upstream of a dam to drive small hydro turbines [25].

Hydrokinetic turbines, which utilize the kinetic energy of river or tidal currents, should not be confused with tidal power that relies on differences in water height between two basins. These turbines are particularly used in off-grid microgrids, often installed in rivers, and typically have small-scale capacities (tens of kilowatts). Biomass accounts for 3.2% of the identified projects [25], and its sources are diverse (IRENA, 2024):

• Forestry residues;

• Agricultural crop waste such as wheat, maize, cassava;

• Animal waste, including manure and bedding;

• Agro-industrial by-products like rice husks and sugarcane bagasse;

• Wood residues from sawmills and factories;

• Biodegradable waste from landfills and construction sites.

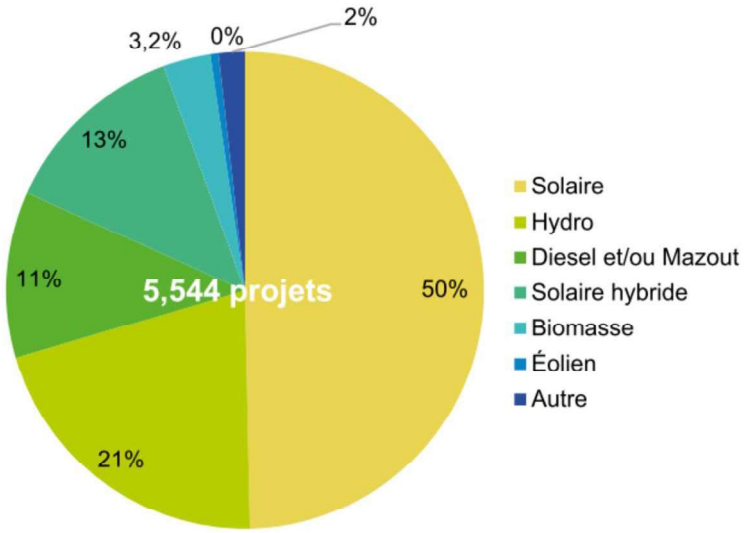

Figure I.6: Rates of Energy Utilization in Microgrid Projects Worldwide

I.8. Topology and Structural Configuration of Microgrid Systems

The following figure I.7 presents the basic classification of hybrid energy systems based on several technical criteria. This includes the mode of operation (isolated or grid-connected) and the configuration of the common bus (DC, AC, or mixed). It also highlights the variety of energy sources used, whether conventional or renewable, with or without storage systems.

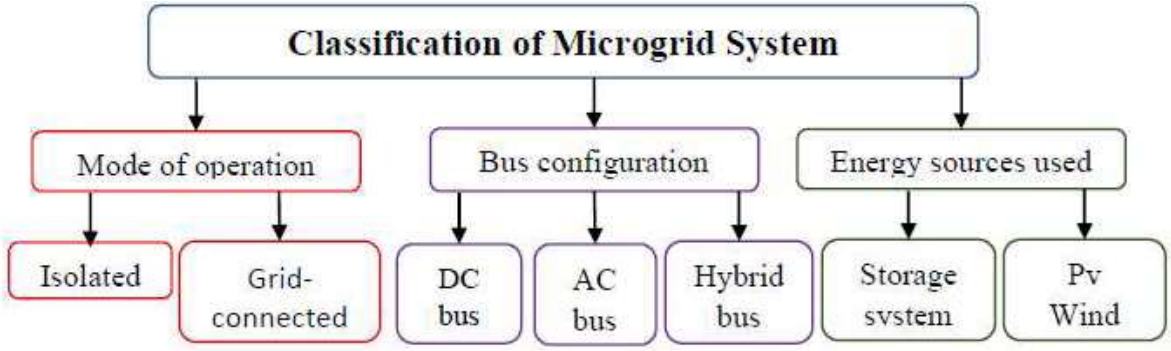

Figure I.7: Typology of Hybrid Energy Systems for Microgrids

I.8.1. Classification of MG Based on Operating Mode and System Structure

Microgrids can be classified according to several key criteria, primarily their operating mode (isolated or grid-connected) and their internal structural configuration:

I.8.1.1. Classification According to Operating Mode

In Figure I.8, a simplified diagram of a microgrid system is shown, which includes renewable energy sources (wind turbines and solar panels), an energy storage unit, and AC loads. The system also features the ability to connect to the main grid through a control switch at the Point of Common Coupling (PCC). Based on this diagram, the two operating modes can be explained as follows:

I.8.1.1.a. Isolated Microgrid Mode (Off-Grid):

When the switch is open, the microgrid operates in isolation from the main grid. In this configuration, local energy demands are met solely by internal sources such as wind turbines, solar panels, and the energy storage system. This setup is essential in remote areas where grid access is not available. However, it presents challenges related to supply reliability, especially during periods of low renewable generation or when the storage system is depleted [26][27].

I.8.1.1.b. Grid-Connected Microgrid Mode (On-Grid):

When the switch is closed, the microgrid is connected to the main utility grid. This allows the system to import electricity during local generation shortfalls and export surplus energy when available. The grid connection enhances overall system performance, enables more reliable supply, and supports advanced energy management strategies. It also contributes to greater economic and operational efficiency by leveraging the flexibility of both local and grid resources [26][27].

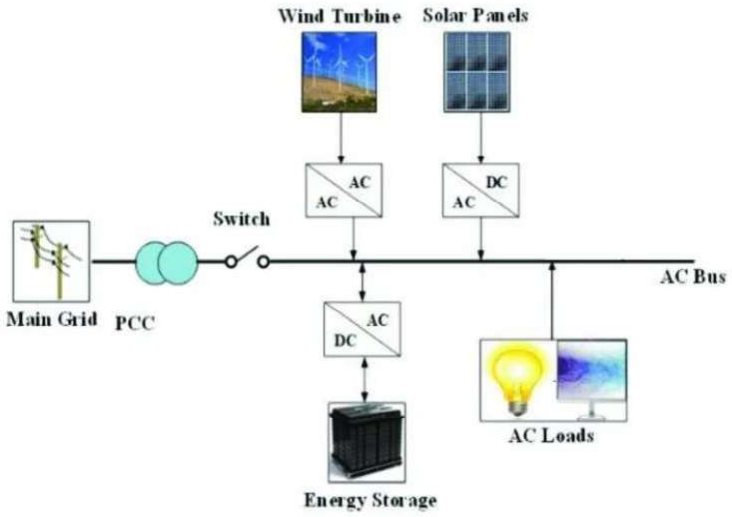

Figure I.8: Operational Structure of a Switchable Microgrid
Grid-Tied and Islanded Modes [26]

I.8.1.2. Classification of Microgrid Architectures Based on Bus Configuration

This classification is based on the type of internal interconnection bus. The main role of this bus is to establish a physical link between all system components while specifying the type and voltage level of the current whether directly generated by the energy sources or conditioned through power converters. There are three main configurations commonly used for integrating various renewable energy sources:

I.8.1.2.a. DC Microgrid

In this architecture, all power sources are connected to a common direct current (DC) bus, where the generated electrical energy is directly injected. DC power sources, such as photovoltaic systems and storage units, are connected using DC-DC converters to maintain voltage stability on the load side. AC power sources, such as wind turbines, are converted to DC using AC-DC converters before being linked to the bus [28].

As illustrated in the figure, this type of microgrid includes renewable energy sources (solar and wind), DC loads (such as electric vehicle chargers and storage devices), and prioritized AC loads (such as hospitals, water pumping stations, and homes). Each component is connected to the bus through a suitable converter to ensure smooth functional integration [29].

This architecture is commonly used in low-power applications due to several advantages, including:

- ✓ Greater flexibility in energy flow control
- ✓ Higher reliability, as the system continues to operate even if one component fails
- ✓ No need for synchronization when adding a new power source

However, it also has some drawbacks, most notably:

- ✓ The need for more converters, which increases system cost and complexity

The Figure I.9 shows a practical example of a DC bus-based microgrid architecture, clearly illustrating the connection of sources and loads and the distribution of power within the system.

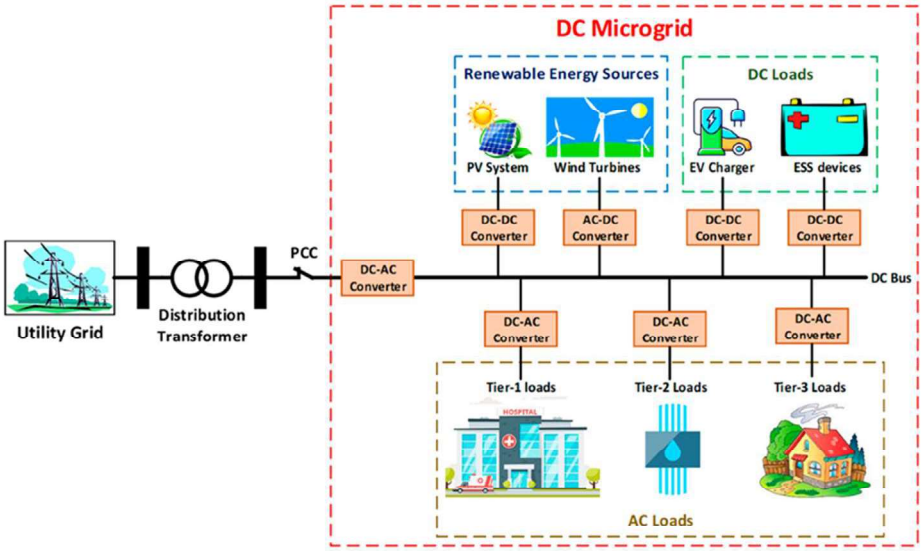

Figure I.9: Simple diagram of a typical DC-MG [28].

I.8.1.2.b. AC Microgrid

The AC bus-based architecture is one of the most widely adopted configurations in medium- and high-power applications due to its technical advantages, primarily the reduced number of converters, which minimizes energy conversion losses and improves overall system efficiency. In this configuration, renewable energy sources such as photovoltaic panels and wind turbines are connected to the AC bus through dedicated converters (DC/AC or AC/DC/AC), depending on the nature of the source. Energy storage systems (ESS) are integrated via bidirectional converters that allow both charging and discharging operations according to system requirements [28]. AC loads are connected directly to the bus without the need for additional conversion, while DC loads are interfaced through AC/DC converters to ensure voltage compatibility. Despite the simplicity of this configuration in terms of reduced conversion stages, it presents several challenges, mainly related to power quality. Inductive and

electronic loads often lead to a low power factor and the generation of electrical harmonics, which can adversely affect system performance and require the implementation of filtering and compensation equipment to maintain system stability. Figure I.10 presents a typical example of an AC bus-based microgrid architecture, illustrating the interconnection of energy sources and various load types, along with the point of common coupling (PCC) with the utility grid [29].

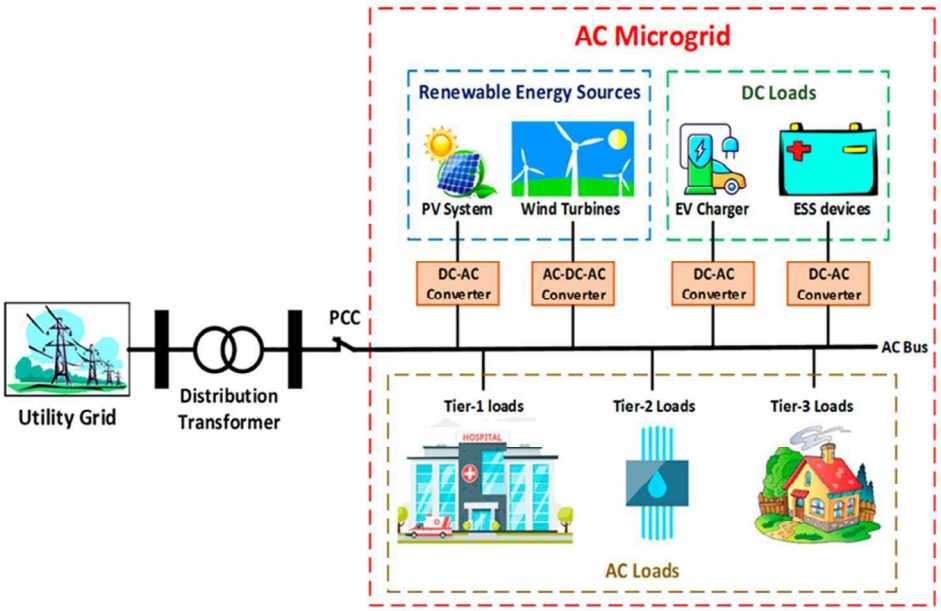

Figure I.10: Simple diagram of a typical AC-MG [22].

I.8.1.2.c. Hybrid AC/DC Microgrid

The hybrid microgrid architecture combines the advantages of both AC and DC bus systems. In this configuration, the two buses are interconnected using a bidirectional DC/AC converter that enables energy exchange between the AC and DC networks as needed. This topology offers higher energy efficiency and lower overall cost compared to purely AC-coupled or DC-coupled systems. These benefits result from fewer energy conversion stages, leading to reduced conversion losses and improved operational performance, especially in systems with mixed types of loads and energy sources. However, the main drawback of the hybrid configuration lies in its complexity in terms of control and energy management [30]. Coordinating the operation of both AC and DC networks requires advanced control strategies to ensure stable and balanced power distribution. Figure I.11 presents an example of a hybrid AC/DC microgrid architecture, clearly illustrating the distribution of loads and energy sources across both networks, as well as the point of common coupling (PCC) with the utility grid [30].

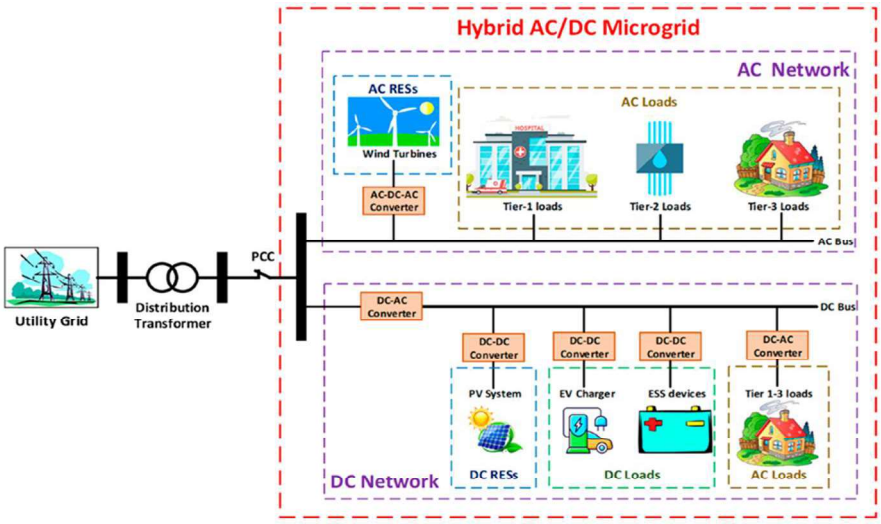

Figure I.11: Simple diagram of a typical HMG.AC/DC [30]

I.8.2. Voltage Levels in Microgrids

Several voltage levels can be identified within a microgrid:

- ✓ **User Connection Voltage:** This is typically the same for all users in a small rural network, ensuring standardized access.
- ✓ **Electricity Distribution Voltage:** This refers to the voltage level of the overhead lines or underground cables connecting generation sources to the loads. Distribution can be done at low or medium voltage depending on the system design.
- ✓ **Generation Coupling Voltage:** This voltage may differ from the distribution voltage, thanks to step-up transformers that adapt the voltage of the generation unit to match the distribution system.
- ✓ **DC Bus Voltage:** One or more DC buses are usually present in a microgrid that includes storage elements interfaced in DC, such as batteries.

The distribution voltage is a key parameter used to classify the type of microgrid. On the generation side, the DC bus voltage characterizes the nature of the equipment. It is common to distinguish:

- ✓ **Extra-Low Voltage Systems (≤ 120 VDC):** Used for batteries and PV converters operating below 120 VDC, typically around 48 VDC.
- ✓ **Low Voltage DC Systems (120 VDC to 1500 VDC):** These systems are used for applications requiring higher power and longer distances, often found in more advanced or larger-scale microgrids.

I.9. The microgrid system used in this thesis

The microgrid system analyzed and adopted in this thesis is based on a real-world implementation the Bella Coola microgrid, located in the remote coastal region of British Columbia, Canada. This system was selected due to its practical relevance, proven performance, and its ability to address challenges similar to those faced by isolated communities without access to a centralized grid. By relying on an actual case study, this work ensures that the

modeling and analysis are grounded in real operational conditions, rather than theoretical assumptions.

Bella Coola is surrounded by mountains and dense forests, making grid extension economically and logistically unfeasible. Figure I.12, taken from Google Maps, shows the town's geographical location and the natural barriers that isolate it from the main power network. In response to these constraints, a fully functional microgrid was designed and implemented during the early 2000s, making Bella Coola one of the first regions in Canada to deploy hydrogen-assisted renewable energy storage [31][32].

Figure I.12: Geographical Location of the Microgrid System in Bella Coola – British Columbia, Canada

The system combines multiple energy sources a small hydro plant (approx. 2 MW), solar panels (1 MW), a wind turbine (1.4 MW), diesel backup generators, and plug-in hybrid electric vehicles (PHEVs) used as mobile storage units. A centralized control system ensures dynamic load-frequency balancing and optimizes energy dispatch across available sources. Figure I.13 displays the actual system architecture implemented in Bella Coola, while and presents a simplified schematic outlining its energy components and technical capacities [31][32].

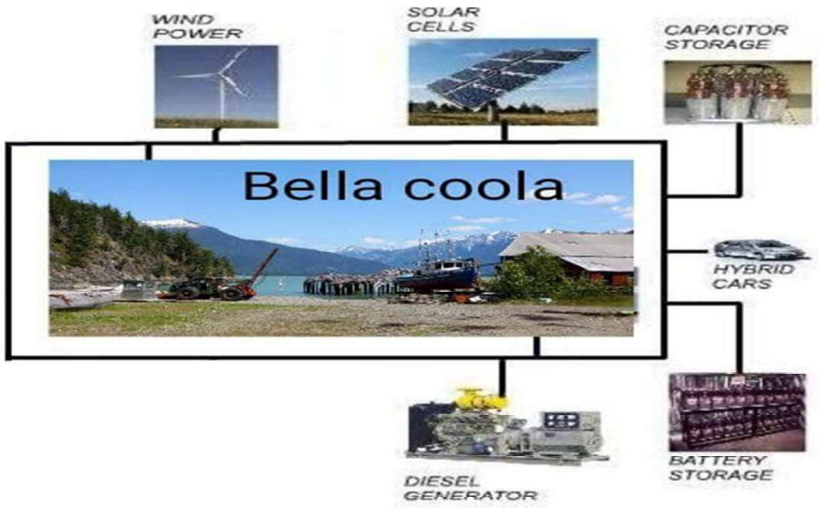

Figure I.13: Composition and structure of bella coola microgrid.

The microgrid offers several advantages: it reduces diesel fuel consumption by over 70% during summer months, cuts greenhouse gas emissions by several hundred tons annually, and improves energy reliability in an off-grid setting. The integration of hydrogen storage and smart control technologies provides additional flexibility and resilience, making the system both efficient and environmentally sustainable [33].

I.10. Energy Sources and Constituent Elements of the Microgrid

The microgrid studied in this thesis is based on a multi-source structure that integrates various types of renewable and conventional energy sources to ensure a stable and reliable power supply for a remote area. The system is composed of a set of units that work together to provide generation, storage, and backup support. This architecture was selected for its ability to adapt to fluctuating demand and the challenges of limited access to a centralized grid. The main elements are as follows:

I.10.1. Solar Energy

Solar energy is one of the fundamental pillars of the global transition toward clean and sustainable energy systems. It is a renewable, inexhaustible, and non-polluting source that allows electricity production without environmental harm. Its origin lies in nuclear fusion reactions occurring at the sun's core, where hydrogen atoms combine to form helium, releasing enormous amounts of energy in the form of electromagnetic radiation that reaches the Earth. It is estimated that the Earth receives more than 170,000 terawatts of solar energy daily many times more than the total global energy demand. With continuous technological advancement, solar systems have become more efficient and cost-effective, enabling widespread use in rural and urban areas, including centralized and decentralized energy systems such as microgrids [34].

I.10.1.1. Solar Energy Utilization Technologies

Solar energy exploitation technologies can be categorized into two main types:

a. Solar Thermal Systems

The heat generated by sunlight is used to heat water or produce steam, which in turn drives turbines to generate electricity, as illustrated in Figure I.14. This technique is employed in large-scale systems such as Concentrated Solar Power (CSP) plants, and is distinguished by its ability to integrate thermal storage systems, ensuring a continuous supply of energy even during periods without sunlight [35].

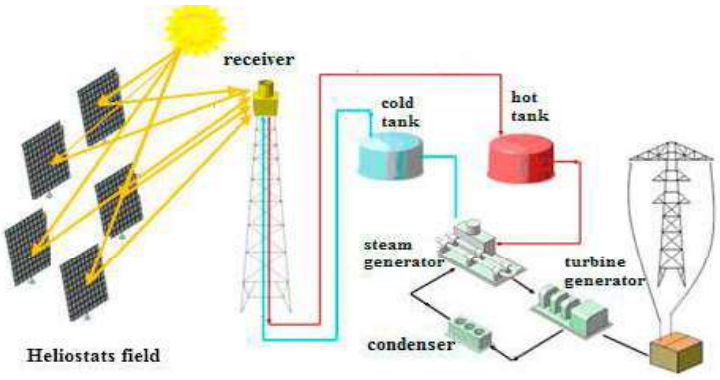

Figure I.14: Diagram of a Central Tower CSP Power Generation System

b. Functioning of Solar Thermal Energy Systems

Solar thermal systems convert solar radiation into heat, used for heating water or air, and for electricity generation in large-scale applications. These systems go through several key stages:

- ✓ **Solar Energy Absorption:** Solar radiation is captured using solar collectors, such as flat-plate collectors or evacuated tube collectors, which convert sunlight into heat.
- ✓ **Heat Transfer**: The generated heat is transferred to a working fluid (commonly water or a special heat-transfer fluid like glycol) circulating through the system.
- ✓ **Heat Storage:** The thermal energy is stored in insulated tanks for later use, especially during nighttime or cloudy conditions.
- ✓ **Final Utilization:** The stored heat is used for domestic water heating, space heating, or to drive steam turbines in large-scale solar thermal power plants for electricity production.

Advantages

- ✓ **Clean and renewable energy:** Does not produce carbon emissions during operation.
- ✓ **High efficiency:** In heating and water heating applications, solar thermal systems are more efficient than photovoltaic systems.
- ✓ **Low operating costs:** Once installed, maintenance and operation costs are relatively low.
- ✓ **Thermal storage capability:** Heat can be stored in tanks for later use, providing greater stability compared to photovoltaic systems.
- ✓ **Long lifespan:** Typically lasts 15–30 years with simple periodic maintenance.

Disadvantages

- ✓ **High initial installation cost:** Can be expensive, especially for residential projects.
- ✓ **Poor performance on cloudy or cold days:** Performance heavily depends on the availability of sunlight.
- ✓ **Requires large space:** Especially in industrial systems or when high energy output is needed.
- ✓ **Difficult to transport:** The generated heat cannot be transferred over long distances, limiting its use to the site of production.
- ✓ **Risk of heat-transfer fluid freezing:** In cold regions, the system may require special protection against freezing.

1.10.1.2. Photovoltaic Systems (PV)

This technology relies on converting sunlight directly into electricity using solar cells. It is characterized by the absence of moving mechanical parts, which reduces maintenance

requirements. This makes it an ideal choice for residential, industrial, and microgrid applications, as illustrated in Figure I.15 It is currently one of the most widespread solar energy technologies, especially with the continuous decline in global solar cell manufacturing costs [35].

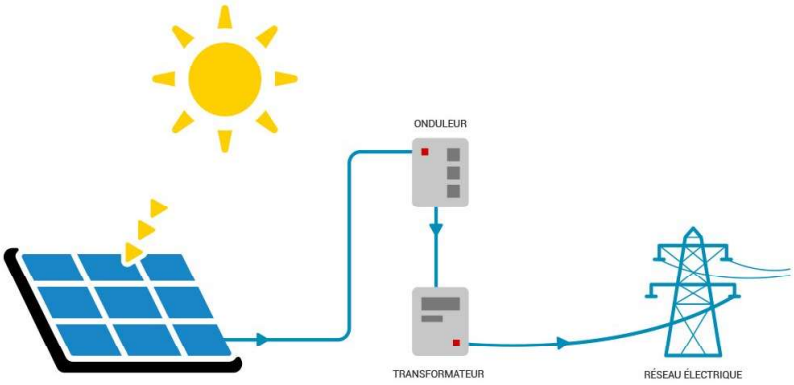

Figure I.15: Photovoltaic Energy Conversion Process

a. Solar Cell and Its Operating Mechanism

A solar cell is a slice of semiconductor material, typically silicon, that is treated to form a PN-type electrical junction. When photons strike the surface of the cell, some of them transfer their energy to electrons in the silicon layer, freeing them from atomic bonds. Due to the electric field at the junction, the electrons move toward one electrode and the holes toward the opposite electrode, generating an electric current as illustrated in Figure I.16 [36]. The performance of the solar cell depends on several factors, including:

- ✓ The type and crystalline structure of the semiconductor material
- ✓ The thickness of the active layer
- ✓ Surface quality and anti-reflective coatings
- ✓ The angle of incidence and the intensity of solar radiation

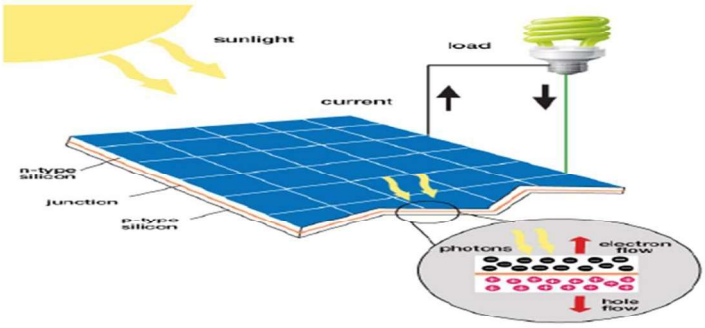

Figure I.16: Photovoltaïque operation

b. Types of Solar Cells

- **Monocrystalline:** These offer the highest efficiency (18–22%) and are typically black in color. They require precise manufacturing processes and have a higher cost, but are ideal when space is limited.

- **Polycrystalline:**These have medium efficiency (15–18%) and a shimmering blue color. They are relatively cheaper and less efficient, making them a popular economical choice.
- **Amorphous Silicon:** Used in portable and small-scale applications, these cells are highly flexible with a low efficiency (6–10%). They perform better under low-light conditions.
- **Thin-Film:** Made from materials like CdTe and CIGS, these cells are lightweight and can be installed on unconventional surfaces. However, they are generally less efficient than traditional silicon cells.

Advantages:

- ✓ **Renewable and Clean Energy Source:** A sustainable energy source that does not produce carbon emissions during operation.
- ✓ **Low Operating Costs:** Relatively low maintenance and operational costs after installation.
- ✓ **Scalability:** Can be installed in various sizes to suit residential, industrial, or commercial needs.
- ✓ **Long Lifespan:** Photovoltaic systems typically last for several decades, often more than 25 years.
- ✓ **Silent Operation:** Operates without generating noise.
- ✓ **Energy Independence:** Reduces dependence on conventional energy sources and power grids.

Disadvantages:

- ✓ **High Initial Cost:** The installation cost is relatively high.
- ✓ **Intermittency:** Electricity production depends on sunlight, making it inconsistent at night or during cloudy days.
- ✓ **Large Area Requirement:** Requires a large surface area to generate significant amounts of electricity, especially for lower-efficiency systems.
- ✓ **Energy Storage Requirement:** Needs storage systems (such as batteries) for nighttime or cloudy-day use, which increases the overall cost.
- ✓ **Efficiency Affected by Weather:** Performance is impacted by weather conditions such as dust, rain, and snow.
- ✓ **Environmental Impact of Manufacturing:** Some manufacturing processes and the disposal of old panels can have environmental consequences.

I.10.2. Wind energy

Wind energy is considered one of the most prominent renewable energy sources, having experienced significant growth in recent years due to its natural abundance, low operational costs, and environmentally friendly nature. This technology relies on harnessing the kinetic

energy of the wind and converting it into usable electrical energy through an integrated system composed of several components that operate in harmony to ensure efficient and stable energy production.

A wind energy conversion system consists of three main interconnected components: the turbine, the transmission system, and the electrical subsystem, which includes the generator, as illustrated in Figure I.17. In the first stage, the wind turbine converts the kinetic energy of the wind into mechanical energy through blades connected to the rotor shaft. In the second stage, the transmission system transfers the mechanical energy from the turbine to the generator while increasing the rotational speed to levels suitable for efficient generator operation. In the final stage, the generator converts the mechanical energy into electrical energy. Power electronics devices are used to regulate and control the characteristics of the electrical output, ensuring compatibility with grid requirements or connected loads [37].

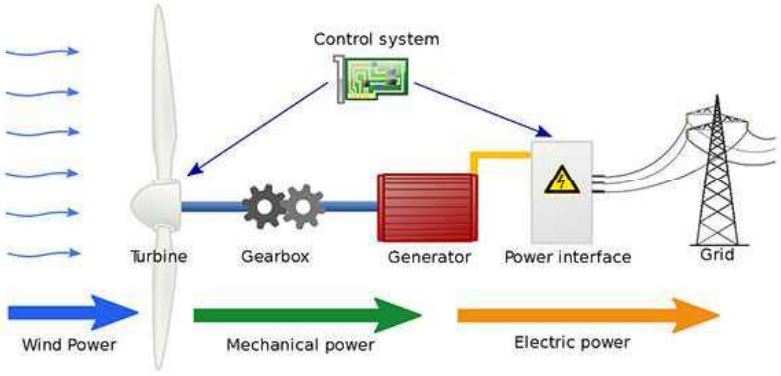

Figure I.17: Principle of the wind energy [36]

In addition to these core components, the system also includes auxiliary elements that do not directly participate in the energy conversion process but are essential for ensuring safe, stable, and reliable operation. These include sensors, control units, and various protection systems.

I.10.2.1. Classification of Wind Turbines

Wind turbines are among the main components in systems that convert wind energy into electrical energy. With technological advancements, various types of turbines have emerged, differing in design and mode of operation. Wind turbines can be classified based on several criteria, the most important of which are the orientation of the rotation axis and the type of electric generator used, as these two factors are key technical determinants of the turbine's performance and its efficiency in power generation. This classification is based on the geometric orientation of the turbine blade rotation axis and is divided into two main types:

I.10.2.1.a. Horizontal Axis Wind Turbines (HAWT)

This type is the most commonly used in commercial applications and represents the traditional design of modern wind turbines. In this configuration, the axis is horizontal and aligned with the direction of the wind, as shown in Figure I.18. These turbines are typically installed at elevated locations to take advantage of strong and steady winds. They are widely used in both onshore and offshore applications due to their high efficiency. However, they also have some drawbacks, such as their heavy weight and noise generation [38].

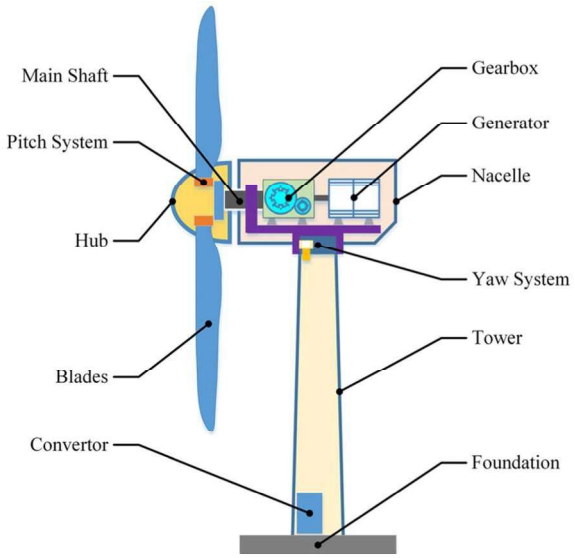

Figure I.18: Horizontal Axis Wind Turbine [36]

I.10.2.1.b. Vertical Axis Wind Turbines

In this type of wind turbine, the axis of rotation is perpendicular to the ground. The blades rotate around the vertical shaft, allowing the turbine to capture wind from any direction without the need for a yaw control system. VAWTs are especially suitable for urban environments or areas with highly variable wind directions. Vertical Axis Wind Turbines are further classified into several main types, including:

- **Darrieus Rotor:**This type of turbine features curved blades shaped like a semicircle or an elliptical arc, resembling an upside down "Ω" or an eggbeater, as shown in Figure I.19. It offers relatively high aerodynamic efficiency; however, it lacks self-starting capability and therefore often requires an external mechanism to initiate rotation [39].

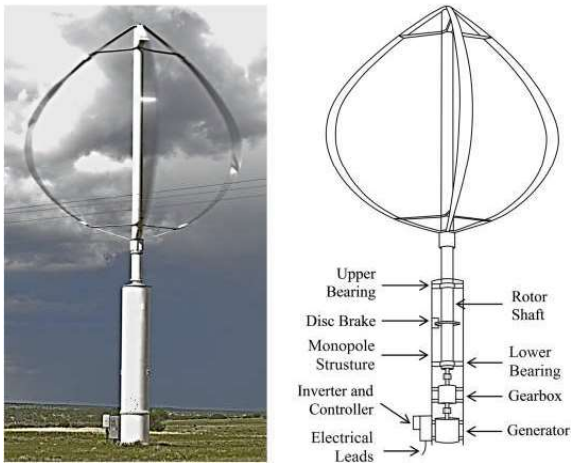

Figure I.19: Darrieus turbine with blades curved in an elliptical arc shape.

- **Helicoidal Rotor (Helical Darrieus Rotor):** This design is an enhancement of the conventional Darrieus rotor, where the blades are shaped in a helical (twisted) form around the vertical axis, as illustrated in Figure I.20 This configuration helps distribute aerodynamic forces more evenly and consistently, which reduces vibrations and improves dynamic stability during operation. The helical rotor also offers higher

efficiency and greater performance stability, particularly under fluctuating wind conditions [39].

Figure I.20. Helical Darrieus Turbine Design for Enhanced Efficiency and Vibration Reduction

- **Rotor (Straight-Bladed Darrieus Rotor):** This type of wind turbine consists of straight vertical blades connected to a central shaft by horizontal supports, forming the shape of the letter "H," as illustrated in Figure I.21. It is characterized by a simple design and ease of manufacturing. Although its aerodynamic efficiency is generally lower than that of curved-blade designs, it is widely used in small to medium-scale applications due to its structural simplicity and ease of maintenance [38][39].

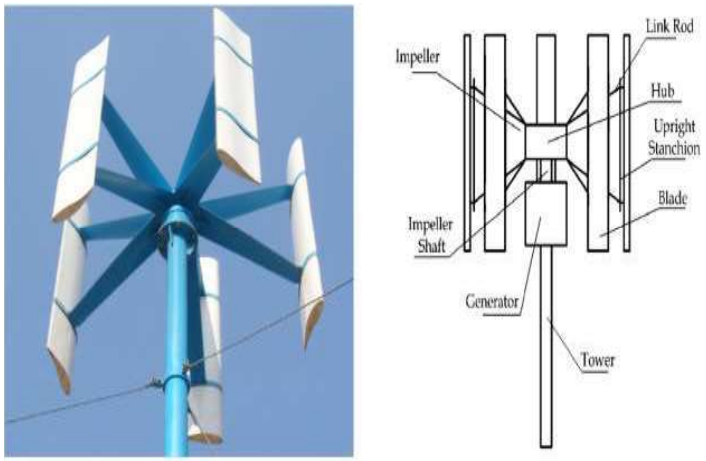

Figure I.21: Straight-Bladed Darrieus Rotor with H-Shaped Configuration

I.10.2.2. General Advantages of VAWT:

- ✓ Do not require a wind direction tracking mechanism.
- ✓ Low startup wind speed.
- ✓ Suitable for urban environments and building integration.
- ✓ Quieter than horizontal axis turbines.

I.10.2.3. General Disadvantages of VAWT:

- ✓ Relatively lower efficiency in large-scale applications.

- ✓ Some types require an auxiliary system to initiate rotation.
- ✓ Less mature and less widely adopted compared to horizontal axis turbines.

I.11. Storage Systems in Microgrids

The microgrid equipped with an Energy Storage System (ESS) is considered a strategic and essential component in the transition toward sustainable smart grids. In light of the global shift towards the use of renewable energy sources such as solar and wind power, challenges related to the intermittency and variability of these sources become increasingly evident. Renewable energy sources are inherently intermittent and time-variable, leading to significant mismatches between production and demand, which places increasing pressure on the stability of the microgrid [28]. On the other hand, electrical load profiles show continuous variations throughout the day, creating gaps between generation and consumption. This imbalance can result in fluctuations in frequency and voltage, which negatively impact the quality and stability of power supply [31]. To address this issue, energy storage systems are employed as intermediaries between generation and consumption. They store the excess energy generated during periods when production exceeds demand and inject it back into the grid during times when demand surpasses generation capacity [38].

Energy storage systems are classified according to several criteria, the most important of which are the form of stored energy and the mechanisms of conversion and storage. These classifications include:

I.11.1. Mechanical Storage Systems

Mechanical storage systems rely on converting excess electrical energy into storable mechanical energy such as kinetic or compressed energy which can later be reconverted into electricity when needed. These systems are characterized by their fast response time and high efficiency during short charge-discharge cycles, making them ideal for applications such as frequency stabilization and grid support during peak demand periods. Generally, these systems are classified into two main types:

I.11.1.1. Flywheel Energy Storage (FES): This system relies on the principle of storing energy in a rotating mass (flywheel) that spins at high speeds inside a vacuum chamber to reduce friction and energy loss. When there is a surplus of electrical energy, it is used to accelerate the rotation of the mass, thereby storing the energy in the form of kinetic energy. When the demand for energy increases, this stored energy is recovered by converting the kinetic energy of the flywheel into electrical energy using a connected generator. Figure I.22 illustrâtes the operating principale of This system [40].

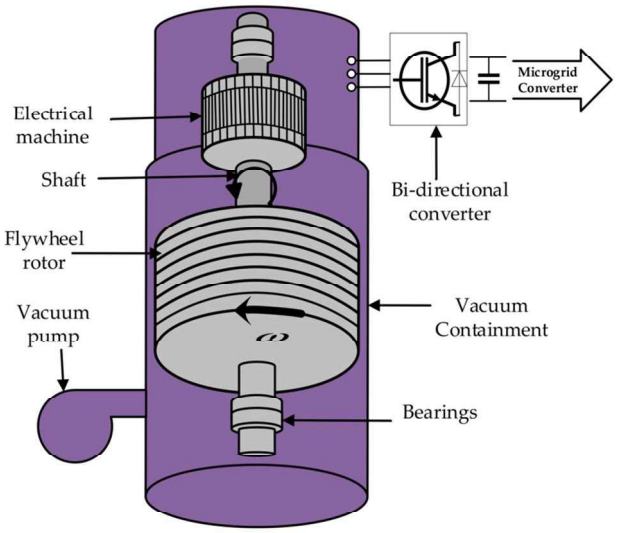

Figure I.22: Operating Principle of a FES System

I..11.1.2. Compressed Air Energy Storage (CAES): This system convert surplus electricity particularly from renewable sources such as wind and solar into mechanical energy by compressing air and storing it in natural underground cavities or industrial high-pressure tanks. When electricity is needed, the compressed air is released, heated using waste heat or auxiliary fuel, and passed through turbines to generate electricity, as illustrated in Figure I.23. This system is characterized by its ability to store large amounts of energy for extended periods, enhancing grid stability [41]. However, its efficiency can be affected by heat losses during the compression and expansion processes. To address this, recent research focuses on developing adiabatic CAES systems that capture and reuse the heat generated during compression, thereby reducing fuel dependency and improving overall system performance [40].

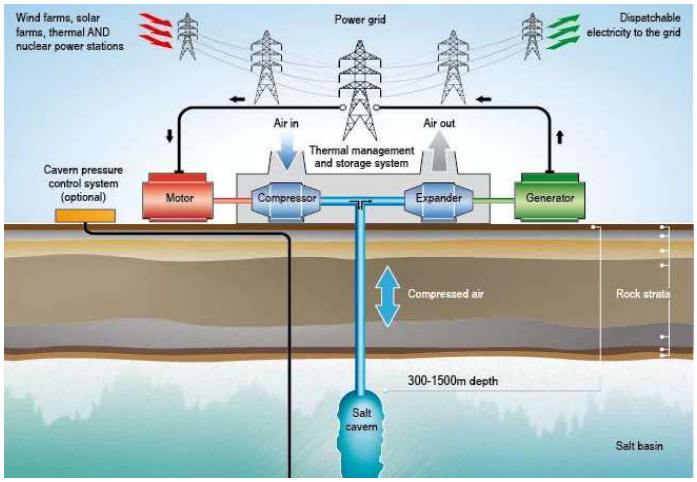

Figure I.23: Schematic Diagram of a CAES System

I.11.2. Electrochemical Storage Systems

Electrochemical storage systems are among the most widely used energy storage technologies worldwide, particularly in the fields of renewable energy, smart grids, and electric vehicles. These systems operate by converting electrical energy into chemical energy through reversible oxidation-reduction (redox) reactions within electrochemical cells, and then

converting it back into electricity when needed. They are classified into several main types, the most notable of which include:

I.11.2.1. Lithium-Ion Battery

Lithium-ion batteries are among the most advanced and widely used electrochemical energy storage technologies today. They are extensively employed in portable electronic devices, electric vehicles, and energy storage systems connected to smart grids. These batteries operate based on the movement of lithium ions between two main electrodes: a positive electrode typically composed of a metal oxide (such as lithium cobalt oxide), and a negative electrode made of graphite. The ions move through a liquid or semi-solid electrolyte during the charge and discharge cycles, as illustrated in Figure I.24 [41].

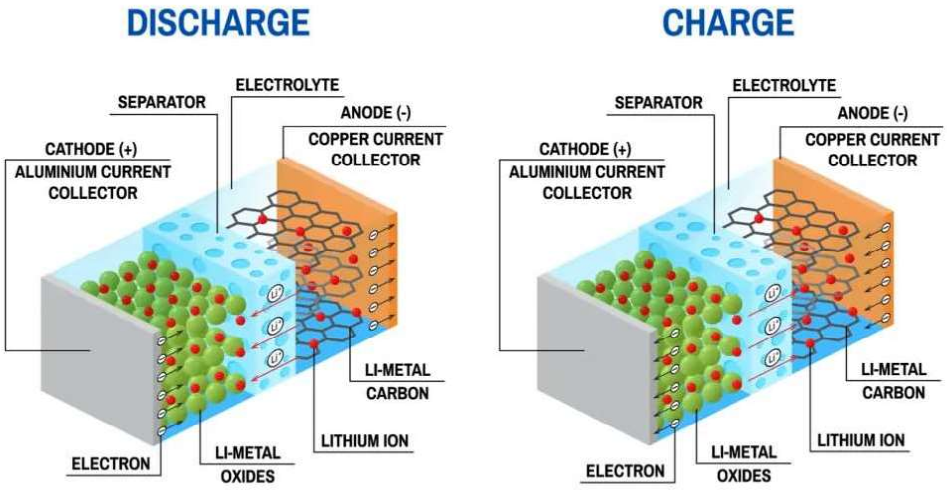

Figure I.24: Operating Mechanism of a Lithium-Ion Battery During Charge and Discharge Cycles

During the charging process, lithium ions migrate from the positive electrode to the negative electrode, where they are stored within the graphite layers, while electrons flow through the external circuit. In the discharging process, the ions return from the negative electrode to the positive electrode, generating an electric current that can be used to power electrical loads [41].

Lithium-ion batteries are known for their high energy density and excellent efficiency, ranging from 90% to 98%, as well as their long service life and lightweight structure, making them an ideal choice for modern applications. However, they require precise thermal management due to their sensitivity to high temperatures, and their cost remains relatively high compared to conventional batteries. Additionally, there are environmental challenges related to material sourcing and recycling. Despite these drawbacks, lithium-ion batteries remain a central focus of ongoing research aimed at developing safer, more efficient, and sustainable solutions, including solid-state battery technologies and advanced battery management systems (BMS) [41].

I.11.2.2. Lead-Acid Batteries

Lead-acid batteries are among the oldest types of rechargeable batteries and remain widely used in various applications, such as conventional vehicles, uninterruptible power

supply (UPS) systems, and certain solar energy systems. Their operation is based on electrochemical reactions between lead and lead dioxide plates immersed in sulfuric acid, as illustrated in Figure I.25 [41].

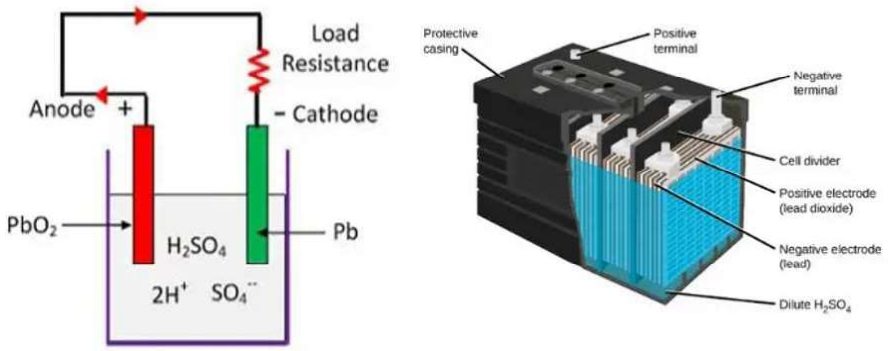

Figure I.25: Electrochemical Operation of a Lead-Acid Battery

Lead-acid batteries are known for their low cost and high current delivery, making them a mature and reliable technology. Despite drawbacks such as low energy density, heavy weight, and the need for periodic maintenance, they remain widely used due to their reliability and availability. They operate through a chemical reaction with sulfuric acid that is reversed during charging and discharging [42].

I.11.2.3. Fuel cell

A fuel cell is an advanced electrochemical device that directly converts chemical energy resulting from the reaction between a fuel, typically hydrogen, and an oxidant such as oxygen into electrical energy without the need for combustion. The cell consists of three main components: the anode, the cathode, and the electrolyte that separates them. When hydrogen enters the anode, it splits into positively charged hydrogen ions and electrons, with the help of a catalyst. The ions pass through the electrolyte toward the cathode, while the electrons are forced to flow through an external electrical circuit, generating an electric current used to power various loads, as illustrated in Figure I.26.[45]

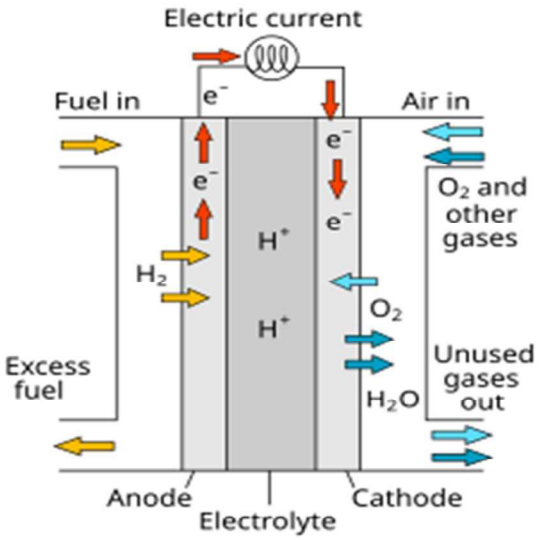

Figure I.26: Basic Operating Principle of a Hydrogen Fuel Cell

Fuel cells are a clean and efficient energy source, producing only water and heat without harmful emissions. They are characterized by high efficiency, silent operation, and quick response, making them suitable for transportation, power generation, and specialized applications such as aerospace. However, their widespread adoption is still limited by high production costs and technical challenges, despite ongoing advancements in the field [45].

I.11.2.4. Supercapacitors

Supercapacitors are energy storage devices known for their exceptionally fast charging and discharging capabilities. They combine higher energy density than conventional capacitors with greater power density than batteries. Their operation is based on storing electrical charge in an electric double layer formed at the surface of the electrodes within an electrolyte, without relying on chemical reactions as in batteries. This enables a remarkably long operational life, reaching up to millions of charge-discharge cycles. The working principle involves the accumulation of electrical charges at the interface between the electrolyte and the electrode surface, forming what is known as the electric double layer. Energy is stored in the form of an electric field between these layers, as illustrated in Figure I.27, allowing for ultra-fast charging and discharging with minimal energy loss. Supercapacitors are classified as high-efficiency storage systems, with efficiencies often exceeding 95% in various applications [44].

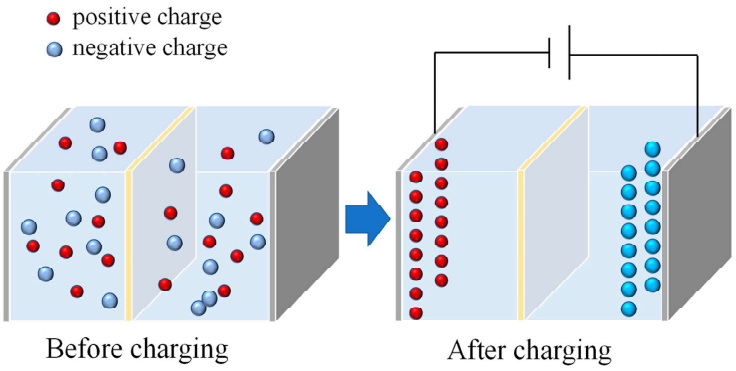

Figure I.27: Operating Principle of Supercapacitors and Formation of the Electric Double Layer

They are used in areas that require an immediate power response, such as voltage stabilization and frequency regulation in power grids, regenerative braking systems in vehicles, and instantaneous power support in industrial and electronic systems. Although their energy density is lower than that of batteries, their rapid response and long cycle life make them an ideal choice for many modern applications particularly when integrated with other storage technologies.

I.12. Adopting Electric Vehicle Batteries as a Main Solution for Energy Storage

In this study, electric vehicle (EV) batteries were selected as a primary and effective solution for storing electrical energy within the microgrid system, due to their dynamic characteristics and high efficiency in charging and discharging processes. This approach represents a modern trend in the field of energy management, as the battery is no longer seen merely as a passive component used to power the vehicle, but rather as an active element that can be integrated into the electrical grid to enhance its flexibility and stability, as illustrated in

Figure I.28. The concept is based on the idea that electric vehicles, when not in use and connected to a smart charging point, can have their stored energy utilized to support the grid during peak demand periods and absorb excess energy during times of high production. In this way, the batteries function as distributed storage units within the network [32][42].

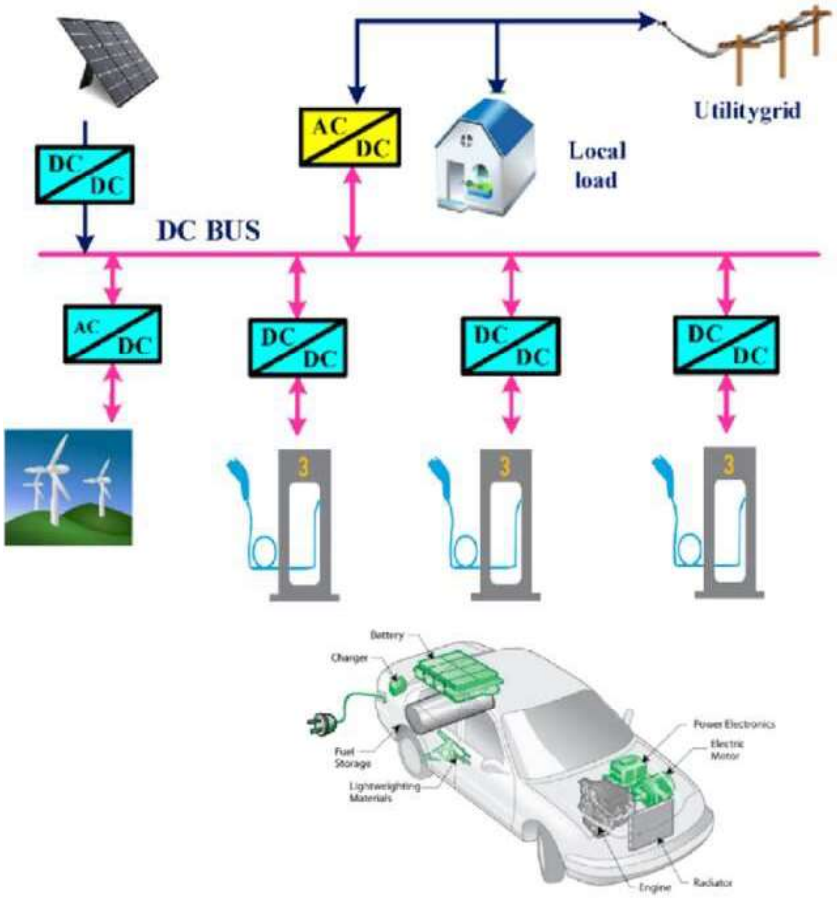

Figure I.28 : Integration of Electric Vehicle Batteries into the Microgrid as Distributed Storage Systems

I.12.1. Types of Electric Vehicles

Modern electric vehicles are divided into several main types, each differing in how it operates and in the extent to which it relies on electric power versus conventional fuel. In what follows, we will discuss the most important of these types: Battery Electric Vehicles (BEVs), Plug-in Hybrid Electric Vehicles (PHEVs), and conventional Hybrid Electric Vehicles (HEVs), highlighting the features and characteristics of each.

I.12.1.1. Battery Electric Vehicles (BEVs)

Battery Electric Vehicles are a type of vehicle powered exclusively by an electric battery, without any components of a gasoline or diesel engine. These vehicles typically support various charging modes, including Fast Charging and Level 2 Charging, and are considered environmentally friendly thanks to producing zero emissions while driving. Figure I.29 illustrates the design of this type of vehicle [46].

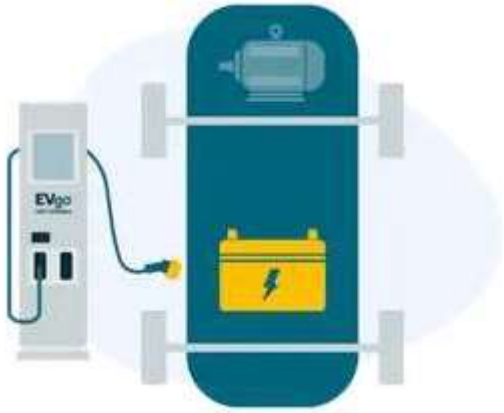

Figure I.29: Structure and Components of a Battery Electric Vehicle (BEV)

I.12.1.2. Plug-in Hybrid Electric Vehicles (PHEVs)

These vehicles combine the advantages of electric and hybrid cars, as they include a larger battery and electric motor compared to conventional hybrids, in addition to an internal combustion engine and a fuel tank. They are also equipped with an external charging port that enables charging using Level 2 Chargers, allowing them to travel a certain distance on electric power alone before switching to fuel use. Figure I.30 shows the components of this type of vehicle [46].

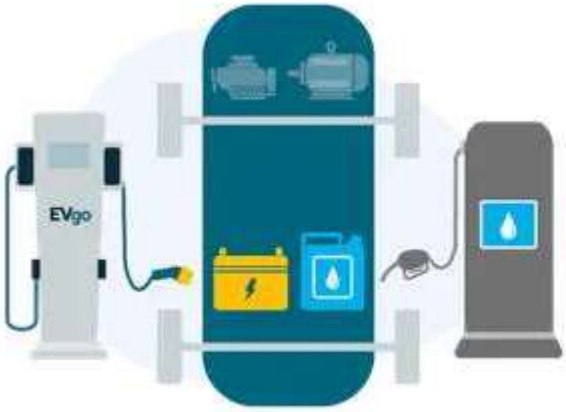

Figure I.30: Structure and Components of a Plug-in Hybrid Electric Vehicle (PHEV)

I.12.1.3. Hybrid Electric Vehicles (HEVs)

These vehicles operate through the integration of an internal combustion engine and a smaller electric motor, where the electric motor is mainly used to support and enhance the performance of the gasoline engine, thereby reducing fuel consumption and emissions. It is worth noting that this type does not have an external charging port and relies entirely on gasoline, without the option to recharge the battery from an external electric source. Figure I.31 displays the basic structure of this type of vehicle [43-46].

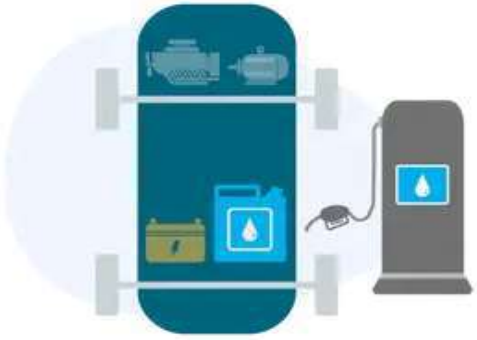

Figure I.31: Structure and Components of a Hybrid Electric Vehicle (HEV)

I.12.2. Reasons for Selecting Electric Vehicle Batteries in This Study

In this study, electric vehicle batteries (EVBs) were selected as a primary solution for electrical energy storage, based on a combination of technical, economic, and practical considerations that support the feasibility of this option in the near future. The world is undergoing a rapid shift toward electric vehicles (EVs), driven by increased environmental awareness, continuous advancements in manufacturing technologies, and the expansion of supportive government policies. This shift has made EVs and consequently their batteries more accessible and affordable for the average consumer. As illustrated in Figure I.32, global EV sales have grown significantly, rising from 0.2 million vehicles in 2013 to 13.8 million in 2023, clearly reflecting the growing interest in sustainable transportation and global efforts to reduce emissions [46]. In light of these trends, this study has adopted the integration of EV batteries into the microgrid system as a realistic and effective energy storage solution that aligns with global environmental objectives and enhances the sustainability and efficiency of the power system.

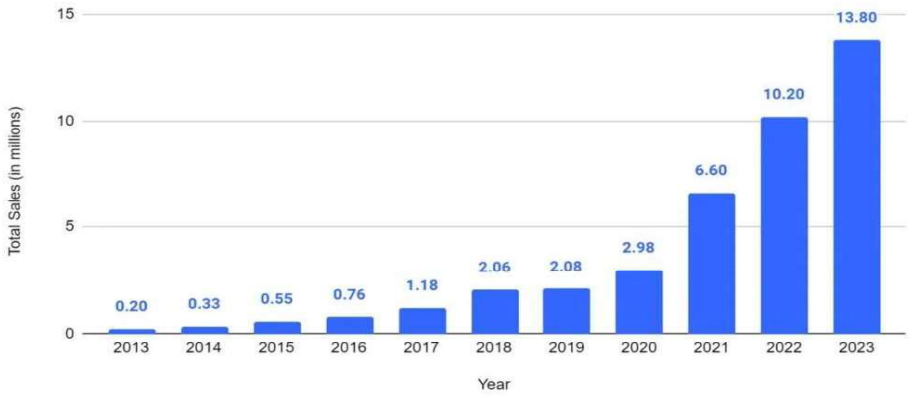

Figure I.32: Global Growth in Electric Car Sales (2013–2023) [46]

This growing availability represents a strategic opportunity to repurpose EV batteries not only for vehicle propulsion but also as energy sources integrated within smart power systems, through the Vehicle-to-Grid (V2G) concept. During long idle periods, whether in residential or institutional parking spaces, the energy stored in these batteries can be partially discharged to support local loads or contribute to grid stabilization [46].

Furthermore, this type of integration not only enhances grid flexibility, but can also significantly contribute to extending the lifespan of the system's stationary battery by

distributing charge and discharge cycles intelligently between mobile and fixed batteries. This distribution reduces the stress on individual batteries and delays their chemical degradation over time. Given that EV batteries are inherently equipped with advanced Battery Management Systems (BMS) and are designed to withstand demanding operating conditions, integrating them into microgrid systems does not require major structural modifications only the development of compatible control and communication interfaces. From this perspective, utilizing EV batteries is not only a proactive and practical solution, but also a sustainable and forward-looking strategy that can redefine the design and operation of future energy systems [32].

I.12.3. Components and Working Principle of Electric Vehicle Batteries

Electric vehicle (EV) batteries typically consist of electrochemical cells integrated into units known as modules, which are then assembled into a complete battery pack. The most widely used type is the lithium-ion (Li-ion) battery, due to its high energy density, low self-discharge rate, and relatively lightweight, making it suitable for mobile applications [42].

The main components of the battery include the positive electrode (usually made of lithium metal oxide), the negative electrode (commonly made of graphite), and an electrolyte that allows lithium ions to move between the electrodes during charging and discharging, as illustrated in Figure 8 related to the lithium battery.

During charging, lithium ions move from the positive electrode to the negative electrode, where they are stored. During discharging, the ions travel in the opposite direction, generating an electric current that can be used to power electrical loads. Within a microgrid system, these processes are managed by an intelligent charge/discharge unit that ensures the battery's efficiency and operational safety. This is monitored by the Battery Management System, which accurately tracks voltage, temperature, and the state of charge (SOC) [42].

I.12.3.1. Advantages of Electric Vehicle Batteries:

Electric vehicle batteries possess several key characteristics that make them highly suitable for energy storage applications, particularly within smart grids and microgrid systems. They offer high charging and discharging efficiency, often exceeding 90%, which enhances their effectiveness in frequent energy cycling. Additionally, they provide rapid response to load fluctuations, a critical feature for maintaining grid stability in the face of sudden changes in demand or supply. Furthermore, their widespread availability driven by the rapid growth of the electric vehicle market ensures that they are accessible in large quantities, facilitating their integration into distributed energy storage infrastructures [42][46].

- **Advantages:**
  - ✓ High energy density.
  - ✓ Dual role (transportation and storage).
  - ✓ Advanced management technologies (BMS).
  - ✓ Good lifespan, reaching 10 years or more.
- **Disadvantages:**
  - ✓ Gradual performance degradation with frequent cycles.

- ✓ High initial investment cost.
- ✓ Need for bidirectional charging stations.
- ✓ Not all users may agree to share their batteries with the grid.

I.12.3.2. Comparison Between Electric Vehicle Batteries and Other Energy Storage Systems

When comparing electric vehicle batteries (EVB) to other types of energy storage systems, it becomes evident that EVBs offer a unique balance of performance, efficiency, and flexibility, particularly in dynamic environments such as microgrids. The table below provides a comparative overview of the most relevant characteristics among different storage technologies:

Table I.1: Comparative Analysis of Electric Vehicle Batteries and Other Energy Storage Technologies

Criterion	ElectricVehicle Batteries (EVB)	Stationary Lithium-Ion Batteries	Lead-Acid Batteries	Supercapacitors	Mechanical Storage
Efficiency	High (>90%)	High (~92%)	Moderate (~70–80%)	Very high (>95%)	Moderate (~70–80%)
Response Speed	Fast	Fast	Moderate	Instantaneous	Relatively slow
Energy Density	High	High	Low	Very low	High (design-dependent)
Lifespan	Good (8–15 years)	Good (10+ years)	Short (3–5 years)	Very long (20+ years)	Very long (30+ years)
Initial Cost	Relatively high	High	Low	High	Very high
Portability	Excellent (mobile, vehicle-based)	Low	Low	Low	Not portable
Environmental Impact	Relatively low	Moderate	High	Low	Low

This comparison demonstrates that electric vehicle batteries provide an effective and flexible energy storage solution, especially suitable for decentralized and smart energy systems. Their dual functionality as both mobile power sources and distributed storage units gives them a distinct advantage over traditional stationary systems. In particular, their ability to integrate seamlessly with Vehicle-to-Grid (V2G) infrastructure makes them ideal for applications where responsiveness, distributed control, and renewable integration are key priorities.

I.13. Major Technical Issues in Microgrid Operation

Microgrid systems are considered among the most advanced solutions for achieving energy sustainability, due to their flexibility to operate either in grid-connected mode or in islanded (standalone) mode. However, integrating these systems into conventional electrical networks poses several technical challenges that may negatively impact operational efficiency and system stability. The main challenges facing microgrid systems can be summarized as follows:

I.13.1. Application of Inverters

Electronic inverters play a pivotal role in microgrids, as they are used to convert the direct current (DC) produced by sources such as solar panels or batteries into alternating current (AC) that can be utilized within the grid. However, this application faces several challenges, especially when operating multiple energy sources simultaneously. Achieving precise synchronization between multiple inverters is difficult and may result in power quality issues, such as waveform distortions and harmonics, as well as voltage or frequency mismatches between sources and loads [47].

I.13.2. Microgrid Protection

Protecting microgrid systems from electrical faults is a major challenge due to the dynamic nature of power flow and changing current direction. In traditional grids, current typically flows in a single, fixed direction, which simplifies protection system design. In contrast, microgrids can experience bidirectional current flow depending on the operating mode whether grid connected or islanded and whether a source is generating or consuming power [48]. This complexity makes traditional protection devices, such as thermal breakers or fuses, inadequate or slow to respond, thereby endangering the system. As a result, adaptive protection systems are adopted, relying on real-time analysis of current, voltage, and phase angle, using smart electronic breakers capable of immediate response to faults. Additionally, intelligent monitoring and time-series data analysis techniques are employed to predict faults before they occur, enhancing the long-term safety and stability of the network [49].

I.13.3. Load Frequency Control

Load frequency control is a fundamental aspect of maintaining stability in microgrid systems, as frequency serves as a direct indicator of the real-time balance between generated and demanded power. In the event of any sudden change in load whether an increase or decrease the system frequency may deviate from its nominal value, potentially leading to operational disturbances, equipment shutdowns, or reduced efficiency [50]. This challenge becomes even more critical in isolated microgrids that are not connected to the main grid, as they lack traditional support sources capable of absorbing such fluctuations. Within the scope of this study, focus will be placed on analyzing the system's frequency behavior under sudden changes in load and generation, with the aim of developing effective solutions to minimize frequency deviation and quickly restore dynamic balance. In addition, the role of energy storage systems and intelligent monitoring will be examined to support frequency stability and enhance the overall reliability of microgrid performance [51].

I.14. Previous Works on Frequency Deviation Control in Microgrid Systems

In recent years, there has been growing interest among researchers in addressing the problem of frequency deviation in isolated microgrid systems, due to its critical role in maintaining system stability and reliability. Various control techniques have been proposed to tackle this issue, each with its own advantages and limitations.

In [52], conventional PID controllers were proposed due to their simplicity and ease of implementation. However, they tend to perform poorly under dynamic conditions and sudden load changes. Fractional-order PID controllers, as shown in [53], offered more accurate and

robust performance, yet they suffer from complex tuning and slower response. Fuzzy logic controllers were used in [54] to improve handling of system nonlinearity and uncertainty, but their design and tuning require significant effort [55]. Type-2 fuzzy logic controllers, such as in [56], enhanced flexibility but introduced higher computational complexity.

On the other hand, some studies such as [57] employed Model Predictive Control (MPC) for its efficiency in dealing with multivariable systems, though its practical implementation demands high computational resources. Sliding Mode Control (SMC), as in [58], provided strong robustness against disturbances but led to high-frequency oscillations. Adaptive neuro-controllers, like the one in [59], showed adaptability to changing dynamics, yet they required extensive training data and significant computational capacity.

Other works, such as [60], explored adaptive control techniques, which allow real-time tuning of controller parameters in response to changing operating conditions. However, they may suffer from stability issues under large disturbances. Optimal control methods [55] and AI-based tuning algorithms such as Genetic Algorithm (GA) [62], Particle Swarm Optimization (PSO) [63], and Swallow Swarm Optimization (SSO) [64] have improved tuning efficiency but faced challenges like slow convergence and sensitivity to initial conditions.

Newer optimization algorithms such as KHA [53], ACO [65], and HSA [66] showed varying levels of effectiveness depending on system characteristics. Additional algorithms like GWO [67], FA [68], Bat Algorithm [69], MFO [70], and CSA [71] have also been tested, though many still require further investigation to validate their practical performance.

In light of the above, this study aims to explore and develop improved control strategies using advanced optimization algorithms, with the goal of enhancing controller performance in isolated microgrids and increasing their efficiency in responding to dynamic operational changes.

I.15. Conclusion

In this chapter, we examined microgrids as an innovative solution to modern energy challenges, exploring their historical development, main components, and various classifications. We also discussed the energy sources used within these systems and their key advantages in promoting environmental sustainability, reliability, and economic efficiency particularly in remote and underserved areas. Additionally, we addressed the major challenges hindering their widespread adoption and reviewed practical applications where microgrids have demonstrated high effectiveness. It is clear that microgrids represent a strategic move toward a more sustainable and flexible energy future.

In the next chapter, we will focus on the modeling and simulation of microgrid systems, presenting the technical and mathematical foundations required to evaluate their performance and enhance their adaptability under varying operational conditions an essential step toward developing smarter and more resilient power networks.

CHAPTER II :

MODELING OF MICROGRID WITH ELECTRIC VEHICLES

II.1. Introduction

This chapter focuses on modeling the main components of the proposed microgrid system, which integrates renewable energy sources such as photovoltaic (PV) panels and wind turbine generators (WTG), along with auxiliary conventional sources like diesel generators and fuel cells. This combination aims to ensure continuous power supply, especially during periods of low renewable energy sources (RES). The proposed system also incorporates an energy storage unit based on electric vehicle batteries, with particular attention given to modeling this vital component due to its key role in energy balancing.

Accurate modeling of each microgrid component forms the foundation for analyzing overall system performance and understanding its behavior under various operating conditions. Given the intermittent and unpredictable nature of renewable energy sources, there is a growing need to develop effective control strategies that enable the system to maintain balance between generation and consumption.

II.2. Microgrid Component Modeling

This figure II.1 illustrates the operating principle of a hybrid microgrid system primarily designed to control frequency deviation caused by sudden fluctuations in power between generation sources and loads. The system integrates renewable energy sources such as photovoltaic panels (with a capacity of 1 MW) and wind turbines (with a capacity of 1.4 MW), as well as mobile storage units like plug-in hybrid electric vehicles (PHEVs), which serve as supporting units to reduce frequency deviation. Additionally, it includes a diesel engine generator (DEG) as a backup source with a capacity of 7.2 MW operating at a lagging power factor [31].

The central controller plays a crucial role in improving overall frequency stability by coordinating the power flows among the various components (ΔP_{PV}, ΔP_{WTR}, ΔP_{DEG}, ΔP_{PHEV}) in response to load changes (ΔP_L) and frequency variations (Δf). This controller makes rapid dynamic decisions to minimize frequency deviation and maintain system reliability by leveraging the flexibility of renewable energy sources, the fast response of hybrid electric vehicles, and the support provided by the diesel generator when necessary [74].

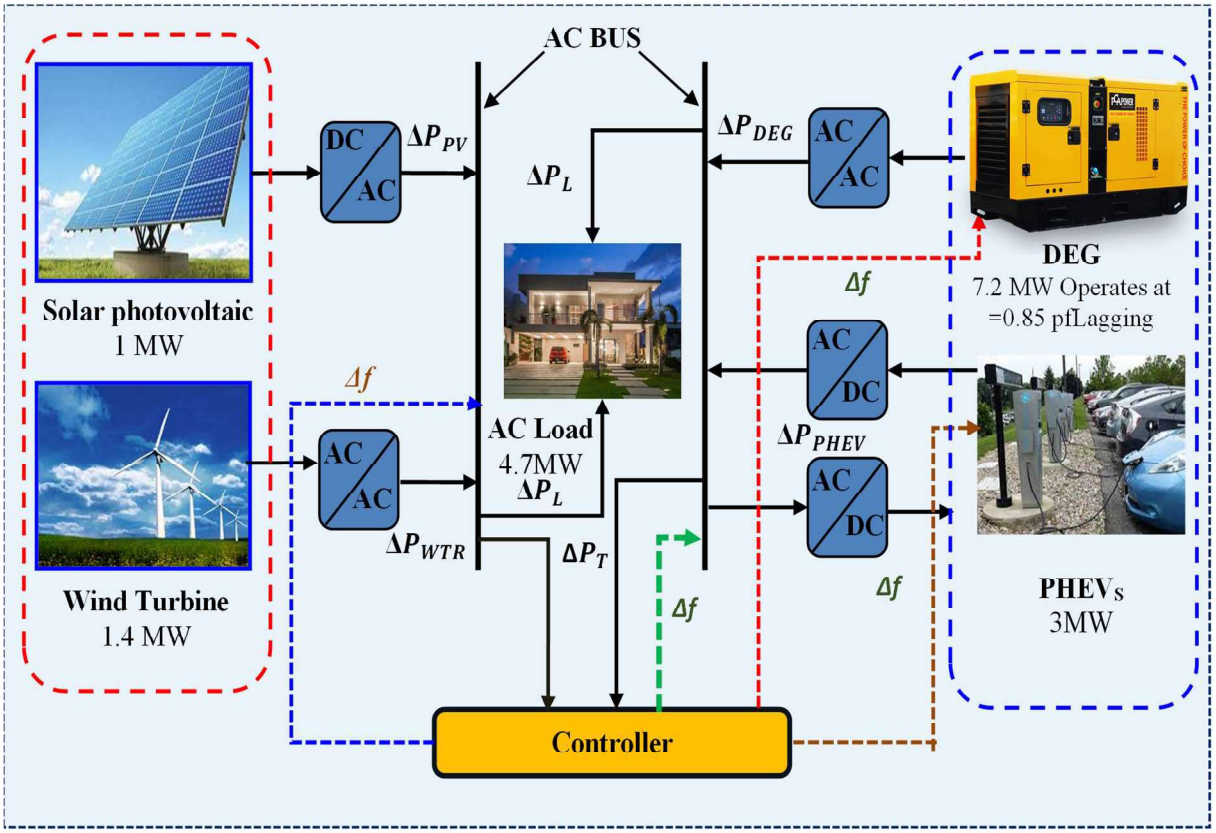

Figure II.1: Overview structure of the MG system.

To understand the system's dynamic variations and select the optimal controller to ensure frequency stability, it is necessary to analyze the system and formulate it into an accurate mathematical model. This model is used to study the system's response to small disturbances and to assess the reliability and stability of the resulting frequency deviations. This analysis starts from the power balance equation (II.1), which expresses the difference between the power demanded by the loads and the power available from generation sources [52].

$$\Delta P = \Delta P_S - \Delta P_S^* \quad \text{(II.1)}$$

$$P_S = P_{PV} + P_{WTG} + P_{DEG} \mp P_{PHEV} \quad \text{(II.2)}$$

Sudden changes in electricity demand (ΔP_L) directly affect the system frequency (Δf) , which necessitates accurate modeling to study this dynamic behavior and to design optimal controllers that ensure frequency stability. To understand the origin of this relationship, we start from the law of conservation of energy and the dynamics of rotation in equation (II.3), which state that any imbalance between the generated and demanded power leads to a change in the kinetic energy stored in the rotating masses of turbines and generators. This kinetic energy is related to the angular speed ω (which is directly linked to the system frequency f) and is expressed by the following relation:

$$E = \frac{1}{2}.J.w^2 \quad \text{(II.3)}$$

Where:

J (J): Moment of inertia.

ω (ω): Angular speed of the generator (directly related to the grid frequency).

When a sudden change in load (ΔP) occurs, it creates an instantaneous imbalance between the generated and consumed power, leading to acceleration or deceleration of the rotating masses and thus causing a change in frequency. This effect can be expressed by stating that the net power entering or leaving the system equals the time rate of change of the stored kinetic energy, according to the relation [36]:

$$\Delta P = \frac{d(E)}{dt} = J.w.\frac{d(w)}{dt} \quad \text{(II.4)}$$

That is, the change in kinetic energy over time equals the net power entering or leaving the system.

The frequency f is directly related to the angular speed ω by the following equation:

$$w = 2.\pi.f \quad \text{(II.5)}$$

Thus:

$$\Delta P = J.w.2.\pi.\frac{df}{dt} \quad \text{(II.6)}$$

In power system engineering, to simplify the dynamic analysis of frequency deviation, the concept of the system's equivalent inertia constant is used, which is defined by the following relation:

$$M = 2.\pi.J.w \quad \text{(II.7)}$$

Using this coefficient, the relationship between the instantaneous change in net power ΔP and the rate of change of frequency (df/dt) can be expressed in the following simplified form:

$$\Delta P = M.\frac{df}{dt} \quad \text{(II.8)}$$

In reality, no mechanical or electrical system can be perfectly ideal; there are always losses arising from various factors such as friction in rotating parts, air resistance, and magnetic and eddy current effects inside generators. These losses are collectively represented by what is known as the damping coefficient D, which indicates the power required to compensate for these losses when a frequency deviation occurs [50].

Consequently, when there is an instantaneous frequency deviation Δf, the power consumed to offset this damping loss is calculated as follows:

$$P_{domping} = \Delta f\ .D \quad \text{(II.9)}$$

Where:

D: Damping coefficient

When a sudden change in power occurs within the electrical power system, part of this power is used to accelerate or decelerate the rotating masses, expressed by the term $M{\cdot}\frac{d(\Delta f)}{dt}$. At the same time, another part is lost due to damping caused by friction and dynamic losses, represented by $D{*}\Delta f$. Consequently, the overall relationship is written as [50-53]:

$$\Delta P = M.\frac{d(\Delta f)}{dt} + D.\Delta f \quad \text{(II.10)}$$

To analyze the dynamic relationship between the change in net power ΔP and the change in frequency Δf in the time domain, the differential equations are often complex and difficult

to solve directly. Therefore, the Laplace transform is used as a powerful mathematical tool that allows us to convert differential equations in the time domain into algebraic equations in the frequency domain (S domain). This step greatly simplifies the process of analysis and controller design, as it enables the study of the system's response and the determination of the transfer function that links the system's inputs and outputs [54].

By applying the Laplace transform to the mathematical model of frequency deviation, we obtain the relationship in the frequency domain:

$$\Delta P(s) = (M.s + D).\Delta f(s) \quad \text{(II.11)}$$

From this, we can derive the transfer function representing the frequency response to power changes:

$$F(s) = \frac{\Delta f(s)}{\Delta P(s)} = \frac{1}{M.s+D} \quad \text{(II.12)}$$

This function shows how changes in the net power affect the system frequency, and it also illustrates the different roles of the inertia and damping coefficients in frequency stability. To further analyze the system's response, we now move on to equation (II.13) the system frequency equation, which explicitly expresses the relationship between frequency and power variations.

$$\Delta f(s) = \frac{1}{M.s+D}\Delta P(s) \quad \text{(II.13)}$$

$$\Delta f(s) = \frac{1}{M.s+D}[\, P_{PV} + P_{WTG} + P_{DEG} \mp P_{PHEV}\,] \quad \text{(II.14)}$$

Based on this, these mathematical models are employed to analyze small-signal behavior and assess the reliability and stability of the system by representing the main microgrid components such as PV, WTG, DEG, and PHEV using first-order transfer functions. This step is essential for developing intelligent control strategies aimed at reducing frequency deviation and ensuring safe and flexible system operation. Accordingly, I will analyze each power source within the microgrid separately to study its dynamic characteristics and its impact on frequency stability.

II.2.1. Photovoltaic systems (PV)

The PV system is an integrated system designed to convert solar radiation energy directly into usable electrical energy, relying on PV cells. This principle is based on converting solar radiation into electricity, a phenomenon discovered by the Becquerel family and presented to the French Academy of Sciences at the end of 1839. The photovoltaic cell is the key element that enables this conversion, as its electrical characteristics resemble those of the photovoltaic power source [32].

Since a single photovoltaic cell typically produces a low voltage, usually not exceeding about 0.6 volts, using it alone does not meet the requirements of practical applications. To overcome this, multiple cells are assembled into a larger unit called a PV module. In these modules, the cells are connected in series and/or parallel and encapsulated within a weather-resistant structure to ensure durability.

For example, a 12V module is usually made up of around 33 or 36 cells connected in series, although the module's open-circuit voltage can exceed this value. There are also modules

containing up to 72 cells connected in series, sometimes known as "42V modules." Some of these modules can be configured in different ways:

- ✓ As a 24-volt module when all 72 cells are connected in series.
- ✓ As a 12-volt module when the cells are divided into two parallel strings, each consisting of 36 cells connected in series.

To obtain higher electrical power, multiple PV modules can be connected in the following ways:

- In series: to increase the voltage.
- In parallel: to increase the electrical current.

Determining the number of modules and how to arrange them is an important step in designing the photovoltaic system to ensure that the required energy needs are met. The complete assembly of these modules is known as a photovoltaic array (PV array), as shown in Figure II.2.

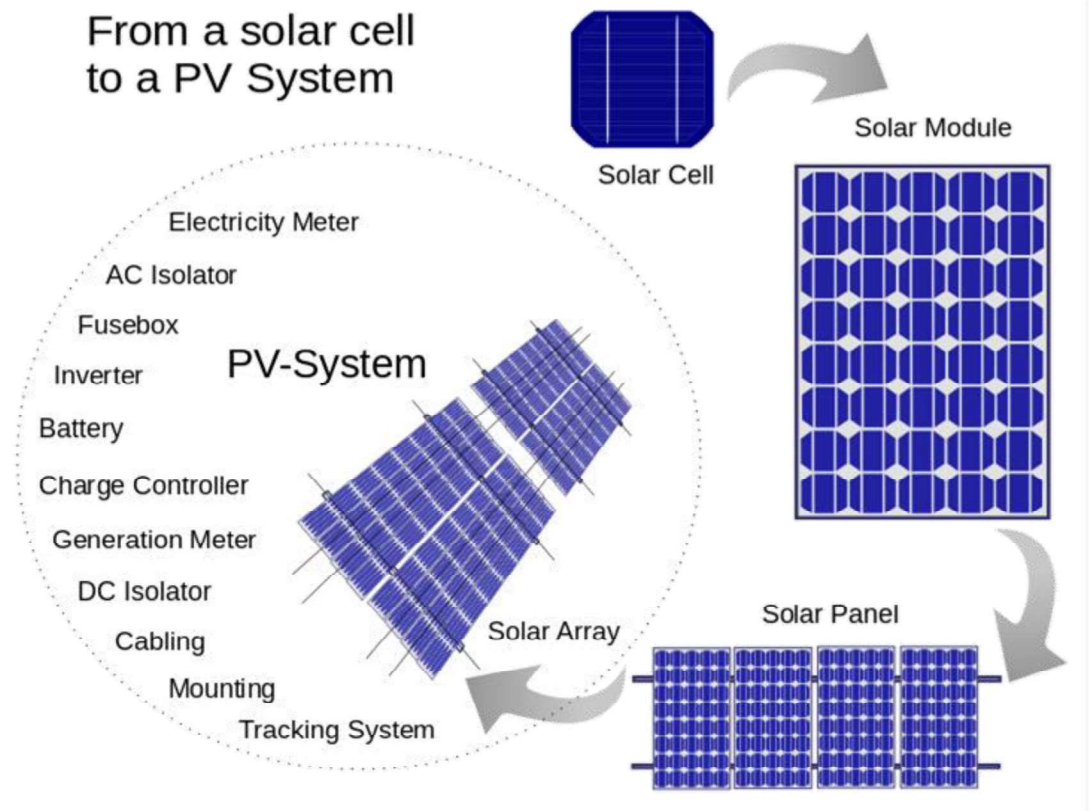

Figure II.2: PV Cell, PV Module, and Array of Modules.

II.2.2.1. Modelling of PV system

PV system can be represented by the well-known electrical equivalent circuit called the single-diode model. It consists of a photocurrent source I_{Ph}, which represents the current generated as a result of photon absorption from solar irradiation; a diode D that models the nonlinear behavior of the P-N junction within the solar cell; a series resistance Rs that accounts for losses in the connections and material; and a parallel resistance Rsh that represents internal leakage currents, as illustrated in Figure II.3 [72].

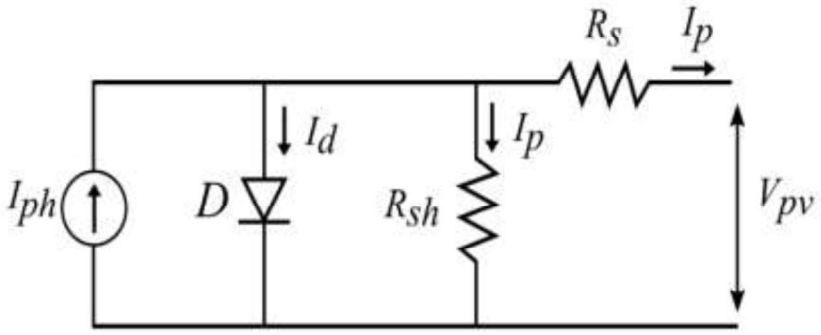

Figure II.3: Model of the PV cell considering voltage and leakage current [72]

Based on Figure II.3, the output current of the solar cell can be expressed by the following equation:

$$I_{sh} + I_D + I_{ph} = I_{pv} \quad \text{(II.15)}$$

Where : I_{Ph}: the current generated by solar irradiation, I_D :the diode current, $I_{sh:}$ is the leakage current through the shunt resistance.

However, when performing dynamic stability analysis, we are often interested only in the small variations around a steady operating point, where the direct effect of changes in solar irradiation is mainly reflected through I_{Ph}. Therefore, in the initial analysis, the effects of I_D and I_{sh} can be neglected to obtain a simplified linear approximation [72-73]

$$I_{ph} = I_{pv} \quad \text{(II.16)}$$

Since the photocurrent I_{Ph} depends quasi-linearly on the solar irradiance I_r, it can be expressed as:

$$I_{ph} = K.I_r \quad \text{(II.17)}$$

Where: K : is a constant that depends on the cell's characteristics and the number of panels.

Since the output power is calculated as the product of voltage and current:

$$P_{PV} = I_{PV}.V_{PV} \quad \text{(II.18)}$$

Therefore, increasing the solar irradiance leads to an increase in the generated current, and consequently, an increase in the output power of the system.

However, the output power of the PV system also depends on the overall system efficiency η_{pv}, which is influenced by several factors. The most important of these are the reference efficiency of the solar cell η_r, the efficiency of the power circuits η_{pc} , and the effect of the cell temperature T_C, which reduces efficiency as the temperature rises. The overall efficiency is given by the following relation:

$$\eta_{pv} = \eta_r.\eta_{pc}\big(1 - \beta(T_c - NOTC)\big) \quad \text{(II.19)}$$

Where: β: is the temperature coefficient representing the efficiency drop due to temperature increase, NOCT: is the nominal operating cell temperature.

The temperature of the solar cell itself depends on the ambient temperature T_a as well as the solar irradiance, and it can be estimated using the following empirical relation:

$$T_C = 30 + 0.017(I_r - 300) + 1.14(T_a - 25) \quad \text{(II.20)}$$

This equation II.20 clearly shows that an increase in solar irradiance I r leads to a rise in the cell temperature Tc, which also depends on the ambient temperature Ta. This rise in temperature results in a reduction of the overall efficiency of the photovoltaic cell, thereby decreasing the output power of the system. To validate these results experimentally, we conducted a test using a solar panel model of type SP75 from SIEMENS company, where the model was developed and simulated using ORCAD [73].

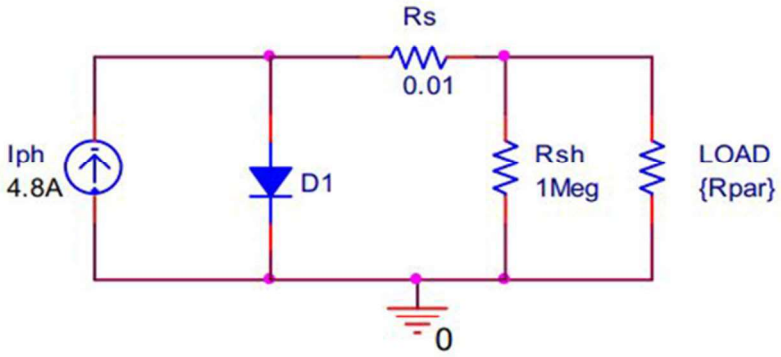

Figure II.4: PV cell model in Orcad

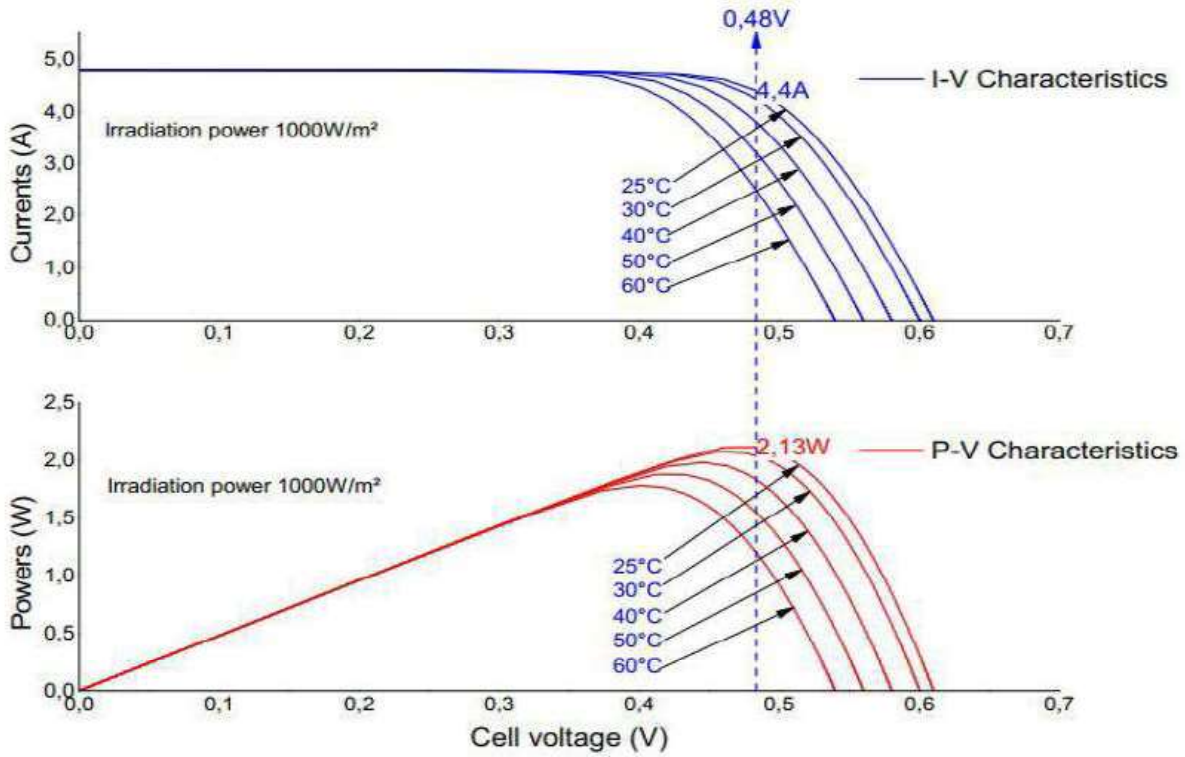

Figures II.5: I-V and P-V Characteristics of the Cell under 1000 W/m² and Variable Temperature

The impact of this temperature rise is clearly observed in the curves presented in Figures II.5 In the current–voltage (I–V) curves, increasing temperature leads to a decrease in the voltage at the maximum power point, while the current remains almost constant. In the power–voltage (P–V) curves, this voltage drop results in a noticeable reduction in the maximum available power of the system.

After combining these factors, the output power can be expressed in a simplified form:

$$P_{pv} = \eta_{pv}.A_{pv}.I_r(t) \quad \text{(II.21)}$$

Where : A_{PV} : the total area of the PV panels.

When the ambient temperature is fixed (or its effect is compensated in advance), the relationship simplifies to:

$$P_{pv} = \eta.A_{pv}.I_r(t) \quad \text{(II.22)}$$

Here, η is considered approximately constant, representing the overall efficiency after accounting for the effect of temperature.

To study the response of the PV system to small fluctuations or disturbances in environmental variables, such as solar irradiance or temperature, we use what is known as small-signal analysis. This method is based on assuming the existence of a fixed operating point, which represents the steady-state condition of the system under specific input values, such as the solar irradiance I_{r0} and the cell temperature T_{c0}[73].

When small disturbances occur around this point, the variables can be represented as follows:

$$I_r = I_{r0} + \Delta I_r \quad \text{(II.23)}$$

$$P_{pv} = P_{pv0} + \Delta P_{pv} \quad \text{(II.24)}$$

where: I_{r0}: the value of solar irradiance at the steady operating point. ΔI_r: the small increase or decrease in irradiance around that point. P_{PV0}: the power produced at the steady operating point.

ΔP_{PV}: the small change in the output power resulting from these disturbances.

The advantage of this analysis is that it transforms the nonlinear system (due to the nonlinear relationships between power, irradiation, and temperature) into a simplified linear model that can be easily studied using linear analysis tools.

This allows us to understand the system's behavior under the influence of rapid or small-scale fluctuations, such as the passing of a light cloud or a slight change in temperature, without the need to solve the full nonlinear model again.

By substituting into power equation (II.22):

$$\Delta P_{pv} = \eta.A_{pv}.\Delta I_r(t) \quad \text{(II.25)}$$

And we define the static gain of the system:

$$K_{pv} = \eta.A_{pv} \quad \text{(II.26)}$$

So it becomes

$$\Delta P_{pv} = K_{pv}.\Delta I_r(t) \quad \text{(II.27)}$$

In reality, the output power of a PV system does not respond instantaneously to sudden changes in solar irradiance. This delay is due to the presence of dynamic elements in the system, such as the response time of Maximum Power Point Tracking (MPPT) algorithms, as well as the effects of DC/DC and DC/AC converters and storage components (e.g., capacitors) within the circuits. To represent this dynamic behavior, the PV system can be modeled as a first-order system characterized by a time constant T_{PV}, which reflects the system's response speed. This model is expressed by the following equation [50-63]:

$$K_{pv}.\Delta I_r(t) = \Delta P_{pv}(t) + T_{PV}.\frac{d\Delta P_{pv}}{dt} \quad \text{(II.28)}$$

Taking the Laplace transform:

$$K_{pv}.\Delta I_r(S) = \Delta P_{pv}(S)(1 + T_{PV}) \quad \text{(II.29)}$$

We obtain the transfer function:

$$G_{pv} = \frac{\Delta P_{pv}(S)}{\Delta I_r(S)} = \frac{K_{pv}}{T_{PV}\,S + 1} \quad \text{(II.30)}$$

II.2.2. Wind Turbine Generator (WTG)

A Wind WTG system fundamentally relies on converting the kinetic energy of the wind into mechanical energy that rotates the turbine shaft, which is then converted into electrical energy using an electric generator (usually an induction generator or a synchronous generator). The wind turbine itself is the main component of the system, and its power output has a nonlinear relationship with wind speeds [36].

For the sake of this research, the wind turbine system considered here is a single wind turbine with variable speed and variable pitch control, featuring a horizontal axis and lift-type blades as illustrated in Figure II.6.

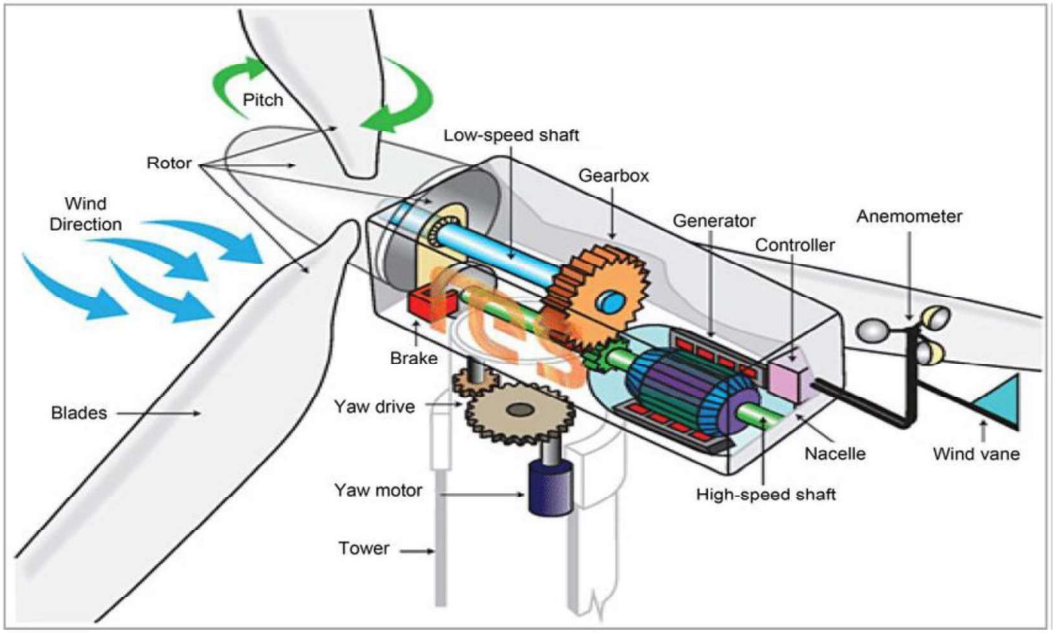

Figure II.6: Components of a Wind Turbine System [51]

II.2.2.1. Modelling of WTG system

The drivetrain consists of a Permanent Magnet Synchronous Generator (PMSG). The generated electrical power is delivered to the Point of Common Coupling (PCC) via a back-to-back converter and filtering system. The voltage source inverter (VSI) operates in grid-feeding mode, assuming a balanced and symmetrical grid, as illustrated in Fig. II.7 [36–38].

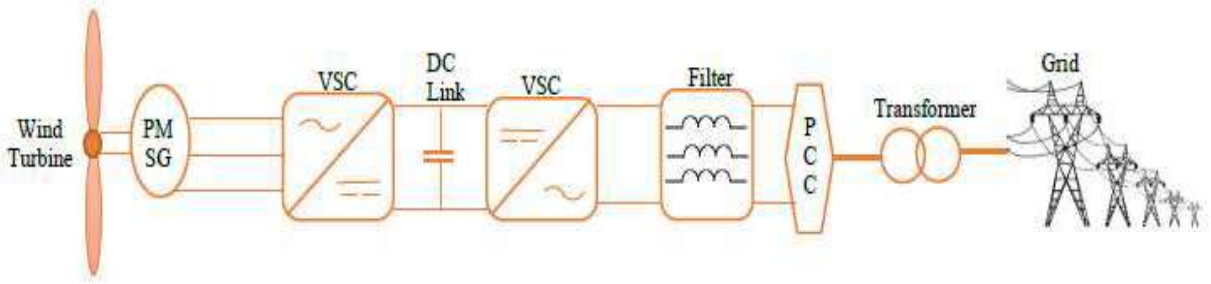

Figure II.7: A Typical Wind Energy Conversion System

With this integrated design, the wind turbine system can effectively convert variable wind energy into electrical power, suitable for either grid-connected applications or standalone systems [36].

The kinetic power of the wind passing through the turbine's swept area is calculated using the equation:

$$P_{WTG} = \frac{1}{2}.\rho.A.V_W^3 \quad \text{(II.31}$$

Where

ρ: air density.

A: swept area = πR².

This equation clearly shows that the power extracted from the wind depends heavily on wind speed (since it is proportional to the cube of the speed), as well as on air density and the effective area of the turbine.

However, in practice, the wind turbine cannot convert all the available kinetic energy of the wind into mechanical energy due to physical and technical limitations. From a physical perspective, it is impossible to completely stop the airflow behind the turbine, as the wind must continue moving to maintain its flow, which naturally leads to a loss of part of the energy. Technically, there are design constraints such as the shape of the blades, their pitch angle, as well as friction losses in the shaft and the overall efficiency of the mechanical components. To account for these factors, the power coefficient Cp is defined, which represents the fraction of the wind's kinetic energy that can be effectively captured by the turbine. Thus, the mechanical power output of the turbine is given by the following equation [52]:

$$P_t = P_{WTG}.C_P(\lambda,\beta) \quad \text{(II.32)}$$

Where,

Cp: Coefficient of power defined by the Betz limit.

P_t: the extracted mechanical power.

The coefficient Cp is defined as a factor that determines the maximum fraction of wind energy that can be converted into mechanical energy, according to Betz's law (Betz limit), which theoretically states that the maximum possible value is around 0.59.

However, in practice, the power coefficient Cp is not constant; rather, it depends on several operational variables, the most important of which are:

– The angular velocity of the shaft ω

– The pitch angle of the blade β

– The tip speed ratio λ which is defined as follows:$\lambda = \frac{R_w}{V_w}$

It is often represented using empirical functions to approximate the actual relationship based on manufacturer data or experiments. For example, in this model we use the following equation [31]:

$$C_P = C_1 \left[\frac{C_2}{\lambda_i} - C_3.\beta - C_4\right] e^{-\frac{C_5}{\lambda_i}} + C_6.\lambda \quad \text{(II.33)}$$

Where: C_1,C_2,C_3,C_4,C_5,C_6 : constants > 0

for the sake of this research, Cp is established as follows [55]:

C_1= 0.0068, C_2=116, C_3= 0.4, C_4 = 5, C_5=21 and C_6= 0.0068

$$\frac{1}{\lambda_i} = \frac{1}{\lambda + 0.008\beta} - \frac{0.035}{\beta^3 + 1} \quad \text{(II.34)}$$

After obtaining the mechanical power extracted from the wind P_{WTG} by the turbine, this power is converted into usable electrical power through a series of electromechanical components. The generator directly converts the mechanical power into electrical power. Subsequently, power converters, such as DC/AC inverters, are employed to regulate the voltage and frequency in accordance with grid or system requirements [53].

The electrical power output from this process is influenced by the overall efficiency of the system, which is calculated as the product of the efficiencies of these three main components:

$$\eta_{WTG} = \eta_{generator} . \eta_{converter} \quad \text{(II.35)}$$

where:

$\eta_{generator}$: the efficiency of the generator, which is affected by its design and power losses in windings and magnets.

$\eta_{converter}$: the efficiency of the power converters, which depends on the conversion technology and its advancement.

Therefore, the actual electrical power obtained at the output of the system can be calculated as:

$$P_{WTG} = P_t . \eta_{WTG} \quad \text{(II.36)}$$

This relationship directly highlights the importance of improving efficiency at every stage of the energy conversion process to increase the amount of electrical power generated from the same amount of mechanical power extracted from the wind.

To study frequency stability in a wind energy system, it is important to understand the effect of small variations in wind speed on the electrical power output of the turbine. Assuming that the instantaneous wind speed V_w deviates slightly around a steady operating point V_{w0}, we can express it as [31]:

$$V_w = V_{w0} + \Delta V_W \quad \text{(II.37)}$$

Similarly, the electrical power output P_{WTG} will also deviate around its nominal value P_{WTG0}

$$P_{WTG} = P_{WTG0} + \Delta P_{WTG} \quad \text{(II.38)}$$

Since the electrical power output of a wind turbine system mainly depends on the cube of the wind speed V_w^3, we can study the effect of small variations in wind speed on the output power by calculating the partial derivative of this relationship. At a steady operating point V_{w0} where the nominal output power is P_{WTG0}, the derivative is given by [54]:

$$\frac{dP_{WTG}}{dV_w} = 3.V_w^3\left(\frac{1}{2}.\eta.C_p.A.\rho\right) \quad \text{(II.39)}$$

We calculate the value of this derivative at the rated wind speed.

$$\frac{P_{WTG}}{V_{w0}} = 3.V_{w0}^3\left(\frac{1}{2}.\eta.C_p.A.\rho\right) \quad \text{(II.39)}$$

But note that the rated power P_{WTG0} is also calculated at the same V_{w0}

$$P_{WT} = 3.V_{w0}^3\left(\frac{1}{2}.\eta.C_p.A.\rho\right) \quad \text{(II.40)}$$

Dividing P_{WTG0} by V_{w0} gives

$$\frac{P_{WTG0}}{V_{w0}} = 3.V_{w0}^2\left(\frac{1}{2}.\eta.C_p.A.\rho\right) \quad \text{(II.50)}$$

$$\frac{\Delta P_{WTG}}{\Delta V_w} = 3.\frac{P_{WTG0}}{V_{w0}} \quad \text{(II.51)}$$

$$\Delta P_{WTG} = 3.\frac{P_{WTG0}}{V_{w0}}.\Delta V_w \quad \text{(II.52)}$$

Accordingly, we define the static gain of the system:

$$K_{WTG} = 3.\frac{P_{WTG0}}{V_{w0}} \quad \text{(II.53)}$$

Therefore :

$$\Delta P_{WTG} = K_{WTG}.\Delta V_w \quad \text{(II.54)}$$

Due to the inherent physical characteristics of WTG, the output power does not respond instantaneously to sudden variations in wind speed. This behavior is primarily attributed to the mechanical rotating components, such as the blades and rotor, which possess mass and rotational inertia. This inertia enables the storage of kinetic energy, thereby smoothing rapid fluctuations and preventing the output power from tracking every minor variation in wind

speed. While this enhances system stability, it also introduces a delay in the power response [50].

Additionally, wind turbine systems typically include control mechanisms such as pitch control systems and speed control systems. These systems require time to process signals, make decisions, and actuate mechanical components, which further slows down the system's response to variations in wind speed [51].

To accurately represent this dynamic behavior, a simplified first-order linear model (first-order transfer function) is often used. This model can be expressed by the following differential equation:

$$K_{WTG}.\Delta V_w = T_{WTG}.\frac{d(\Delta P_{WTG})}{dt} + \Delta P_{WTG} \quad \text{(II.56)}$$

where:

T_{WTG}: the time constant, representing how quickly the system reacts to changes.

K_{WTG}: the static gain, which defines the steady-state relationship between wind speed variations and output power changes.

ΔV_w: the instantaneous change in wind speed.

ΔP_{WTG}: the resulting change in the turbine's output power.

This model helps us better understand and predict how the system responds when wind speed fluctuates. It is also used in design and analysis processes to ensure the turbine operates within safe and desired performance limits.

To represent the dynamic behavior of the wind turbine power output, we use the frequency domain through the Laplace transform. This representation captures the effect of inertia and the delay in the system's response to changes in wind speed. As a result, we obtain a first-order transfer function expressed as:

$$G_{WTG} = \frac{\Delta P_{WTG}(S)}{\Delta V_w(S)} = \frac{K_{WTG}}{T_{WTG}\ S+1} \quad \text{(II.57)}$$

II.2.3. Plug-in Hybrid Electric Vehicles (PHEV)

Figure II.8 shows the shape of the PHEV, which is considered an active and flexible component in the architecture of modern microgrid systems. It performs two main and complementary functions. The first function is acting as electrical loads when their batteries are charged from the grid. The second, and more important function in the context of system stability, is the ability of these vehicles to act as power sources when needed; they can feed the energy stored in their batteries back into the grid, helping to compensate for sudden drops in the production of renewable energy sources such as wind and solar power [32].

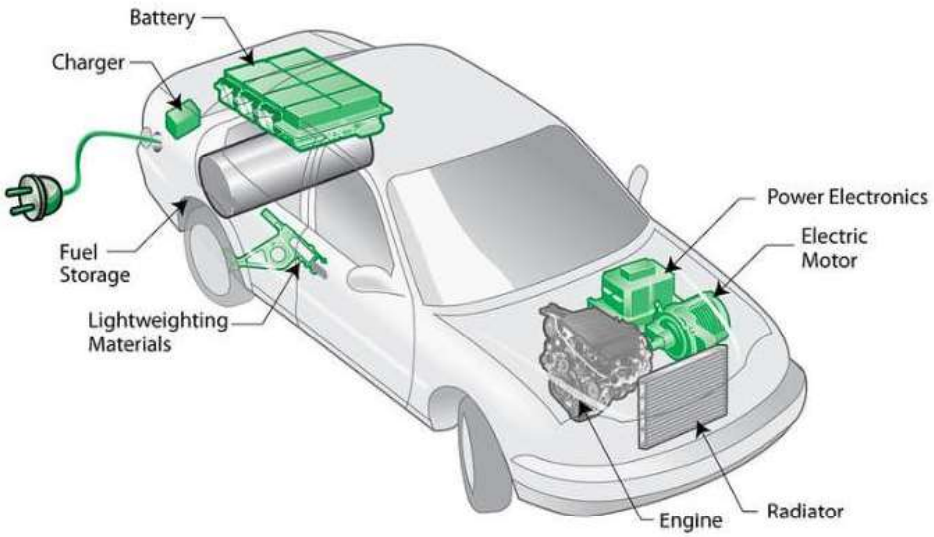

Figure II.8: Structure of Plug-in Hybrid Electric Vehicles (PHEVs) in modern MG

II.2.3.1. Modelling of PHEV System

The response of PHEV vehicles is controlled by the frequency deviation signal in the grid (Δf). When there is a drop in frequency (Δf < 0), this indicates a shortage in generation capacity, so the vehicles discharge part of the energy stored in their batteries to support the grid. Conversely, if there is an increase in frequency (Δf > 0) due to excess generation, the vehicles start charging to absorb this surplus and help restore the frequency to its nominal value. This response is mathematically represented by a control output signal K_{EV}, which is directly related to the frequency deviation [74]:

$$K_{EV} = K_{EV\,max}.\Delta f \tag{II.58}$$

where:

$K_{EV\max}$: the maximum value that the participation factor can reach, determined during the design phase based on the battery's characteristics.

Δf : the frequency deviation from the nominal value.

After determining the value of the participation factor K_{EV} , which represents the level of contribution of PHEVs to grid stability, as well as defining the droop characteristic that is used to reduce the system's excessive sensitivity to frequency deviations, the central controller calculates and generates the control signal ΔU_C according to the following relation [54]:

$$\Delta U_C = K_{EV} - Y.\Delta f \tag{II.59}$$

Where: K_{EV}: Represents the required response or the maximum participation capacity that can be provided by the electric vehicles.

$\Delta f \cdot Y$: Represents the effect of the droop characteristic applied to reduce the sudden change in the system's response due to the frequency deviation Δf, through the droop constant Y.

$$Y = \frac{K_{EV}}{R_{av}} \tag{II.60}$$

Rav: reflects the flexibility of the system's response.

When a frequency deviation Δf from the nominal value occurs, PHEV vehicles are used to support the grid by charging or discharging their batteries. The output power from a single vehicle, ΔP_{PHEV}, depends linearly on the frequency deviation, while taking into account the physical constraint represented by the maximum power limit Pmax, according to the following equation.

$$\Delta P_{PHEV} = \begin{cases} -\Delta P_{MAX}, U_C < -\Delta P_{MAX} \\ -\Delta P_{MAX}, U_C > -\Delta P_{MAX} \\ U_C, |U_C| \leq \Delta P_{MAX} \end{cases} \quad \text{(II.61)}$$

Here appears the participation gain $K_{EV,i}$ for vehicle i, which is not constant but depends on the battery's state of charge (SOC), as illustrated in Fig. II.9. Within the ideal SOC range between SOCa and SOCb, the gain remains at 1 ($K_{EV,i}$ =1), ensuring full participation in supporting the grid, while it gradually decreases outside this range until it reaches zero at SOCa or SOCc. This adaptive strategy, shown in Figuer. II.9, ensures that the vehicle neither charges nor discharges in a way that could harm the battery or reduce its lifespan [54].

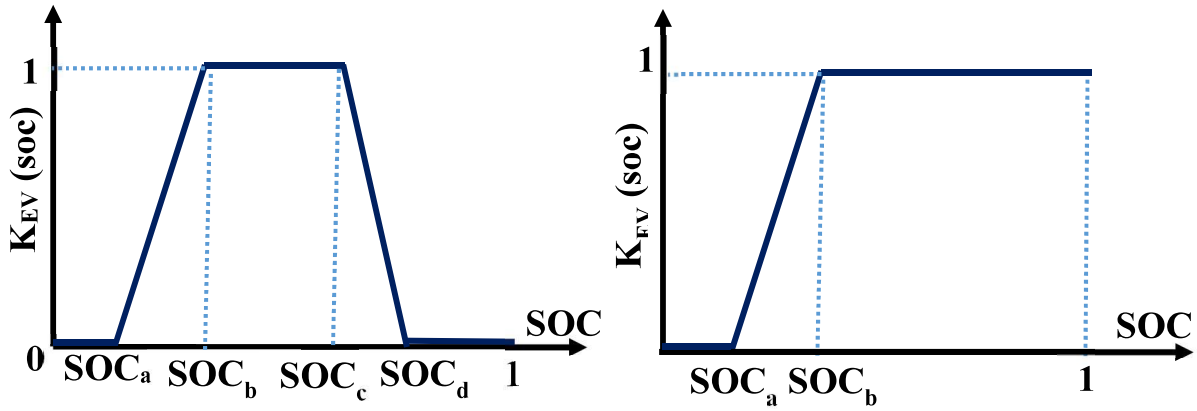

Figure II.9: Representing the charging and discharging EV

When a deviation in the grid frequency occurs, PHEVs collectively contribute to supporting grid stability by charging or discharging their batteries. To calculate the total power output from all participating vehicles, the following equation is used:

$$\Delta P_{PHEV} = N_{EV} * \Delta P_{PHEV\,i} \quad \text{(II.62)}$$

Where: N_{EV}: represents the number of vehicles participating in the support process:

Electric vehicle batteries, specifically PHEVs, cannot respond instantaneously to sudden changes in grid frequency due to their internal physical and electrical limitations. Among these are the internal resistance of the battery, the current inertia presents in the associated electronic circuits, and the constraints of the control and management systems that process the charge and discharge commands. To accurately represent these dynamic behaviors, the model incorporates what is known as the battery time constant T_{EV}. This parameter describes the approximate time required for the battery to reach its target output power following a change in the control signal [31-54].

This leads to a first-order differential equation that describes the evolution of the output power from the fleet of PHEVs over time:

$$N_{EV}.(\Delta U_C - \Delta f.Y) = T_{EV}\frac{d(\Delta P_{PHEV})}{dt} + \Delta P_{PHEV} \quad \text{(II.63)}$$

where:

ΔP_{PHEV}: the change in output power provided to support the grid.

N_{EV}: the number of participating vehicles.

ΔU_C: the centralized control signal generated by the controller.

Δf: the deviation of the frequency from its nominal value.

Y: the droop coefficient that smooths the system's response.

This equation shows that the output power does not immediately follow changes in the control signal. Instead, it gradually evolves over time according to the time constant T_{EV} . In other words, when a sudden change occurs in the control signal or frequency, the battery's response is not instantaneous; it ramps up progressively until it reaches the new target value.

By including this dynamic model, the system reflects real-world behavior more accurately, which helps in designing a more effective control system that accounts for the battery's physical limitations and ultimately improves the stability of the electrical grid.

To analyze stability in the frequency domain, we apply the Laplace transform to Equation II.63.

$$\big(Y.\Delta f(S) - \Delta U_C(S)\big).N_{EV} = \Delta P_{PHEV}.(1 + T_{EV}) \quad \text{(II.64)}$$

Thus, we obtain the transfer function:

$$G_{PHEV} = \frac{N_{EV}.(\Delta U_C(S) - \Delta f(S).Y)}{S.T_{EV}+1} \quad \text{(II.65)}$$

II.2.4. Diesel Energy Generator (DEG)

The DEG is one of the essential conventional components in a microgrid system, especially in cases where there is a shortage in power generated from renewable energy sources such as wind and solar. The diesel generator is characterized as a dispatchable power source, making it suitable for maintaining grid stability. However, it is subject to physical limitations such as response delay and mechanical control system characteristics. Moreover, the diesel engine is considered a reliable backup option once the energy from renewable sources is depleted and the electric vehicle batteries are discharged, as it can be relied upon to supply the minimum required power for system continuity [50].

A DEG consists of a diesel engine and an electric generator. It works by converting the chemical energy stored in diesel fuel into usable electrical energy. The engine transforms diesel fuel into mechanical energy by rotating the crankshaft as a result of fuel combustion in the cylinders. This mechanical energy is then used to drive the alternator, which converts the mechanical power into electrical energy through magnetic induction. An Automatic Voltage Regulator (AVR) ensures stable output voltage levels. Additionally, the diesel generator includes other components such as mechanical couplings, speed regulators, a supporting chassis, a startup battery, a fuel tank, and a control panel. Figure II.10 illustrates a simplified block diagram of the diesel generator [54-63].

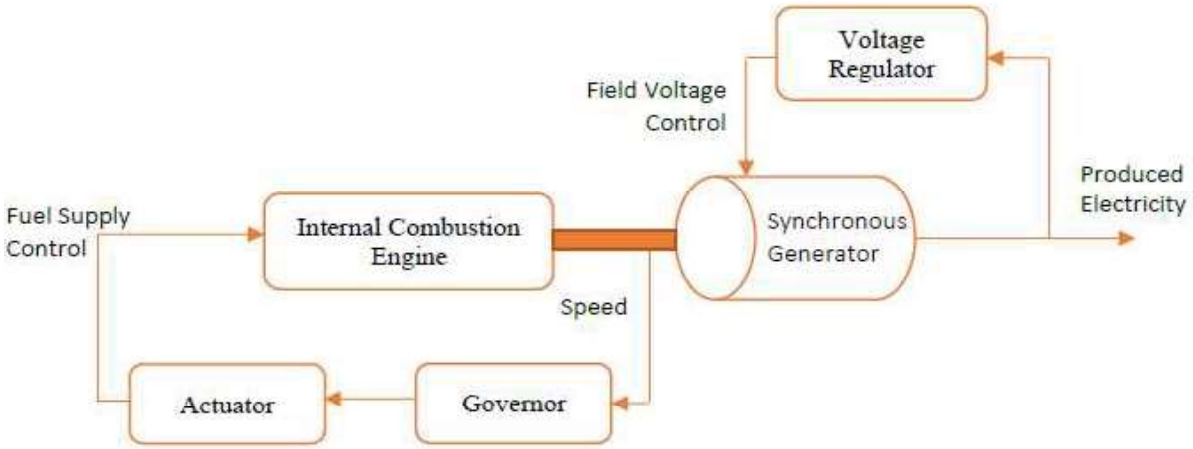

Figure II.10: Functional Block Representation of the Diesel Generator

II.2.4.1. Modelling of DEG System

The DEG relies on an internal combustion engine running on diesel fuel to drive an electric generator and produce power. When a frequency deviation (Δf) occurs in the grid, the amount of fuel supplied to the engine can be adjusted to increase or decrease the output power, aiming to restore the nominal frequency. This process is managed by the mechanical control system (Governor), which automatically regulates the fuel input based on the frequency deviation. However, due to the inertia of the rotating components, the response is not instantaneous. The relationship between mechanical power and frequency deviation is given by [74]:

$$\Delta P_{DEG} = -\frac{1}{R_{DEG}}.\Delta f \tag{II.66}$$

Where:

ΔP_{DEG}: the change in the mechanical power delivered to the generator.

R_{DEG}: the droop coefficient of the generator (represents the allowed frequency deviation in response to a change in power).

The governor's effect in a DEG is not instantaneous, as there is a delay in response due to the mechanical system's characteristics. This delay is modeled by introducing a time constant T_{DEG}, leading to a first-order differential equation that describes the mechanical power response as follows:

$$-\frac{1}{R_{DEG}}.\Delta f = \Delta P_{DEG} + T_{DEG}.\frac{d(\Delta P_{DEG})}{dt} \tag{II.67}$$

Where: T_{DG}: The time constant, which depends on the characteristics of the generator, engine, and control system.

To analyze the system behavior in the frequency domain, the Laplace transform is used:

$$-\frac{1}{R_{DEG}}.\Delta f(S) = \Delta P_{DEG}(S)(T_{DEG} + 1) \tag{II.68}$$

$$G_{DEG} = \frac{\Delta P_{DE}}{\Delta f(S)} = -\frac{1}{R_{DEG}(1+S.T_{DEG})} \tag{II.69}$$

II.3. Design and Modeling of the Microgrid in MATLAB Environment

After conducting a detailed mathematical analysis of each energy source such as PV systems, WTG, DEG, and PHEV a complete MG system was developed using the MATLAB environment. This was achieved by creating custom functions for each individual component. Each source was modeled using its own differential equations or transfer functions, and the components were then integrated into a unified structure through an Energy Management System (EMS), which coordinates power generation, storage, and load supply. Figure II.11 illustrates the overall architecture of the microgrid, where the various energy sources are interconnected in a way that reflects their interactive behavior within the system. It is worth noting that all constant values and parameters used in modeling the system components are listed in Table II.1.

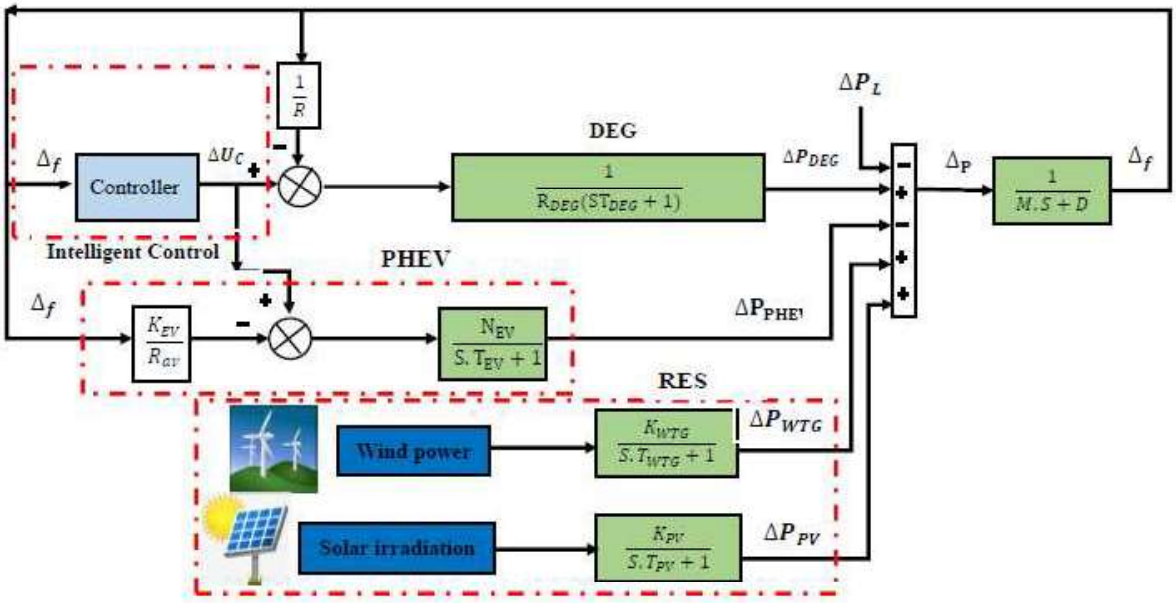

Figure II.11: Proposed Overall Structure of the Integrated Microgrid System in MATLAB Environment

Table II.1: Parameters and Constants Used in Modeling the Microgrid Components [71]

Parameter	Value	Parameter	Value
M(S)	0.1667	T_{DEG}	0.025
D(puMW)	0.015	K_{DEG}	2
T_{PV}(S)	1.8	T	250
T_{WTG}	2	K_{PV}	1
T_{EV}	0.1	K_{WTG}	1
R_{av}(HZ/puMW)	2.4	N_{EV}	600

II.4. Modeling the Temporal Variations of RES and Load

The inherent intermittency and randomness of renewable energy sources (RES), such as solar and wind power, represent a major challenge in maintaining system frequency and stability in microgrid applications. These sources are highly dependent on environmental conditions, such as solar irradiance and wind speed, which exhibit non-linear and stochastic

behaviors. Therefore, it is essential to incorporate mathematical models that accurately reflect these variations by combining randomness and sudden temporal shifts [53]-[63].

To simulate these characteristics, the following general equation is used to represent the power output from each energy source:

$$p = \left(\frac{\phi.n.\sqrt{\beta}.(1-G(s))+\beta}{\beta}\right).T = T.X \quad \text{(II.70)}$$

Where:

p: Power generated by the source (solar or wind)

ϕ: Randomness coefficient (modeled as a uniform distribution)

β: Average generated power

n: Conversion coefficient of generated power

G(s): Transfer function representing system dynamics

T: Sudden change rate in power output

X: Per-unit standard value of the energy type

II.4.1. Modeling Variations in Solar Energy

Solar power output is directly affected by solar irradiance, which fluctuates due to cloud cover, atmospheric conditions, and the sun's position. Hence, modeling its variability requires considering both random and sudden changes in irradiance [53].

The following parameters are used to simulate solar energy fluctuations:

$$\phi \simeq U(1,1), \qquad \eta = 0.8\,, \qquad \beta = 10\,, \qquad G(s) = \frac{1}{10^4+1}$$

$$T = 0.24.h(t) - 0.04.h(t-140) \quad \text{(II.71)}$$

- ϕ is modeled as a uniformly distributed random variable (though in this case, constant).
- η represents the efficiency of solar energy conversion.
- The function T includes a sudden drop at t=140 seconds, mimicking a transient reduction in irradiance (e.g., cloud shadowing).
- The Heaviside function h(t) is used to simulate these abrupt transitions.

II.4.2. Modeling Variations in Wind Energy

Wind power generation is sensitive to the randomness of wind speed and direction, which fluctuates significantly even over short time periods. A similar modeling approach is adopted here, with adjusted parameters reflecting wind dynamics:

$$\phi \simeq U(1,1), \qquad \eta = 0.9\,, \qquad \beta = 10\,, \qquad G(s) = \frac{1}{10^4+1}$$

$$T = 0.05.h(t) - 0.02.h(t-180) \quad \text{(II.72)}$$

- Wind energy has a slightly higher conversion efficiency η =0.9A
- A sudden decrease in power output is simulated at t=180 seconds.
- The difference between the positive and negative terms in T reflects a slower and more dispersed response in wind energy systems compared to solar PV systems.

II.4.3. Modeling Variations in Electrical Load

Frequency deviations in the microgrid are not only caused by fluctuating generation, but also by time-varying loads. These loads may change abruptly due to industrial processes, consumer behavior, or switching events. The load variation model accounts for a series of sudden shifts over time [63]:

$$\phi \simeq U(1,1), \qquad \eta = 0.9\,, \qquad \beta = 10\,, \qquad G(s) = \frac{1}{10^4 + 1}$$

$$T = 0.05.h(t) - 0.02.h(t - 180) \tag{II.73}$$

The change in the load is based on the following parameters:

$$\phi \simeq U(1,1), \qquad \eta = 0.8\,, \qquad \beta = 10\,, \qquad G(s) = \frac{1}{300.S + 1} + \frac{1}{1800.S + 1}$$

$$T = \frac{1}{X}\begin{bmatrix} 0.9.h(t) + 0.03.h(t - 110) + 0.03.h(t - 130) + \\ 0.03.h(t - 150) - 0.15.h(t - 170) + \\ 0.1h(t - 190 \end{bmatrix} + 0.02.\mathrm{h(t)} \tag{II.74}$$

The figure II.12 represents the mathematical model that combines randomness and temporal variations in energy production from renewable sources, reflecting the impact of sudden fluctuations on the electrical system. It also illustrates how the function T(t) is used to represent the instantaneous changes in solar and wind energy as well as load variations within the network.

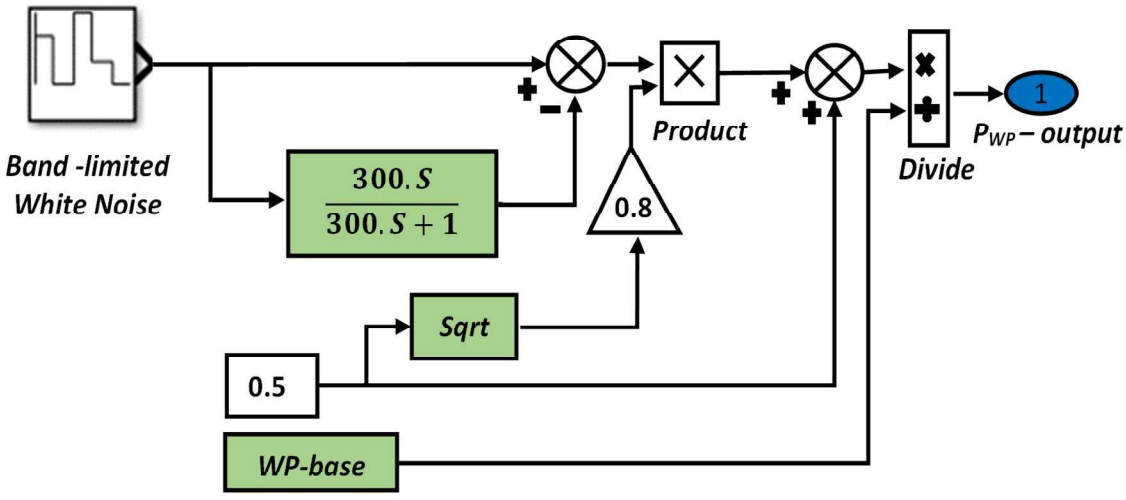

Figure II.12: Dynamic Model of Renewable Energy and Load Variations Incorporating Randomness and Sudden Changes

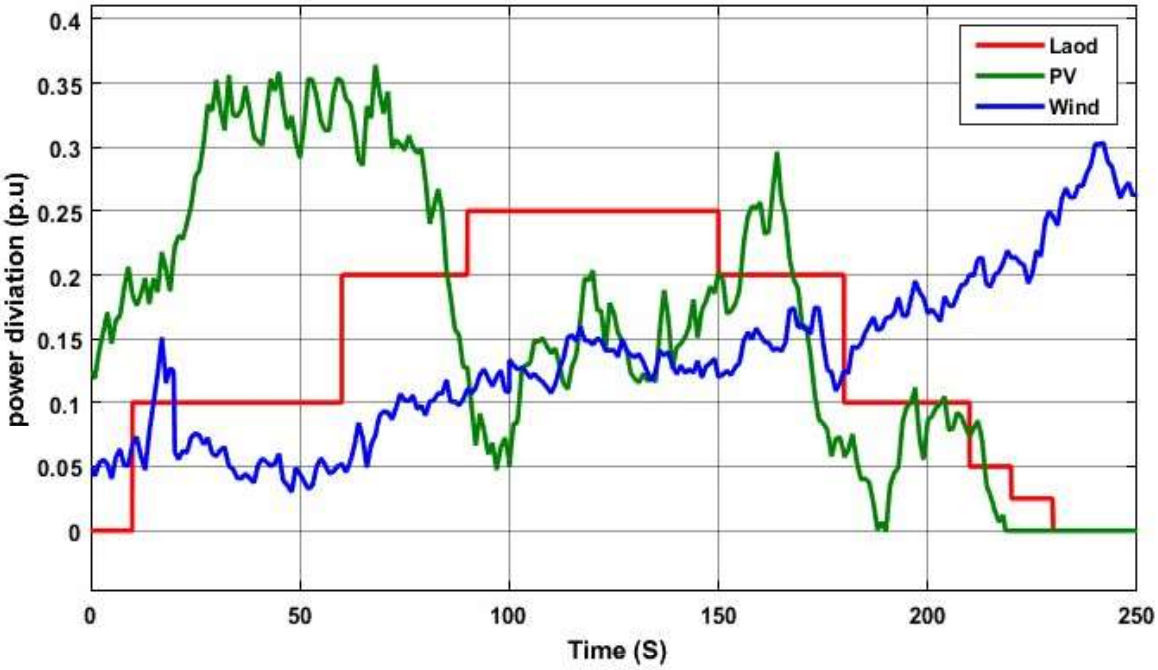

Figure II.13: Graphic of load, wind and PV power variation

The figure II.13 represents the variation in energy output from renewable sources (solar and wind) and the change in electrical load over time. It is generated based on the application of the mathematical models and equations previously presented. The green curve reflects the output from the solar energy variation model, while the blue curve illustrates the wind energy behavior. The red curve represents the load variation as defined in the model. This figure is used to analyze the impact of randomness and sudden temporal changes on the stability of the electrical system within the microgrid environment.

II.5. conclusion

In conclusion, this chapter has presented accurate mathematical models for the components of the proposed microgrid, including renewable energy sources such as photovoltaic panels, wind turbines, and hydroelectric generators, as well as conventional sources like fuel cells and diesel generators. The modeling also included electric vehicle batteries, which represent one of the most important modern storage technologies for supporting grid stability and enhancing operational efficiency. For the purpose of frequency-domain analysis in the small-signal model and the implementation of various control strategies, all components were represented using first-order transfer functions. These models form a solid foundation for system stability analysis and the design of effective controllers. Building on this foundation, the next chapter will move to the simulation phase, where various types of controllers will be utilized alongside optimization algorithms and techniques, aiming to improve the efficiency and stability of microgrid operation.

CHAPTER III:

FREQUENCY STABILIZATION OF MICROGRID USING MULTI-STAGE PID CONTROLLER AND OPTIMIZATION TECHNIQUES

III.1. Introduction

In this chapter, the focus is placed on one of the major challenges facing microgrid systems, namely frequency fluctuations resulting from sudden changes in load demand or renewable energy generation. Such disturbances can directly affect system stability and quality of service, which necessitates the adoption of effective control strategies to mitigate their impact.

Initially, the Multi-Stage PID (MPID) controller is studied, and its parameters are tuned using conventional methods such as Ziegler–Nichols (ZN) and Coefficient diagram method (CDM). Subsequently, intelligent optimization algorithms, including the Cuckoo Search Algorithm (CSA) and Ant Colony Optimization (ACO), are employed to further improve tuning efficiency and enhance the dynamic performance of the system. This chapter also presents a comparative analysis between the classical PID controller and the MPID controller in order to highlight the advantages achieved by the proposed approaches. All tuning and optimization methods are tested under a set of potential disturbances affecting the microgrid system, and the frequency deviation responses are analyzed and discussed.

III.2. Problem Statement and Motivation

Figure II.11 represents the islanded microgrid system in the absence of any control mechanisms. In this model, the system's response relies solely on the intrinsic characteristics of each energy source, without the presence of a control unit to regulate and coordinate frequency balance. Moreover, Figure III.1 illustrates the impact of climatic factors on frequency deviation and system instability, highlighting the urgent need for an effective control strategy to ensure system stability and reliable operation.

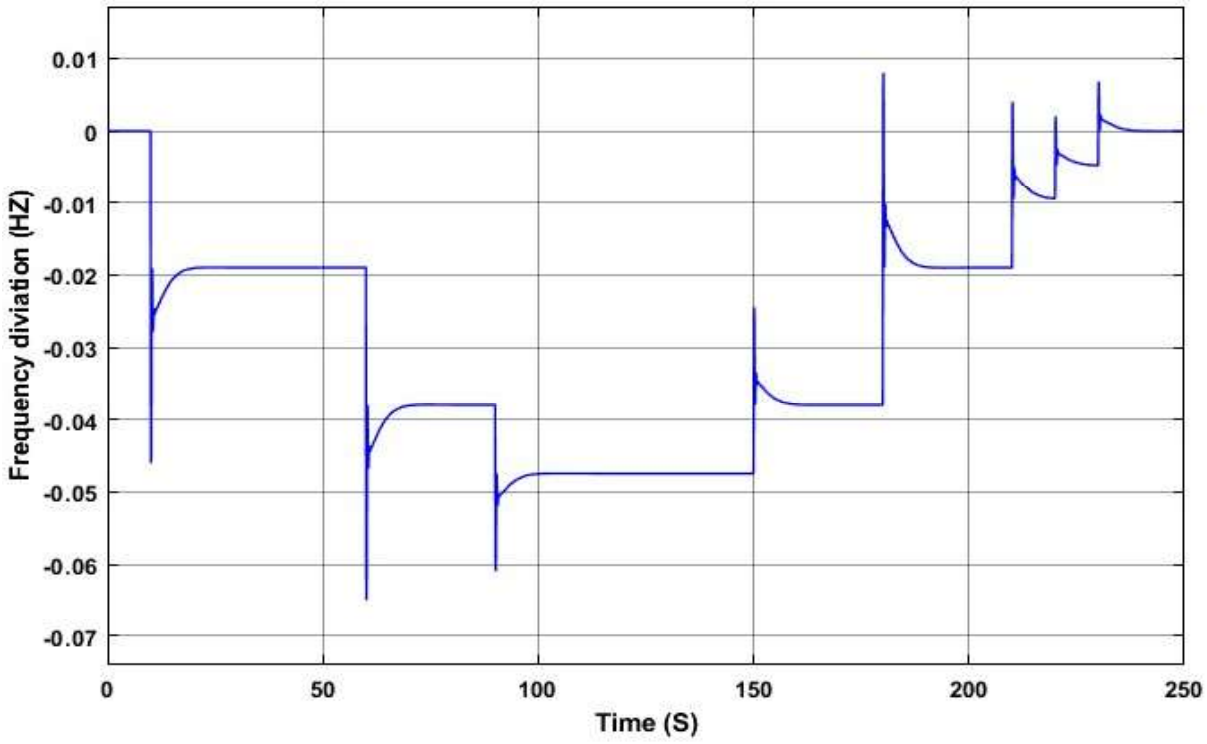

Figure III.1: Simulation Results Prior to Enhancement

Before selecting the appropriate controller to manage frequency deviation in the microgrid system, it is essential to represent the entire system using a unified transfer function that reflects its overall dynamic behavior. This representation enables the analysis of the system's response to various disturbances and the study of its stability in both the time and frequency domains. It is achieved by integrating the individual models of the different energy sources and linking them to the overall system dynamics, which are typically simplified into a single-block model, as illustrated in Figure III.2. This unified representation is a fundamental step toward understanding the system's dynamic characteristics and identifying the most suitable controller to enhance performance and ensure stability under load fluctuations and changing weather conditions.

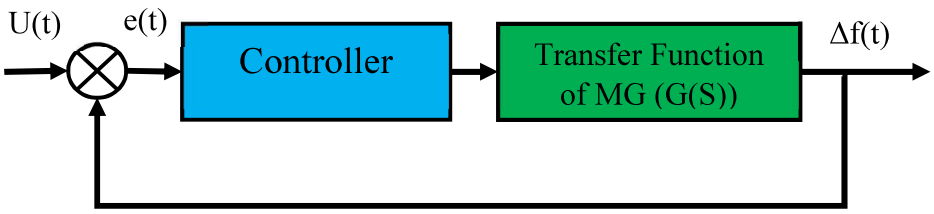

Figure III.2: Simplified Block Diagram of the Microgrid System with Controller

Based on this simplified representation, the transfer function of the microgrid system shown in Figure II.11 can now be derived. This function mathematically expresses the relationship between the system's input disturbances namely load variations and fluctuations in renewable energy sources and the resulting frequency deviation at the output. It serves as a fundamental tool for analyzing the system's dynamic response and is used in the design of appropriate control strategies. The transfer function encapsulates the essential dynamic behavior of the interconnected components within the system, thereby enabling the application of control techniques. It is represented as follows:

Based on the model illustrated in Figure (II.7) and Equation (II.14), the transfer function that relates the load variation $\Delta P_L(s)$ to the frequency deviation $\Delta f(s)$ can be derived. and is given as follows:

$$\Delta f(s) = \frac{1}{M.s+D}\left[P_{PV} + P_{WTG} + \Delta f(s) + \frac{N_{EV.}}{R_{EV}(S.T_{EV}+1)}.\Delta f(s).\frac{1}{R_{DEG}(1+S.T_{DEG})} - \Delta P_L\right] \quad \text{(III.1)}$$

RES such as solar and wind power, as illustrated in Figure II.7, are not directly affected by frequency deviations. Instead, they depend on external factors like solar irradiance and wind speed, which are not related to the dynamic changes caused by load variations. In other words, the energy produced by these sources does not constitute an automatic response to frequency deviation but rather represents independent inputs that enter the system externally [32]-[50].

Therefore, when analyzing a complex system with multiple inputs such as loads and renewable energy sources, it becomes difficult to isolate the impact of each input on the final output. For this reason, it is common in linear system analysis to hold all other inputs constant (i.e., temporarily assume them to be zero,) while deriving the transfer function between a specific input and a given output. This approach allows us to analyze the relationship between the load and the frequency without interference from other input effects [32]-[71].

Thus, the transfer function between ΔP_L (s) and $\Delta f(s)$ becomes:

$$\Delta f(s) = \frac{1}{M.s+D}\left[\Delta f(s) + \frac{N_{EV.}}{R_{EV}(S.T_{EV}+1)}.\Delta f(s) + \Delta f(s).\frac{1}{R_{DEG}(1+S.T_{DEG})} - \Delta P_L(s)\right] \quad \text{(III.2)}$$

Δf(s) on the left-hand side:

$$\Delta P_L \frac{1}{M.s+D} = \Delta f(s)\left[\frac{1}{M.s+D}\left(\frac{N_{EV.}}{R_{EV}(S.T_{EV}+1)} + \frac{1}{R_{DEG}(1+S.T_{DEG})}\right) - 1\right] \quad \text{(III.3)}$$

$$G(s) = \frac{\Delta f(s)}{\Delta P_L(s)} = \frac{-1}{\left[\frac{N_{EV.}}{R_{EV}(S.T_{EV}+1)} + \frac{1}{R_{DEG}(1+S.T_{DEG})}\right] - (M.s+D)} \quad \text{(III.4)}$$

III.3. Study of Two Controllers for Frequency Deviation Control in a MG System

In this work, the focus will be on studying and analyzing two different types of controllers with the aim of reducing frequency deviation resulting from sudden changes and instability within the microgrid system. Precise frequency control is essential to maintain system stability and ensure power quality, especially in systems that rely on intermittent renewable energy sources. Through this study, we will examine two different types of controllers, which are as follows:

III.3.1. PID controller structure

The PID controller is one of the most widely used controllers in industrial systems, due to its simple structure and ease of use. The PID controller calculates the error as the difference between the measured value and the reference value to be achieved. It then attempts to minimize this error using adjustable variables [52].

The PID controller consists of three independent constant parameters, commonly referred to as a three-term controller: the proportional (P), integral (I), and derivative (D) terms. These components are connected in parallel, as illustrated in Figure III.3. Their relationship is also simplified by the following mathematical equation.

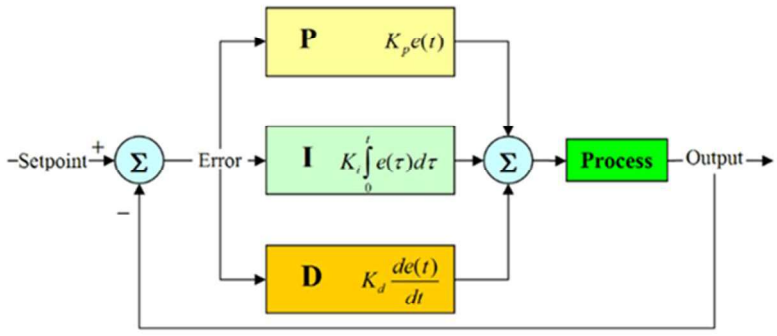

Figure III.3: PID controller models.

$$C(S) = K_p e(S) + K_i \frac{e(S)}{S} + k_d.S.e(S) \quad \text{(III.4)}$$

Each of these constants plays a specific role in adjusting the system's response:

- The proportional term (P) addresses the current error.
- The integral term (I) handles the accumulation of past errors, helping to eliminate steady-state error.

- The derivative term (D) predicts future error trends by analyzing the rate of change of the error, which helps reduce oscillations and limit overshoot.

III.3.2. Multi-Stage PID (MPID) Controller Design

The Multi-Stage PID (MPID) controller is a modern development of the conventional PID controller, designed to address some of the limitations encountered in microgrid systems particularly the issue of equal or closely related control parameters (Kp, Ki) under certain microgrid operating conditions. This equality or direct proportionality between the variables has weakened the system's ability to adapt to dynamic changes, resulting in prolonged settling times, increased oscillations, and overall reduced system stability [32].

The MPID controller consists of two independent units: a PI unit and a PD unit connected in series, as illustrated in Figure III.4. The PD unit comes first and its main function is to anticipate the error and improve the system's response speed to sudden changes in frequency (Δf). The resulting signal is then passed to the PI unit, which contributes to enhancing long-term signal stability through integration and correction of the remaining deviations. This helps keep the system frequency within the required limits in the standalone case [71].

Thus, the structure of the MPID controller offers high flexibility compared to the conventional controller, allowing each unit's positive characteristics to be exploited independently, while ensuring better tuning of all parameters.

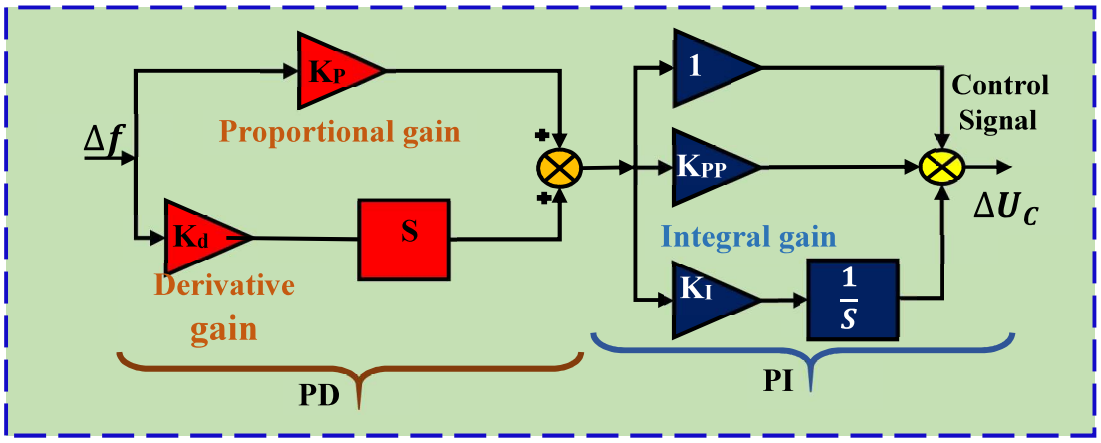

Figure III.4: Block diagram representation of a multistage PID controller (MPID).

The mathematical model of the MPID controller can be formulated by connecting the PD model to handle the transient inputs, followed by the PI model for the steady-state condition, as will be illustrated later in equation (III.5). This facilitates system analysis in both the frequency domain and time response

$$\frac{\Delta U_C}{\Delta_f} = (Kp + Kd.S)(1 + K_{PP} + \frac{K_i}{S}) \quad \text{(III.5)}$$

III.4. The Various Approaches to Optimization

In this part of the work, the control parameters were tuned using a set of optimization techniques, including conventional and intelligent optimization algorithms. The main objective was to enhance the system's overall performance by improving its stability, reducing the response time, and minimizing error rates. Among the most prominent algorithms employed are:

III.4.1. Optimization methods

III.4.1.1. Coefficient diagram method (CDM)

III.4.1.1.a. General concept

Some systems, such as the MG system, present significant challenges in terms of control and selecting an appropriate controller. This is due to the complexity of manufacturing dynamics and the precise performance requirements, including settling time, response speed, and long-term stability. Moreover, these systems are often described by complex mathematical equations in which the number of unknowns exceeds the number of available equations, making it difficult to obtain accurate solutions.

In light of these challenges, the CDM is considered an effective approach for tuning the parameters of the PID controller. This method combines both classical and modern control techniques and relies on performance analysis through the coefficient diagram, while also comparing the system's mathematical model with the well-known Manabe equation. Developed by the researcher Manabe, this method provides a structured framework for exploring the solution space by introducing initial coefficients that aid in constructing suitable solutions. Figure III.5 illustrates the typical structure of the CDM approach, as referenced in [72–73].

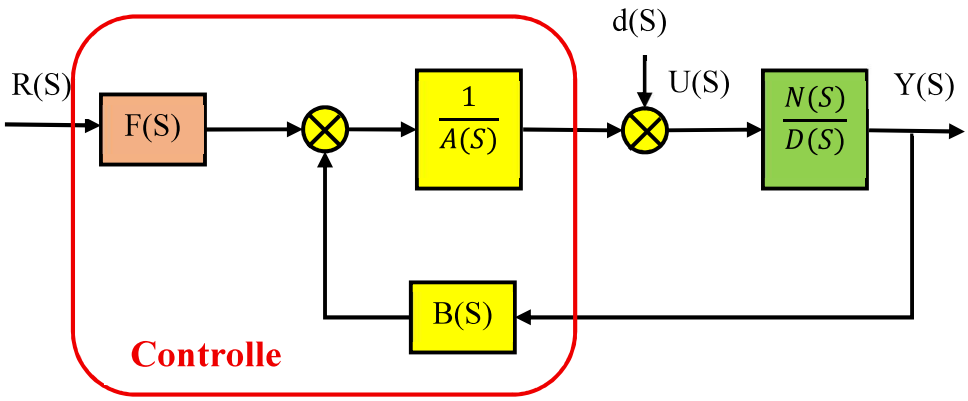

Figure III.5: Mathematical model of the CDM method

III.4.1.1.b. CDM description

The previously described closed-loop system is considered, where y denotes the system output, $U$is the control input, and $Y(s)$ represents the reference signal (setpoint), while d accounts for the random disturbance affecting the system. The terms $A(s)$,$F(s)$ and $B(s)$ correspond to the controller polynomials, whereas $N(s)$ and $D(s)$ represent the numerator and denominator of the system's dynamic model, respectively [50].

The general form of the characteristic polynomial for a linear closed-loop system is expressed through the following equation, which serves as the foundation for analyzing system stability and response behavior [74]:

$$\mathrm{Y(S)} = \frac{1}{\mathrm{P(S)}}\left(\mathrm{N(S).F(S).R(S) + A(S).N(S).d(S)}\right) \quad \text{(III.6)}$$

Since $P(s)$ denotes the characteristic polynomial of the closed-loop system [44], it can be formulated as follows:

$$\mathrm{P(S)} = a_n.s + a_{n1}.s^{n-1} + \ldots + a_1 + a_0 = \sum_i^n a_i s^i \quad \text{(III.7)}$$

With:

$$P(S) = A(S).D(S) + B(S).N(S) \quad \text{(III.8)}$$

In order to construct the CDM controller diagram effectively, three core parameters must be taken into account: the equivalent time constant (τ), the stability index (Υ_i), and the stability limit (Υ_i^*). These parameters are derived from the coefficients of the system's characteristic polynomial and play a vital role in shaping the structure and performance of the CDM controller. Understanding and accurately calculating these values is essential for ensuring a stable and well-tuned control system [50].

$$\Upsilon_i = \frac{a_i^2}{a_{i+1}.a_{i-1}} \qquad i = 1.2.3 \ldots \ldots . n-1 \quad \text{(III.9)}$$

$$\Upsilon_0 = \Upsilon_n = \infty$$

$$\tau = \frac{a_1}{a_0} \quad \text{(III.10)}$$

$$\Upsilon_i^* = \frac{1}{\Upsilon_{i-1}} + \frac{1}{\Upsilon_{i+1}} \quad \text{(III.11)}$$

The characteristic polynomial, as defined in Equations (III.8) and (III.9), is reformulated using the parameters $a0$, the equivalent time constant τ, and the stability indices, as shown below.

$$P_t(S) = a_0 \left[\left\{ \sum_{i=2}^{n} \left(\prod_{j=1}^{i-1} \frac{1}{\Upsilon_{i-j}^{j}} \right) (\tau.S) \right\} + \tau.S + 1 \right] \quad \text{(III.12)}$$

The time constant (τ_i) is defined as follows:

$$\tau_i = \frac{a_{i+1}}{a_i} \quad \text{(III.13)}$$

We can deduce the following relationship:

$$a_i = \frac{a_0.\tau^2}{\Upsilon_{i-1}.\Upsilon_{i-2}^2 \ldots\ldots \Upsilon_2^{i-2}.\Upsilon_{i-1}} \quad \text{(III.14)}$$

III.4.1.1.c. Stability condition of this method

The stability and control criteria of systems sharing similar characteristics with the MG have been extensively examined using the CDM across several research studies [72–75]. Below is a summary of the key findings from these works:

- The system stability condition of order three is as follows:
  $a_2.a_1 > a_0.a_3 \longrightarrow \Upsilon_1.\Upsilon_2 > 1$ (III.15)
- The system stability condition of order four is as follows:

  $$a_2 > \frac{a_1.a_4}{a_3} + \frac{a_0.a_3}{a_1} \longrightarrow \Upsilon_2 > \Upsilon_2^* \quad \text{(III.16)}$$
- The stability condition five and above is given as follows:
  $\Upsilon_i > 1.12.\Upsilon_i^* \qquad i = 2 \ldots \ldots \ldots . (n-2)$ (III.17)
  $\Upsilon_i \Upsilon_{i+1} \leqslant 1 \qquad i = 2 \ldots \ldots \ldots . (n-2)$ (III.18)

This approach was originally introduced by the researcher Manabe, who established a set of fixed values later known as Manabe constants to simplify the evaluation of system stability and performance. These constants serve as reference points in the analysis process [73–76].

$$\Upsilon_i = [2\ \ 2\ \ 2\ \ 2\ \ \dots\dots\dots\dots\ \ 2.5]\,, \quad i = 1 \dots\dots\dots\dots (n-1) \quad \Upsilon_0 = \Upsilon_n = \infty$$

III.4.1.1.d. Implementation of CDM to optimize the MPID controller

To determine the parameters of the MPID controller using the CDM method, the first step involves calculating the closed-loop transfer function $FTS(s)$ of the system. Once this function is obtained, the constants of the MG system, as presented in Table II.1, are substituted into the equation. As a result, the transfer function can then be expressed in terms of the MPID controller parameters {Kp, Ki, Kd, Kpp}, as shown in references [50]-[76].

$$FT_S(S) = \frac{N_S(S)}{D_S} = \frac{\Delta_f}{\Delta_U} \qquad n = 6 \tag{III.19}$$

$$N_s(S)\begin{cases} S^5(0.75Kd - 0.75Kd.Kpp) + S^4\begin{pmatrix}34Kd - 34Kd.Kpp - 0.75Kp\\ +0.75Kd.Kpp + 0.75Ki.Kd\end{pmatrix} + \\ S^3(1.95Kd - 1.95Kd.Kpp - 34Kp + 34Kp.Kpp + 34Ki.Kd - 0.75Ki.Kp) + \\ S^2(4Kd - 4Kd.Kpp - 1.95Kp + 1.95Kp.Kpp + 1.95Ki.Kd - 34Ki.Kp) \\ +S(4Kp - 4Kp.Kpp - 4KiKd - 1.95Ki.Kp) - 4Ki.Kp \end{cases}$$

$$D_s(S)\begin{cases} 0.0025.S^6 + S^5(0.0138 + 0.75Kd - 0.75Kd.Kpp) \\ +S^4\begin{pmatrix}0.9751 + 34Kd - 34Kd.Kpp\\ -0.75Kp + 0.75Kd.Kpp + 0.75KiKd\end{pmatrix} \\ +S^3\begin{pmatrix}-0.97503 - 1.95Kd + 1.95Kd.Kpp -\\ 34Kp + 34Kp.Kpp + 34Ki.Kd - 0.75Ki.Kp\end{pmatrix} \\ +S^2\begin{pmatrix}-10.018 + 4Kd - 4Kd.Kpp - 1.95Kp\\ +1.95Kp.Kpp + 1.95Ki.Kd - 34Ki.Kp\end{pmatrix} \\ +S(-1.215 + 4Kp - 4Kp.Kpp - 4KiKd - 1.95Ki.Kp) - 4Ki.Kp \end{cases}$$

Through the basic rules of the CDM method, this equation can be deduced

$$P(S) = D_s(S) \tag{III.20}$$

To effectively design a controller using the CDM method, it is crucial to identify key parameters such as the equivalent time constant (τ) and the stability indices (Υ_1, Υ_2, Υ_3, Υ_4, and Υ_5). Within this framework, the desired characteristic polynomial can be formulated as a function of τ and the stability indices Υ_i, where η represents the degree of the polynomial.

$$P_t(S) = \sum_{i=0}^{n} at_i.S^i \qquad n = 6 \tag{III.21}$$

With:

$$P_t(S) = \frac{a_0\tau^6S^6}{\Upsilon_5.\Upsilon_4^2.\Upsilon_3^3.\Upsilon_2^4.\Upsilon_1^5} + \frac{a_0\tau^5S^5}{\Upsilon_4.\Upsilon_3^2.\Upsilon_2^3.\Upsilon_1^4} + \frac{a_0\tau^4S^4}{\Upsilon_3.\Upsilon_2^2.\Upsilon_1^3} + \frac{a_0\tau^3S^3}{\Upsilon_2.\Upsilon_1^2} + \frac{a_0\tau^2S^2}{\Upsilon_1} + a_0\tau S + a_0 \tag{III.22}$$

The general mathematical method of CDM is expressed in the form of matrices as follows:

$$[A]_{(n+1).n}.[M]_{n.1} = [B]_{(n+1).1} \quad \text{(III.23)}$$

Where:

[A]: Represents the MG system matrix.
[B]: Represents the CDM matrix.
[M]: Represents the multi-stage PID controller matrix.

With:

$$[A]_{7*6} = \begin{bmatrix} 0 & 0 & 0 & 0 & 0 & 0 \\ 0.75 & -0.75 & 0 & 0 & 0 & 0 \\ 34 & -34 & -0.75 & 0.75 & 0.75 & 0 \\ -1.95 & 1.95 & 34 & -34 & -34 & -0.75 \\ 4 & -4 & -1.95 & 1.95 & 1.95 & -34 \\ 0 & 0 & 4 & -4 & -4 & -1.95 \\ 0 & 0 & 0 & 0 & 0 & -4 \end{bmatrix} \quad \text{(III.24)}$$

$$[B]_{7*1} = \begin{bmatrix} \frac{a_0\tau^6}{\Upsilon_5.\Upsilon_4^2.\Upsilon_3^3.\Upsilon_2^4.\Upsilon_1^5} - 0.0025 \\ \frac{a_0\tau^5}{\Upsilon_4.\Upsilon_3^2.\Upsilon_2^3.\Upsilon_1^4} - 0.0138 \\ \frac{a_0\tau^4}{\Upsilon_3.\Upsilon_2^2.\Upsilon_1^3} + 0.9751 \\ \frac{a_0\tau^3}{\Upsilon_2.\Upsilon_1^2} - 0.97503 \\ \frac{a_0\tau^2}{\Upsilon_1} + 10.018 \\ a_0\tau^1 - 1.215 \\ a_0 \end{bmatrix} \quad \text{(III.25)}$$

In order to simplify the calculations, we set the controller parameters:

$$Kp = Kp\ , Kd = Kd\ , Kd * Kpp = Kdpp \quad \text{(III.26)}$$

$$Kp.Kpp = Kppp\ , Ki * Kd = Kid\ ,\ \ Ki * Kp = Kip \quad \text{(III.27)}$$

$$[M]_{6.1} = \begin{bmatrix} Kd \\ Kdpp \\ Kp \\ Kpp \\ Kid \\ Kip \end{bmatrix} \quad \text{(III.28)}$$

Then write Equation (III.23) in this form, meaning we put the unknowns on one side and the features on one side

$$\begin{bmatrix} Kd \\ Kdpp \\ Kp \\ Kpp \\ Kid \\ Kip \end{bmatrix} = ([A]^t.[A])^{-1}.[A]^t[B] \quad \text{(III.29)}$$

For numerical applications, I suggest using Manabe constants [44]:

$\tau = 2.8$, $a_0 = 1$ $\Upsilon_1 = 2.5$, $\Upsilon_2 = \Upsilon_3 = \Upsilon_4 = \Upsilon_5 = 2$

After solving the system equations using Manabe constants, we determine the values for the MPID controller parameters.

$$Kd = 1.312 \quad , Kp = 1.2807 \quad , Ki = 4.5407 \quad , Kpp = 0.987$$

The proposed control strategy follows a structured sequence of steps to determine the parameters of the MPID controller using the CDM method. A flowchart illustrating this approach is presented in Figure III.6. The process begins with system modeling and the derivation of its transfer function to capture the underlying dynamics. Based on desired performance metrics such as stability, damping, and response time a target characteristic polynomial is then constructed. This polynomial is converted into a coefficient diagram, which provides a visual representation of the system's stability and dynamic behavior. Using this diagram, the MPID controller parameters are carefully adjusted to achieve optimal system performance. This systematic methodology ensures that the controller is effectively tailored to meet the operational requirements of the system.

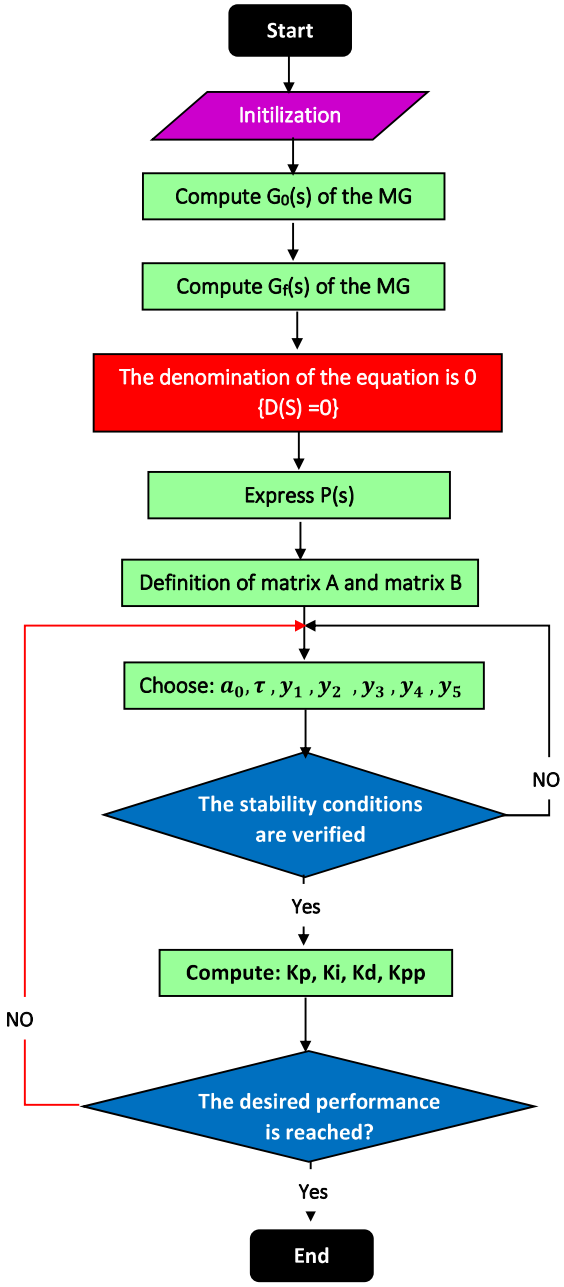

Figure III.6: Flowchart of the CDM method for tuning the MPID controller parameters

III.4.1.2. Ziegler Nichols method (ZN)

III.4.1.2.a. General concept

Several experimental methods have been developed to determine the coefficients of a PID controller. In 1942, Ziegler and Nichols proposed two experimental approaches designed to quickly tune the parameters of P, PI, and PID controllers. The first requires recording the step response of the open-loop system, while the second involves bringing the closed-loop system to the verge of instability. It is important to note that these methods generally apply only to systems without oscillatory behavior and whose phase shift at high frequencies exceeds -180 degrees. Such systems often exhibit pure time delay and/or multiple time constants and are commonly found in physic chemical processes such as temperature, level, and pressure control [78]. This method is based on knowledge of the critical point of the Nyquist diagram of the

process. The PID controller parameters are determined based on the characteristics $K0$ and $T0$, where $K0$ is the gain that brings the system to the limit of oscillation, and $T0$ is the oscillation period. The Ziegler Nichols method was developed through simulations on a large number of cases. The design criterion is to obtain a decay ratio d=1/4 for disturbance rejection, which corresponds to a damping coefficient ζ of 0.22. These values are satisfactory for good disturbance rejection but are too low for setpoint change responses. Table III.1 presents the results obtained from applying the Ziegler Nichols method, which is based on the critical values of the system. This table is provided as part of the explanation of how this method is used to tune the PID controller parameters based on experimental procedures [79-80].

Table III.1: Calculation of PID Controller Parameters Based on $K0$and $T0$ [79]

Parameter tuning			
Controller	Kp	Ki	Kd
PID	$0.6K_0$	$2K_P/T_0$	$K_0T_0/8$

III.4.1.2.b. Application of Ziegler Nichols method to optimize the MPID controller

The ZN is one of the well-known classical approaches for tuning PID controller parameters. At this stage, an improved version of this method was developed and applied to a multistage MPID controller in order to reduce frequency fluctuations in a standalone microgrid. A new control variable, Kpp, was introduced to enhance performance, particularly under the dynamic and unstable conditions typical of microgrids based on renewable energy sources [80].

This modification was driven by one of the main challenges in microgrid operation frequency deviation caused by fluctuations in both power generation and load demand, especially when integrating variable energy sources such as solar and wind. These deviations can degrade power quality and threaten the continuity of power supply [77-78].

A two-step implementation of the modified ZN method was adopted to tune the MPID controller parameters effectively:

Stage 1:

In this stage, the classical Ziegler–Nichols rules were applied to calculate the initial values of the conventional controller parameters: Kp, Ki, and Kd. The Kpp parameter was initially set to zero in order to assess the baseline system performance using only the traditional tuning method without any enhancements.

Stage 2:

The new parameter Kpp was then integrated into the tuning model, and its value was gradually increased, starting from a small initial value (Kpp = 0.1), until the system achieved a stable dynamic response and effective frequency regulation. At each tuning step, the system performance was evaluated using stability indicators such as settling time, maximum deviation, and oscillation rate.

To improve frequency regulation in the microgrid system, a gradual tuning strategy was implemented. The approach began with the adjustment of the basic PID parameters, followed

by the integration of an additional gain, Kpp, to further enhance the system's dynamic performance. This tuning process was structured into four main stages, as outlined below:

Step 1: Initialization

Set all controller parameters to zero:

Kp = Ki = Kd = Kpp = 0

Step 2: Identify critical values.

Determine the ultimate gain (Ku) and the ultimate period (Tu).

Step 3: Compute initial PID parameters.

Kp = 0.6 * Ku

Ki = 2 Kp / Tu or Ki = 0.5 Tu

Kd = Kp Tu / 8 or Kd = 0.125 Tu

Step 4: Optimize Kpp

Increment Kpp gradually until the desired level of frequency stability is achieved.

Figure III.7 illustrates the flowchart of the enhanced Ziegler–Nichols-based tuning strategy. The practical implementation of this approach was carried out through the following structured steps:

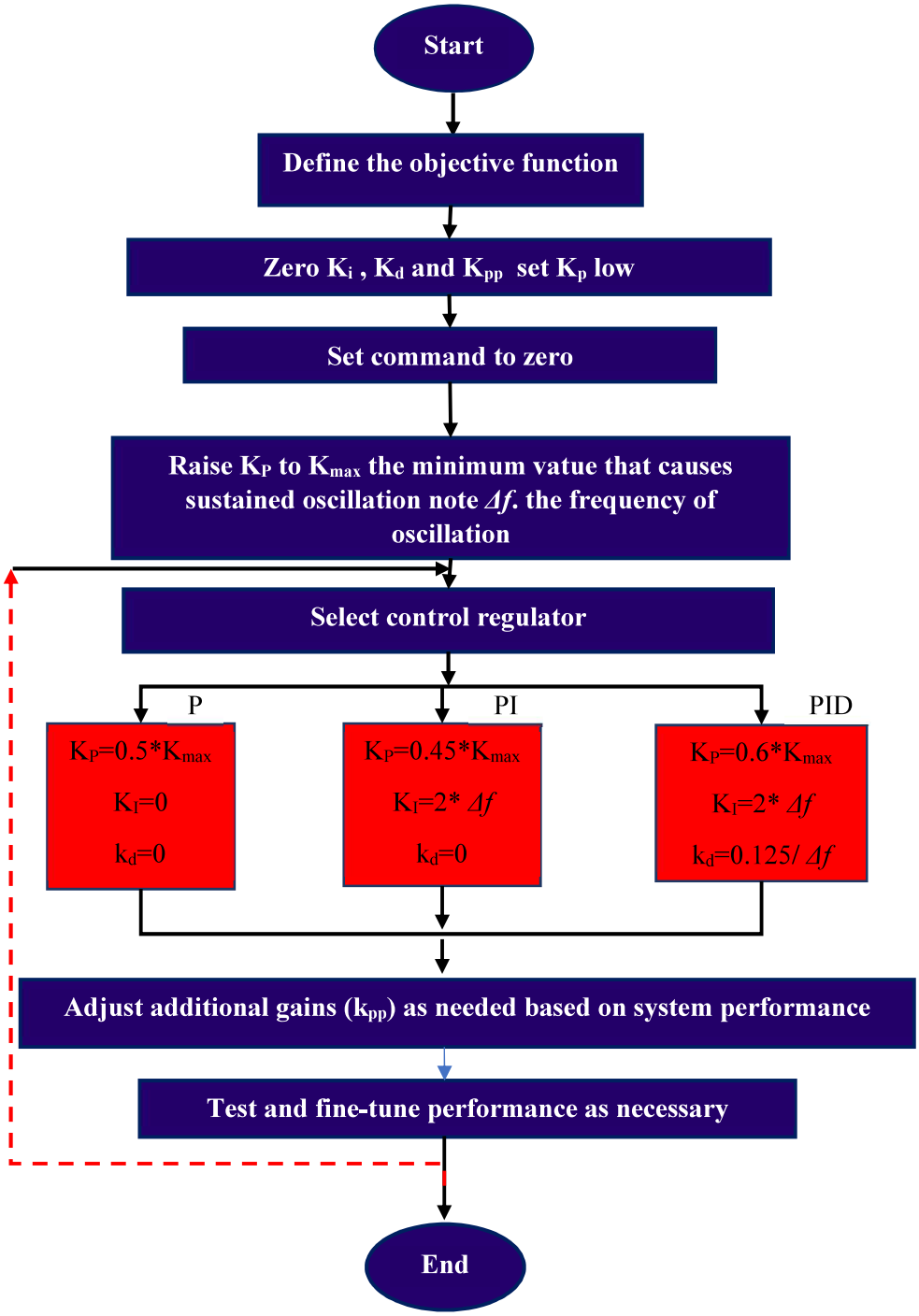

Figure III.7: Flowchart of the ZN method for tuning the MPID controller parameters

III.4.2. Optimization algorithms.

III.4.2.1. Cuckoo Search Algorithm (CSA)

III.4.2.1.a. General concept

The algorithm, introduced by the researcher X.S [80], draws inspiration from the natural behavior of cuckoo birds. It is based on the reproductive strategy of female cuckoos, which lay their eggs in the nests of other bird species to avoid the energy and time required for nest-

building and chick-rearing. The core mechanism of the algorithm revolves around two fundamental principles. for its success [80-82]:

- The female cuckoo randomly selects the best nests built by other birds.
- She discards the original eggs far from the nest and lays her own eggs at each stage, repeating this process until only one egg from the other species remains.

In this algorithm, the eggs represent potential solutions, with the cuckoo's egg symbolizing a newly generated solution. This new solution is produced using the Lévy flight distribution, as described in [32]-[70].

$$x_j(t+1) = x_i(t) + a \oplus levy(\lambda) \quad \text{(III.30)}$$

$$levy(\lambda) = s * (x_i(t) - x_{best}) \quad \text{(III.31)}$$

$$i = 1.2.3 \ldots N$$

Where

λ represents the Lévy exponent, S denotes the step size, α is a scaling constant, X best refers to the current best solution, and ⊕ indicates the entry wise (element-wise) multiplication operator.

$$s = \sigma_u * u * |V|^{-1/\beta} \quad \text{(III.32)}$$

If the host bird detects the presence of a cuckoo egg indicating that the condition r1 < Pa is satisfied it discards the egg, meaning the new solution is rejected and replaced by another one calculated as follows:

$$x_j(t+1) = x_i(t) + rand(n_1 - n_2) \quad \text{(III.33)}$$

$$n_1, n_2 \ldots N$$

III.4.2.1.b. Application of CSA algorithm to optimize the MPID controller

The CSA has proven its effectiveness in solving complex problems. In this study, CSA is employed to tune the parameters of the MPID controller to enhance system performance and stability. Therefore, it will be applied according to the following steps to achieve optimal tuning results [71]:

- Step 1: Initialization

  A set of random candidate solutions is generated within the nest search space, and each solution is evaluated based on the defined objective function.

- Step 2: MPID Controller Setup

  The multi-stage PID (MPID) controller is initialized by setting the values of its parameters (Kp, Ki, Kd, and Kpp), along with the initial error conditions, including current, cumulative, and previous errors.

- Step 3: Parameter Update via Lévy Flights

  In each iteration, the parameters of the MPID controller are updated using Lévy flight-based strategies to explore the search space more effectively.

- Step 4: Iterative Search
- Steps 2 and 3 are repeated continuously until convergence is achieved or the predetermined maximum number of iterations is reached.
- Step 5**:** Optimal Solution Selection

  The best-performing parameter set obtained throughout the optimization process is selected as the final solution for tuning the MPID controller.

I have developed a program based on the Cuckoo Search Algorithm (CSA) to optimize the parameters of the MPID controller as follows:

Begin
Define the objective function
Define the maximum number (n) of iterations and other parameters
while (x < MaxGeneration):
Obtain a cuckoo randomly via Levi's flights and then we determine the MPID parameters
Evaluate its fitness Fi
Choose a nest among n (say j) randomly
if Fi>Fj
Replace Fj with the new parameters
End if
End while
A group of bad nests is abandoned, and one nest is chosen as the best solution, which expresses the values of the constants for MPID controller.
End.

I have summarized this program in a flowchart that illustrates the sequence of steps of the CSA for tuning the MPID controller parameters, starting from defining the objective and setting the parameters, through the search and evaluation process, and ending with selecting the optimal solution [71].

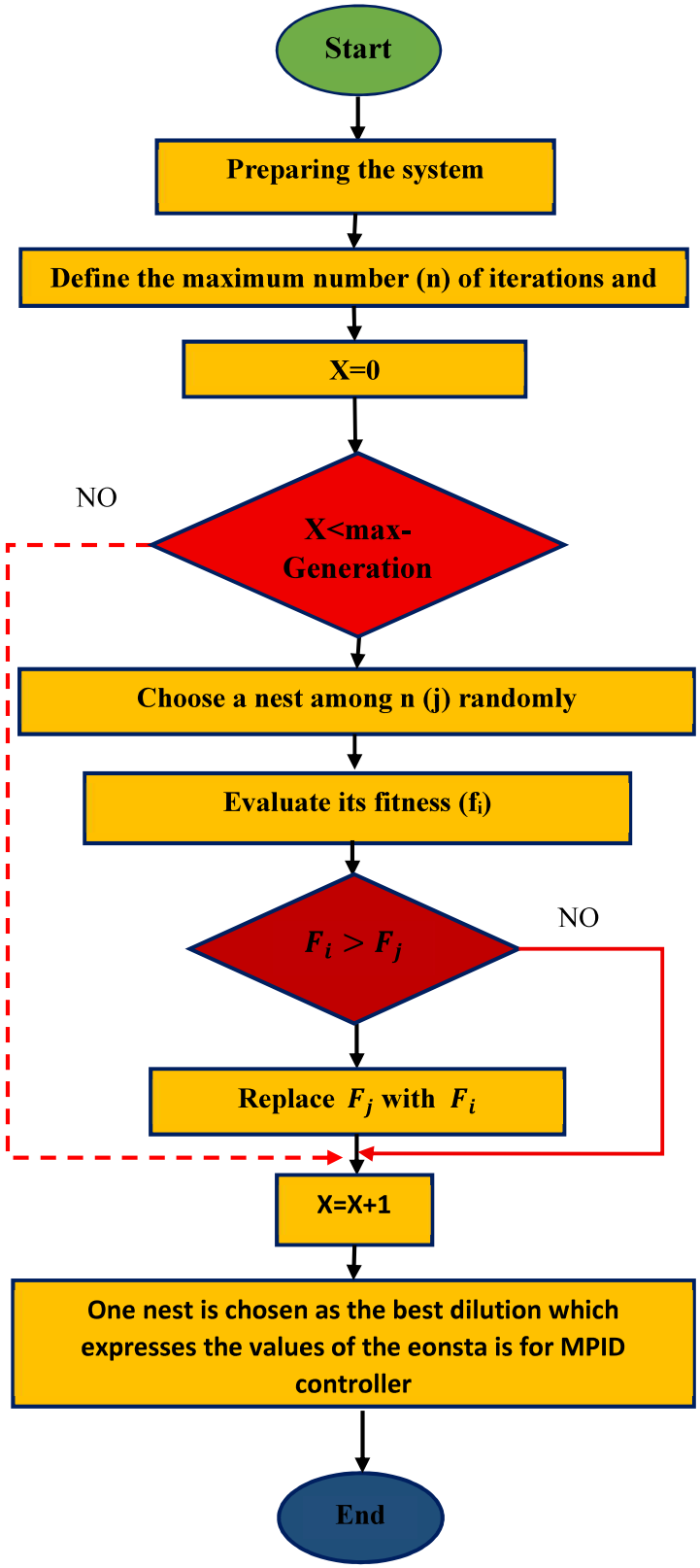

Figure III.8: Flowchart of the CSA-MPID Controller Parameter Optimization

III.4.2.2. Ant Colony Optimization (ACO)

III.4.2.2.a. General concept

The ACO algorithm is specifically designed to find solutions to problems with different cases or instances. This method relies on cooperation among ants within the colony to identify effective solutions. Due to the strong similarity between the algorithm and the behavior of ant colonies in nature, it is characterized by flexibility and high adaptability, making it applicable to multiple versions of the same problem as well as to various types of problems [83].

The basic concept of this algorithm was first proposed in 1992 by Dorigo, inspired by the foraging behavior of ants. In nature, ants work together to find the shortest route between their nest and a food source. This route may include multiple intersections, requiring ants to make decisions at each junction to choose the optimal path with the goal of minimizing the total traveled distance [83-84].

This cooperation is achieved through the release of pheromones, which are chemical substances secreted by individuals of the same species, serving as an effective means of communication. Ants leave a trail of pheromones along the path they travel, and the amount of pheromone depends on how frequently the path is used and how quickly the food is reached. Since shorter paths are traveled in less time, they accumulate more pheromones. Consequently, ants are more likely to select paths with higher pheromone concentrations [85-86].

Pheromones evaporate over time, which prevents ants from following non-optimal paths indefinitely. However, shorter paths maintain a higher pheromone level due to frequent and rapid usage, eventually causing most ants to converge on the shortest path. Figure III.9 visually illustrates this process. Colors are used to represent pheromone concentration levels along different paths:

Red: Indicates paths with a low level of pheromones, often representing longer or less frequently used routes.

Orange: Represents a medium pheromone level, typically found on paths still under exploration or serving as alternatives to the optimal path.

Green: Denotes a high pheromone concentration, usually corresponding to the shortest route that the ants settle on after several search iterations.

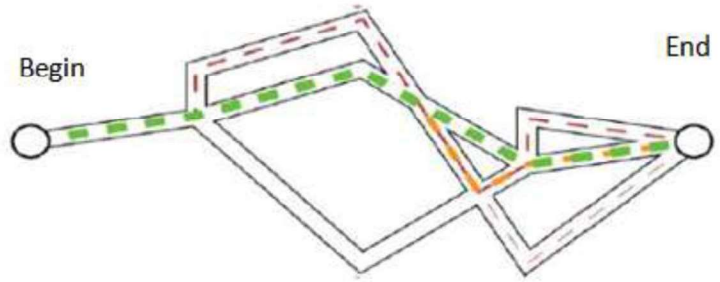

Figure III.9: The shortest path ants to find the pheromone [86]

This color gradient demonstrates how the ants' initially random movement gradually transforms into an organized pattern following the optimal route, driven by pheromone accumulation.

III.4.2.2.b. Application of ACO algorithm to optimize the MPID controller

In our work, we employ the ACO algorithm to tune the parameters of an MPID controller, which consists of four parameters: Kp, Ki, Kd, and Kpp. To fully exploit ACO's capabilities, we represent the optimization problem directly using a construction graph, where each ant incrementally builds a solution by sequentially selecting the parameter values. In the proposed design (modified from Figure III.10), the representation of the parameters is organized into two consecutive branching stages as follows:

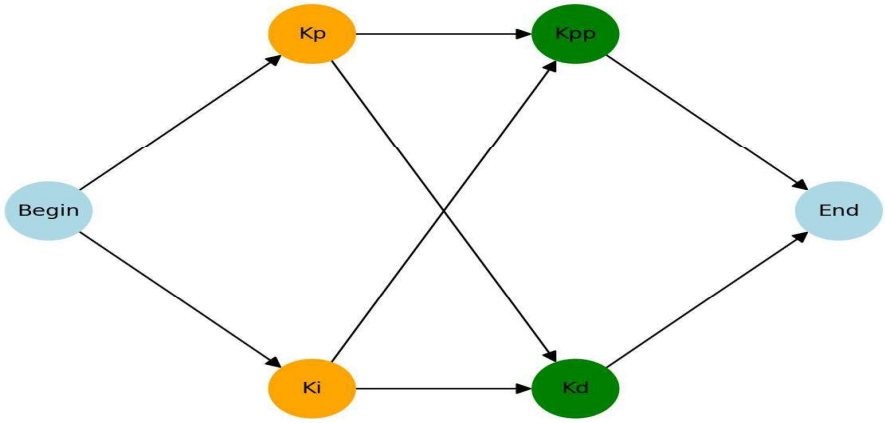

Figure III.10: Construction Graph of ACO-Based Optimization for MPID Controller Parameters

Stage 1: Represents two parallel options Kp and Kd meaning that the ant selects a value for either Kp or Ki from a coded set of possible values.

Stage 2: Represents the next parallel group Kpp and Ki where the ant then selects a value for either Kpp or Ki

In the numerical implementation for the current study, each possible value of a parameter is encoded. Each node in the construction graph represents an encoded value for a specific parameter. Once a single ant's path through the two branching layers is complete, it yields a candidate set of values (Kp, Ki, Kpp, Kd). During the iterative process of the algorithm, pheromone levels on the graph's edges are updated so that better parameter combinations become increasingly likely, guiding convergence toward the optimal set of parameters.

Regarding the modified Figure III.11 for MPID: The figure presents each branching layer as a set of nodes, where each node denotes an encoded value for a given parameter. Multiple connecting edges indicate the possible transitions ants can take when selecting parameter values.

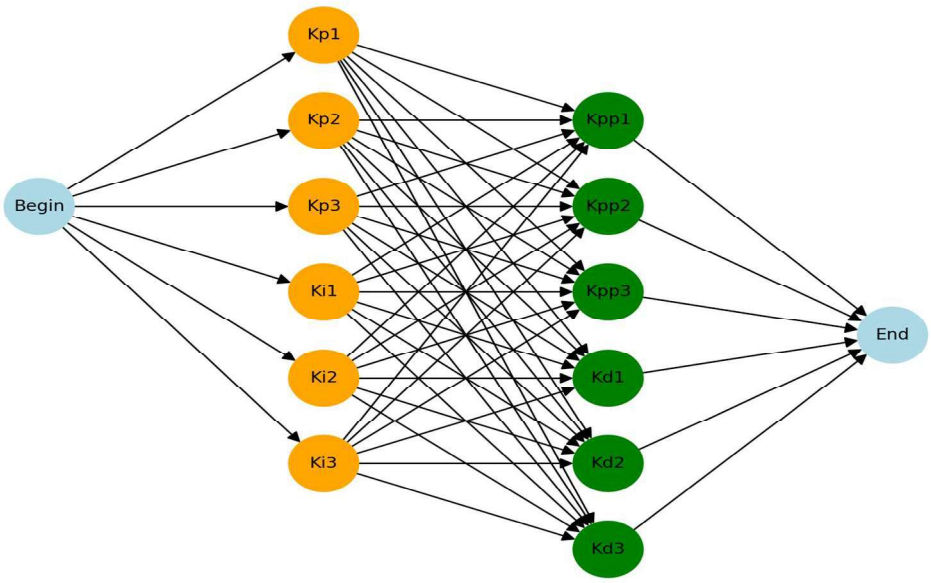

Figure III.11: Construction graph for MPID optimization n values per parameter

To learn more about the ACO and how to tune MPID parameters, we will explain it in detail, step by step:

Step 1: Initialization

1- Defining the System to be Controlled

The Transfer Function (TF) of the system to be tuned is specified.

2- Initializing the Ant Colony

- Define the number of ants (num Ants), representing the number of candidate solutions explored in each iteration.
- Define the number of iterations (num Iterations), which determines how many rounds the algorithm will execute to find the optimal values.
- Set the initial pheromone levels so that all paths have equal probability at the start.

3- Initialize the ACO parameters:

α: Controls the influence of previous pheromone levels on the selection of new values.

β: Controls the influence of heuristic information (newly discovered values).

ρ: Evaporation rate of pheromones.

Q: Reinforcement factor applied to solutions that improve system performance.

Step 2: Generating Initial Random Solutions

Different sets of values (Kp, Ki, Kd and Kpp) are randomly generated within the defined limits. Each ant selects MPID values randomly.

Step 3: Evaluating the Performance of Each Solution

1- Create an MPID controller for each ant; the controller is defined as a transfer function.

2- Analyze the closed-loop system response by closing the feedback loop between the controller and the system to obtain the actual response.

3- Calculate the objective function (Integral of Time-weighted Absolute Error – ITAE) to evaluate solution quality.

Step 4: Pheromone Update

1- Evaporation: Reduce the influence of old pheromones for all paths using an evaporation formula.

2- Reinforcement: Add new pheromone amounts to paths that result in better performance.

Step 5: Iterative Optimization

Select new values for MPID parameters and repeat the process for a set number of iterations.

Step 6: Extracting Results and Visualization

Print the best discovered MPID values. At the end of the iterations, the optimal values found are printed.

After reviewing the steps of the ACO algorithm in tuning the MPID parameters, the diagram below summarizes the entire process clearly.

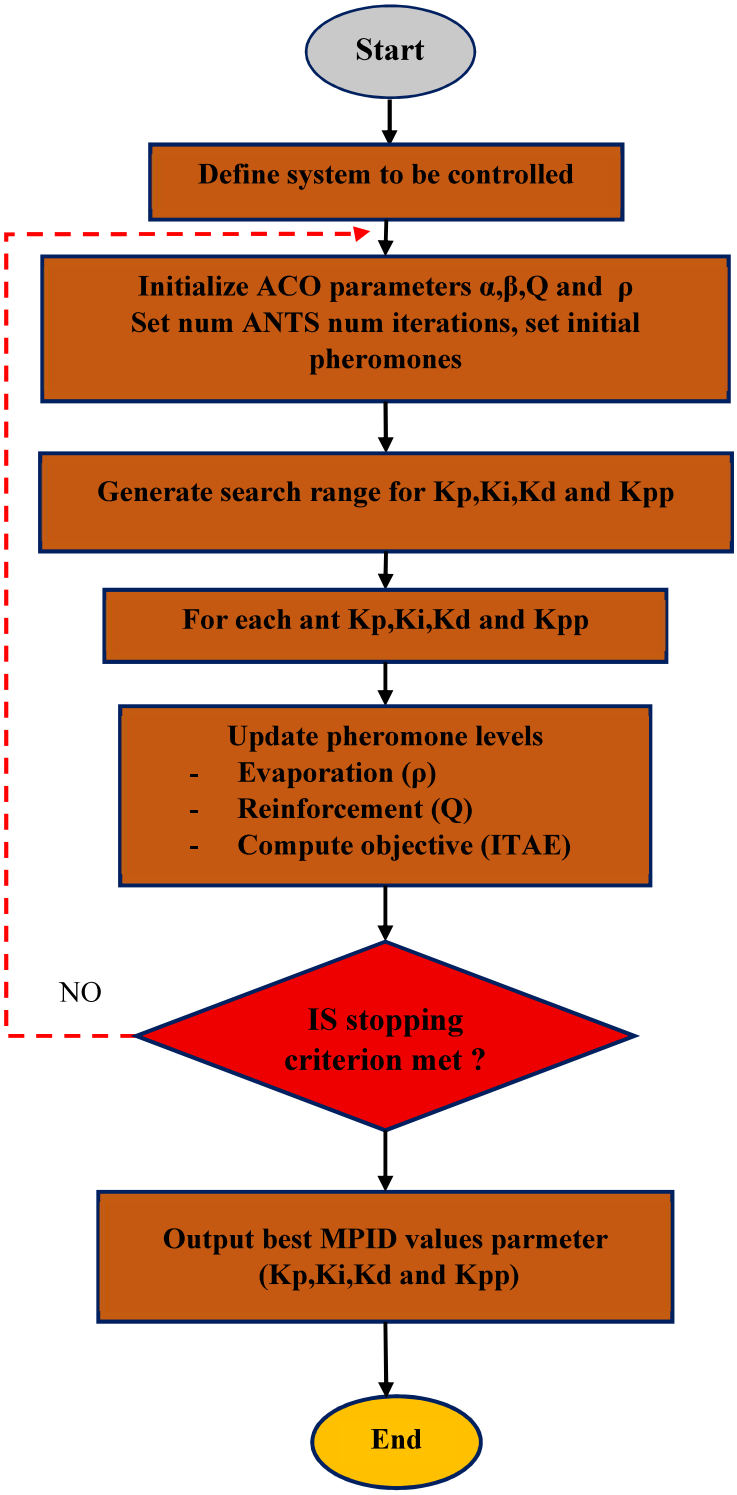

Figure III.12: Flowchart of ACO algorithm.

III.5. Simulation Results and Discussion

This section presents the simulation of a microgrid system connected to multiple energy sources, including electric vehicle batteries, using two types of controllers: the conventional PID controller and MPID controller. The parameters of both controllers were tuned using a set of advanced optimization algorithms, with the aim of providing a comprehensive comparison

of their performance in reducing frequency deviation and enhancing system stability under different operating conditions.

I have relied in this thesis on the ITAE index (Integral of Time multiplied by Absolute Error), which is defined as the time integral of the absolute value of the error multiplied by time, as shown in equation (III.34). This index gives greater weight to sustained and delayed errors. Its importance lies in its ability to evaluate the dynamic performance of the microgrid system by focusing on measuring the speed of response in reducing long-term oscillations and seeking effective solutions. Accordingly, the ITAE index was used as a fundamental criterion for comparing the simulation results of frequency deviation in the microgrid system, with the aim of determining the effectiveness of different tuning methods in enhancing system stability.

$$ITAE = \frac{1}{T}\int |e(t)|\mathrm{dt} \qquad \text{(III.34)}$$

In terms of the number of iterations, we write:

$$ITAE = \sum_{k=0}^{n} t_k |e(k)|\,\Delta t \qquad \text{(III.35)}$$

Where:e[k]: the error at sample ,k (e.g., Δf[k] for frequency deviation).T_k: the sampling time. N: the number of iterations until the end of the simulation.

The simulations were carried out using the MATLAB Simulink 2023 environment, and Figure III.13 illustrates the connection between the Simulink–MATLAB simulation environment and the MATLAB workspace.

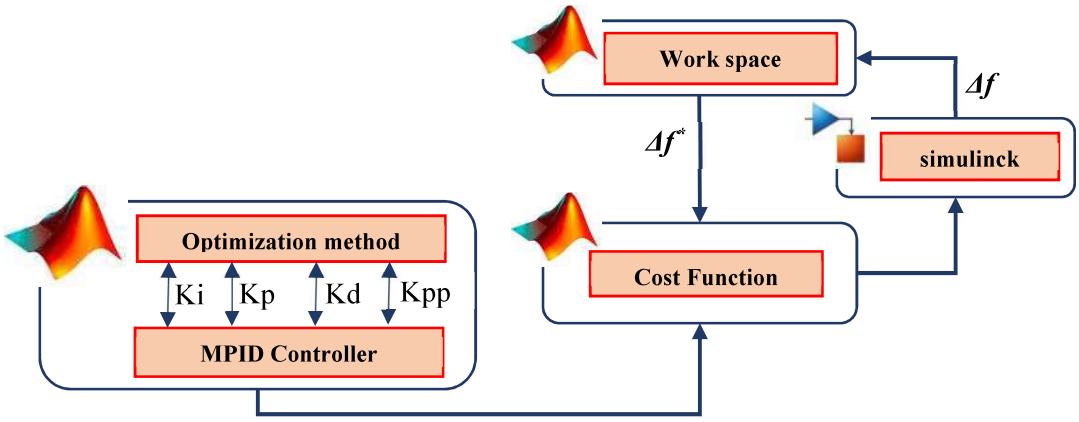

Figure III.13: Flowchart showing the interaction between MATLAB Simulink and the workspace for setting the frequency deviation parameter in the objective function

I divide the simulation into two main parts: the first focuses on using optimization methods, while the second applies the optimization algorithm to tune the MPID controller parameters. This division aims to organize the work and clarify the differences between the two approaches.

The first part: In this section, the focus is on using optimization methods to tune the MPID controller parameters. Two different methods have been used for this tuning, and a set of scenarios will be implemented to test the MPID controller's ability to reduce frequency deviation. These scenarios are divided as follows:

Scenario I: The MPID controller parameters will be tuned using both the Ziegler Nichols method and the CDM method.

Case 1: Effect of CDM parameter constants on the frequency deviation performance of an MPID-controlled microgrid system.

Based on the stability conditions established for the CDM method discussed earlier in this study, additional calculations were carried out to derive new coefficient values for controlling the operation of the MPID controller. All constants defined by Manabe were adopted, except for the parameter Υ_2, which was modified as presented in Table III.2. The obtained results clearly showed a notable impact on the Δf.

This stage aims to demonstrate the effectiveness of the CDM method in ensuring system stability and in determining its optimal settings. The approach relied on Manabe's findings regarding the constants of a system equation related to the distortion ratio and settling time, with carefully introduced changes to one of these parameters. As illustrated in Figure III.13 and supported by previous studies, modifying the CDM parameters directly affects the overshoot ratio in the response. Figure III.14 shows that selecting $\Upsilon_2 = 1.4$ produced a favorable system response compared to other values, although it led to an increase in the settling time. Conversely, setting $\Upsilon_2 = 2.9$ increased the overshoot ratio but helped reduce the settling time. Based on these observations, the CDM method can be considered an effective choice for studies seeking to balance settling time and distortion ratio, whether by prioritizing one over the other or by considering both simultaneously.

Table III.2: Performance measurement coefficients MPID-CDM against variation .

Υ_2	Ki	Kp	Kd	Kpp
1.4	2.62238	2.3051	0.8785	0.8873
2.2	3.7182	1.4362	0.3836	0.9013
2.9	4.42	1.1478	0.1	1.023

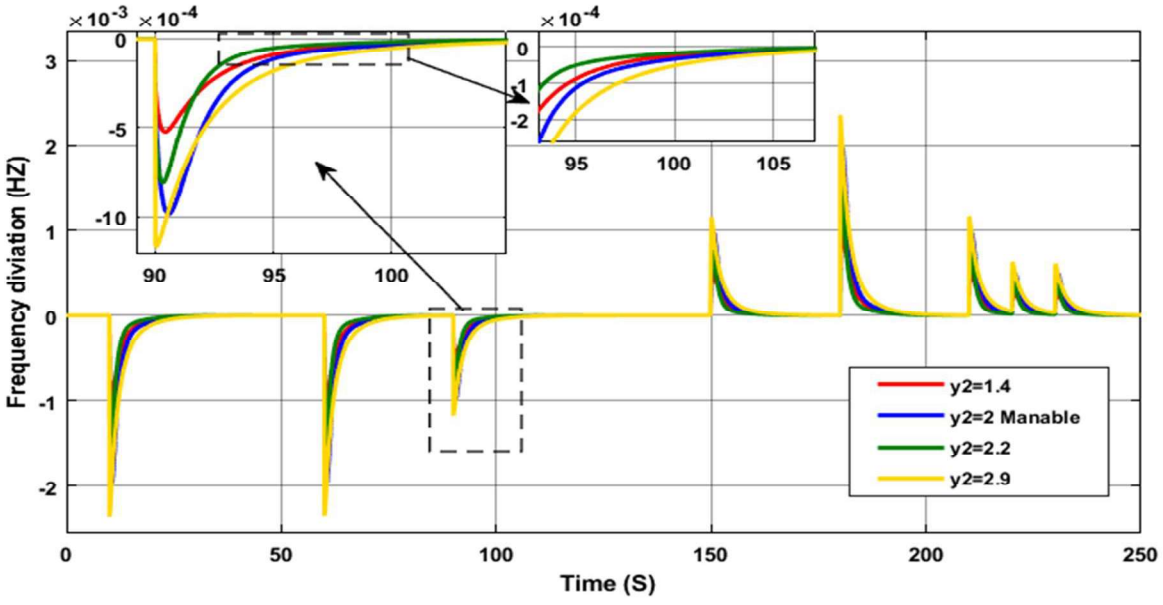

Figure III.14: Frequency deviation response under different Υ_2 values using the CDM–MPID approach

The figure III.14 illustrates the effect of changing the Υ_2 value on the system's frequency deviation response when using the CDM method with the MPID controller. It can be observed that when $\Upsilon_2 = 1.4$ (red line), the overshoot is significantly reduced compared to other values, although the settling time is longer. In contrast, increasing Υ_2 to 2.9 (yellow line) results in a higher overshoot but a shorter settling time. The reference value $\Upsilon_2 = 2$ set by Manabe (blue line) provides an intermediate performance between the two cases, while $\Upsilon_2 = 2.2$ (green line) offers a relative balance between overshoot and settling time. This analysis highlights the critical role of the Υ_2 parameter in optimizing system performance according to operational requirements.

Case 2: We tested the MPID controller with the Ziegler–Nichols method after optimizing the Kpp value.

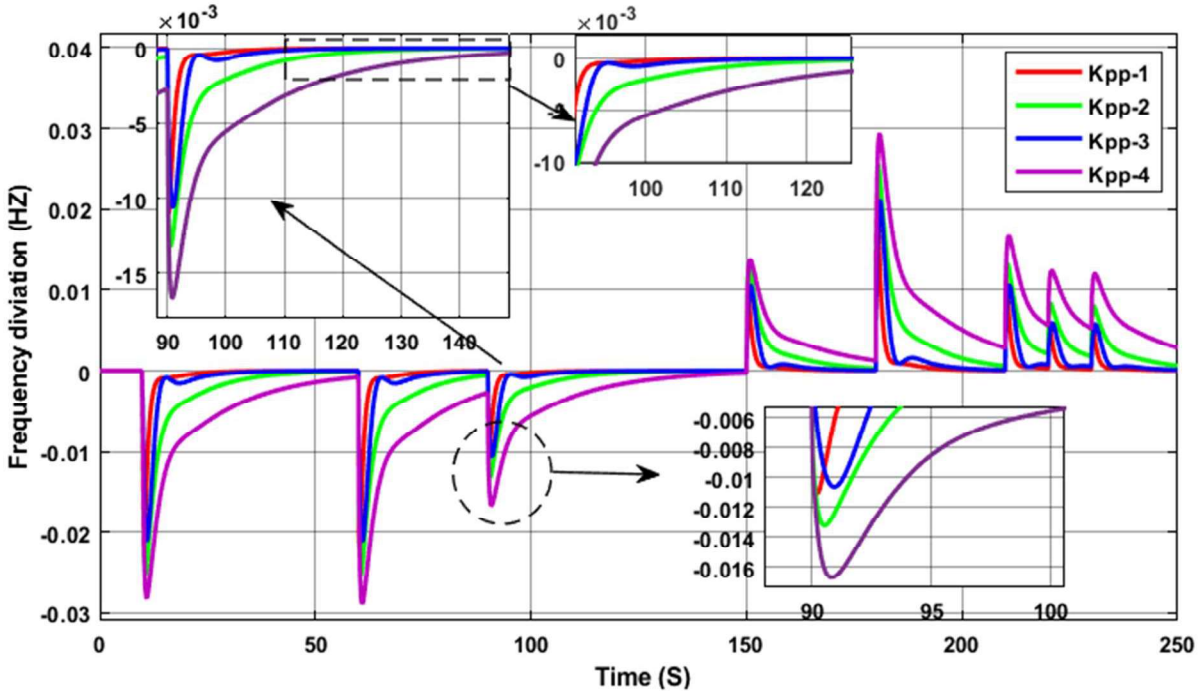

Figure III.15: Impact of Kpp optimization on the Δf response of the microgrid system.

Figure III.15 illustrates the effect of optimizing the Kpp value on controlling the Δf of the microgrid system. The results show that varying Kpp has a significant impact on system stability, either by reducing disturbances or by accelerating the settling process. For instance, at a certain value such as (Kpp2), the positive peak deviation increases compared to the other values, indicating higher sensitivity of the response. In contrast, other values such as (Kpp1 and Kpp3) reduce the deviation magnitude and provide a smoother response. The zoomed-in section further highlights the influence of Kpp during critical moments, where stabilization is achieved with noticeable differences in damping speed. Overall, optimizing the Kpp value after applying the ZN method enhances the system's performance by improving stability and reducing frequency deviation, while enabling the selection of the optimal value that balances fast response with minimal oscillations.

Scenario II: we focus on comparing the classical PID controller and the MPID controller using the CDM and ZN methodes, by controlling the Δf of the microgrid system under load variation, as shown in Figure III.16. As illustrated in Figure III.17 and Figure III.18, the graph shows the frequency deviation response of the system when controlled using these different methods

under various loading conditions (ΔP_L), while Table III.3 presents the percentage change in the ITAE value for each meth Table III.5 Optimal parameters of the PID and MPID controllers-based CDM and ZN,

Table III.3: Optimal parameters of the MPID and PID controller-based CDM and ZN

Methods	Optimized gains			
	KP	KI	KD	KPP
CDM – MPID	1.2807	4.5407	0.5212	0.987
CDM – PID	0.5496	3.4514	0.1368	-
ZN-MPID	3.601	3.6	0.9	0.1
ZN-PID	2.2971	3.594	2.87	-

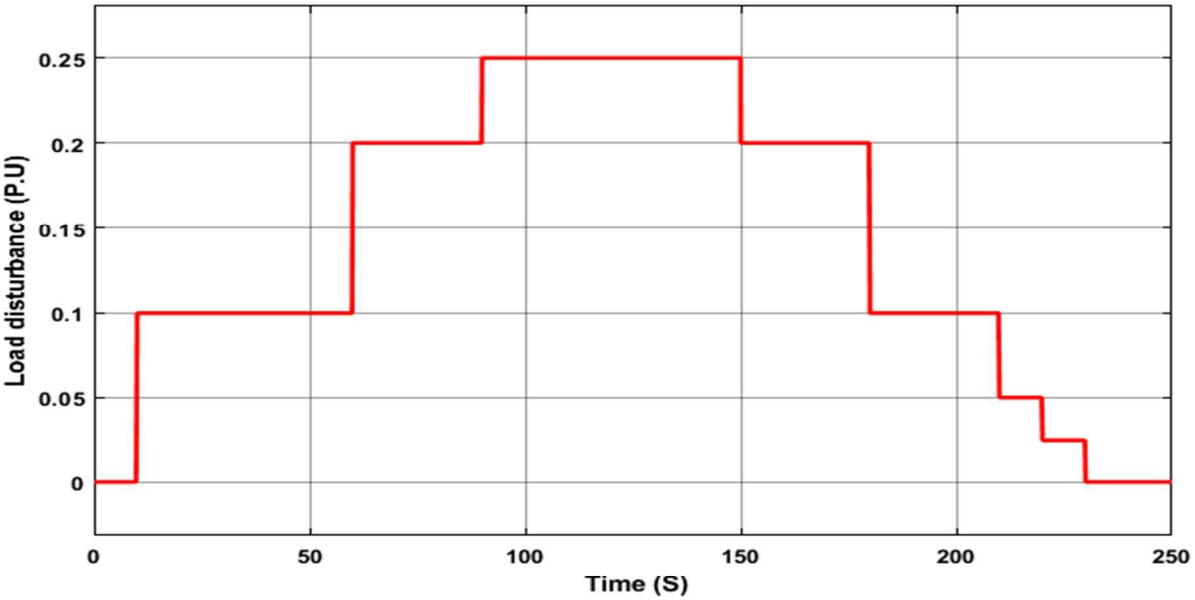

Figure III.16: Multistep load disturbances in MG

Table III.4: Comparison of the performance indicators of PID, MPID controllers using ZN and CDM

Methods	Performance Indices			
	Peak undershoot (HZ)	Peak Overshoot (HZ)	Settling Time (S)	ITAE
ZN- PID	-0.007498	0.00264	19s	0.01736
CDM - PID	-0.001592	0.000075	16S	0.000534
ZN - MPID	-0.003328	0	8S	0.00711
CDM - MPID	-0.00178	0	7S	0.000138

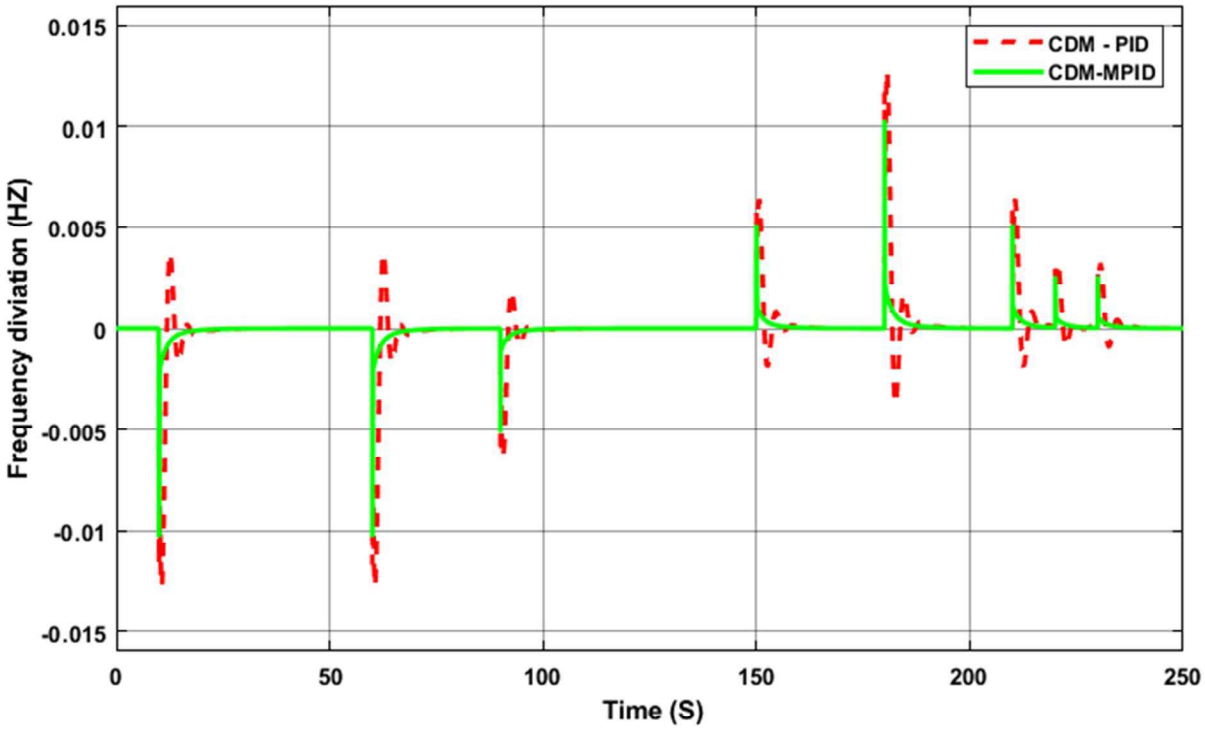

Figure III.17: Δf dynamic response of PID and MPID controller based on CDM

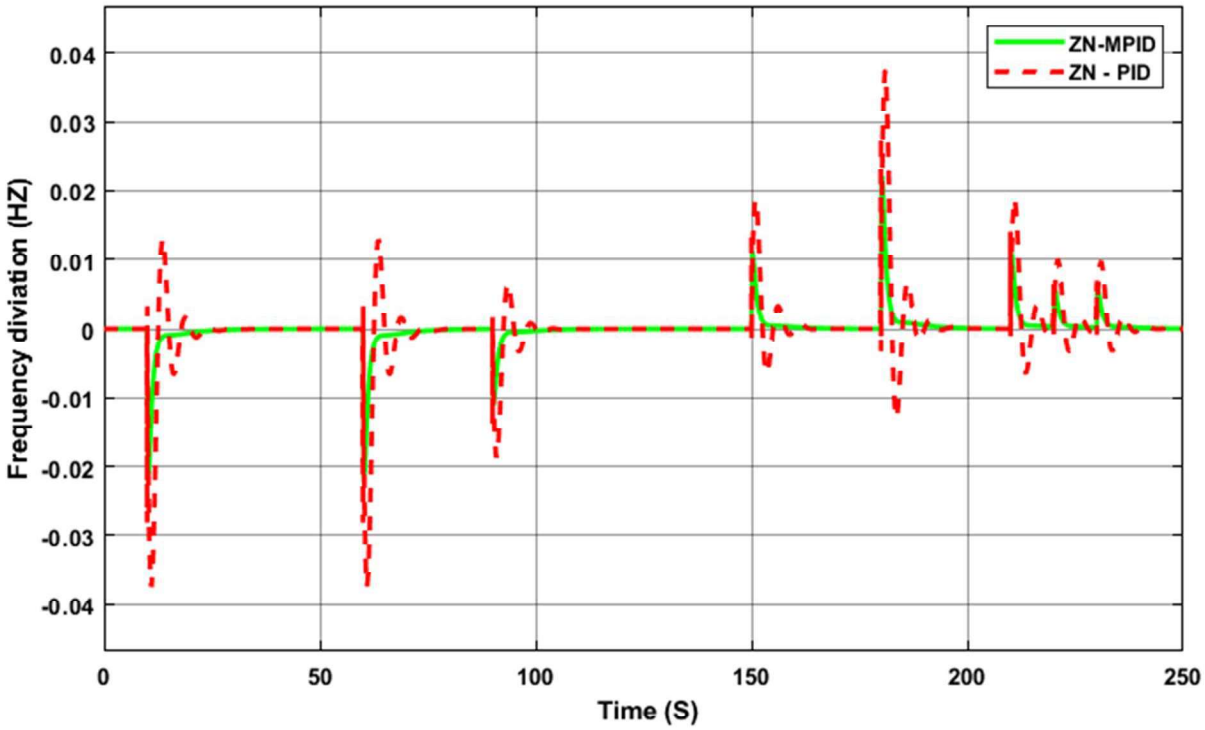

Figure III.18: Frequency perturbation dynamic response of PID and MPID controller based on ZN

The results indicate that employing the MPID controller yields the best dynamic performance in reducing Δf in the microgrid system, particularly when its parameters are tuned using the CDM method, achieving zero overshoot, a settling time of 7 seconds, and the lowest ITAE value of 0.000138. Moreover, using CDM with a PID controller significantly improves performance compared to ZN tuning, especially in reducing overshoot and ITAE. In contrast, switching from PID to MPID even with ZN tuning demonstrates a noticeable reduction of the positive peak to zero and a shorter settling time. Although CDM-MPID shows a slight increase in the negative peak compared to CDM-PID, the improvements in overall quality metrics (settling time and ITAE) make CDM-MPID the optimal choice for controlling frequency oscillations under load disturbances.

Scenario III: The MPID controller was tested under a set of potential disturbances affecting the microgrid system, along with a comparison between the CDM and ZN methods. The MG frequency deviation (Δf) was simulated under various operating conditions as follows:

Case 1: The MG is subjected to the load change (ΔPL) shown in Figure III.15, with the resulting frequency deviation (Δf) illustrated in Figure III.19.

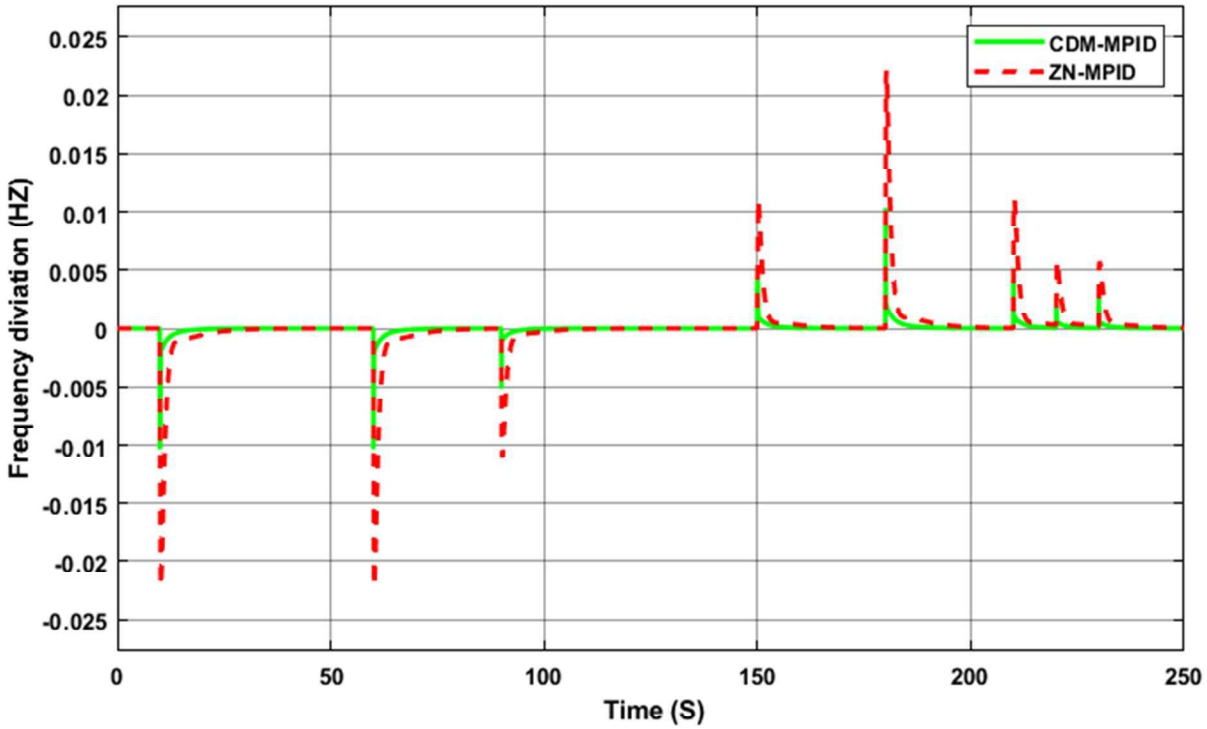

Figure III.19: Δf dynamic response of MPID controller based on CDM and ZN methods.

Case 2*:* The MG is subjected solely to solar power disturbances (ΔP_{PV}) as depicted in Figure III.20, while the resulting frequency deviation (Δf) is illustrated in Figure III.21.

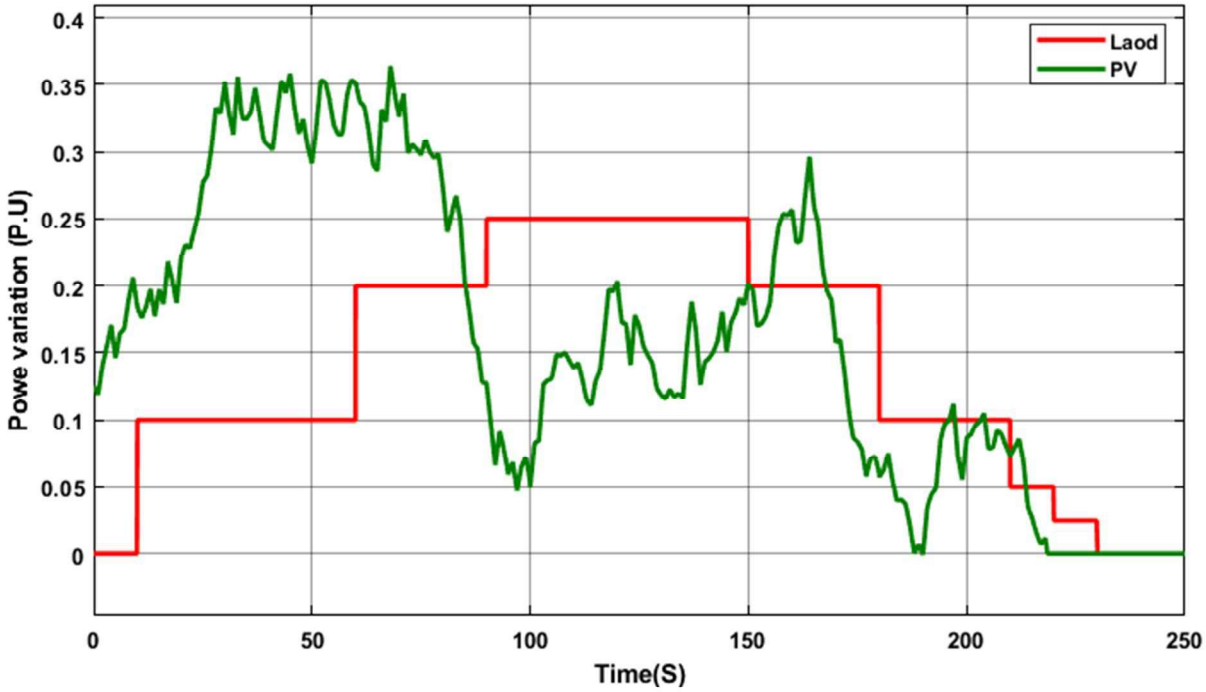

Figure III.20: Graphic of load and solar power variation

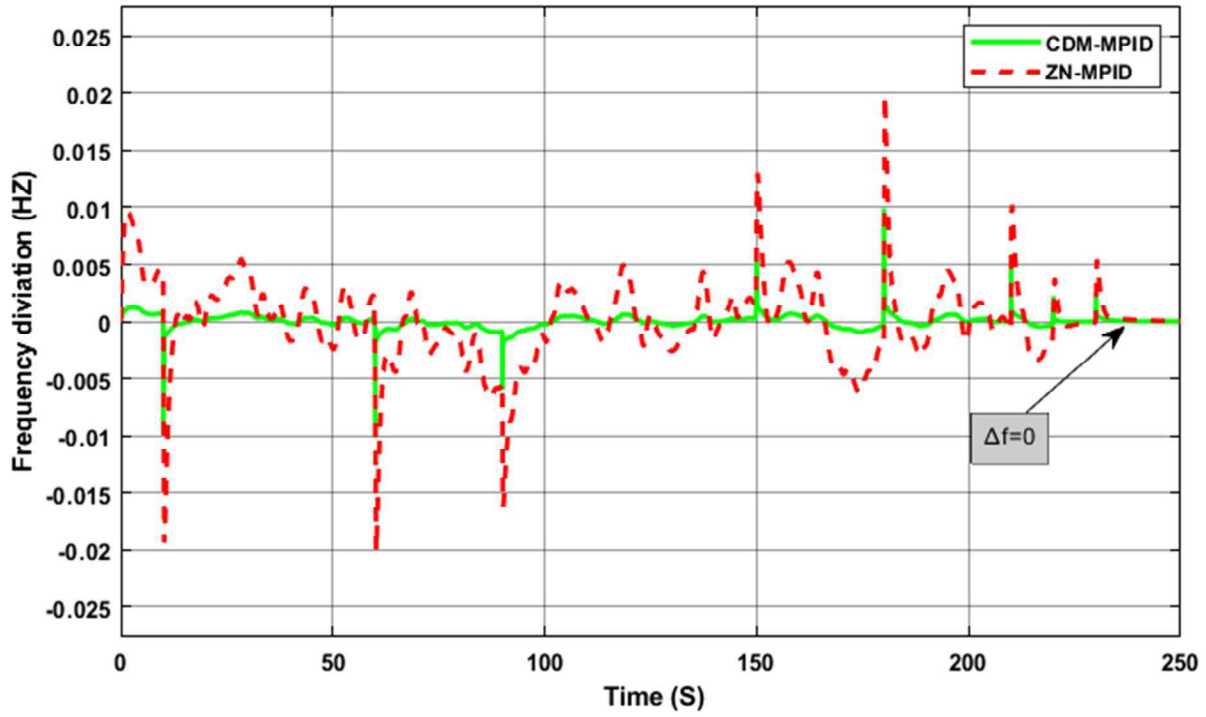

Figure III.21: Frequency response of MG against PV power variations

Case 3: The MG is subjected solely to wind power disturbances (ΔP_{wind}) as depicted in Figure III.22, while the resulting frequency deviation (Δf) is illustrated in Figure III.23.

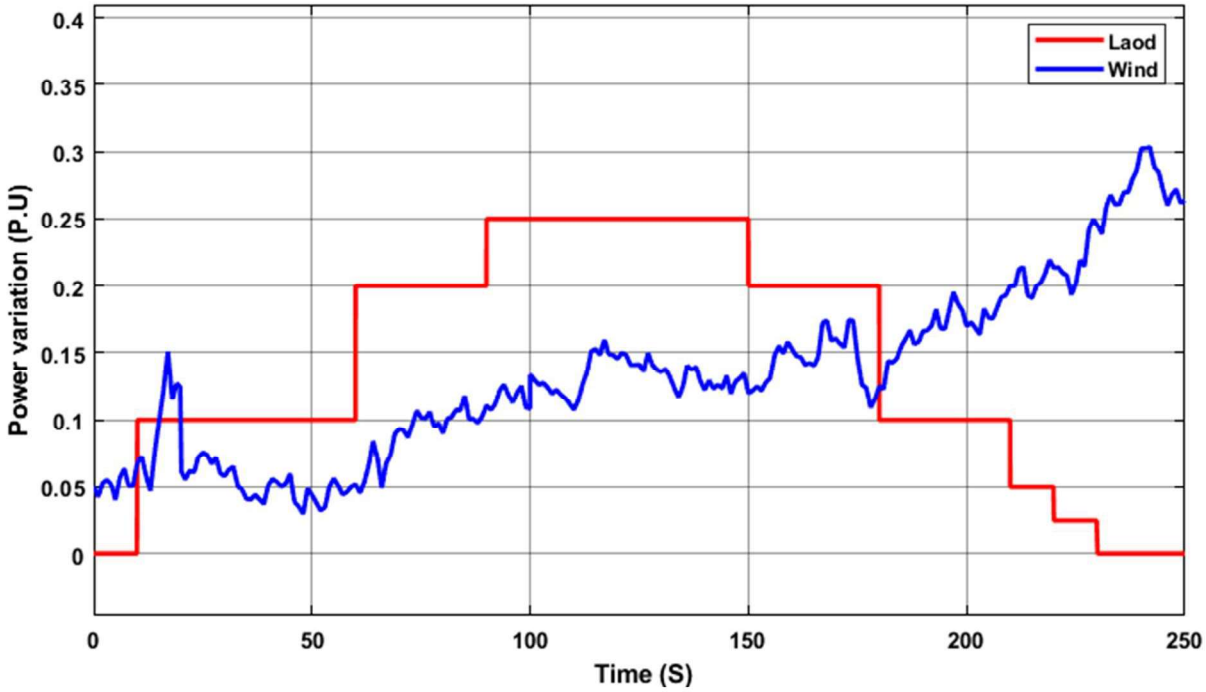

Figure III.22: Graphic of load and wind power variation

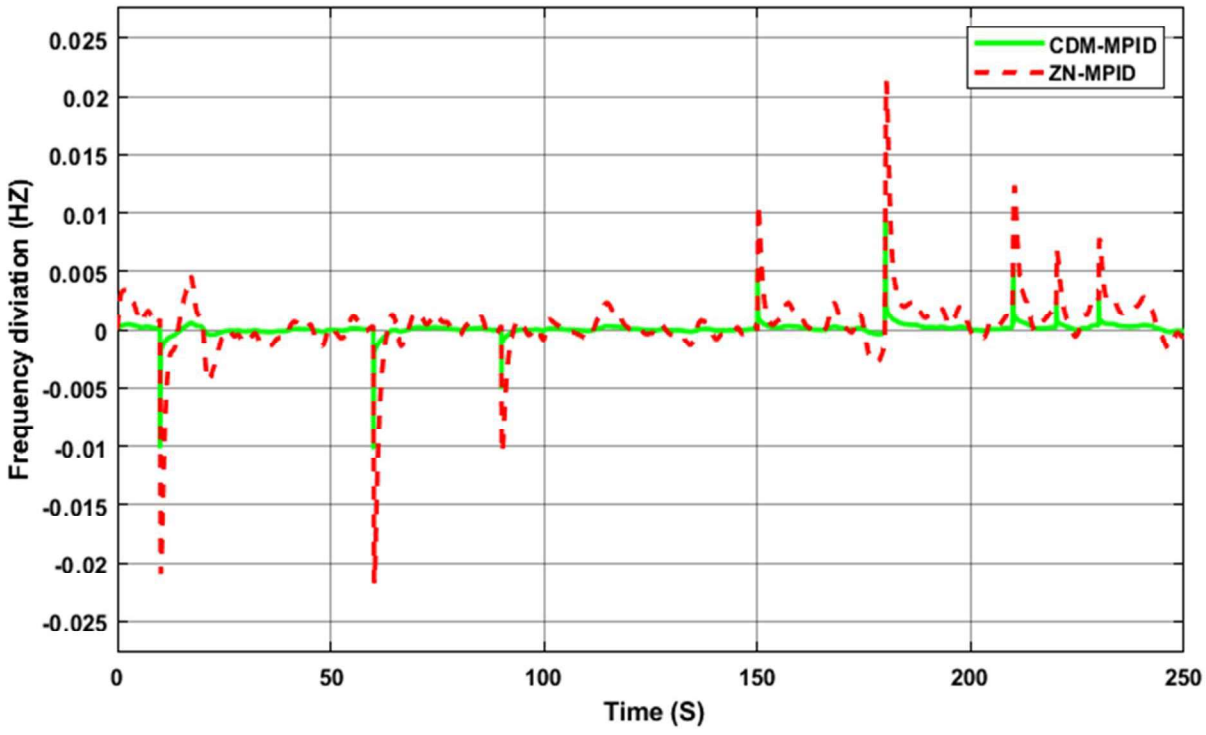

Figure III.23: Frequency response of MG against Wind power variations

Case 4: The MG is subjected to wind power disturbances (ΔPwind) and solar power disturbances (ΔP_{PV}) depicted in Figure III.24, while the resulting frequency deviation (Δf) is illustrated in Figure III.25.

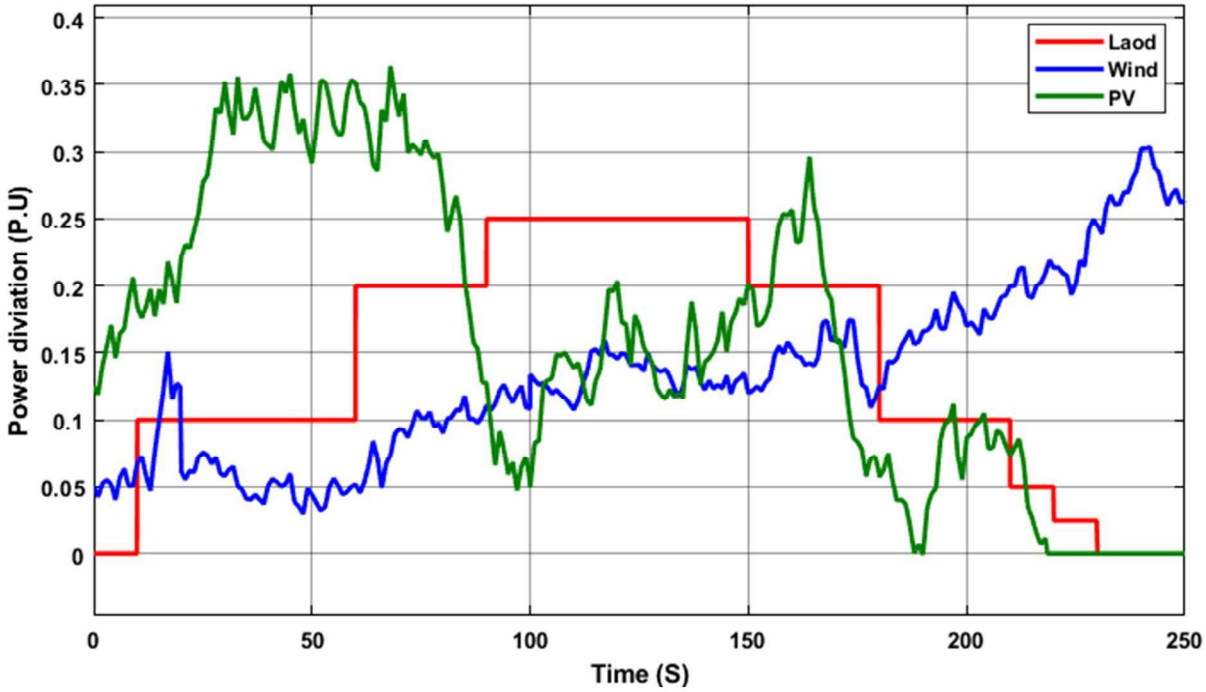

Figure III.24: Graphic of load, wind and PV power variation

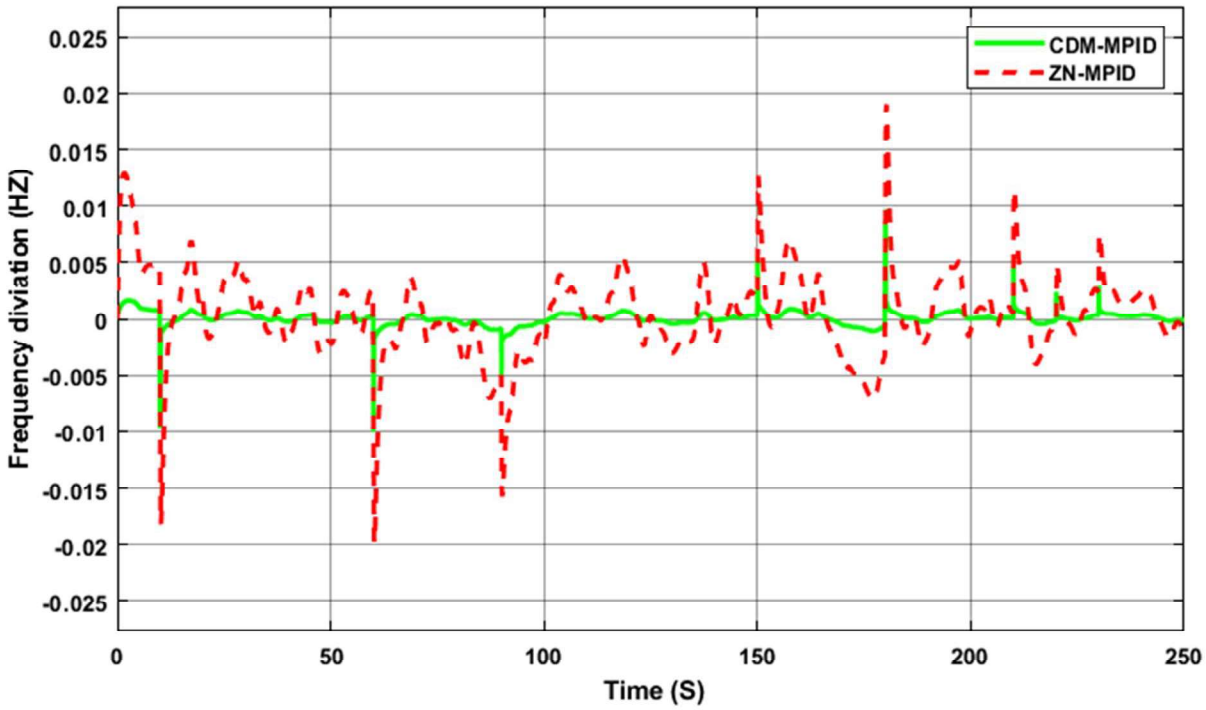

Figure III.25: Frequency response of MG against PV power variations, Wind power variations and multi-step load disturbance

Table III.5: Performance evaluation of CDM-MPID and ZN-MPID controllers.

Cases	Methods	Performance Indices			
		Undershoot (Hz)	Overshoot (Hz)	Peak	ITAE
Case 1	ZN- MPID	-0.0223	0	0.0013	0.0000757
	CDM –MPID	-0.0056	0	0.00014	0.0000307
Case 2	ZN- MPID	-0.0194	0.0246	0.0044	0.00026
	CDM –MPID	-0.00907	0.00049	0.0009	0.00007
Case 3	ZN- MPID	-0.02405	0.00327	0.0043	0.00036
	CDM –MPID	-0.009719	0.000901	0.000905	0.000959
Case 4	ZN – MPID	-0.019	0.0207	0.0087	0.000374
	CDM –MPID	-0.0096	0.01204	0.00019	0.0000425

The Figure III.19 , Figure III.21, Figure III.23, Figure III.25 and the table III.5 together provide a comprehensive view of the MPID controller performance when tuned using Ziegler–Nichols (ZN) and CDM methods under different disturbance conditions. The figures illustrate the frequency deviation response of the system in four cases: load variations only, solar power fluctuations, wind power fluctuations, and the combined case of solar and wind power. It is evident that the CDM-MPID controller ensures a more stable response by reducing oscillations and deviations compared to the ZN-MPID in all scenarios, while also accelerating the return of frequency to its reference value. The table III.5 confirms these observations through the quantitative values of performance indices (Undershoot, Overshoot, Peak, ITAE), where the CDM-MPID consistently achieves lower values, reflecting improved dynamic performance and faster stabilization in both short-term and long-term behavior. Overall, the simulation results demonstrate that tuning the MPID controller using the CDM method significantly enhances microgrid stability and efficiency in handling complex and combined renewable energy variations while maintaining frequency stability and reliable operation.

The second part: **the parameters of the MPID controller were optimized using modern optimization algorithms, and several scenarios were conducted to evaluate its effectiveness in minimizing frequency deviation.**

Scenario I: The MPID controller parameters will be tuned using both the ACO algorithm and the CSA algorithm.

Case 1: Impact of ACO parameter tuning on the frequency deviation response of the microgrid system with MPID control.

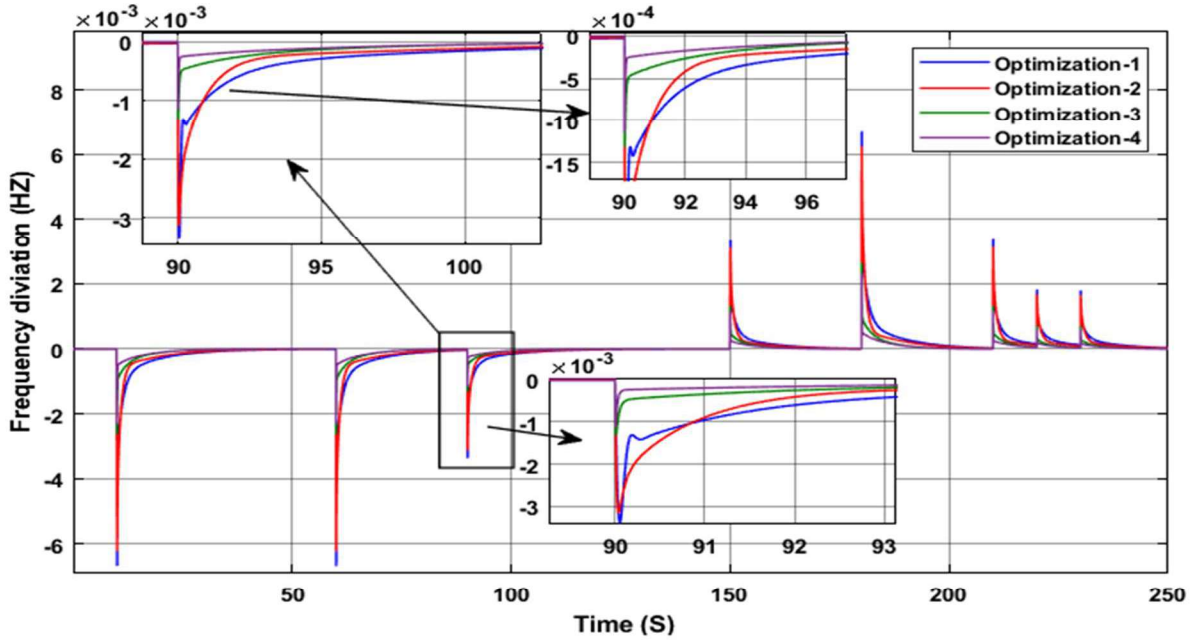

Figure III.26: Δf of the MG under different ACO parameter tuning strategies using the MPID controller.

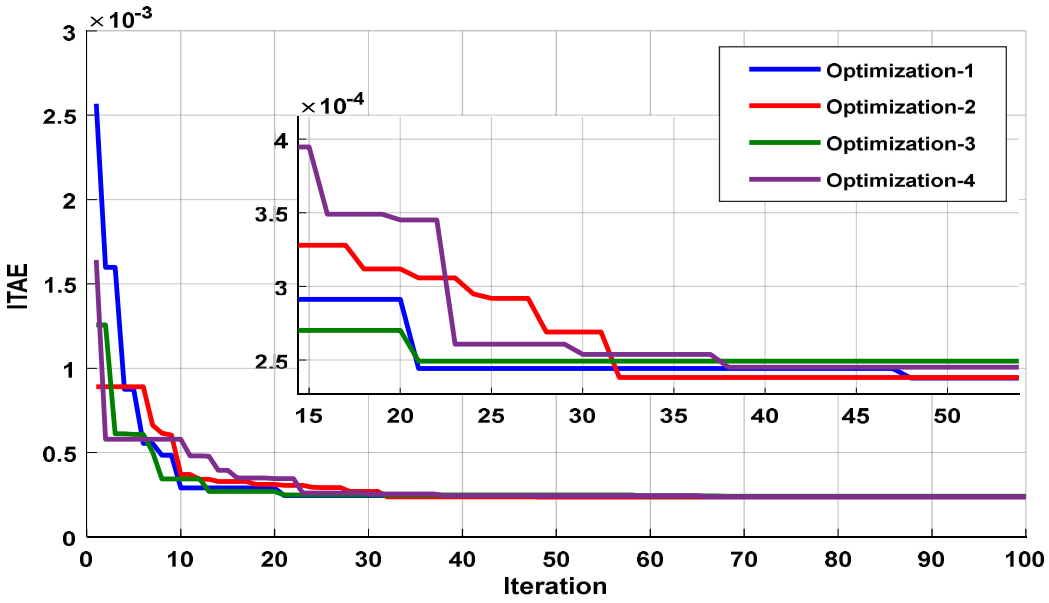

Figure III.27: Convergence over iterations for different ACO parameter tuning strategies

The results obtained in Figures III.26 and III.27 demonstrate that tuning the parameters of the ACO algorithm has a direct impact on the performance of the MPID controller in reducing frequency deviation within the microgrid system. From Figure 5, it can be observed that all tuning strategies reduced the frequency deviation following the load change, as illustrated in Figure III.15. However, Optimization-2 exhibited the best response in terms of faster settling time and lower overshoot compared to the other methods, while Optimization-1 was relatively slower in reaching steady state. Figure III.26 highlights the convergence process of the algorithm, where it is evident that Optimization-2 achieved the fastest and most accurate convergence toward the optimal solution, whereas Optimization-4 remained at higher values, which negatively affected its performance. Therefore, it can be concluded that selecting appropriate parameters for the ACO algorithm significantly enhances the performance of the

MPID controller by reducing oscillations and settling time, ensuring a more reliable system response.

Case 2*:* Impact of CSA parameter tuning on the frequency deviation response of the microgrid system with MPID control.

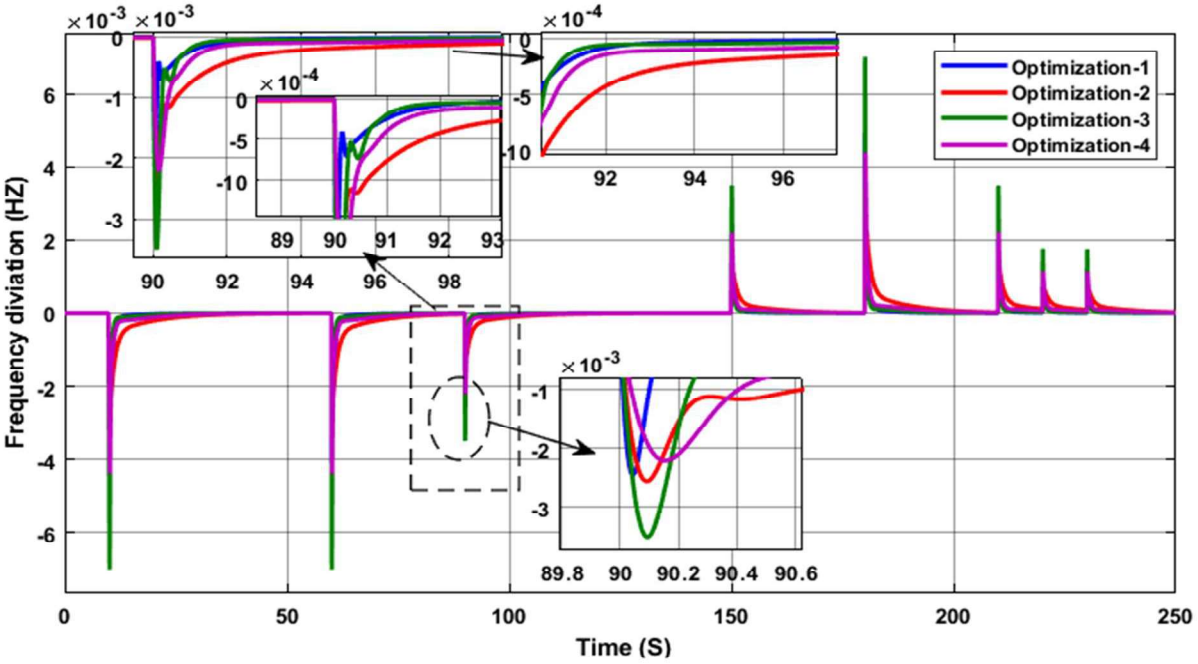

Figure III.28: Δf of the MG under different CSA parameter tuning strategies using the MPID controller.

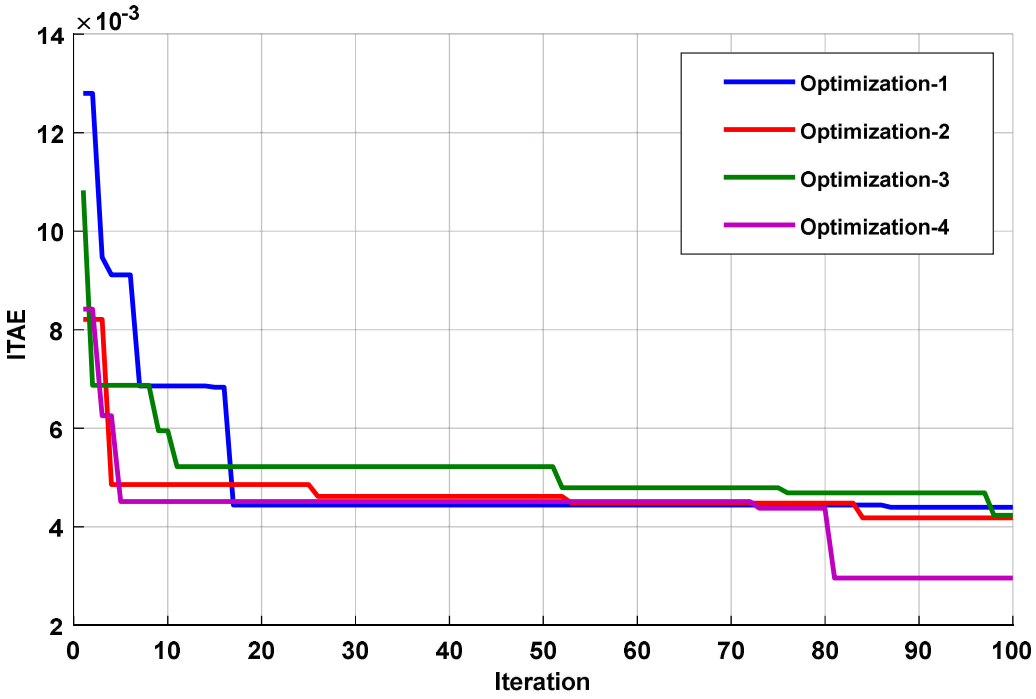

Figure III.29: Convergence over iterations for different CSA parameter tuning strategies

Figure III.28 illustrates the response of the microgrid system in controlling frequency deviation by tuning the MPID controller parameters using the CSA algorithm with four different optimization strategies. The results demonstrate the crucial role and effectiveness of

proper CSA parameter tuning, showing that Optimization-4 achieved the best performance in terms of reaching the lowest deviation value. This impact is clearly reflected in the frequency deviation response, where optimal tuning contributed to reducing the deviation magnitude, accelerating the stabilization process, and minimizing oscillations, as well as attaining the lowest ITAE value, as shown in Figure III.29. Although Optimization-2 exhibited a faster initial response, Optimization-4 achieved better long-term stability. These findings highlight that the choice of optimization strategy within CSA plays a key role in enhancing control efficiency and achieving a balance between response speed and system stability.

Scenario II: We focus on a comparative analysis between the classical PID controller and the MPID controller, optimized using the ACO and CSA algorithms, for regulating the Δf of the microgrid system under load variations, as illustrated in Figure III.16. Table III.6 summarizes the optimal parameters obtained for both PID and MPID controllers using the CSA and ACO algorithms. Figures III.30 and III.31 present the system's frequency deviation response under different control strategies and varying load conditions (ΔPL). Furthermore, Figure III.32,III.33 and Table III.4 highlight the percentage variation in ITAE for each method.

Table III.6: Optimal parameters of the MPID and PID controller-based CDM and ZN

Methods	Optimized gains			
	KP	KI	KD	KPP
ACO – MPID	1.2807	4.5407	0.5212	0.987
ACO– PID	0.5496	3.4514	0.1368	-
CSA-MPID	3.601	3.6	0.9	0.1
CSA-PID	2.2971	3.594	2.87	-

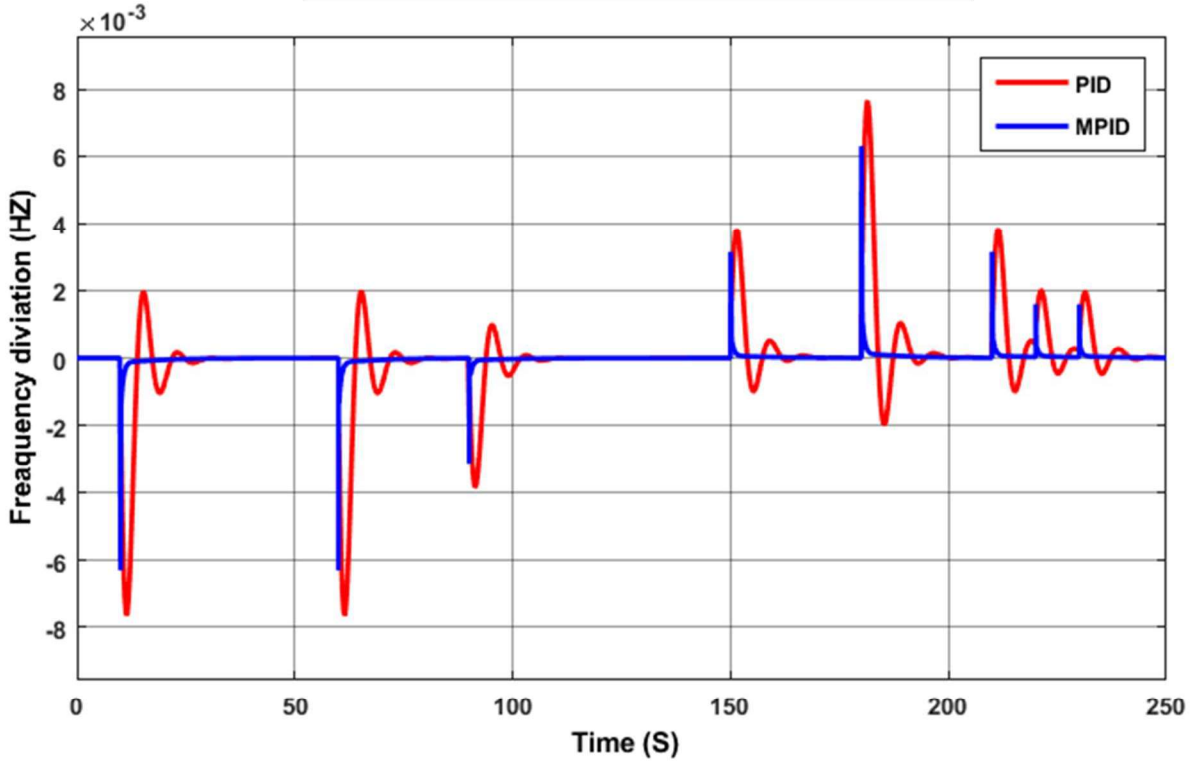

Figure III.30: Δf dynamic response of PID and MPID controller based on ACO

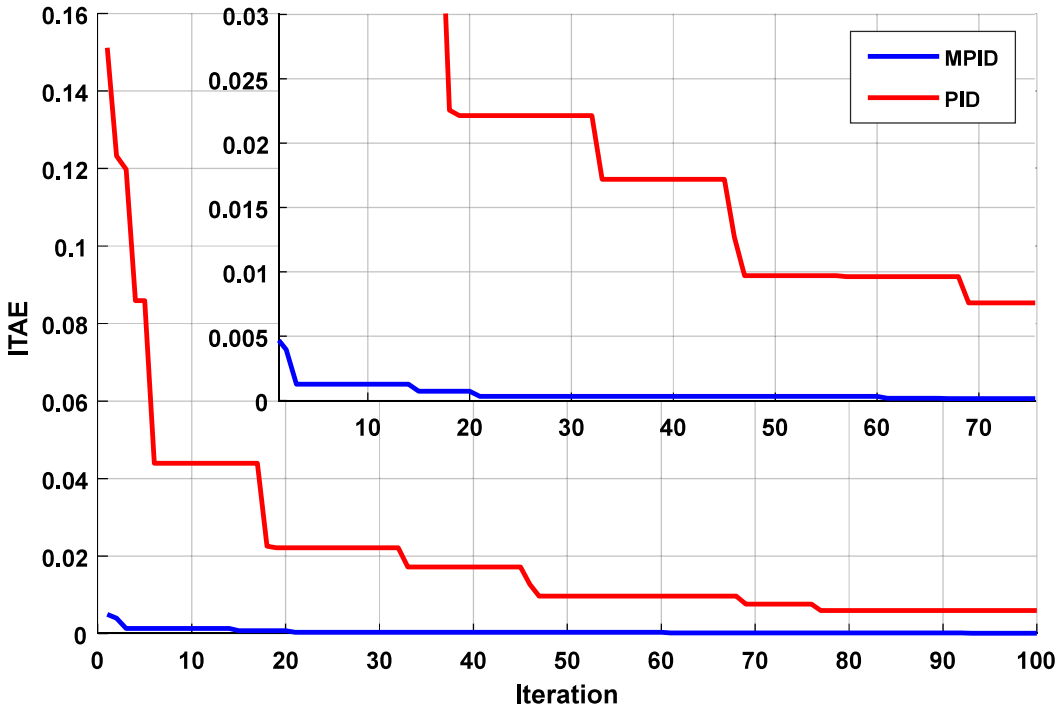

Figure III.31: Convergence behavior across iterations under various ACO parameter tuning strategies

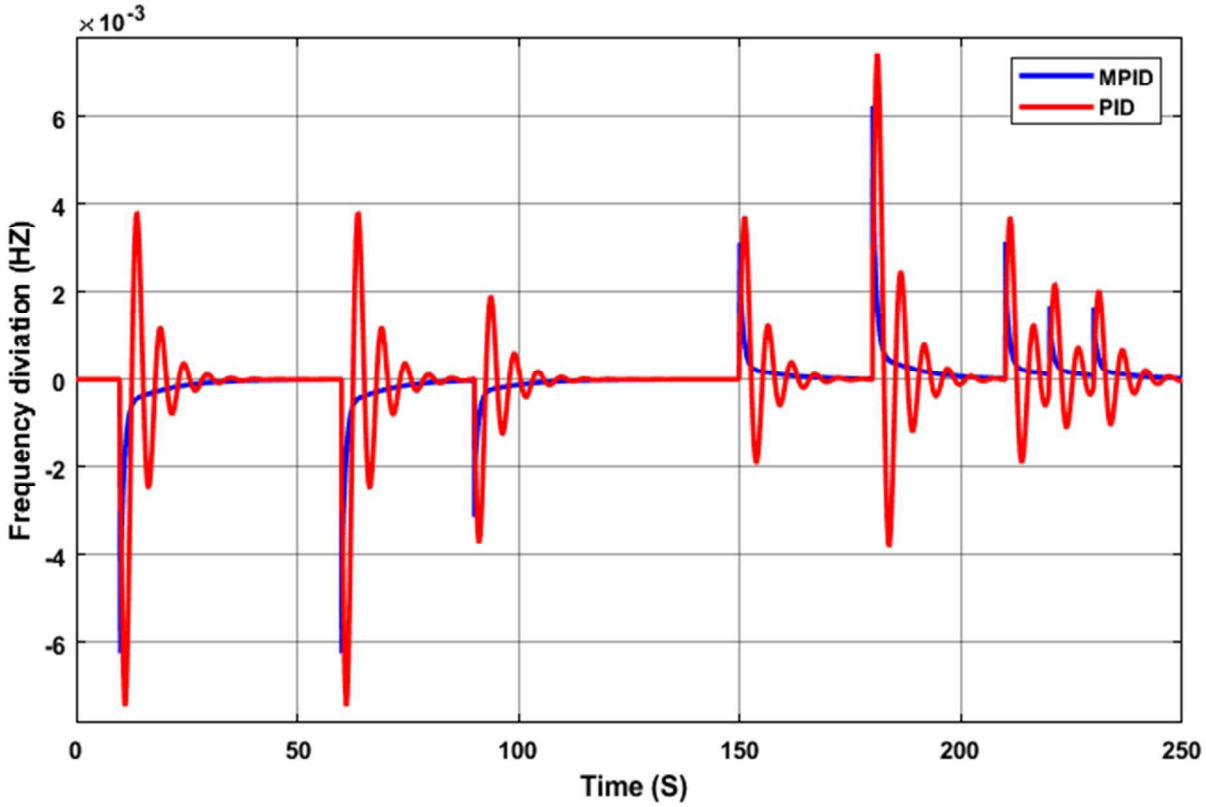

Figure III.32: Δf dynamic response of PID and MPID controller based on CSA

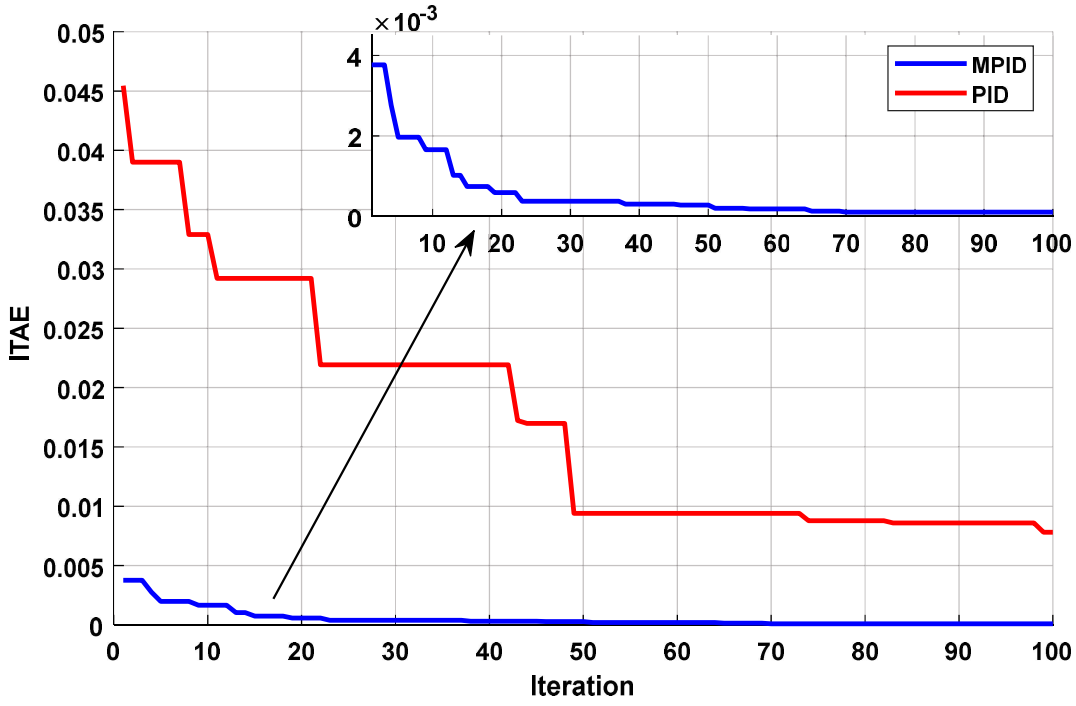

Figure III.33: Convergence behavior across iterations under various ACO parameter tuning strategies

Table III.7: Comparison of the performance indicators of PID, MPID controllers using ACO and CSA

Methods	Performance Indices			
	Peak undershoot (HZ)	Peak Overshoot (HZ)	Settling Time (S)	ITAE
ACO- PID	-0.00798	0.00264	25s	0.007
CSA - PID	-0.00792	0.00475	18S	0.009
ACO - MPID	-0.006128	0	6S	0.000711
CSA- MPID	-0.00678	0	9S	0.000138

The results presented in Figures (III.30, III.31, III.32 and III.33) clearly demonstrate the superiority of the MPID controller over the classical PID controller, despite employing two different optimization algorithms, CSA and ACO. The system's response with the PID controller exhibited significant deviations and frequent oscillations under disturbances, with deviation values reaching relatively high levels, highlighting its limited ability to maintain frequency stability. In contrast, the MPID controller delivered a more stable response, significantly reducing frequency deviations and accelerating the system's return to the reference value with minimal oscillations.

Furthermore, Figures (III.31 and III.33) clearly illustrate the difference in performance criteria, where the error with PID remained relatively high despite a gradual decrease, while MPID rapidly reached an almost negligible error and maintained it at a steady level, indicating its high accuracy and optimal response. Accordingly, it can be concluded that adopting the

MPID controller effectively enhances the system's dynamic stability compared to the conventional PID controller.

Based on these results, the scenario aims to achieve two main objectives: first, to evaluate the superiority of the MPID controller over the conventional PID controller in terms of improving system stability and reducing distortions in both frequency and voltage; and second, to validate the effectiveness of the proposed approach through the performance index (ITAE), as confirmed by Figures (III.31 and III.33) and Table III.7. This superiority is attributed to the MPID controller's ability to manage and tune a larger number of parameters compared to the PID controller, which can only adjust a limited set of parameters, making it less suitable for complex systems with multiple control requirements.

Scenario III: The MPID controller was evaluated under different potential disturbances impacting the microgrid system, with a comparative analysis between the CSA and ACO algorithms. The microgrid frequency deviation (Δf) was simulated across various operating conditions as outlined below:

Case 1: The MG undergoes a load variation (ΔPL) as depicted in Figure III.16, while the corresponding frequency deviation (Δf) is presented in Figure III.34.

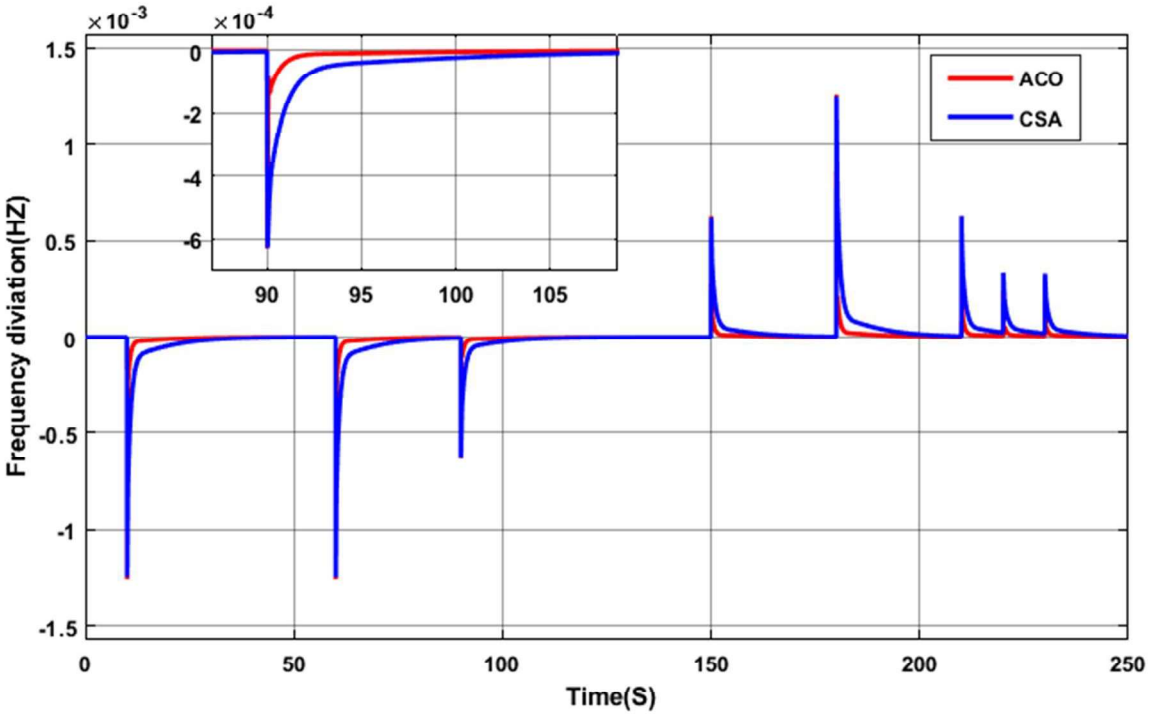

Figure III.34: Frequency response of the MG under load variations

Case 2: The MG undergoes a solar power disturbance (ΔP_{PV}) as depicted in Figure III.20, while the corresponding frequency deviation (Δf) is presented in Figure III.35.

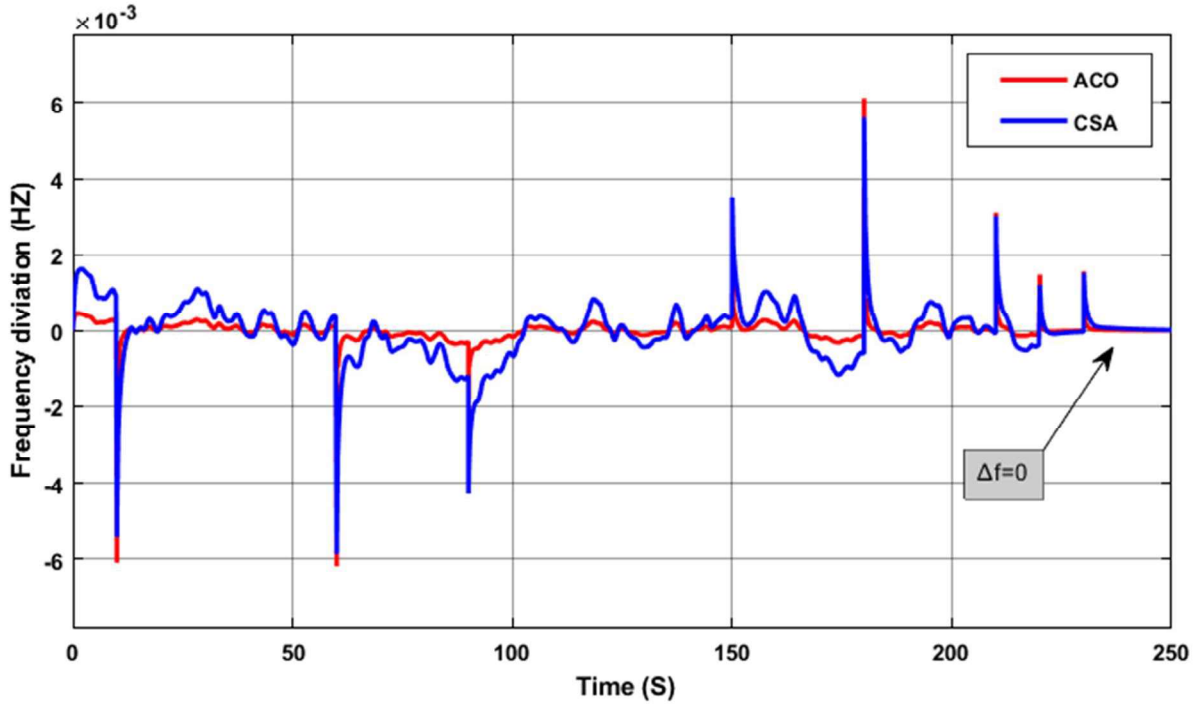

Figure III.35: Frequency response of MG against PV power variations

Case 3: The MG undergoes a wind power disturbance (ΔPwind) as depicted in Figure III.22, while the corresponding frequency deviation (Δf) is presented in Figure III.36.

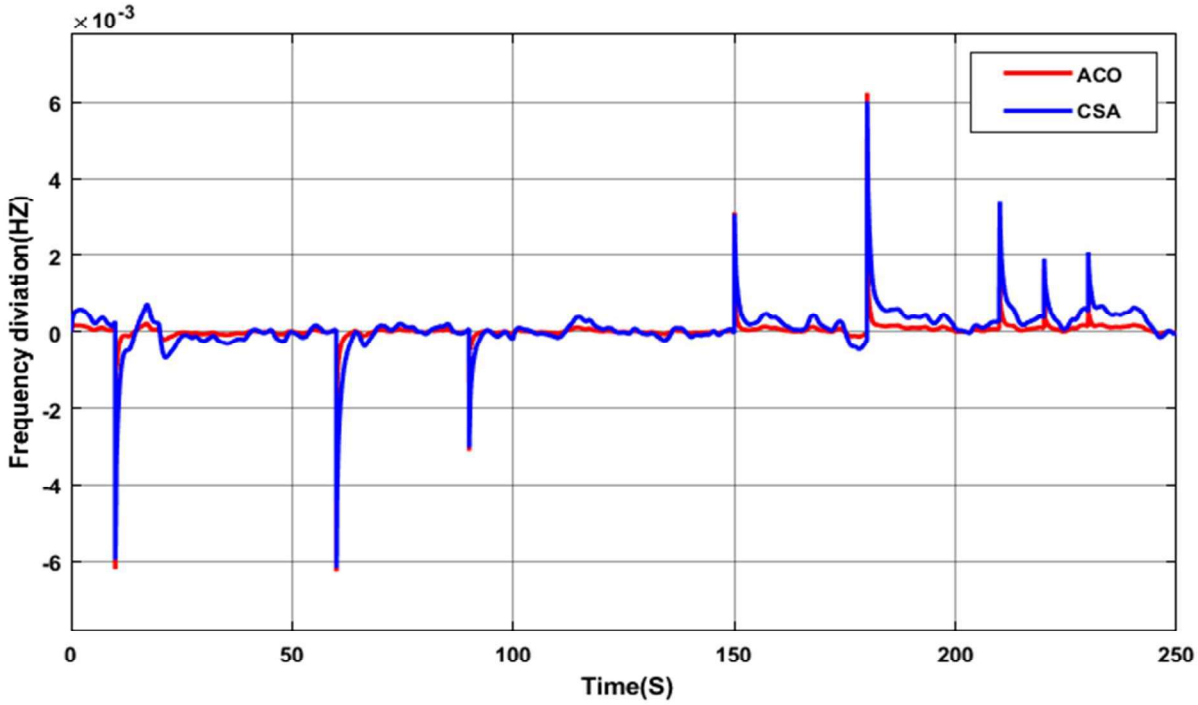

Figure III.36: Frequency response of MG against wind power variations.

Case 4: The microgrid is exposed to solar power disturbances (ΔP_{PV}) and wind power disturbances (ΔPwind) as illustrated in Figure III.24, whereas the corresponding frequency deviation (Δf) is shown in Figure III.37.

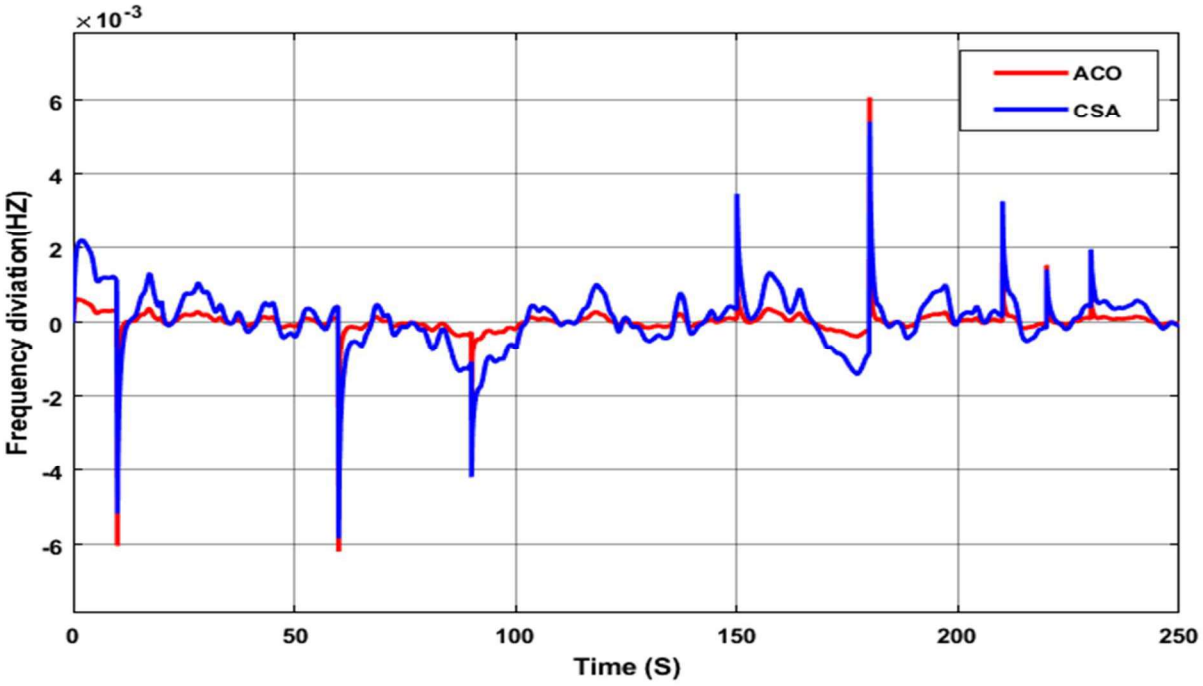

Figure III.37: Frequency response of MG against PV power variations, wind power variations, and multi-step load disturbance

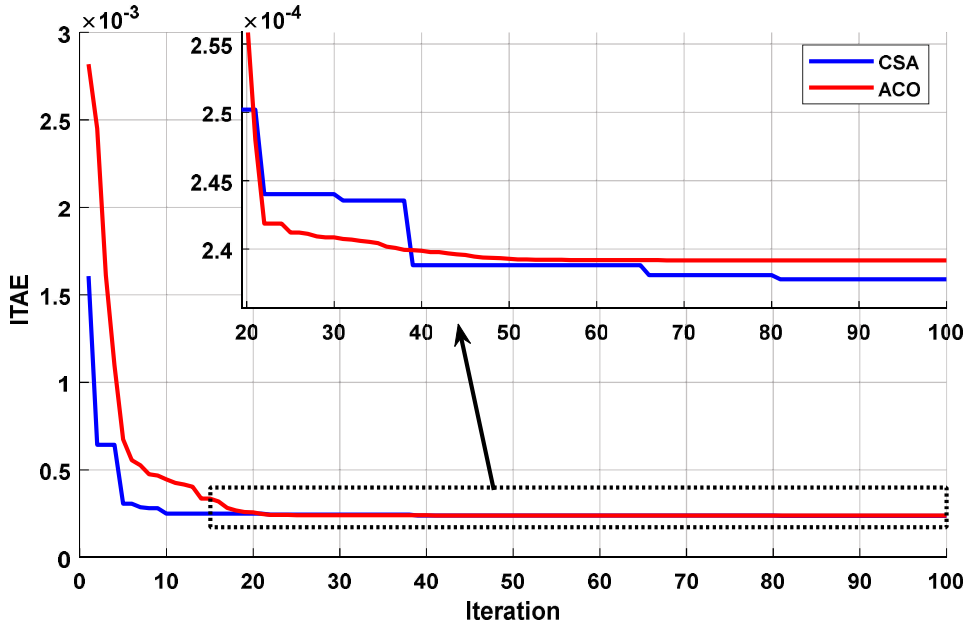

Figure III.38: ITAE analysis over iterations for different control strategies

The obtained results in this scenario present a comparison between the performance of the MPID controller when tuned using the ACO and CSA algorithms. From the first figure, it can be observed that both methods successfully reduced the Δf and maintained its stability after the microgrid system was subjected to sudden disturbances. As illustrated in Figures III.34, III.35, III.35, and III.36, the results demonstrate the superiority of the MPID controller in terms of system stability and reduction of distortions under all operating conditions, whether considering the impact of solar energy alone, wind energy alone, or their combined effect. This is attributed to the MPID controller's ability to handle multiple inputs effectively. However, the

response of the ACO-tuned controller was characterized by smoother dynamics and better oscillation reduction compared to CSA, reflecting its effectiveness in improving the dynamic performance of the system. The figure III.38, on the other hand, confirms the convergence behavior of the performance function over iterations, where CSA demonstrated faster convergence toward the optimal solution during the initial stages, while ACO converged more slowly but provided clearer stability at the final steady state. Therefore, it can be concluded that CSA is characterized by faster convergence, whereas ACO ensures more stable performance in response to disturbances.

III.6. Analysis of results in general

Based on the simulation results obtained for tuning the parameters of the Multi-Stage PID (MPID) controller for microgrid frequency regulation, a two-stage approach was adopted. In the first stage, conventional methods such as the Ziegler Nichols (ZN) method and the Coefficient Diagram Method (CDM) were used to tune the controller parameters. In the second stage, modern metaheuristic algorithms, namely the Cuckoo Search Algorithm (CSA) and the Ant Colony Optimization (ACO), were employed to determine the controller parameters and evaluate its performance under various disturbance scenarios.

The results revealed that modern algorithms achieve superior performance compared to conventional methods, thanks to their ability to explore a wider solution space and exploit collective search mechanisms, which enhance accuracy and robustness. This is mainly because optimization algorithms search for optimal solutions through their inherent exploration and exploitation capabilities, particularly in mathematically formulated systems. In contrast, conventional methods rely primarily on algebraic relationships that yield a single solution, thereby limiting their adaptability to complex systems.

Nevertheless, conventional methods cannot be disregarded, as they remain fundamental in providing initial search domains for optimization algorithms and offering useful preliminary estimates for modern approaches, in addition to serving as benchmarks for comparison and performance evaluation.

III.7. Conclusion

In this chapter, the frequency regulation problem in microgrid systems was addressed through the design and tuning of a Multi-Stage PID (MPID) controller. Both conventional approaches, namely Ziegler–Nichols (ZN) and the Coefficient Diagram Method (CDM), as well as advanced optimization algorithms such as the Cuckoo Search Algorithm (CSA) and Ant Colony Optimization (ACO), were applied to optimize the controller's parameters. The obtained results demonstrated that intelligent optimization significantly improves the system's dynamic performance, achieving faster convergence and better stability compared to classical tuning techniques. Moreover, the comparative analysis with the traditional PID controller highlighted the superior effectiveness of the MPID controller in mitigating frequency deviations under various disturbance scenarios.

Building upon these findings, the next chapter will extend the study by investigating the application of Fuzzy Logic controllers (Type-1 and Type-2) for the enhancement of MPID performance. This will provide a deeper insight into the potential of intelligent control strategies in further improving system robustness and adaptability in microgrid environments.

CHAPTER IV :

ENHANCING MG PERFORMANCE USING MPID CONTROLLER TUNED WITH TYPE-2 FUZZY

IV.1. Introduction

This chapter aims to investigate and develop advanced intelligent control strategies to improve frequency stability in islanded microgrids, based on the use of a Multistage PID (MPID) controller tuned with Type-1 Fuzzy Logic (T1-FL) and Type-2 Fuzzy Logic (T2-FL). In addition, the performance of the proposed approach is compared with the conventional PID controller. The islanded microgrid is considered one of the most significant innovations in modern power systems, as it ensures autonomous power supply by integrating multiple energy sources such as photovoltaic (PV) systems, wind turbines (WTG), plug-in hybrid electric vehicles (PHEVs), and diesel generators.

In this context, the PID controller remains one of the most widely used classical controllers in power systems due to its simplicity and ease of implementation. However, its effectiveness becomes limited when facing the stochastic fluctuations of renewable energy sources or large-scale disturbances. To overcome these limitations, the Multistage PID (MPID) controller was developed, consisting of interconnected PI and PD units, which provides greater flexibility and improved dynamic response. Type-1 Fuzzy Logic (T1-FL) offers an effective tool for tuning the parameters of both PID and MPID controllers by handling uncertainties in the system. Nevertheless, Type-2 Fuzzy Logic (T2-FL) demonstrates superior flexibility in managing complex and uncertain operating conditions, leading to more stable and efficient performance.

This chapter presents simulation results that compare the performance of the conventional PID controller with the MPID tuned by T1-FL and T2-FL, followed by a comprehensive discussion of the advantages and limitations of each method. Finally, the chapter provides an in-depth analysis of the results, emphasizing the practical implications of these strategies in enhancing the reliability and efficiency of future microgrid systems.

IV.2. Proposed MG structure

Figure IV.1 presents the schematic of an integrated hybrid energy system designed for renewable sources and EV charging with intelligent control. The system relies on renewable resources, mainly solar and wind, for electricity generation [71]. To strengthen storage capacity, it incorporates energy storage units, including EVs that serve as mobile batteries. Additionally, a diesel generator is employed to ensure the balance between energy production and consumption, thereby enhancing both grid efficiency and stability. At the core of the system lies the intelligent control unit, which combines an MPID controller with Type-2 Fuzzy Logic (T2-FL). This controller continuously monitors energy and frequency deviations (Δp, Δf) arising from fluctuations in load demand or variations in power generation, and it takes corrective actions to regulate these deviations accordingly [30].

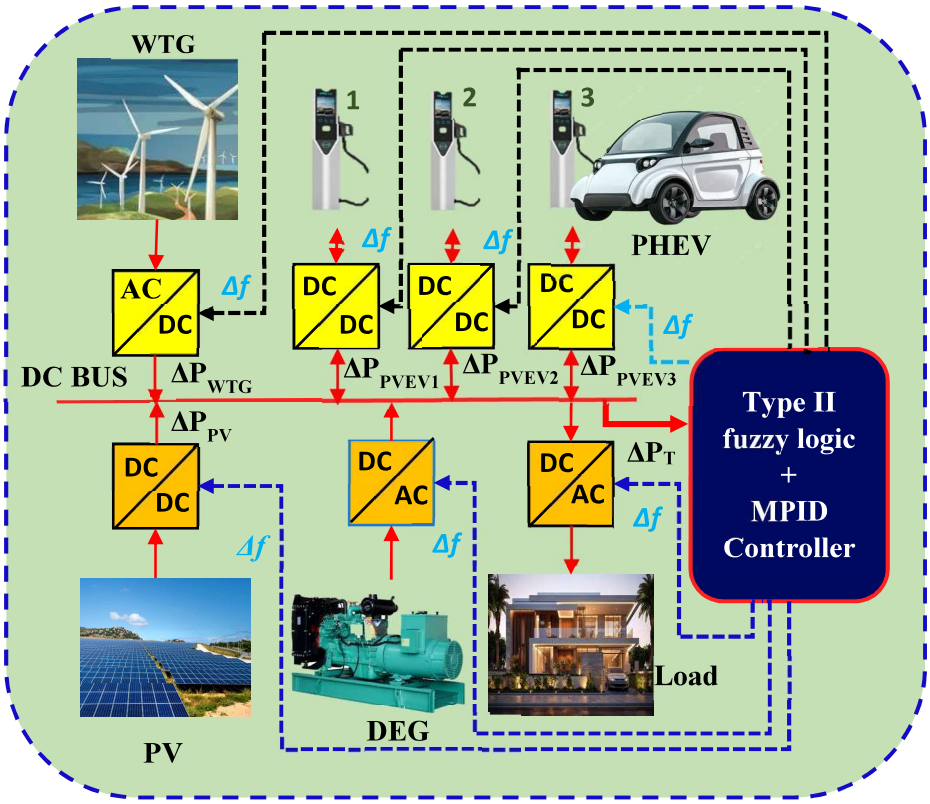

Figure IV.1. Schematic of an integrated hybrid energy system combining renewable sources and EV charging with Type 2 fuzzy logic

Based on this figure, I employed a mathematical representation of the various energy sources that constitute the microgrid system, with the aim of describing the behavior of each source individually and its role in maintaining the system's balance. This mathematical representation is an essential step toward simplifying and understanding the system dynamics, as well as developing a suitable controller for mitigating frequency deviation. The detailed models and mathematical equations are presented in Chapter III, including the formulations for solar energy, wind energy, batteries, electric vehicles, and the diesel engine-generator. This ensures accurate simulation of system performance and provides a solid basis for evaluating the effectiveness of the proposed control strategies.

IV.3. Design of a proposed multistage PID controller optimized with T2-FL

In this work, I relied on the multi-stage PID controller (MPID) to regulate the frequency deviation within the microgrid system. This controller is an evolution of the classical PID controller, as many researchers have previously focused on eliminating one of the PID parameters to transform it into either the PI or PD form. Others combined these two units and introduced a new parameter, resulting in the formulation of the MPID controller, which consists of five parameters (Kp, Ki, Kd, and Kpp), as illustrated in Figure III.4. This controller was integrated into the microgrid system, as shown in Figure IV.2, to reduce frequency deviation and ensure overall system stability for tuning the parameters of the MPID controller, I studied the fundamentals of fuzzy logic [30].

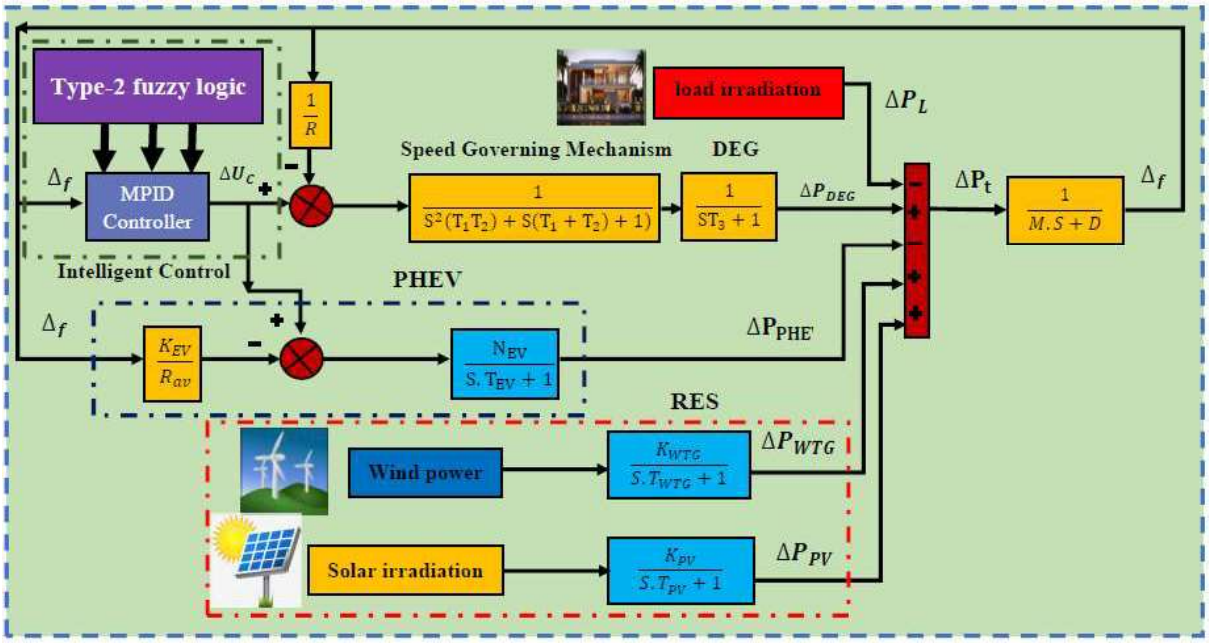

Figure IV.2. Hybrid architecture of integrating Type-2 Fuzzy Logic with an MPID controller in a Microgrid system

Figure IV.2 and Figure IV.3. illustrates the hybrid architecture for integrating T2-FL with a MPID controller to improve frequency deviation performance in a microgrid system. The role of the fuzzy logic is to process the frequency deviation input (Δf) and the desired reference value (Δf*), through adaptive adjustment of the MPID controller's basic parameters: Kp, Ki, Kd, and Kpp. This adjustment is performed in real time according to the system's dynamic operating conditions, ensuring an effective response under various disturbances and uncertainties [87].

As shown in the diagram, the fuzzy controller inputs (Δf and Δf*) are processed within a fuzzy inference mechanism that relies on a set of fuzzy rules and type-II membership functions. This type differs from traditional fuzzy logic (type-I) by incorporating an additional dimension for representing uncertainty, known as the Footprint of Uncertainty (FOU). This feature makes it more capable of handling nonlinearities and sudden fluctuations caused by renewable energy sources. The fuzzy controller outputs are the optimal values of the MPID parameters (Kp, Ki, Kd, and Kpp), which are then fed into the controller modules. Here, Kp and Kd tune the PD loop to ensure a fast response and dampen oscillations, while Ki and Kpp operate within the PI structure to eliminate steady-state errors and achieve long-term stability. The additional parameter Kpp acts as a flexible factor, providing the controller with greater adaptability compared to a conventional PID controller [88].

By combining these two structures, the MPID controller achieves a balance between fast response in transient states (enabled by the PD loop) and accuracy in steady states (enabled by the PI loop). Consequently, the system becomes more adaptable to load variations, renewable energy fluctuations, and sudden disturbances. The T2-FL's automatic tuning mechanism makes the adjustment process dynamic rather than static, enhancing system resilience and stability, reducing frequency deviations, and improving the overall efficiency of the MG [89].

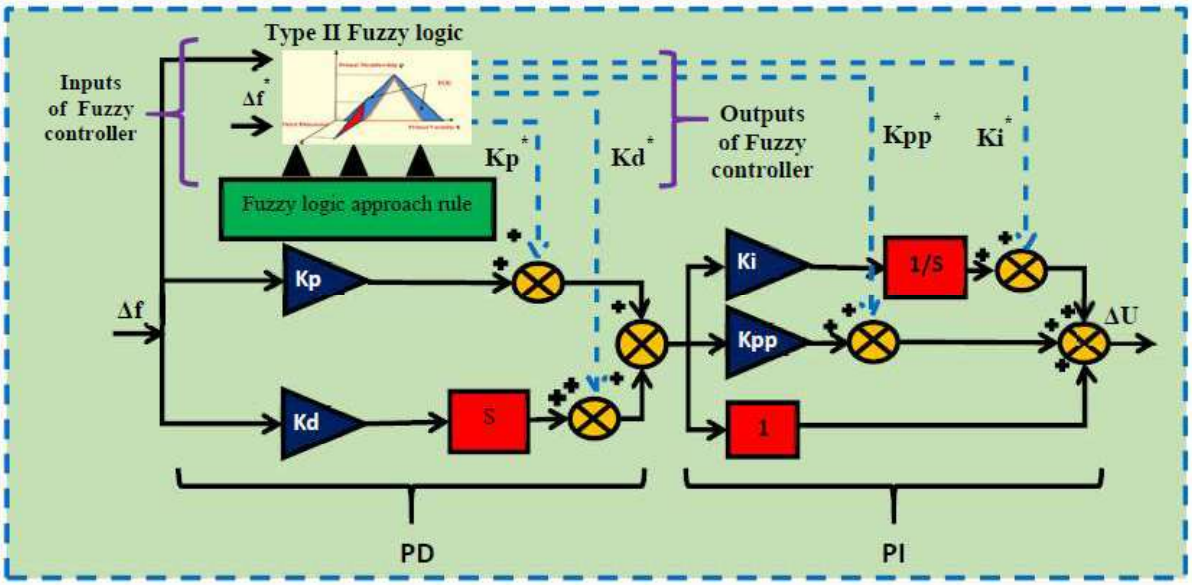

Figure IV.3. Adaptive tuning mechanism of MPID controller parameters using T2-FL

IV.4. Generality on Fuzzy logic controller

Fuzzy logic is a practical approach developed to address problems that are difficult to express mathematically. Unlike classical logic, which relies only on binary values (true or false), fuzzy logic is based on the idea that real-world phenomena are not always clearly defined but may fall within intermediate or partial states. Therefore, it allows values to be represented in degrees ranging from 0 to 1. This feature has made fuzzy logic an effective tool in many fields, such as control systems, artificial intelligence, and decision-making. It helps deal with ambiguity and uncertainty in a manner similar to human reasoning by relying on flexible rule-based structures. Based on these general concepts, two main types of fuzzy logic can be distinguished: first-level fuzzy logic and second-level fuzzy logic, each with its own characteristics and applications, as follows [87].

IV.5. Structure and formulation of Type-2 Fuzzy Logic Control System

T-2 FL is considered an advancement over traditional Type -1 fuzzy logic (T1-FL), as it does not only represent uncertainty in the membership functions but also extends it to the fuzzy sets themselves. This provides a wider range of possible membership values within the fuzzy sets [88], thereby enhancing the system's ability to deal with higher levels of uncertainty and imprecision in data. Consequently, T2-FL is more suitable for complex decision making and control applications in uncertain environments, such as microgrid systems. It is represented as follows:

IV.5.1. Fuzzification

In this phase, all system inputs are transformed into fuzzy values by applying membership functions. The main inputs are the Area Control Errors (ACE1, ACE2, ACE3 … ACEn), which represent the frequency deviations in each control area of the microgrid. Each ACE_i is calculated as [87] :

$$ACE_i = \Delta P_i + \Delta f_i + \beta_i \quad \text{(IV.1)}$$

where:

Bi: is the frequency bias factor of area i

Δfi: is the frequency deviation in area i

ΔPi is the deviation in tie-line power exchange for area i

In the studied microgrid, the ACE values reflect the deviations caused by disturbances in solar power, wind power, and load variations. These crisp ACE values are then converted into fuzzy values through membership functions. The mathematical representation of the T2-FL membership function can be expressed as [88]:

$$f(x,u) = \{x \in X, u \in P_x \subseteq [1\ 0]\ \mid (\delta f\ (x\ ,u),(x,u))\} \quad \text{(IV.2)}$$

where
$f(x,u)$ is the T2-FL set.
$\delta f\ (x,u)$ is the membership function that takes values between 0 and 1.
x: represents the inputs (ACE values),
u: The outputs or resulting values that can be regulated based on the inputs.
A T2-FL set can be expressed using a double integral as follows:

$$f = \int_u^p \int_x^X \delta f\ (x\ ,u)(x,u)^{-1} du\ dx \quad \text{(IV.3)}$$

This integral formula reflects the inclusion of all possible input values and their corresponding membership degrees, enabling the controller to effectively deal with the uncertainty in frequency deviations caused by renewable energy fluctuations and load disturbances [89].

The figure IV.4 illustrates the structure of the Type-2 Fuzzy Logic System based on the Sugeno model. The left side shows the system inputs, namely Δf and frequency value (F), which are fuzzified into membership functions. These inputs are processed through the Rule Editor, where fuzzy rules are applied. On the right side, the outputs represent the controller parameters Ki, Kp, d, and Kpp. This fuzzy system dynamically tunes the multistage PID controller parameters according to microgrid operating conditions, thereby enhancing stability and adaptability under disturbances.

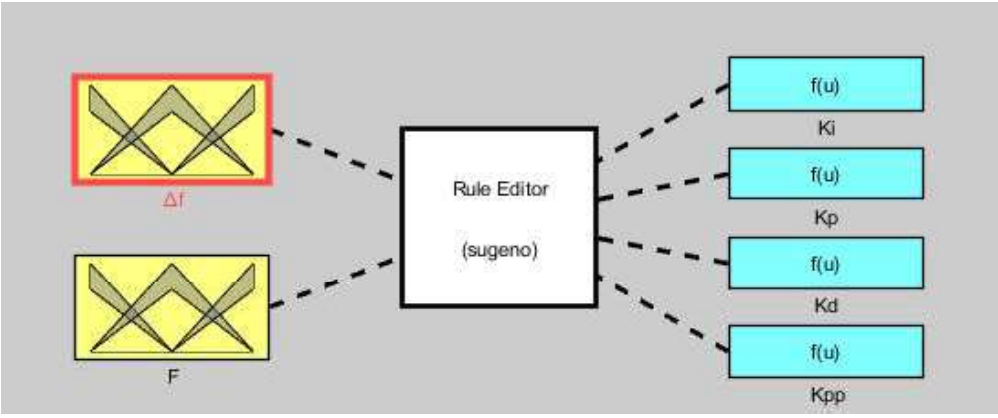

Figure IV.4. Structure of Type-2 Fuzzy Logic in Microgrid using MATLAB

IV.5.2. Footprint of Uncertainty

At this stage, the ambiguity in the T2-FL set is expressed as the region that encompasses all primary membership functions, confined between their lower and upper membership function values [90].

$$0 \leqslant \delta f\,(x, u) \leqslant 1 \qquad \text{(IV.4)}$$

This inequality defines the search domain of uncertainty in the system, arising from variations in the membership functions.

IV.5.3. Fuzzy Rule Base

Fuzzy logic rules are determined based on fluctuations outside the power sources. Using these inputs and outputs and also relying on Equation 5, a typical basic rule for T2-FL logic can be formulated as follows [90-91]:

$$If\ ACE_1 = \check{F}_1^i\ and\ \frac{d(ACE)}{dx} = \check{F}_2^i, then\ U = \check{G}^i \quad (22) \qquad \text{i= 1,2,3,3 . . . N} \qquad \text{(IV.5)}$$

where,
ACE_1 is the Accumulated Error.
$\frac{d(ACE)}{dx}$ is the Derivative of Accumulated Error (rate of change of accumulated error).
$\check{F}_1^i\ and\ \check{F}_2^i$ are the fuzzy sets representing the inputs.
$\check{G}^i$ Ou U is the output resulting after applying the fuzzy rule.
N represents the maximum number of rules that can be formulated, which is equal to five membership functions (5 x 5)
Figure IV.5 illustrates the architecture of a T2-FL control system, consisting of several interconnected components that work together to improve control performance.

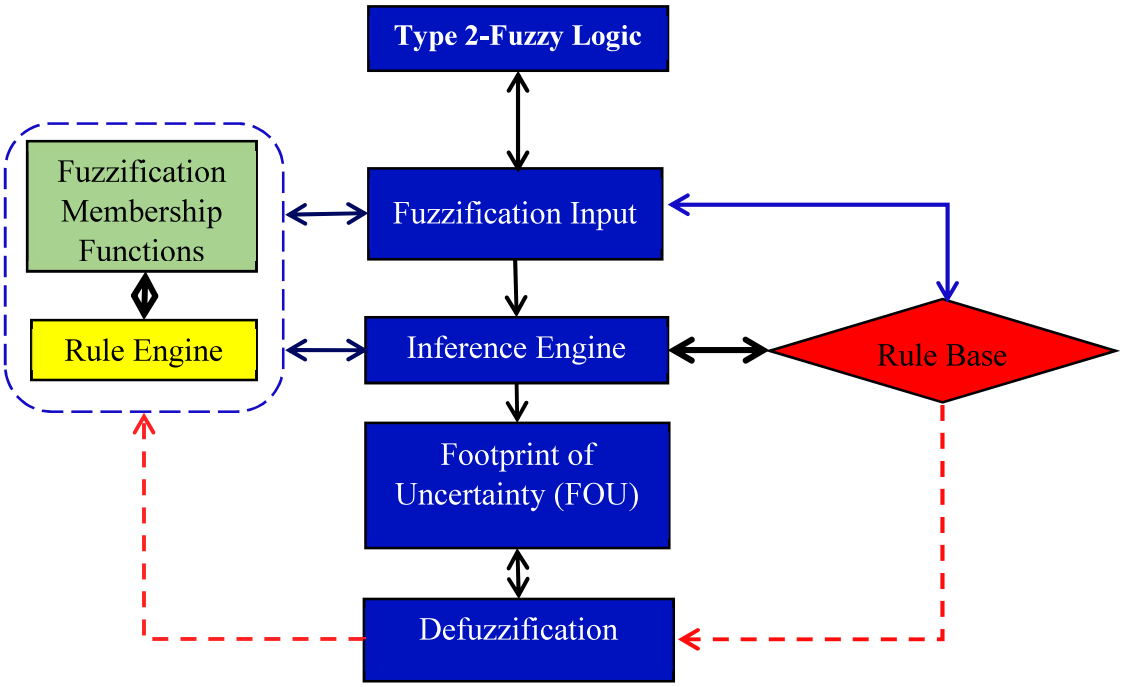

Figure IV.5. Flowchart of T2-FL logic controller.

Figure IV.6. shows the five linguistic variables, denoted as LN (Large Negative), LP (Large Positive), MN (Medium Negative), and MP (Medium Positive), represented using the triangular form of Mamdani T2-FL logic. These variables were selected for their relevance to the present study. The linguistic rules outlined in Table IV.1, Table IV.2, and Table IV.3 were obtained from equation (IV.5) [92].

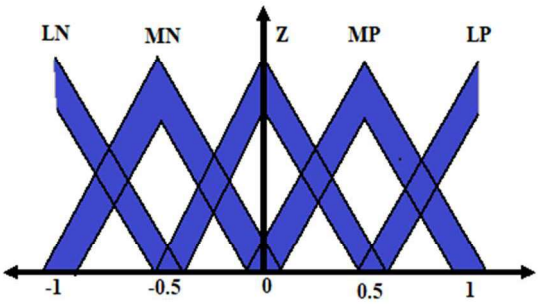

a) Triangular

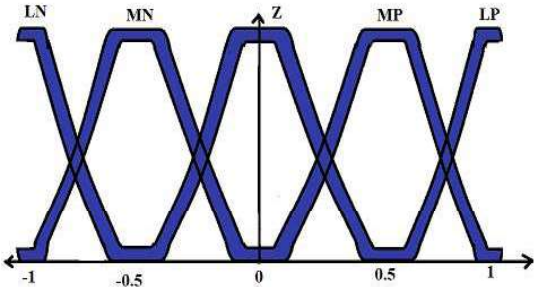

b) Triangular-tarapezoidal

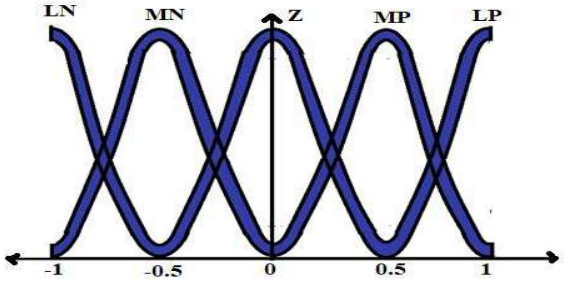

d) Goussian

Figure IV.6. Membership functions (MF) for inputs and outputs in the T2-FL Logic.

Table IV.1. T2-FL Logic Approach Rule Base for ΔK_P and ΔK_{PP}.

Δf* / Δf	LN	MN	Z	MP	LP
LN	LP	LP	LP	MP	Z
MN	LP	LP	MP	Z	MN
Z	LP	MP	Z	MN	LN
MP	MP	Z	MN	LN	LN
LP	Z	MN	LN	LN	LN

Table IV.2. T2-FL Approach Rule Base for ΔK_i.

Δf* / Δf	LN	MN	Z	MP	LP
LN	LN	LN	LN	NM	Z
MN	LN	LN	MN	Z	MP
Z	LN	MN	Z	MP	LP
MP	MP	Z	MP	LP	LP
LP	Z	MP	LP	LP	LP

Table IV.3. T2-FL Approach Rule Base for ΔK_d.

Δf* / Δf	LN	MN	Z	MP	LP
LN	MP	MN	LN	LN	MP
MN	MP	MN	MN	MN	Z
Z	Z	MN	MN	MN	Z
MP	Z	MP	MP	MP	LP
LP	LP	LP	MP	MP	LP

The figure IV.7 shows MATLAB's Membership Function Editor (FIS Editor) after applying Equation (IV.5) to generate fuzzy rules and membership shapes. The membership functions for the input variable F (range [-1, 1]) are plotted linguistic terms (e.g. LN, MN, Z, MP, LP) are represented by triangular membership functions (trimf). The right panel displays the parameters and type of the currently selected MF (highlighted in red), while the left panel lists the FIS variables. This GUI is used to enter and tune the IF–THEN fuzzy rules derived from Equation (IV.5) before running full-system simulations.

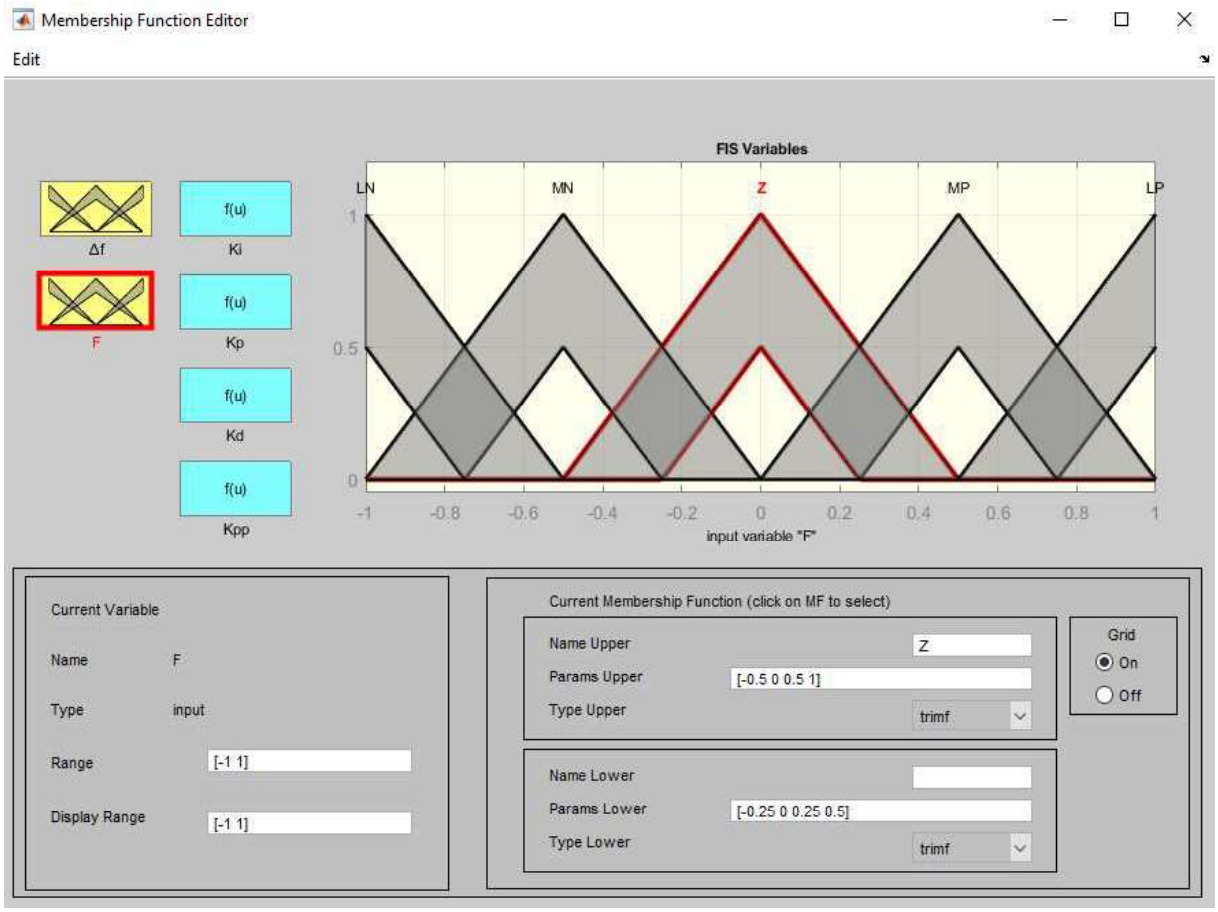

Figure IV.7. Membership Function Editor in MATLAB

IV.5.4. Inference System

At this stage, the collected results are utilized to compute the parameters of the MPID controller and to obtain the initial outcomes using the following equations [88].

$$K_p = \sum_1^N \check{G}_p^i . f_k(x) \quad \text{(IV.6)}$$

$$K_i = \sum_1^N \check{G}_i^i . f_k(x) \quad \text{(IV.7)}$$

$$K_d = \sum_1^N \check{G}_d^i . f_k(x) \quad \text{(IV.8)}$$

$$K_{pp} = \sum_1^N \check{G}_d^K . f_k(x) \quad \text{(IV.9)}$$

IV.5.5. Type-Reduction

To accurately tune the MPID controller parameters, it is necessary to determine the maximum and minimum output values using the Karnik-Mendel method, derived from

equations (IV.10). This approach is primarily intended to minimize the error of nonlinear functions by computing the centroid average of fuzzy logic [93], as expressed in equation (IV.11). The procedure is repeated until convergence is attained or the required values are achieved.

$$L_{Ki,p,d,pp} = \frac{\sum_{i=1}^{N} x_i.\underline{u}(x_i)}{\sum_{i=1}^{N} \underline{u}(x_i)} \quad \text{(IV.10)}$$

$$u_{Ki,p,d,pp} = \frac{\sum_{i=1}^{N} x_i.\overline{u}(x_i)}{\sum_{i=1}^{N} \overline{u}(x_i)} \quad \text{(IV.11)}$$

where
$\overline{u}(x_i)$: The upper bounds of the membership function.
$\underline{u}(x_i)$: The lower bounds of the membership function.
$L_{Ki,p,d,pp}$: Lower Bound Centroid.
$u_{Ki,p,d,pp}$: Upper Bound Centroid.

IV.5.6. Defuzzification

At this stage, the fuzzy values are converted into crisp values using the center of gravity method. After determining the upper and lower limits of the fuzzy logic, the final optimal parameters of the MPID controller are computed through the central equation (IV.11) and the iterative formula [93], which is based on the convergence principle between the two values $L_{Ki,p,d,}$ and $u_{Ki,p,d,pp}$.

$$C = \frac{\sum_{i=1}^{N}(x_i.u_i^c(x_i))}{\sum_{i=1}^{N} u_i^c(x_i)} \quad \text{(IV.12)}$$

$u_i^c(x_i)$: is the membership value determined at x_i based on the current C value.

After incorporating the optimized parameters into the T2-FL controller, the resulting final expression of the MPID controller can be written as follows:

$$u(s) = e(s)\big((k_p - k_p^*) + (k_{pp} - k_{pp}^*)\big) + \mathrm{e(s)}.\frac{N.S}{S+N}.(k_{d-}k_d^*) + \frac{(k_i - k_i^*)e(s)}{s} \quad \text{(IV.13)}$$

Equation (IV.13) is subsequently converted from the Laplace domain into the time domain, as expressed in equation (IV.14). This transformation enables the assessment of the system's dynamic response during time-based simulations, providing clearer insight into how each controller parameter influences overall system performance.

$$u(t) = e(t)\big((k_p - k_p^*) + (k_{pp} - k_{pp}^*)\big) + \frac{de(t)}{dt}(k_{d-}k_d^*) + (k_i - k_i^*)\int e(t)\,dt \quad \text{(IV.14)}$$

k_p^* k_{pp}^* k_d^* k_i^*Parameters dynamically tuned using T2-FL.
$e(t)$ Frequency deviation Δf.

IV.6. Results and Discussion

In this section, the application of the proposed T2-Fuzzy-MPID controller is examined for frequency regulation in MG systems. The suggested method addresses active power flow management and frequency deviation control under various operating scenarios. The MG system under study consists of PV units, WTG, PHEV, and DEG used as storage and backup

sources. The T2-Fuzzy-MPID controller is assessed under changing weather conditions and fluctuating load demands, considering the integration of PHEV batteries, which pose a notable challenge for MG operation. To verify its effectiveness, several simulations were performed to analyze the controller's performance in terms of sensitivity to both internal and external disturbances and to compare it with conventional optimization-based PID, fractional-order PID (FOPID), and MPID controllers. The controller is tuned through real-time T2 fuzzy logic parameters to cope with system uncertainties and nonlinear behaviors. Frequency stability is further supported by PHEV batteries, acting as mobile energy storage systems (MESS) thanks to their flexible storage capacity. The simulations were carried out in MATLAB/Simulink (2023b) on a computer equipped with an Intel Core i7 processor and 8 GB RAM, and the controller was tested under multiple scenarios.

In this chapter, the Integral of Time-weighted Absolute Error (ITAE) is employed as the main performance index to evaluate the controllers and compare the results between the proposed T2-FL strategy and other benchmark methods. The ITAE index is widely recognized in control system analysis due to its ability to account for both transient and steady-state performance, as it penalizes sustained errors more heavily over time. This characteristic leads to faster settling and reduced steady-state deviation. Unlike Chapter III, where ITAE was expressed with respect to the number of iterations to assess the convergence behavior of the optimization algorithms, in this chapter ITAE is evaluated in the time domain to capture the dynamic response of the microgrid system under disturbances[65-69]. The ITAE is mathematically defined as:

$$ITAE = \int_0^T |e(t)|.dt \quad \text{(IV.15)}$$

where

e(t) represents the error signal over time and T is the total simulation time. A lower ITAE value indicates better control performance, characterized by faster response and lower accumulated error.

First scenario:

In In this scenario, the MPID controller based on Mamdani T2-FL will be applied to investigate the impact of different membership function shapes on system performance. Three membership function types will be examined: triangular, triangular–trapezoidal, and Gaussian. The study aims to emphasize the importance of selecting the appropriate membership function shape in improving the controller's accuracy and stability by comparing the results under the same operating conditions.

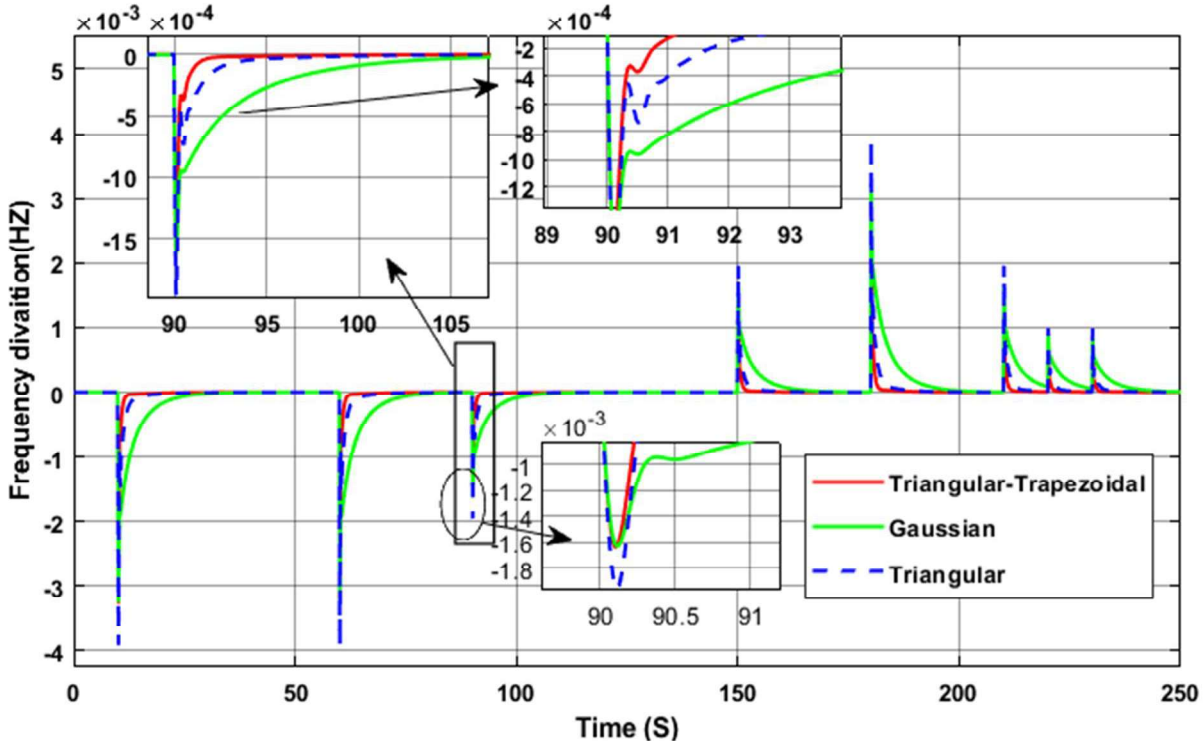

Figure IV.8. Impact of membership function type on frequency deviation in the MG

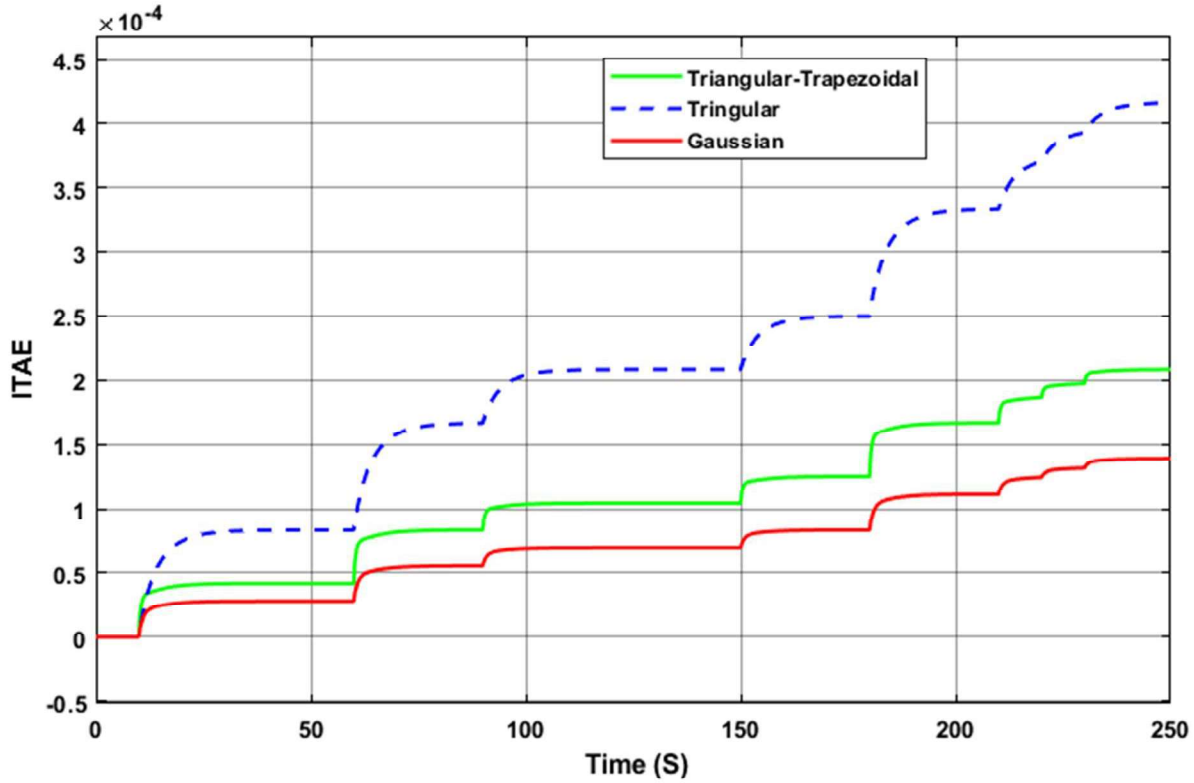

Figure IV.9. Impact of membership function type on ITAE criterion in the MG

The results in the figure IV.8 and Figure IV.9. clearly demonstrate the direct impact of membership function selection on the performance of fuzzy logic controllers. From Figure 1 (frequency deviation), it can be observed that the triangular-trapezoidal function (green) achieved the smallest maximum deviation of approximately -1.6×10^{-3} Hz at $t \approx 90$ s, with a faster stabilization compared to the other functions. The Gaussian function (red) recorded a

maximum deviation of around -1.8×10^{-3} Hz, while the triangular function (blue dashed) performed the worst, reaching nearly -2.2×10^{-3} Hz along with repeated oscillations after each disturbance at t = 90 s, 150 s, 200s and 250 s. From Figure 2 (ITAE criterion), the Gaussian function (red) provided the best performance, with an ITAE value of approximately 1.4×10^{-4} at t = 200 s. In comparison, the triangular-trapezoidal function (green) reached about 2.1×10^{-4}, while the triangular function (blue dashed) produced the highest cumulative error of roughly 4.1×10^{-4}.

Overall, these findings confirm that the triangular-trapezoidal function is more effective in reducing instantaneous deviations and improving frequency stability, whereas the Gaussian function achieves the lowest cumulative error in the long term. The triangular function, however, is the least efficient in both aspects, exhibiting the highest deviations and ITAE. This highlights that the choice of membership function is not merely a formal step, but rather a fundamental design decision that determines the accuracy and stability of the system.

Second scenario:

In this scenario, a load disturbance was introduced into the MG system, as illustrated in Figure III.15, to evaluate the performance of the proposed T2-FL compared to the T1-FL technique in tuning the PID and MPID controller parameters, as well as the T1-FL , representing previous works in this field. Furthermore, Table IV.4 presents the optimized values of the PID and MPID controller parameters obtained using the T2-FL and T1-FL approaches, which serve as the basis for the comparative analysis.

Table IV.4. The optimal parameters of PID, and MPID controllers using T2-FL and T1-FL.

Methods	Optimized gains			
	Kp	Ki	Kd	Kpp
T2- FUZZY-PID	1.549	3.459	1.1368	-
T2-FUZZY-MPID	2.692	4.358	3.289	2
T1-FUZZY-PID	1.723	1.5614	2.9136	-
T1-FUZZY-MPID	2.381	3.087	1.785	0.741

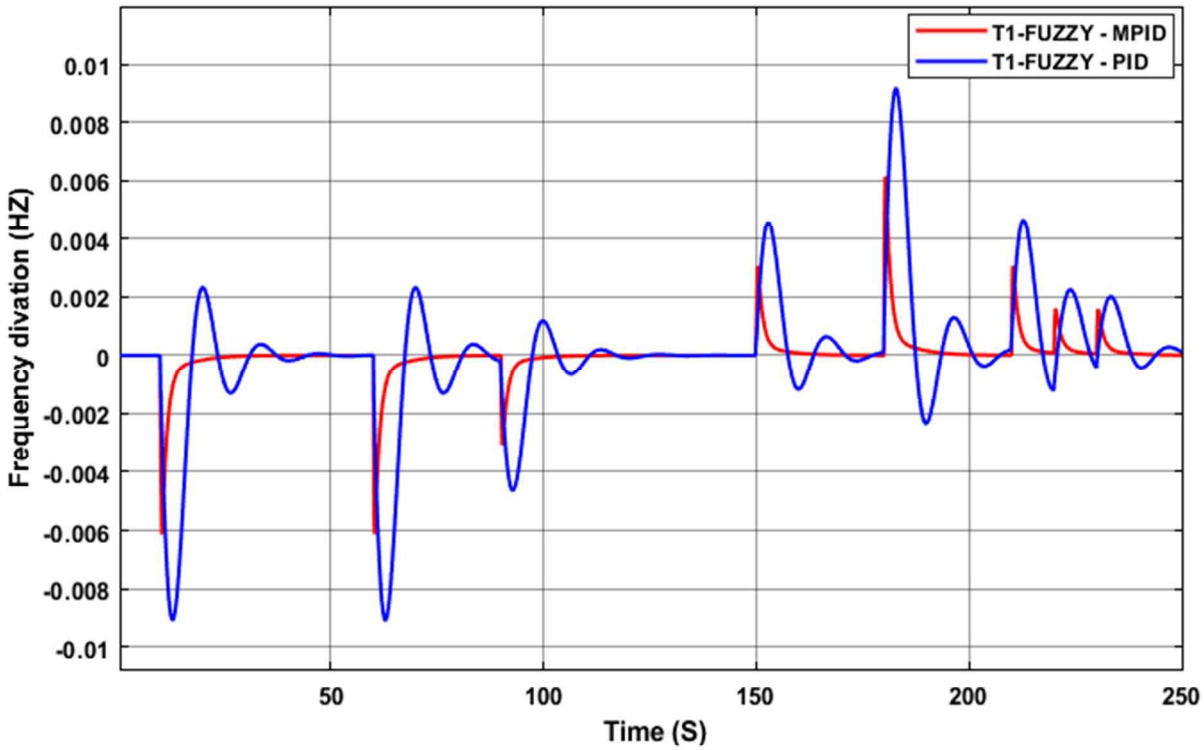

Figure IV.10. Performance comparison of PID and MPID controllers tuned with T1-FL

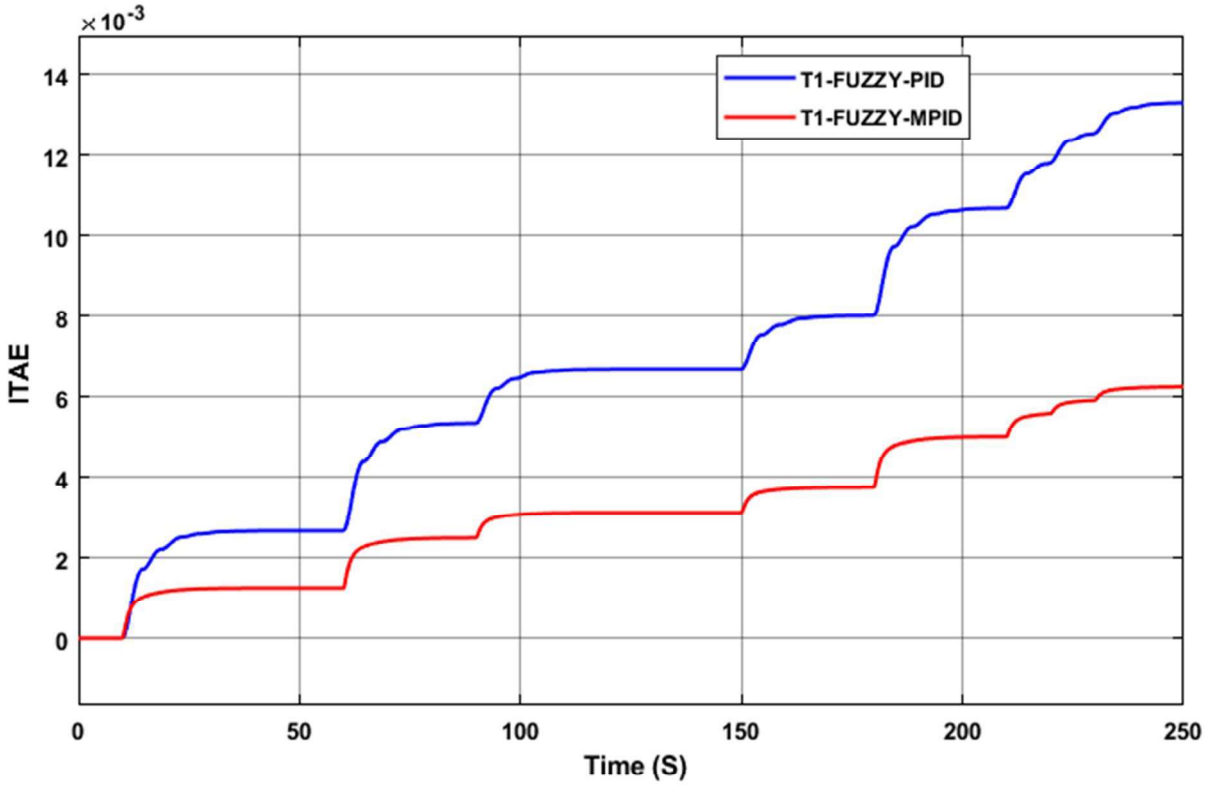

Figure IV.11. ITAE performance index results of PID and MPID controllers tuned with T1-FL

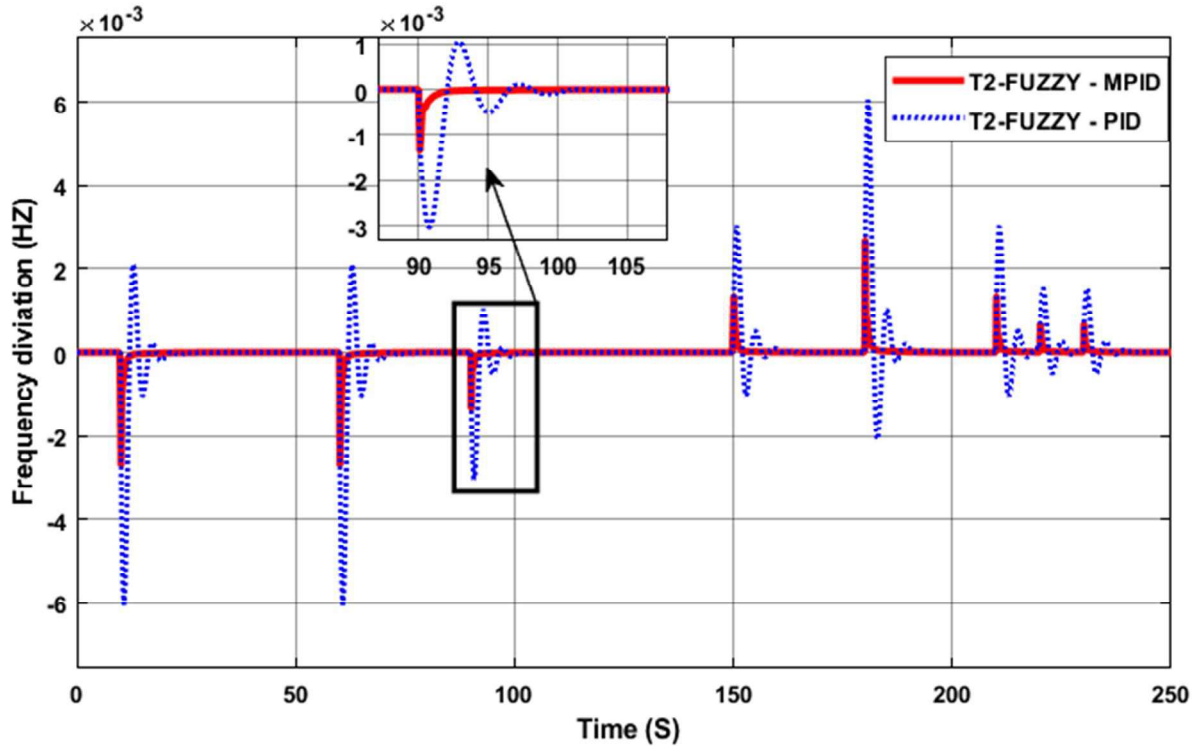

Figure IV.12. Performance comparison of PID and MPID controllers tuned with T2-FL

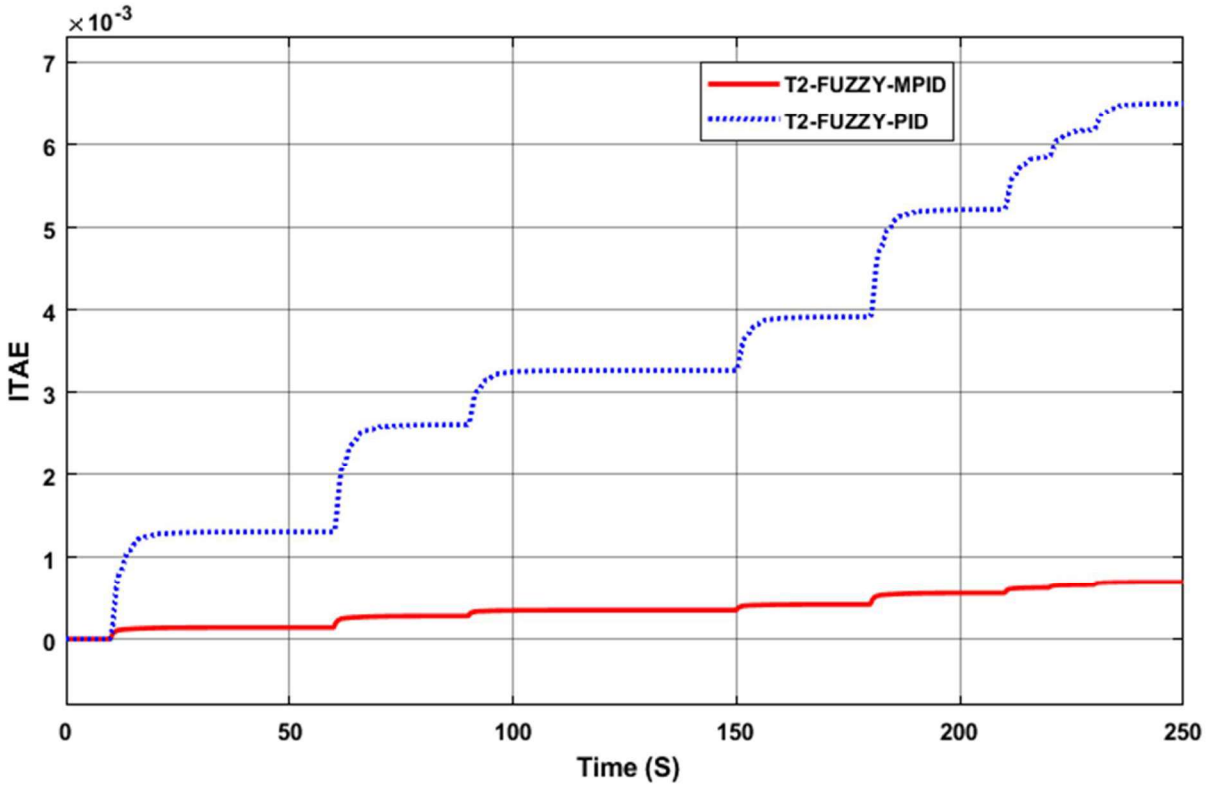

Figure IV.13. ITAE performance index results of PID and MPID controllers tuned with T2-FL

The simulation results provide a comparative evaluation between the conventional PID controller and the MPID controller when tuned using both T1-FL and T2-FL. As illustrated in Figure IV.10, applying T1-FL with the PID controller leads to a relatively unstable system,

which is evident from the large oscillations and repeated frequency deviations that weaken the system's ability to maintain stability. In contrast, combining T1-FL with the MPID controller significantly improves performance, where oscillations are reduced and the system achieves a higher degree of stability due to the additional control parameter Kpp.
In Figure IV.12, which presents the results based on T2-FL tuning, oscillations are considerably minimized for both PID and MPID controllers. Despite the improvements observed with both controllers, the MPID still demonstrates clear superiority in terms of faster stabilization and reduced fine deviations, reflecting the effectiveness of Type-2 fuzzy logic in handling uncertainty and achieving a more efficient response.
Moreover, the ITAE performance index results, as shown in Figures IV.11 and IV.13, further validate these observations. The MPID controller tuned with T2-FL achieved the lowest ITAE values compared to the other configurations, indicating reduced accumulated error and improved transient response. This quantitative assessment is consistent with the graphical analysis and confirms that the combination of MPID and T2-FL provides the most effective strategy for enhancing microgrid frequency stability under disturbances.

- **Third scenario:**

The robustness of the T2-FL MPID controller was evaluated through multiple case studies, demonstrating its capability to regulate frequency under diverse internal and external disturbances. The applied T2-FL tuning approach proved effective in minimizing frequency deviation within the MG system, thereby ensuring system stability even in the presence of uncertainties and the stochastic behavior of renewable energy sources alongside load variations.

Case 1: In this case, the performance of the MG in terms of frequency deviation response is investigated based on the load disturbance in Figure III.15. To this end, the analysis aims at as sassing systematic stability and the efficacy of the suggested control strategy. The changes made by this solution in the frequency deviation are given in Figure IV.14, which tests the controller's ability to manage disturbances while operating in unstable conditions.

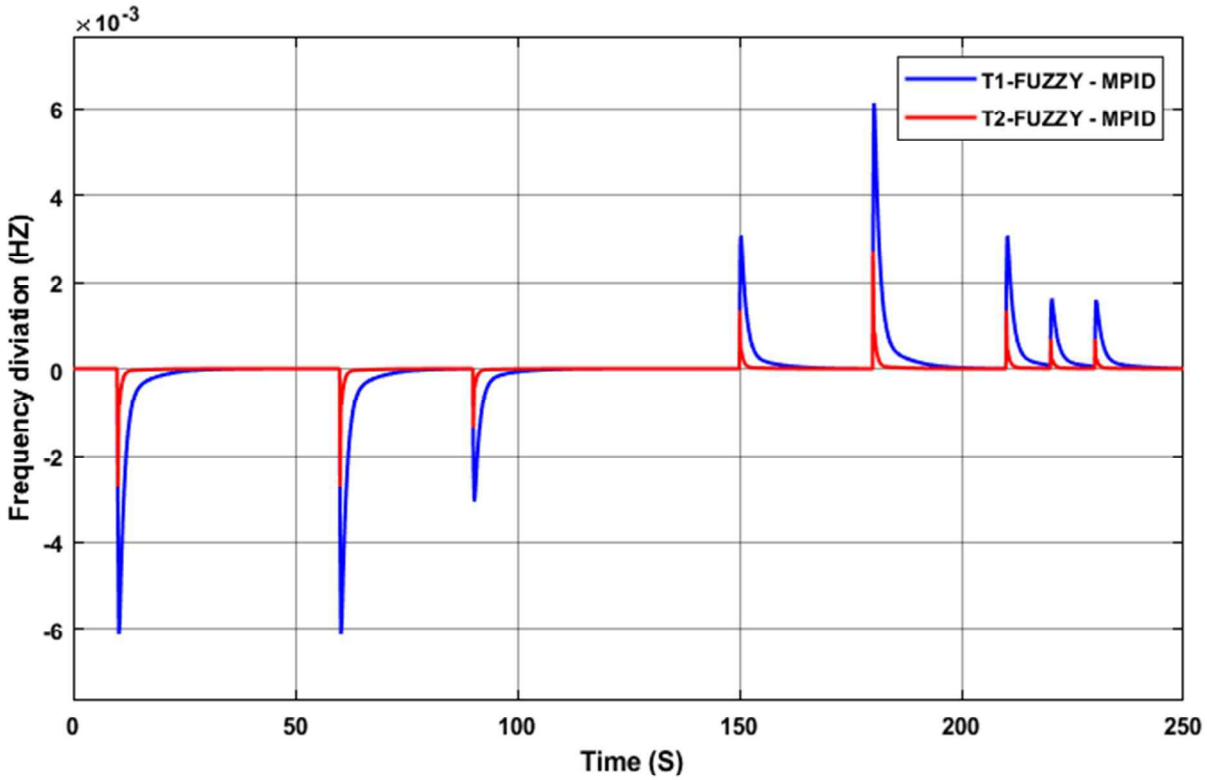

Figure IV.14. Frequency deviation response of the MG under load variations using MPID controller with T1-FL and T2-FL

The figure IV.14 illustrates the frequency deviation response of the MG under load variations, comparing the performance of the MPID controller when using both T1-FL and T2-FL. The results show that the frequency deviation with T1-FL exhibits larger peak values and sharper responses at disturbance moments, reflecting its limited capability in suppressing oscillations. In contrast, the T2-FL curve demonstrates superior damping ability and reduced deviations, maintaining the frequency closer to zero with a faster recovery after disturbances. The magnified section between 60 and 70 seconds further highlights the effectiveness of T2-FL in minimizing oscillations and ensuring better system stability. Therefore, it can be concluded that employing T2-FL with the MPID controller significantly enhances frequency stability in the microgrid under load variations compared to T1-FL.

Case 2: In this Case, only the impact of wind speed fluctuations is taken into account, as illustrated in Figure III.21. The resulting frequency deviation of the MG, caused by variations in wind power, is presented in Figure IV.15.

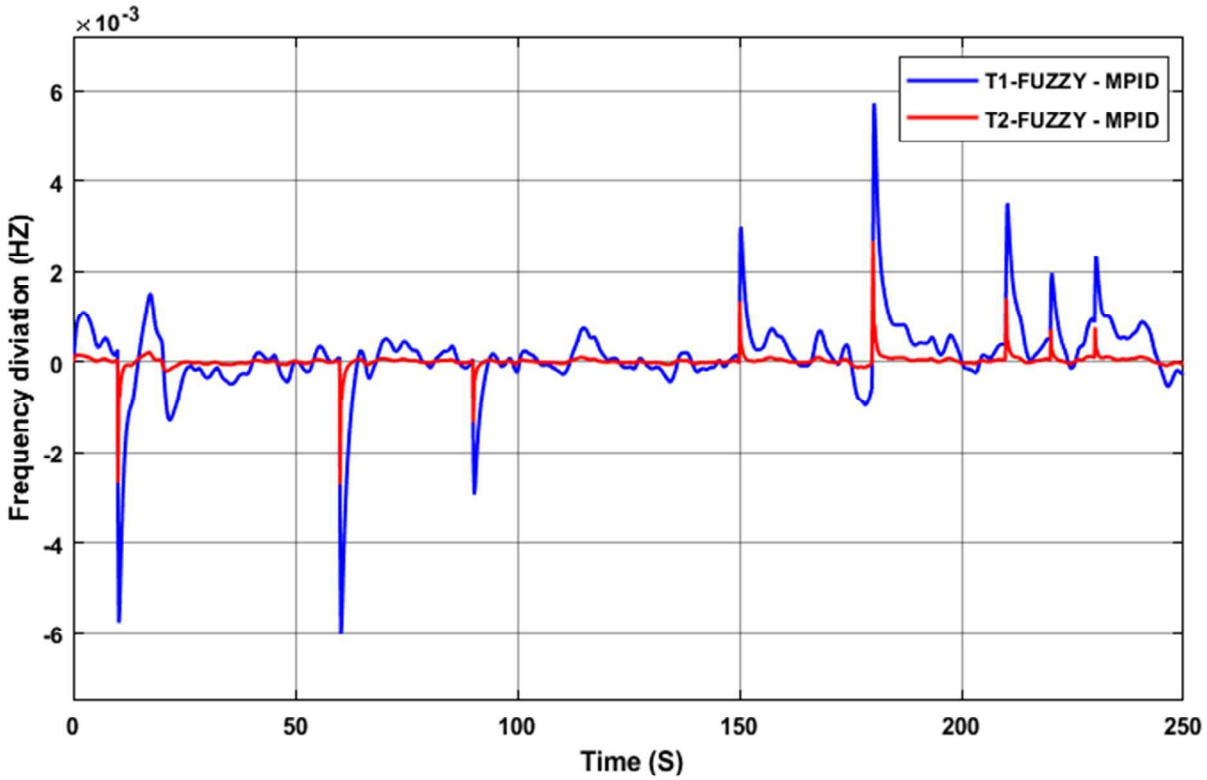

Figure IV.15. Frequency deviation response of the MG under wind power fluctuations using MPID controller with T1-FL and T2-FL

The figure IV.15 presents the frequency deviation response of the microgrid under wind power fluctuations, comparing the performance of the MPID controller with T1-FL and T2-FL. It is evident that the blue curve T1-FL exhibits sharp oscillations and peak frequency deviations exceeding 6×10^{-3} Hz, reflecting its limited ability to suppress the random effects caused by wind speed variations, with oscillations persisting for longer durations. In contrast, the red curve (T2-FL) demonstrates a more stable performance by reducing the deviation magnitude, keeping the frequency closer to its nominal value, and achieving faster damping of oscillations. Therefore, it can be concluded that integrating T2-FL with the MPID controller significantly enhances frequency stability and improves system reliability when dealing with fluctuations from renewable energy sources, particularly wind power.

Case 3: the MG is subjected solely to disturbances caused by solar energy, as illustrated in Figure III.19. The corresponding frequency deviation resulting from these disturbances is presented in Figure IV.16, which demonstrates the controller's capability to preserve the stability of the MG under fluctuating solar power generation.

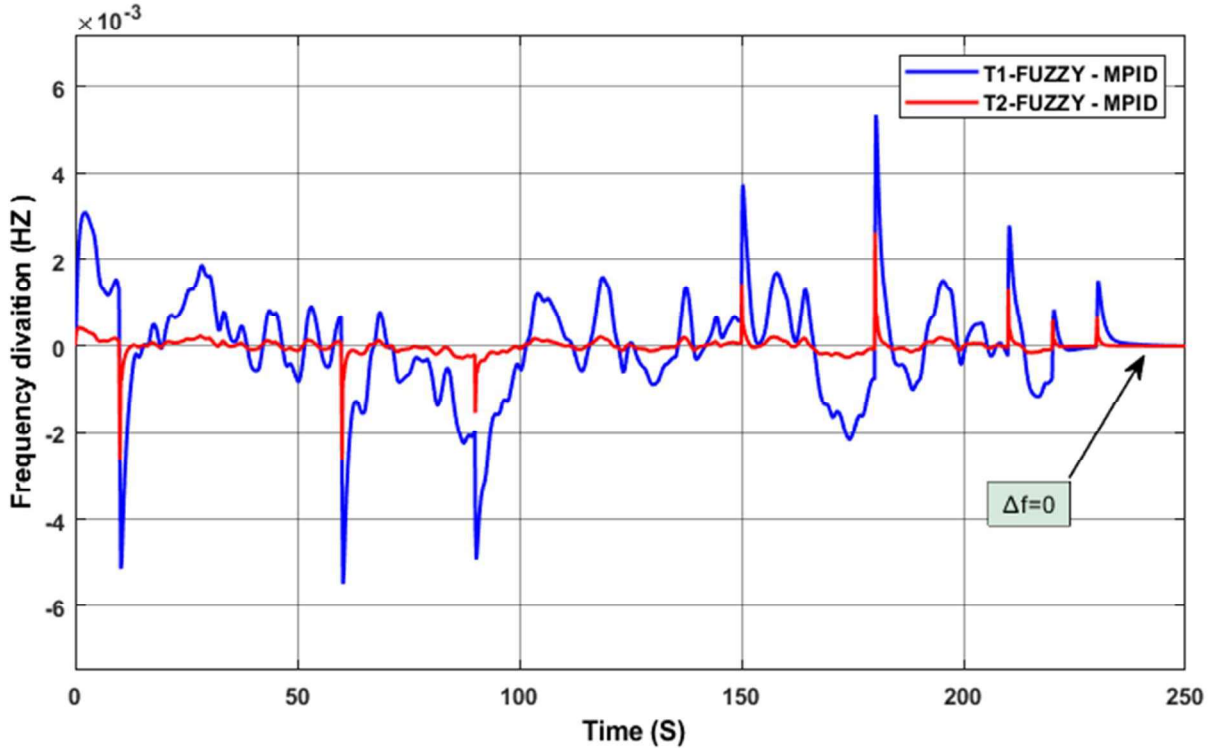

Figure IV.16. Frequency deviation response of the MG under solar power variations using MPID controller with T1-FL and T2-FL

The figure IV.16 present illustrates the frequency deviation response of the microgrid system under solar power variations, using both the T1-FL controller (blue) and the T2-FL-MPID controller (red). It is clearly observed that the proposed T2-FL controller outperforms the T1-FUZZY-MPID by significantly reducing oscillations and maintaining the frequency deviation close to zero. In the period between 220s and 250s, the frequency deviation gradually decreases and approaches zero, which is due to the assumption that solar power becomes zero in this stage (nighttime). This highlights the efficiency of the T2-FUZZY-MPID controller in ensuring frequency stability even under highly variable and complex operating conditions.

Case 4: The MG is subjected to all disturbance sources, including load variations, fluctuations in PV output, and changes in wind speed generation. The resulting frequency deviation is illustrated in Figure IV.17, confirming the influence of these disturbances on the overall system stability.

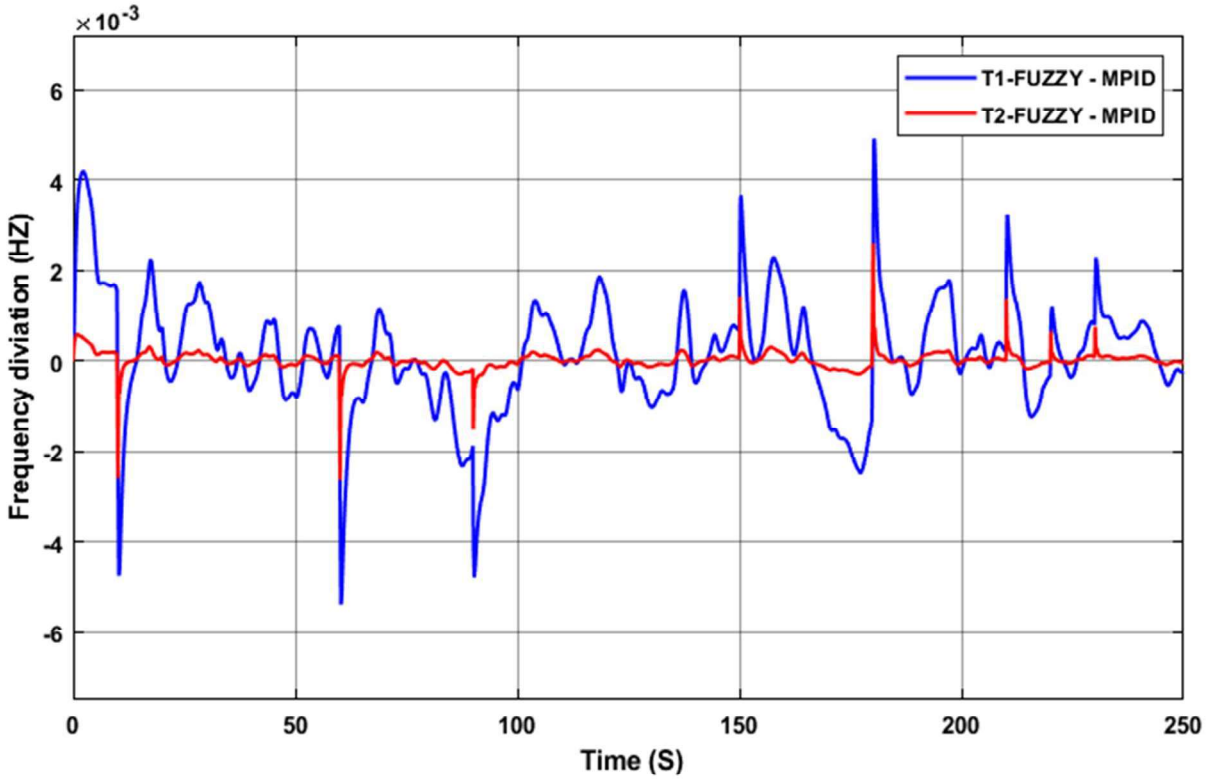

Figure IV.17. Frequency deviation response of the MG under the combined influence of wind power and load variations using T1-FL and T2-FL

The figure IV.17 illustrates the frequency deviation response of the MG under the combined influence of wind power and load variations. It can be observed that sudden changes in energy sources lead to a noticeable increase in frequency deviation when using the T1-FL controller (blue curve), where sharp oscillations and larger deviation amplitudes are evident. In contrast, the T2-FL controller (red curve) demonstrates a more stable performance, maintaining the frequency deviation close to zero with a significant reduction in oscillations. This highlights its superior ability to adapt to the complex fluctuations of both wind power and load variations, thereby ensuring effective frequency stability.

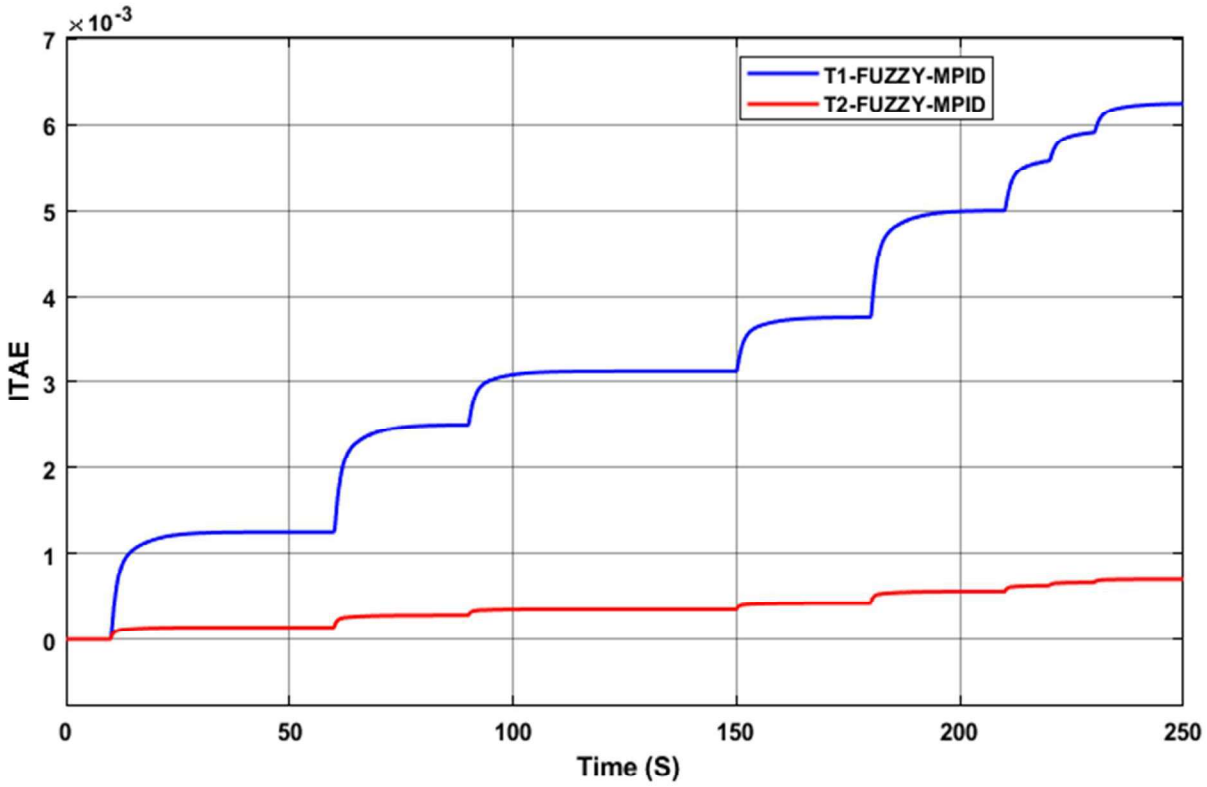

Figure IV.18. Variation of ITAE index over time comparing T1-FL-MPID and T2-FL-MPID controllers in the MG

The presented figure IV.18 shows the variation of the ITAE index over time when comparing the performance of the T1-FUZZY-MPID controller (purple curve) and the T2-FUZZY-MPID controller (green curve). It can be observed that the ITAE value increases significantly when using the T1-FUZZY-MPID controller due to the accumulation of errors over time, reflecting its limited ability to mitigate oscillations and frequency deviations. In contrast, the T2-FUZZY-MPID controller demonstrates superior performance by maintaining very low ITAE values throughout the operation period, indicating its high effectiveness in reducing cumulative error and minimizing the impact of disturbances. This superiority confirms that the Type-2 fuzzy-based controller is more suitable for such microgrid applications, where higher precision and stability are required to cope with continuous variations in energy sources and loads.

- **Fourth scenario:**

In this scenario, the PHEV integrated into the microgrid was tested to evaluate its effectiveness in frequency stabilization. As explained previously, when the PHEV battery is unable to supply the required load demand, the diesel generator intervenes to compensate for the deficit. However, in this scenario, the DEG was disconnected in order to specifically assess the capability of the PHEV battery. The tests were carried out in two stages: in the first stage, the battery performance was examined under charging and discharging conditions, while in the second stage, different states of charge (SoC) were tested to measure their contribution to compensating the energy demand on the frequency deviation (Δf) in the microgrid system.

Case 1: In this case, the PHEV was tested through its battery under charging and discharging conditions, in order to evaluate its performance and its capability to contribute to energy balance within the microgrid system.

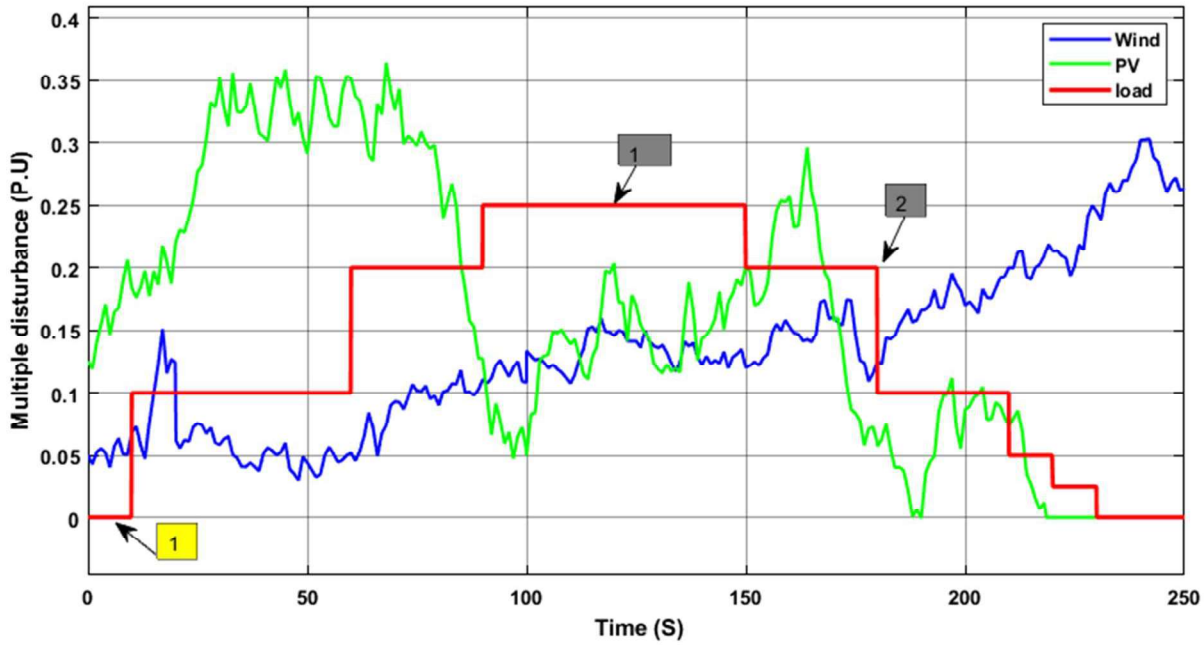

Figure IV.19. Variation of RES (wind and solar) with load over time in the MG

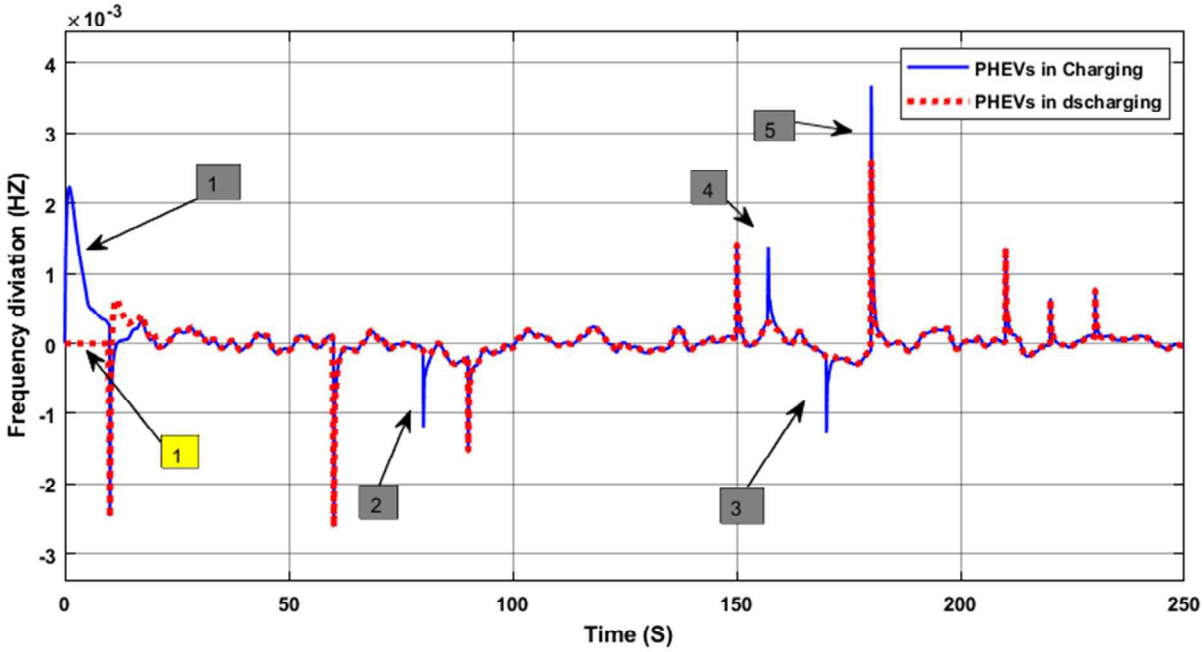

Figure IV.20. Frequency deviation response of the MG during charging and discharging of the PHEV battery

Figure IV.19 illustrates the variation of renewable energy sources (wind and PV) along with the load over time. It is clearly observed that renewable energy sources are inherently intermittent and fluctuating, which leads to frequent mismatches between the generated power and the load demand. In regions (1) and (2), the load exceeds the power generated from renewable sources, creating critical periods within the system that require additional energy to compensate for the deficit. This imbalance between generation and demand highlights the necessity of a storage element or an alternative source that can act as a buffer to maintain system stability.

Figure IV.20 shows the Δf response of the MG when the PHEV battery is tested under charging and discharging conditions. In region (1), shaded in yellow, it is observed that in the discharging state the frequency remains close to zero, which indicates that the system is stable and the load is fully supplied. However, in the same region during charging, a frequency deviation appears despite the load being equal to zero. This is due to the fact that the battery was empty at that moment and absorbed energy from the grid for charging, resulting in a noticeable deviation. Furthermore, in regions (1, 2, 3, and 4), larger deviations occur during charging because the load demand exceeded the power produced by renewable sources, and the charging process imposed an additional burden on the system. In region (5), two simultaneous events occurred: a sudden change in the load and a reduction in available power, which together caused a significant frequency deviation.

From these two figures, it can be concluded that the PHEV battery plays a dual role within the microgrid: on the one hand, it acts as an additional load during charging, and on the other hand, it functions as a vital energy source when needed to compensate for generation shortages. This dual role makes PHEV batteries an essential component in enhancing frequency stability and ensuring a continuous balance between supply and demand in MG.

Case 2: In this case, the impact of the PHEV state of charge (SOC) — 10%, 40%, 60%, and 80% — on the frequency stability of the microgrid was investigated through the vehicles' ability to compensate for the energy deficit in coordination with the T1-FL-PID and T2-FL controllers. To achieve variations in the SOC levels, the parameters of the electric vehicle battery were adjusted according to the specifications presented in Table IV.5, enabling a realistic representation of the differences in the available battery capacities for discharging.

Table IV.5. Ratio variation in PHEVs

Percentage variation	Parameters PHEVs			
	R_{av}	T_{Ev}	K_{Ev}	N_{Ev}
±10%	0.24	0.01	0.18	60
±40%	0.96	0.04	0.72	240
±60%	1.44	0.06	1.08	360
±80%	1.92	0.08	1.44	480

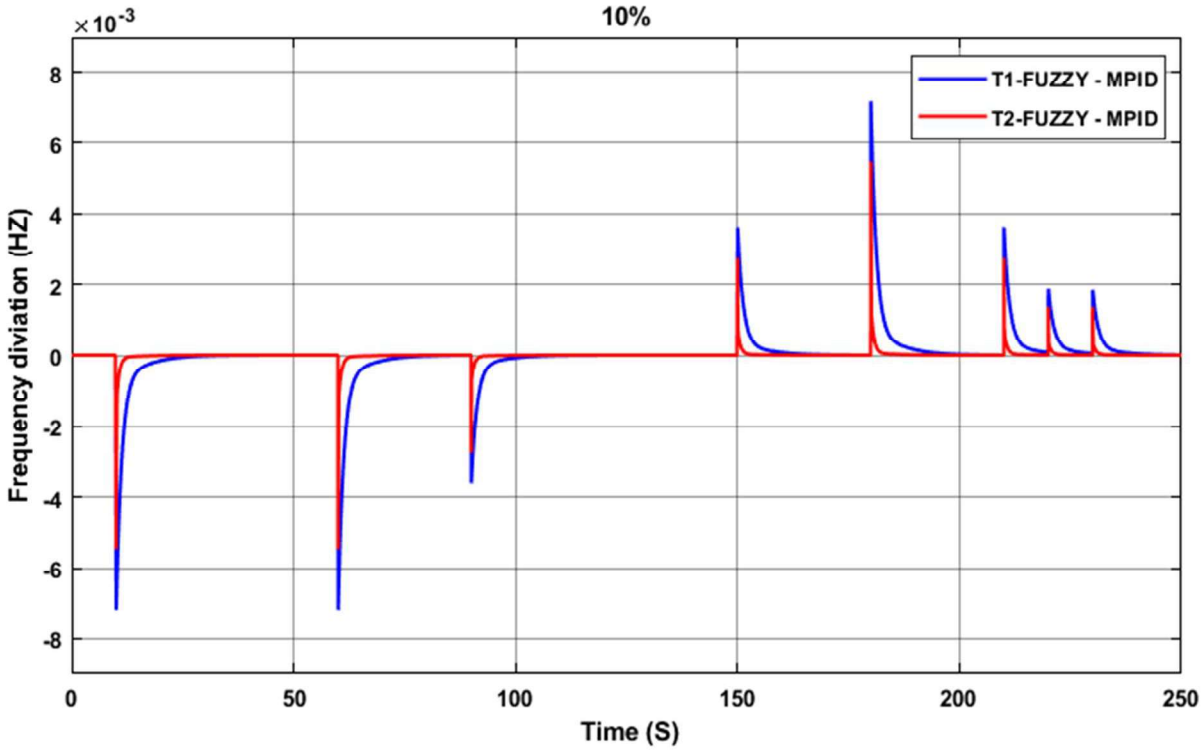
10%
×10-3
T1-FUZZY - MPID
T2-FUZZY - MPID
Frequency diviation (HZ)
Time (S)

a)

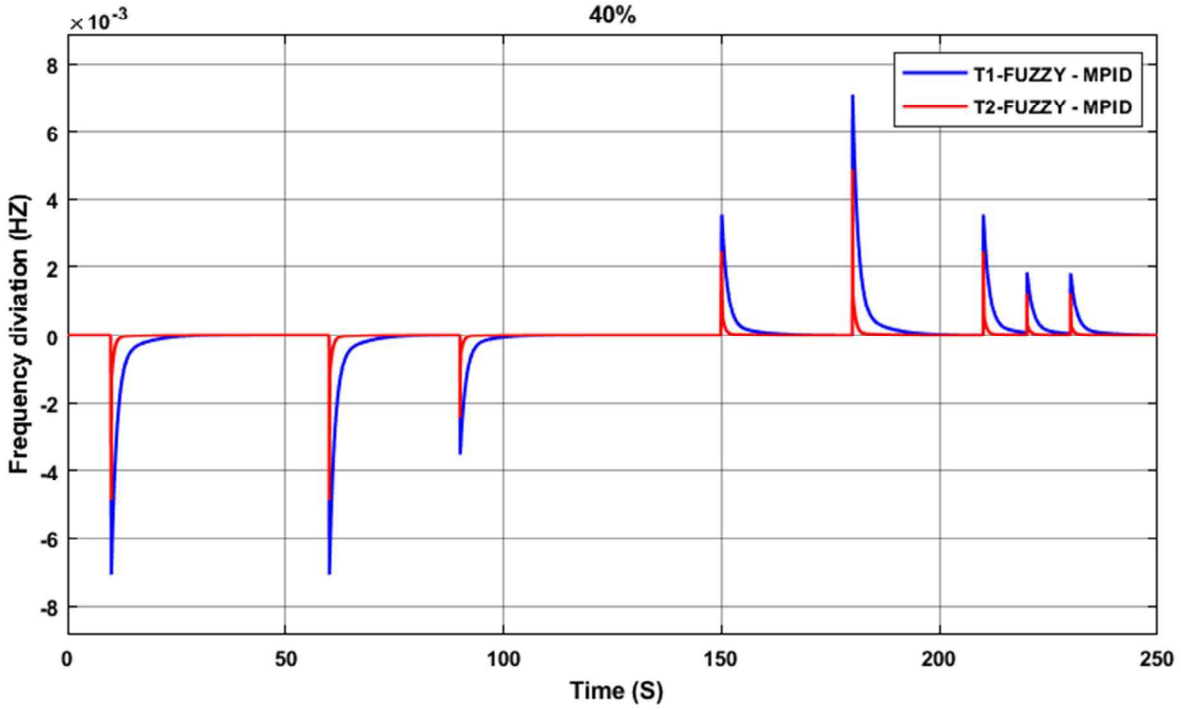
40%
×10-3
T1-FUZZY - MPID
T2-FUZZY - MPID
Frequency diviation (HZ)
Time (S)

b)

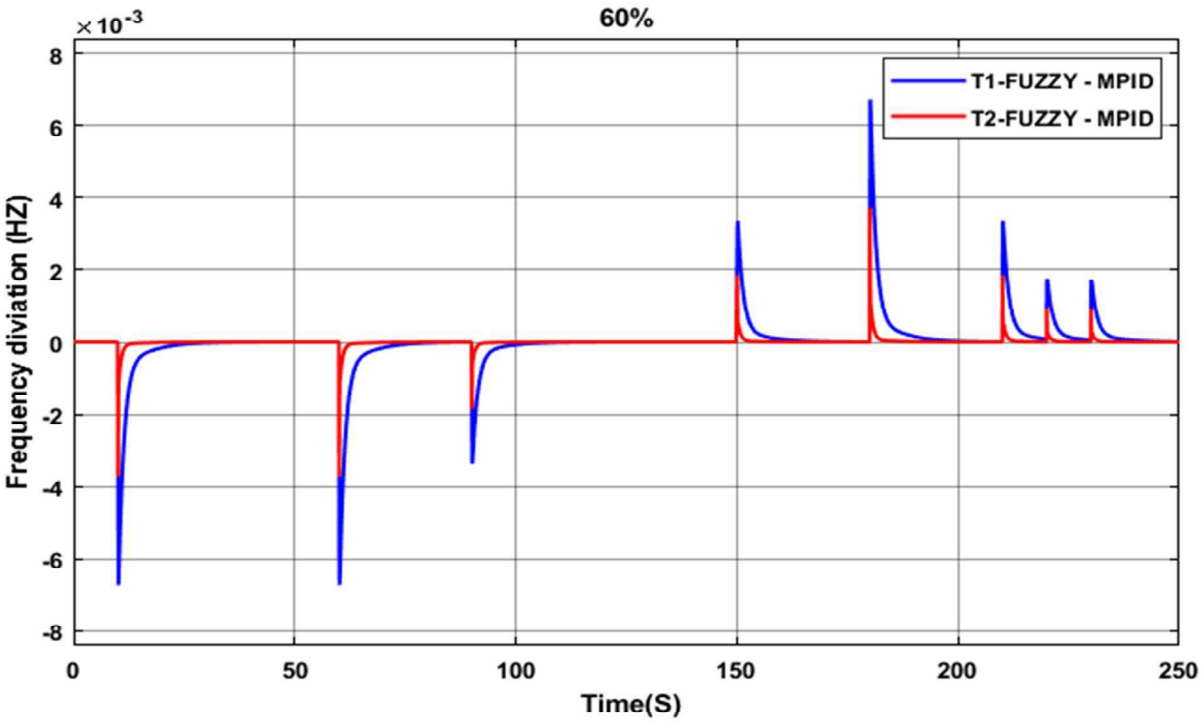

c)

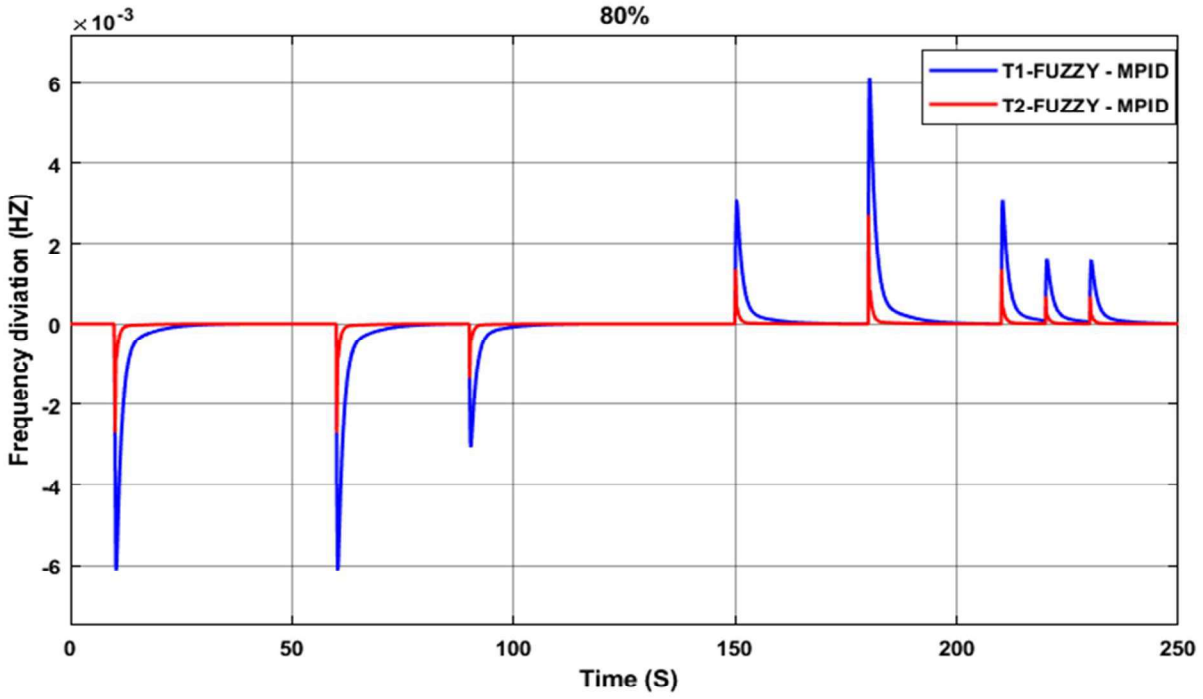

d)

Figure IV.21: Frequency deviation response of the microgrid under different states of charge (SOC) of electric vehicle batteries (**a-** 10%, **b-** 40%, **c-** 60%, and **d-** 80%) using the T1-FUZZY-MPID and T2-FUZZY-MPID controllers

The results presented in the four figures IV.21 illustrate the impact of the state of charge (SOC) of electric vehicle batteries on the frequency stability of the microgrid when using the T1-FUZZY-MPID and T2-FUZZY-MPID controllers. At SOC = 10%, a larger frequency

deviation with pronounced oscillations is observed, where the performance of the T1 controller is less efficient compared to the T2 controller, which successfully reduced the deviation rapidly and restored the frequency to its reference value. As the SOC is increased to 40%, the stability improves due to the greater discharge capacity, with noticeable reduction in oscillations, especially when using the T2 controller. At SOC = 60%, further improvement is achieved, as the battery's ability to balance the power deficit increases, resulting in additional reduction of oscillations and maintaining the frequency deviation close to zero, particularly with the T2 controller. At SOC = 80%, the battery reaches its highest efficiency in compensating the power shortage, leading to the best frequency stability, where the T2-FUZZY-MPID controller demonstrates clear superiority by minimizing oscillations to the lowest level compared to T1. Therefore, it can be concluded that increasing the SOC from 10% to 80% results in a gradual and significant enhancement in frequency stability, with the T2 controller consistently showing more effective and reliable performance across all cases.

IV.7. Analysis of results in general

The simulation results showed that using T2-FL with the MPID controller achieved superior performance in terms of frequency stability, faster disturbance response, and higher energy utilization efficiency. Applying T2-FL with the PID controller also demonstrated noticeable improvements compared to the T1-FL with PID, as it helped reduce oscillations and enhance stability, although its performance remained relatively lower than when combined with MPID. In contrast, using T1-FL with the PID controller was simpler and required fewer computational resources, making it more suitable for applications with limited capabilities. For scenarios that demand high performance and greater adaptability to changing operating conditions, T2-FL with MPID is considered the most appropriate choice, while the combination of T1-FL with PID remains a practical option for simpler systems. For future work, it is recommended to conduct further testing under diverse operating conditions to assess the robustness of these control schemes, in addition to exploring hybrid strategies that integrate the strengths of PID and MPID with both Classic andT2-FL, which could provide balanced and comprehensive performance improvements.

IV.8. Conclusion

In conclusion, this chapter has provided a comprehensive investigation into the application of classical and advanced control strategies for frequency stabilization in islanded microgrid systems. The analysis highlighted the limitations of the conventional PID controller when exposed to the intermittent nature of renewable energy sources and sudden load variations. To address these challenges, the Multistage PID (MPID) controller, supported by fuzzy logic tuning methods, demonstrated superior adaptability and enhanced dynamic response. The simulation results confirmed that Type-1 Fuzzy Logic (T1-FL) improves the performance of PID and MPID controllers by managing system uncertainties, while Type-2 Fuzzy Logic (T2-FL) further enhances stability under complex and fluctuating conditions. These findings underline the critical role of intelligent tuning techniques in reinforcing the operational reliability of islanded microgrids. Overall, the comparative evaluation established the MPID controller tuned with T2-FL as the most effective strategy among the studied approaches, ensuring robust performance and greater resilience of microgrid systems.

GENERAL CONCLUSION

General Conclusion

This thesis has provided a comprehensive study on the modeling, analysis, and control of hybrid microgrid systems, with a particular focus on frequency stability. The work addressed one of the most critical challenges in modern power systems, namely the integration of renewable energy sources and the mitigation of their intermittent nature to ensure reliable and stable operation.

In Chapter I, a thorough review of the microgrid concept was presented, including its historical development, main components, and different classifications. The discussion emphasized its advantages in reducing emissions, improving energy efficiency, and ensuring reliable electricity supply, particularly in remote and isolated areas. This theoretical framework laid a solid foundation for understanding the characteristics of microgrids and the challenges they face, with frequency stability identified as a central issue.

Chapter II focused on the accurate modeling of the proposed hybrid microgrid system. Mathematical representations were developed for renewable energy sources such as photovoltaic panels and wind turbines, as well as conventional sources including diesel generators and fuel cells. Plug-in Hybrid Electric Vehicles (PHEVs) were also incorporated as flexible and mobile storage units due to their growing importance in supporting system stability. The models were built using first-order transfer functions to facilitate frequency-domain analysis, thus establishing the necessary groundwork for studying system dynamics and designing effective control strategies.

In Chapter III, the frequency regulation problem was analyzed in depth through the design of a Multi-Stage PID (MPID) controller. Its parameters were tuned using conventional techniques such as Ziegler–Nichols (ZN) and the Coefficient Diagram Method (CDM), in addition to advanced optimization algorithms like the Cuckoo Search Algorithm (CSA) and Ant Colony Optimization (ACO). The results clearly demonstrated that optimization-based tuning significantly enhanced system performance by reducing frequency deviations, improving stability, and accelerating dynamic response. The comparative analysis further showed that the MPID controller outperformed the classical PID controller under a wide range of operating conditions.

Chapter IV extended the study by applying fuzzy logic techniques (Type-1 and Type-2) to enhance the adaptability of the MPID controller. The results revealed that Type-1 Fuzzy Logic offered an efficient approach to handling uncertainties, while Type-2 Fuzzy Logic achieved superior robustness in dealing with the stochastic behavior of renewable energy and sudden load disturbances. These findings underscored the vital role of advanced control strategies in improving the reliability and flexibility of microgrid systems.

From this study, several key points can be highlighted:

- ✓ Microgrids represent a strategic solution for meeting the growing electricity demand while reducing environmental impact and increasing reliance on renewable energy sources.
- ✓ Accurate modeling of microgrid components is essential for understanding system dynamics and developing effective control approaches.

- ✓ The MPID controller significantly outperforms the classical PID controller in reducing frequency deviations and improving overall system stability.
- ✓ The integration of advanced tuning strategies, such as metaheuristic optimization and fuzzy logic, contributes to greater robustness and adaptability under uncertain and variable operating conditions.
- ✓ The use of PHEVs as mobile storage units enhances system flexibility and stability, representing a promising field for further research and development.

In conclusion, this thesis has demonstrated that frequency control is the cornerstone of ensuring reliable operation of microgrids, particularly in islanded mode where system inertia is low and the variability of renewable energy sources becomes more pronounced. Without effective frequency regulation, microgrids are exposed to severe oscillations that negatively affect power quality and overall stability, and in extreme cases, may even lead to partial or complete system collapse. Therefore, achieving frequency stability is not merely a technical necessity but a fundamental prerequisite for expanding the integration of renewable energy sources and promoting the widespread deployment of microgrids across different environments.

The proposed models and control strategies developed in this work provide a valuable framework for both research and practice. From a scientific perspective, they contributed to a deeper understanding of the dynamic behavior of hybrid microgrids and highlighted the critical role of controller design and tuning in mitigating frequency deviations. The comparative assessment between conventional and advanced controllers particularly the Multi-Stage PID (MPID) helped address an existing research gap and established a solid reference point for future investigations.

From a practical standpoint, the findings offer significant guidance for engineers, system operators, and policymakers in developing more efficient and sustainable microgrids. The integration of renewable energy sources, supported by advanced control techniques and flexible storage units such as Plug-in Hybrid Electric Vehicles (PHEVs), demonstrates a clear pathway toward enhancing network flexibility, reducing dependence on fossil fuels, and minimizing harmful emissions.

Ultimately, this study confirms that hybrid microgrids, when equipped with effective frequency control strategies, represent a fundamental pillar of the future power system landscape. They enable the transition toward decentralized, flexible, and clean energy networks capable of reliably meeting the rapidly increasing global demand for electricity, while simultaneously supporting sustainability goals and energy security in both developed and developing countries.

Future work

Based on the findings of this thesis, several promising research directions can be pursued to further enhance the reliability and stability of microgrid systems.

First, the development of hybrid optimization techniques represents a highly promising avenue, as combining multiple algorithms can achieve superior dynamic performance compared to relying on a single method. Such hybrid approaches are particularly effective in improving frequency stability under variable operating conditions. In addition, the integration

of fuzzy logic with newly developed algorithms offers an opportunity to strengthen the ability of controllers to handle nonlinearity and uncertainties associated with renewable energy sources

Second, the exploration of novel controllers such as the Triple Integral Derivative (TID) and Model-Free Control (MFC) is strongly recommended. These controllers may provide more flexible and efficient control solutions compared to conventional strategies, enabling improved adaptability to sudden disturbances and system uncertainties.

Third, future work should focus on the study of hybrid microgrids composed of multiple interconnected sub-microgrids, which play a key role in ensuring energy continuity and enhancing operational resilience when facing disturbances or generation fluctuations.

Finally, advancing toward experimental research is crucial. This involves validating the proposed models in real microgrid environments, collecting operational data under realistic conditions, and conducting extensive testing with different load profiles, storage technologies, and weather scenarios. Such efforts are essential to bridge the gap between theoretical simulations and practical deployment, ensuring the applicability and reliability of the proposed solutions.

Bibliography

1. Kakran, S., Rathore, J. S., Sidhu, A., & Kumar, A. (2024). Solar energy advances and CO2 emissions: A comparative review of leading nations' path to sustainable fu-ture. Journal of Cleaner Production, 143598.
2. Ma, S. (2024). Optimal scheduling of electric vehicle aggregators for frequency regulation and cost efficiency in renewable-powered grids. Computers and Electrical Engineering, 118, 109317.
3. Bouddou, R., Benhamida, F., Zeggai, A., Ziane, I., & Belgacem, M. (2020). The dynamic economic dispatch in an integrated wind-thermal electricity market using simulated annealing algorithm. Przeglad Elektrotechniczny, 96(11), 55-60.
4. Ahmad, S., Shafiullah, M., Ahmed, C. B., & Alowaifeer, M. (2023). A review of microgrid energy management and control strategies. IEEE Access, 11, 21729-21757.
5. Cisneros-Saldana, J. I. D., Samal, S., Begovic, M. M., & Samantaray, S. R. (2024). On protection schemes for ac microgrids: challenges and opportunities. IEEE Transactions on Industry Applications.
6. Karim El Mezdi, A. E. Magri, and Lhoussain Bahatti, “Advanced control and energy management algorithm for a multi-source microgrid incorporating renewable energy and electric vehicle integration,” Results in Engineering, vol. 23, pp. 102642–102642, Aug. 2024, doi: https://doi.org/10.1016/j.rineng.2024.102642.
7. Heidari, M., Soleimani, A., Dzikuć, M., Heidari, M., Dolatabadi, S. H. H., Kuryło, P., & Khan, B. (2024). Exploring synergistic ecological and economic energy solutions for low-urbanized areas through simulation-based analysis. AIMS Energy, 12(1), 119-151. doi: https://doi.org/10.3934/energy.2024006.
8. Ibrahim Alhamrouni, Wahab, W., Salem, M., Nadia, & Awalin, L. (2019). Modeling of micro-grid with the consideration of total harmonic distortion analysis. Indonesian Journal of Electrical Engineering and Computer Science, 15(2), 581–581.
9. Dekker, J., Nthontho, M., Chowdhury, S., & Chowdhury, S. P. (2012). Economic analysis of PV/diesel hybrid power systems in different climatic zones of South Africa. International Journal of Electrical Power & Energy Systems, 40(1), 104–112.
10. D. C. Das, A. K. Roy, and N. Sinha, “GA based frequency controller for solar thermal–diesel–wind hybrid energy generation/energy storage system”, Int J. Electr. Power Energy Syst., vol. 43, no. 1, pp.262–279, 2012.
11. Mesa Solutions. “Microgrid Controllers: Functions and Benefits.” Mesa Solutions, 18 May 2023, 247mesa.com/microgrid-controllers-functions-and-benefits
12. Cohn, Lisa. “History of Microgrids in the US: From Pearl Street to Plug-And-Play.” Microgrid Knowledge, 22 July 2019, www.microgridknowledge.com/about-microgrids/article/11429549/history-of-microgrids-in-the-us-from-pearl-street-to-plug-and-play.

13. . Li, Fusheng, et al. Microgrid Technology and Engineering Application. London, Uk ; San Diego, Ca, Usa, Academic Press Is An Imprint Of Elsevier, 2016.

14. Thirunavukkarasu, M., Sawle, Y., & Lala, H. (2023). A comprehensive review on optimization of hybrid renewable energy systems using various optimization techniques. Renewable and Sustainable Energy Reviews, 176, 113192.

15. Chambalile, M., Su, B., & Illo, F. (2024). The State-of-the-Art Review on Wind and Photovoltaic Solar Hybrid Renewable Energy and Its Impending Potential in Eastern and Southern Africa. Journal of Energy Research and Reviews, 16(8), 23-43.

16. IEA. "Growth in Global Energy Demand Surged in 2024 to Almost Twice Its Recent Average - News - IEA." IEA, 24 Mar. 2025, www.iea.org/news/growth-in-global-energy-demand-surged-in-2024-to-almost-twice-its-recent-average.

17. Center for Climate and Energy Solutions. "Microgrids | Center for Climate and Energy Solutions." Center for Climate and Energy Solutions, 16 Oct. 2017, www.c2es.org/content/microgrids/.

18. "The Rise of Microgrids in Developing Countries." Www.hivepower.tech, 18 Jan. 2021, www.hivepower.tech/blog/the-rise-of-microgrids-in-developing-countries.

19. "Developing Energy Flexibility in Clusters of Buildings: A Critical Analysis of Barriers from Planning to Operation." Energy and Buildings, vol. 300, 1 Dec. 2023, p. 113608, www.sciencedirect.com/science/article/pii/S0378778823008381?ref=pdf_download&fr=RR-2&rr=81a0b603ade104bc, https://doi.org/10.1016/j.enbuild.2023.113608.

20. Doğrul, Mürsel, and Yokota Takayuki. "The Political Economy of Japan's Net-Zero Vision in the Context of Energy Security." Ege Akademik Bakis (Ege Academic Review), vol. 25, no. 1, 4 Feb. 2025, pp. 241–254, dergipark.org.tr/en/pub/eab/issue/90033/1575092, https://doi.org/10.21121/eab.20250115. Accessed 24 Mar. 2025.

21. Zahid, Herman, et al. "A Review on Socio-Technical Transition Pathway to European Super Smart Grid: Trends, Challenges and Way Forward via Enabling Technologies." Results in Engineering, Jan. 2025, p. 104155, https://doi.org/10.1016/j.rineng.2025.104155.

22. "The Key to Africa's Off-Grid Energy Breakthrough? A Clear Legal Framework | UNDP Climate Promise." UNDP Climate Promise, 2024, climatepromise.undp.org/news-and-stories/key-africas-grid-energy-breakthrough-clear-legal-framework.

23. Bhoi, Ashok, et al. "Optimal Harmonic Estimation in Renewable Integrated Power System Using Grasshopper Optimisation Algorithm and Recursive Least Square Approach." TENCON 2024 - 2024 IEEE Region 10 Conference (TENCON), 1 Dec. 2024, pp. 1328–1332, https://doi.org/10.1109/tencon61640.2024.10903090. Accessed 14 May 2025.

24. Hitchens, Kathy. "Bloomberg NEF: Microgrids, Sustainable Energy Thrive in 2024." Microgridknowledge.com, Microgrid Knowledge, 26 Feb. 2025,

www.microgridknowledge.com/microgrids/news/55270854/bloombergnef-microgrids-sustainable-energy-thrive-in-2024.

25. "IRENA Renewable Energy Statistics Year 2024." SlideShare, Slideshare, 2024, fr.slideshare.net/slideshow/irena-renewable-energy-statistics-year-2024/270219114. Accessed 23 June 2025.

26. Tran, Quynh T, et al. "Isolation Microgrid Design for Remote Areas with the Integration of Renewable Energy: A Case Study of Con Dao Island in Vietnam." Clean Technologies, vol. 3, no. 4, 3 Nov. 2021, pp. 804–820, https://doi.org/10.3390/cleantechnol3040047.

27. Kanimozhi, Gunasekaran, and Karmel Arockiasamy. Blockchain Technology for Hybrid AC–DC Microgrids. Elsevier, 1 Mar. 2024, pp. 233–258, www.sciencedirect.com/science/article/abs/pii/B9780443221873000102.

28. Wu, Xiong, et al. "Hybrid AC/DC Microgrid Planning with Optimal Placement of DC Feeders." Energies, vol. 12, no. 9, 9 May 2019, p. 1751, https://doi.org/10.3390/en12091751. Accessed 16 Mar. 2022.

29. Ullah, Shahid, et al. "Assessment of Technical and Financial Benefits of AC and DC Microgrids Based on Solar Photovoltaic." Electrical Engineering, vol. 102, no. 3, 21 Feb. 2020, pp. 1297–1310, https://doi.org/10.1007/s00202-020-00950-7.

30. Anil Annamraju, and Srikanth Nandiraju. "A Novel Fuzzy Tuned Multistage PID Approach for Frequency Dynamics Control in an Islanded Microgrid." International Transactions on Electrical Energy Systems, vol. 30, no. 12, 10 Nov. 2020, https://doi.org/10.1002/2050-7038.12674.

31. Raju, Gotte Vikram, and Nandiraju Venkata Srikanth. "Frequency Control of an Islanded Microgrid with Multi-Stage PID Control Approach Using Moth-Flame Optimization Algorithm." Electrical Engineering, 20 June 2024, https://doi.org/10.1007/s00202-024-02518-1.

32. Hajimiragha, A. H., & Dadash, M. R. (2013). Research and development of a microgrid control and monitoring system for the remote community of Bella Coola: Challenges, solutions, achievements and lessons learned. in 2013 IEEE International Conference on Smart Energy Grid Engineering (SEGE), 2013, pp. 1–6. https://doi.org/10.1109/sege.2013.6707898

33. M. R. S. Shaikh and S. Labade, "A review paper on electricity generation from solar energy," International Journal for Research in Applied Science and Engineering Technology, Sep. 2017. doi: 10.22214/ijraset.2017.5022.

34. Edouard, Mboumboue, and Donatien Njomo. "Mathematical modeling and digital simulation of PV solar panel using Matlab software." International Journal of Emerging Technology and Advanced Engineering 3.9 (2013): 24-32.

35. Chen, Zhenyu, et al. "Synthesis and Applications of Three-Dimensional Graphene Network Structures." Materials Today Nano, vol. 5, 1 Mar. 2019, pp. 100027–100027, https://doi.org/10.1016/j.mtnano.2019.01.002. Accessed 24 Apr. 2023.

36. Huang, Sheng, et al. “Application of Model Predictive Control in Wind Farm.” Elsevier EBooks, 30 Sept. 2022, pp. 155–164, https://doi.org/10.1016/b978-0-12-821204-2.00137-9. Accessed 23 June 2025.

37. Abdullah, Muhammad. “Lift and Drag Force.” Scribd, 2025, fr.scribd.com/document/559091093/Lift-and-drag-force. Accessed 23 June 2025.

38. Vu. “Pham Nam Phong.” Vu Phong Energy Group, 28 Jan. 2022, vuphong.com/four-fascinating-facts-about-wind-power/. Accessed 23 June 2025.

39. Soomro, Abid, et al. “Hybrid PV System with High Speed Flywheel Energy Storage for Remote Residential Loads.” Clean Technologies, vol. 3, no. 2, 20 Apr. 2021, pp. 351–376, https://doi.org/10.3390/cleantechnol3020020.

40. “Compressed Air Energy Storage (CAES).” Oil Free Air, 16 Feb. 2018, www.oilfree-air.eu/compressed-air-energy-storage-caes/.

41. Muhamad Azim, M.K., et al. “Recent Progress in Emerging Hybrid Nanomaterials towards the Energy Storage and Heat Transfer Applications: A Review.” Journal of Molecular Liquids, vol. 360, Aug. 2022, p. 119443, https://doi.org/10.1016/j.molliq.2022.119443. Accessed 7 July 2022.

42. Petrovic, Slobodan. “Lead–Acid Batteries.” Springer EBooks, 30 Oct. 2020, pp. 47–71, https://doi.org/10.1007/978-3-030-57269-3_3.

43. Ma, Ning, et al. “Aging Mechanism and Models of Supercapacitors: A Review.” Technologies, vol. 11, no. 2, 1 Apr. 2023, p. 38, www.mdpi.com/2227-7080/11/2/38, https://doi.org/10.3390/technologies11020038. Accessed 25 May 2023.

44. “Engineered Nanomaterials for Energy Applications.” Handbook of Nanomaterials for Industrial Applications, 2018, pp. 751–767, www.sciencedirect.com/science/article/pii/B9780128133514000432, https://doi.org/10.1016/b978-0-12-813351-4.00043-2.

45. Zhao, Jingyuan, and Andrew F. Burke. “Electric Vehicle Batteries: Status and Perspectives of Data-Driven Diagnosis and Prognosis.” Batteries, vol. 8, no. 10, 24 Sept. 2022, p. 142, https://doi.org/10.3390/batteries8100142. Accessed 27 Sept. 2022.

46. El-Hendawi, Mohamed, et al. "Control and EMS of a grid-connected microgrid with economical analysis." Energies 11.1 (2018) : 129.

47. Bevrani, Hassan, Bruno François, and Toshifumi Ise. Microgrid dynamics and control. John Wiley & Sons, 2017.chapter Microgrids : Concept, Structure, and Operation Modes

48. Bae, In-Su, and Jin-O. Kim. "Reliability evaluation of customers in a microgrid." IEEE Transactions on Power Systems 23.3 (2008) : 1416-1422.

49. M’hamed Helaimi, Gabbar, H. A., Taleb, R., & Regad, M. (2023). Frequency control scheme based on the CDM-PID controller for the hybrid microgrid system with stochastic renewable generators. Automatika, 64(3), 484–495. https://doi.org/10.1080/00051144.2023.2192380

50. Hamid, M. N. A., Banakhr, F. A., Mohamed, T. H., Ali, S. M., Mahmoud, M. M., Mosaad, M. I., ... & Hussein, M. M. (2024). Adaptive Frequency Control of an Isolated Microgrids Implementing Different Recent Optimization Techniques. International Journal of Robotics and Control Systems, 4(3), 1000-1012.

51. B. Alouache, M. Helaimi, A. Belhadj Djilali, H. Allouache, and A. Yahdou, "Load Frequency PID Controller Design Based on Pole Placement Method of an Islanded Microgrid," Journal of Renewable Energies, Oct. 2024, doi: https://doi.org/10.54966/jreen.v1i3.1303.

52. Regad, M., & Helaimi, M. (2020). Frequency control of microgrid with renewable generation using fractional order PID controller based Krill Herd. Indonesian Journal of Electrical Engineering and Informatics, 8(1), 11-20.

53. Annapoorani, K. I., Rajaguru, V., Padmanabhan, S. A., Kumar, K. M., & Venkatachalam, S. (2022). Fuzzy logic-based integral controller for load frequency control in an isolated micro-grid with superconducting magnetic energy storage unit. Materials Today: Proceedings, 58, 244-250.

54. Mehbodniya, A., Kumar, P., Changqing, X., Webber, J. L., Mamodiya, U., Halifa, A., & Srinivasulu, C. (2022). Hybrid Optimization Approach for Energy Control in Electric Vehicle Controller for Regulation of Three-Phase Induction Motors. Mathematical problems in engineering, 2022(1), 6096983.doi: https://doi.org/10.1155/2022/6096983.

55. Mohammadzadeh, A., & Kayacan, E. (2020). A novel fractional-order type-2 fuzzy control method for online frequency regulation in ac microgrid. Engineering Applications of Artificial Intelligence, 90, 103483.

56. Jan, M. U., Xin, A., Rehman, H. U., Abdelbaky, M. A., Iqbal, S., & Aurangzeb, M. (2021). Frequency regulation of an isolated microgrid with electric vehicles and energy storage system integration using adaptive and model predictive controllers. IEEE Access, 9, 14958-14970.

57. Prasad, S. (2023). Robust sliding mode controller for frequency regulation in a microgrid. Transactions of the Institute of Measurement and Control, 45(10), 1947-1964.

58. Zhang, Y., Liu, Ali, S. Q., & Hasanien, H. M. (2012). Frequency control of isolated network with wind and diesel generators by using adaptive artificial neural network controller. International Review of Automatic Control, Praise Worthy Prize, 5(2).

59. Minchala-Avila, L. I., Garza-Castañón, L. E., Vargas-Martínez, A., & Zhang, Y. (2015). A review of optimal control techniques applied to the energy management and control of microgrids. Procedia Computer Science, 52, 780-787.

60. Qin, Y., Zhao, G., Hua, Q., Sun, L., & Nag, S. (2019). Multiobjective genetic algorithm-based optimization of PID controller parameters for fuel cell voltage and fuel utilization. Sustainability, 11(12), 3290.

61. Rajesh, K. S., & Dash, S. S. (2019). Load frequency control of autonomous power system using adaptive fuzzy based PID controller optimized on improved sine cosine algorithm. Journal of Ambient Intelligence and Humanized Computing, 10, 2361-2373.

62. Regad, M., Helaimi, M., Taleb, R., Othman, A. M., & Gabbar, H. A. (2020). Frequency Control in Microgrid Power System with Renewable Power Generation Using PID Controller Based on Particle Swarm Optimization. In Smart Energy Empowerment in Smart and Resilient Cities: Renewable Energy for Smart and Sustainable Cities (pp. 3-13). Springer International Publishing.

63. El-Fergany, A., & El-Hameed, M. (2017). Efficient frequency controllers for autonomous two-area hybrid microgrid system using social-spider optimizer. IET Generation, Transmission & Distribution, 11(3), 637-648.

64. Kumarakrishnan, V., Vijayakumar, G., Boopathi, D., Jagatheesan, K., Saravanan, S., & Anand, B. (2022). Frequency regulation of interconnected power generating system using ant colony optimization technique tuned PID controller. In Control and Measurement Applications for Smart Grid: Select Proceedings of SGESC 2021 (pp. 129-141). Singapore: Springer Nature Singapore.

65. Asgari, S., Suratgar, A. A., & Kazemi, M. (2021). Feedforward fractional order PID load frequency control of microgrid using harmony search algorithm. Iranian Journal of Science and Technology, Transactions of Electrical Engineering, 45(4), 1369-1381.

66. Mishra, D., Nayak, P. C., Bhoi, S. K., & Prusty, R. C. (2020, December). Grey Wolf Optimization algorithm based Cascaded PID controller for Load-frequency control of OFF-Grid Electric Vehicle integrated Microgrid. In 2020 IEEE International Symposium on Sustainable Energy, Signal Processing and Cyber Security (iSSSC) (pp. 1-6). IEEE.

67. Khan, R., Gogoi, N., Barman, J., Latif, A., & Das, D. C. (2019, June). Virtual power plant enabled co-ordinated frequency control of a grid connected independent hybrid microgrid using firefly algorithm. In 2019 IEEE Region 10 Symposium (TENSYMP) (pp. 795-800). IEEE.

68. Putra, D. F. U., Firdaus, A. A., Arof, H., Putra, N. P. U., & Kusuma, V. A. (2023). Improved load frequency control performance by tuning parameters of PID controller and BESS using Bat algorithm. Bulletin of Electrical Engineering and Informatics, 12(5), 2624-2634

69. Sanki, P., Mazumder, S., Basu, M., Pal, P. S., & Das, D. (2021). Moth flame optimization based fuzzy-PID controller for power–frequency balance of an islanded microgrid. Journal of The Institution of Engineers (India): Series B, 102(5), 997-1006.

70. Abriz, A. F., Ghavifekr, A. A., Soltaninejad, M., Tavana, A., Safari, A., & Ziamanesh, S. (2023, February). Modified cuckoo optimization algorithm for frequency regulation of microgrids. In 2023 8th International Conference on Technology and Energy Management (ICTEM) (pp. 1-5). IEEE.

71. B. Alouache, et al. “Optimal Tuning of Multi-Stage PID Controller for Dynamic Frequency Control of Microgrid System under Climate Change Scenarios.” Electrical Engineering & Electromechanics, no. 1, 2 Jan. 2025, pp. 8–15, https://doi.org/10.20998/2074-272x.2025.1.02. Accessed 8 July 2025.

72. Nyawat CW, Srisiriwat N. Temperature control of solid oxide fuel cell system with coefficient diagram method. Adv Eng Res. 2016;90:38–45.

73. GiernackiW. A comparative analysis of tracking quality for CDM and PID control. 10th Portuguese conference on automatic control (CONTROLO'2012); 2012 July 16–18; Funchal.

74. Tarek Hassan Mohamed, Zaki, A. A., & Hussein, M. M. (2015). Application of Linear Quadratic Gaussian and Coefficient Diagram Techniques to Distributed Load Frequency Control of Power Systems. Applied Sciences, 5(4), 1603–1615. https://doi.org/10.3390/app5041603

75. Amarnani D, Rajvant R, Thirunavukkarasu I, et al. Implementation of CDM based PID controller for a stable and double integrating process. J Mechatron Automation. 2015; 2:15–22.

76. Shunji Manabe, "Importance of Coefficient Diagram in Polynomial Method", Proceedings of the 42nd IEEE Conference on Decision and Control Maui, Hawaii USA, December 2003

77. Kumar, B., Adhikari, S., Datta, S., & Sinha, N. (2021). Real time simulation for load frequency control of multisource microgrid system using grey wolf optimization based modified bias coefficient diagram method (GWO-MBCDM) controller. Journal of Electrical Engineering & Technology, 16(1), 205-221.

78. Reza Sarwo Widagdo, Balok Hariadi, and Kukuh Setyadjit, "Modelling and Analysis of Ziegler-Nichols and Chien-Hrones-Reswick Tuning PID on DC Motor Speed Control,"Jurnal Teknologi Elektro, vol. 14, no. 1, pp. 23–23, Feb. 2023, doi:https://doi.org/10.22441/jte.2023.v14i1.005.

79. Ellis, George. "Ziegler Nichols Method - an Overview | ScienceDirect Topics." Www.sciencedirect.com, 2012, www.sciencedirect.com/topics/computer-science/ziegler-nichols-method.

80. Meshram, P. M., and Rohit G. Kanojiya. "Tuning of PID Controller Using Ziegler-Nichols Method for Speed Control of DC Motor." IEEE Xplore, 1 Mar. 2012, ieeexplore.ieee.org/document/6216102.

81. Vo D.N., Schegner P., Ongsakul W. Cuckoo search algorithm for non-convex economic dispatch. IET Generation, Transmission & Distribution, 2013, vol. 7, no. 6, pp. 645-654. doi: https://doi.org/10.1049/iet-gtd.2012.0142.

82. Thao N.T.P., Thang N.T. Environmental Economic Load Dispatch with Quadratic Fuel Cost Function Using Cuckoo Search Algorithm. International Journal of U- and e-Service, Science and Technology, 2014, vol. 7, no. 2, pp. 199-210. doi: https://doi.org/10.14257/ijunesst.2014.7.2.19.

83. Bey, Mohamed, et al. "Result-Adaptive PID Control Based Ant Colony Optimization Tuning for Battery Operation Control in Standalone PV System with Consumption Side Power Management." ELECTRICA, vol. 24, no. 3, 23 Oct. 2024, pp. 710–721, https://doi.org/10.5152/electrica.2024.24041. Accessed 27 Aug. 2025.

84. Mahmood Mahdi, Shaymaa, et al. "PID CONTROLLER TUNING USING ANT COLONY METHOD for SERVO HYDRAULIC SYSTEM." Journal of Mechanical Engineering Research & Developments, vol. 42, no. 4, 11 June 2019, pp. 148–152, https://doi.org/10.26480/jmerd.04.2019.148.152. Accessed 23 Apr. 2021.

85. REN, JIN-ZHI, and WEI XIANG. "Application of Ant Colony-Particle Swarm Optimization Algorithms in Path Planning of Security Robots." DEStech Transactions on Computer Science and Engineering, no. iceit, 8 Mar. 2018,

https://doi.org/10.12783/dtcse/iceit2017/19847. Accessed 29 Oct. 2021.

86. Mahfoud, Said, et al. “ANT-Colony Optimization-Direct Torque Control for a Doubly Fed Induction Motor : An Experimental Validation.” Energy Reports, vol. 8, Nov. 2022, pp. 81–98, https://doi.org/10.1016/j.egyr.2021.11.239. Accessed 18 Jan. 2023.
87. Y. Arya and N. Kumar, “BFOA-scaled fractional order fuzzy PID controller applied to AGC of multi-area multi-source electric power generating systems,” Swarm and Evolutionary Computation, vol. 32, pp. 202–218, Feb. 2017, doi: https://doi.org/10.1016/j.swevo.2016.08.002.
88. A. Anand, P. Aryan, N. Kumari, and G. L. Raja, “Type-2 fuzzy-based branched controller tuned using arithmetic optimizer for load frequency control,” Energy Sources, Part A: Recovery, Utilization, and Environmental Effects, vol. 44, no. 2, pp. 4575–4596, May 2022, doi: https://doi.org/10.1080/15567036.2022.2078444.
89. N. KUMARI, P. Aryan, and G. L. L. Raja, “Optimal Type-2 Fuzzy Based Secondary Control Strategy for Three-Area Hybrid Power System Integrating Renewable Sources Under Various Deregulated Market Scenarios,” SSRN Electronic Journal, 2022, doi: https://doi.org/10.2139/ssrn.4163795.
90. S. R. Paital, P. Ray, and S. R. Mohanty, “A robust dual interval type-2 fuzzy lead–lag based UPFC for stability enhancement using Harris Hawks Optimization,” ISA Transactions, vol. 123, pp. 425–442, Apr. 2022, doi: https://doi.org/10.1016/j.isatra.2021.05.029.
91. R. Kumar Khadanga, A. Kumar, and S. Panda, “Frequency control in hybrid distributed power systems via type-2 fuzzy PID controller,” IET Renewable Power Generation, Mar. 2021, doi: https://doi.org/10.1049/rpg2.12140.
92. Tawfiq Aljohani, “Intelligent Type-2 Fuzzy Logic Controller for Hybrid Microgrid Energy Management with Different Modes of EVs Integration,” Energies, vol. 17, no. 12, pp. 2949–2949, Jun. 2024, doi: https://doi.org/10.3390/en17122949.
93. R. Saraswat and S. Suhag, “Type-2 fuzzy logic PID control for efficient power balance in an AC microgrid,” Sustainable Energy Technologies and Assessments, vol. 56, p. 103048, Mar. 2023, doi: https://doi.org/10.1016/j.seta.2023.103048.